Alma Mater Studiorum – Università di Bologna

DOTTORATO DI RICERCA IN

Ingegneria Civile, ambientale e dei materiali

Ciclo XXVIII

Settore Concorsuale di afferenza: 03/B2

Settore Scientifico disciplinare: CHIM/07

SYNTHESIS AND CHARACTERIZATION OF NEW ALIPHATIC BIODEGRADABLE POLYESTERS FOR PACKAGING APPLICATIONS

Presentata da: *Laura Genovese*

Coordinatore Dottorato

Chiar.mo Prof. Alberto Lamberti

Relatore

Chiar.mo Prof. Andrea Munari

Correlatore

Chiar.ma Prof.ssa Nadia Lotti

Esame finale anno 2016

TABLE OF CONTENTS

1.

INTRODUCTION

1 INTRODUCTION

1.1 Plastic Industry

Over the last 60 years, plastics have brought economic, environmental and social advantages; synthetic polymeric materials have found wide applications in every aspect of life and industries (Figure 1.1).

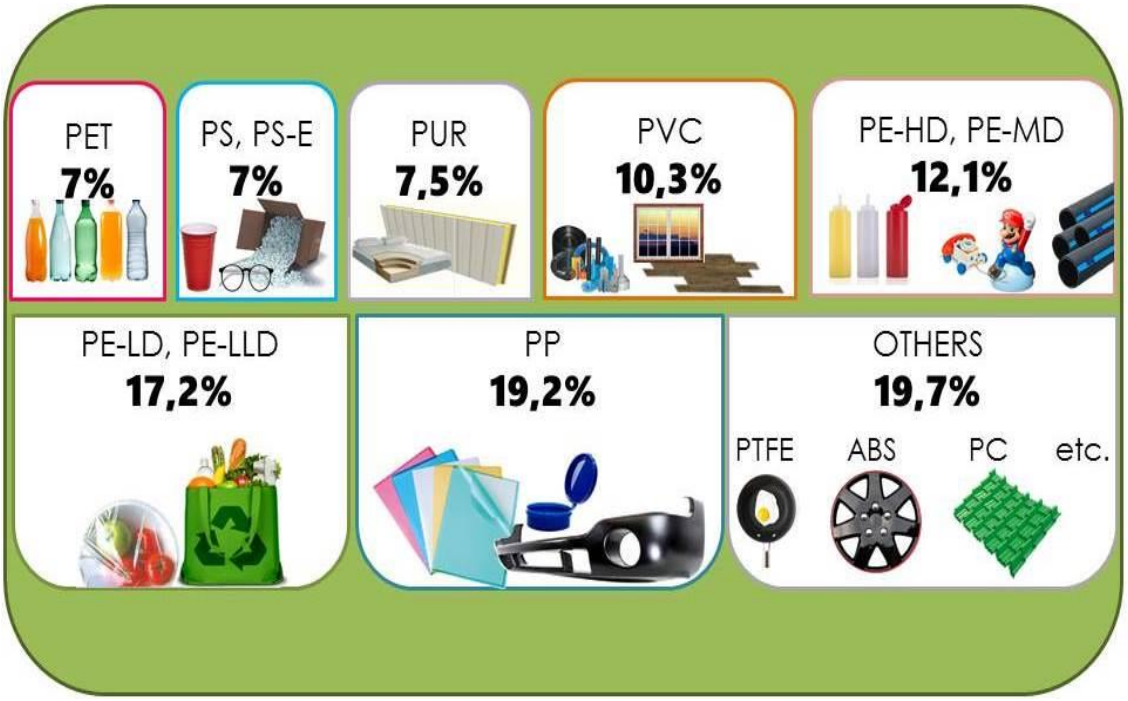

Figure 1.1: European plastics demand by polymer type 2014.
Source: Plastic Europe

Such success is mainly due to their low cost, their reproducibility, and their resistance to physical aging and biological attacks [Vert, 2005]. Petroleum plastic is in fact, versatile, lightweight, flexible, moisture resistant, biologically inert, strong, and relatively inexpensive.

In 2014, the global plastic consumption worldwide has been estimated at 311 million tons (Figure 1.2) and more than 99% of these polymeric materials was obtained from petrochemicals, but within a short time period almost half of them are disposed to the environment. In 2014 alone, about 8 million tonnes of plastic waste were landfilled in Europe (figure 1.3).

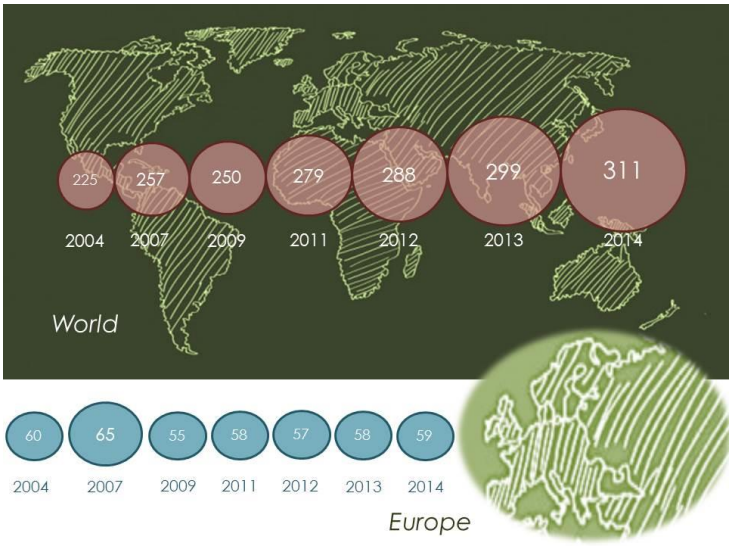

Figure 1.2: World and European plastics production in million tonnes.
Source: Plastic Europe

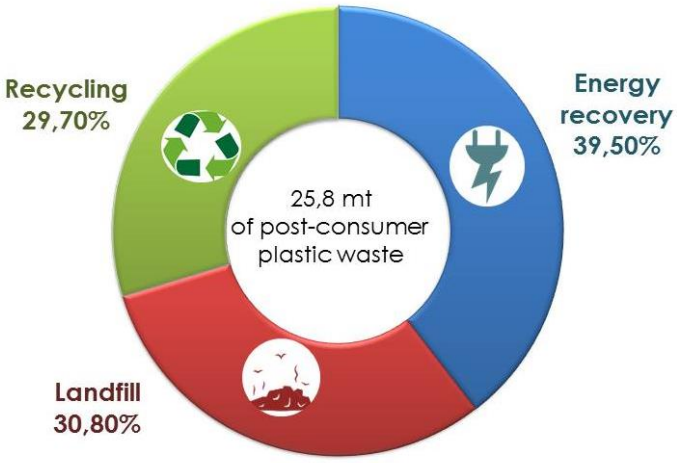

Figure 1.3: Treatment for post-consumer plastics waste in Europe.
Source: Plastic Europe

The main sources of plastic waste are typically represented by those fields where the highest plastic consumption occurs. Figure 1.4 shows the contribution of the different sectors to the plastic consumption in Europe in 2014. Packaging is the largest contributor to plastic demand (39.5%), well ahead of "Others" (22.7%), which includes furniture, medical waste, etc. The remaining sectors are automotive (8.6%), electrical and electronic equipment (EEE, 5.7%), building & construction (20.1%) and agriculture (3.4%) [Plastic Europe 2015].

The resistance of synthetic polymers to the degrading action of living systems is becoming highly problematic, particularly in those domains where they are used for a limited period of time before becoming wastes. It is the case in surgery, pharmacology, agriculture, and in the packaging as well. In these fields, time-resistant polymeric wastes are no longer acceptable.

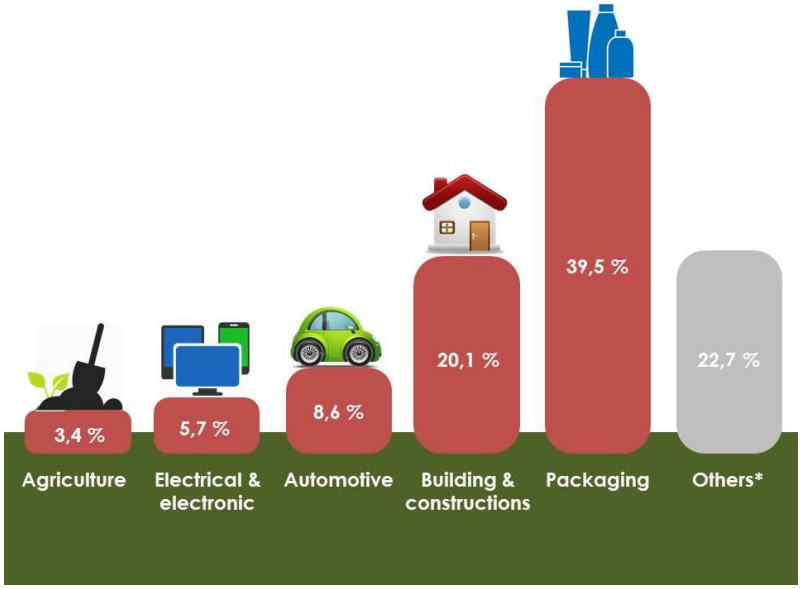

Figure 1.4: Distribution of European plastic demand by segment in 2014.
Source: Plastic Europe

Extensive littering, in combination with a continuous increase in consumption of low biodegradable plastic materials is causing, in fact, large-scale accumulation of plastics in our environment. Plastic pollution can unfavorably affect lands, waterways and oceans. Living organisms, particularly marine animals, can also be affected through entanglement, direct ingestion of plastic waste, or through exposure to chemicals within plastics that cause interruptions in biological functions. Immediate global action and measures to reduce littering are essential to protect our oceans, coastlines, fresh water ecosystems and terrestrial environment from plastic pollution. This actual dramatic scenario together with climate changes, the limited fossil fuel resources and their price fluctuations are the strong drivers for governments, companies and scientists to find alternatives to the petro-based polymers. In particular, for short term and single-use application there is the urgent need to strengthen the development of partially or fully

biobased plastic materials, that are completely degradable in the environment. For these reasons, bioplastics are experiencing a renaissance, with a global bioplastics production capacity, which is set to grow 350% by 2019 [www.european-bioplastics.org.] .

On this ground, there is a fast-growing industrial and academic interest for the production of a great variety of controlled life span materials; optimally designed polymers must be resistant during their use and must degrade at the end of their useful life [Lucas *et al*., 2008]. Biodegradable plastics can be broadly divided into different categories based on the origin of the raw materials (petroleum-based or renewable, Figure 1.5) and on the processes used in their manufacture.

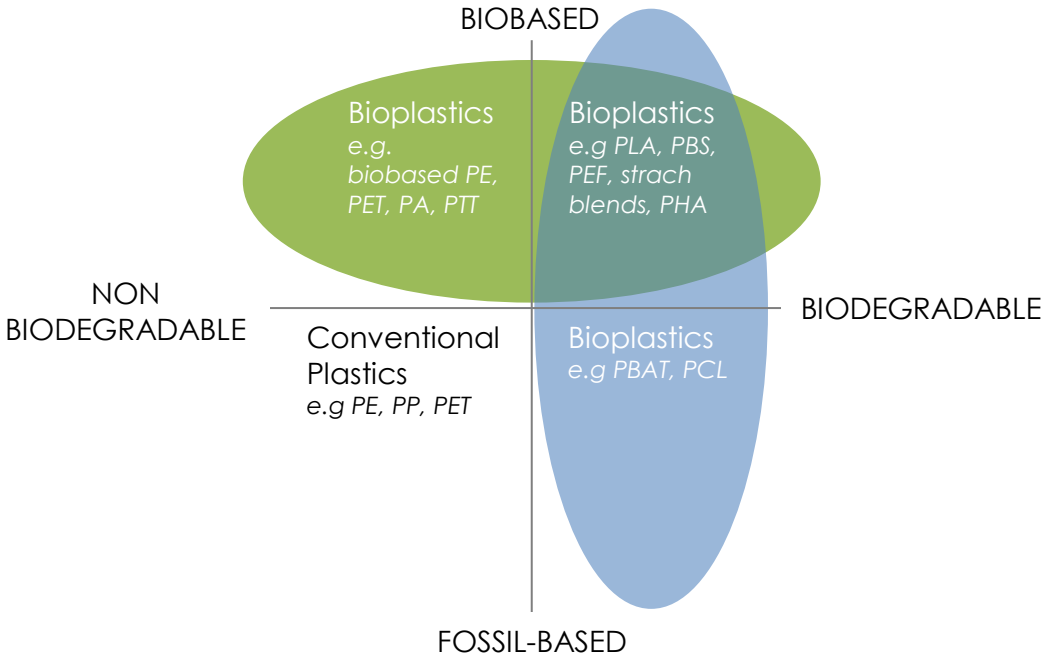

Figure 1.5: Bioplastic categories.
Source: European Bioplastics.

Four main approaches can be used for the design of biodegradable polymers. The easiest one is to add to cheap synthetic traditional polymers a biodegradable or photooxidizable component. A more expensive solution is to change the chemical structure by introducing hydrolysable or oxidizable groups in the main chain of nondegradable synthetic polymers. The third way is to replace traditional plastics with natural biopolymers, such as starch, chitosan, chitin or their derivatives, and last, but not least, is to tailor new hydrolysable structures such as polyesters, polyanhydrides, polyurethanes and polyamides [Luckachan & Pillai, 2011].

Scientific efforts toward the design, synthesis and production of sustainable or *green* polymers have expanded tremendously in the last two decades. These last, overcome several of the disadvantages of petrochemical-based polymers, i.e. (a) declining oiland gas resources; (b) increasing oil and gas prices during recent decades; (c) environmental concerns for their degradation or incineration and global warming; (d) uneconomical costs and cross-contaminations in their recycling; and € consumer toxicity risks about their monomers or oligomers migrating to edible materials.

Biodegradable polymers disposed in bioactive environments degrade by the enzymatic action of microorganisms such as bacteria, fungi, and algae. Their polymer chains may also be broken down through non-enzymatic processes, such as chemical hydrolysis. Biodegradation converts them to CO_2, CH_4, water, biomass and other natural substances. Biodegradable plastics are thus naturally recycled by biological processes. The use of biodegradable plastics is of interest specially if the products can provide economical and/or ecological benefits beyond simply "disappearing from view" by being buried in soil or incorporated into the organic waste stream. For example, if conventional plastic garbage bags for organic waste are not separated from their contents in a time-consuming process, then incineration remains the only possibility for disposing of the filled bags. This makes no sense from the energy standpoint, since organic waste is about two-thirds water. If, however, a biodegradable garbage bag is used, separation is not anymore necessary, and the organic waste together with the bag undergoes organic disposal. There are various possibilities in this last case: first of all, composting, secondly, anaerobic fermentation during which the biomass is converted into biogas (methane), providing a source of energy. In this way, biodegradable plastics represent not only a cost-effective disposal solution, but can also give an important contribution to efficient management of organic waste. Target markets for biodegradable plastics include packaging materials (trash bags, wrappings, loose-fill foam, food containers, film wrapping, laminated paper), hygiene products (diaper back sheets, cotton swabs), consumer goods (fast-food tableware, containers, egg cartons, razor handles, toys), and agricultural tools (mulch films, pots) [Gross & Kalra, 2002].

1.2 Aliphatic polyesters

Aliphatic polyesters are a class of polymers, which contain the ester functional groups along the main chain (Figure 1.6).

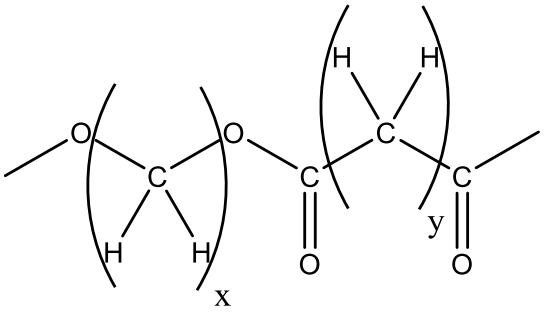

Figure 1.6 Chemical structure of aliphatic polyesters

Because of their favorable features of biodegradability and biocompatibility, they represent one of the most important classes of synthetic biodegradable polymers and are nowadays available commercially in a variety of types according to the final application: pharmaceutical, medical, and biomedical engineering, including drug delivery systems, artificial implants, and functional materials in tissue engineering.

The history of aliphatic polyesters begins in the late 1920s when the American chemist Wallace Carothers and his research group at DuPont began pioneering work concerning the synthesis of polyesters, starting from aliphatic diacids and aliphatic diols, in order to obtain appropriate polymers for the production of fibers. Their pioneering studies established a firm base for systematic studies of mechanisms of aliphatic polyester formation [Mark & Whitby, 1940]. In particular, these included proof of the high molecular weight nature of the polyesterification products, determination of the so called Carothers equation relating the conversion degree of functional groups with the number average degree of polymerization of the resulting linear polyester, and the importance of ring-chain equilibria in the polyester synthesis. Further studies by Flory (a former assistant of Carothers) at Cornell University (Flory, 1936, 1939, 1942, 1953) led to the development of the principles of kinetics of polyesterification and of polyester molar mass distribution. However, only some soft materials with low molecular weights and high susceptibility to hydrolytic degradation were produced. [Bikiaris cap 4; 2015]

Some properties of the aliphatic polyesters, such as hydrolytic instability, low melting temperatures, and solubility in common organic solvents were considered at that time as being detrimental from the practical application point of view, and this led to a strong delay in development of these polymers. More recently, since the environmental concerns together with the necessity of controlled life span materials are attracting growing interest, aliphatic polyesters are spotlighted because of their peculiar biodegradability; indeed their application as both biomedical and commodity degradable materials is being intensively studied.

Biodegradable aliphatic polyesters are found also in nature as some type of microorganisms can synthesize aliphatic polyesters such as polyhydroxyalkanoates (PHAs) in order to store "energy" .Polyhydroxybutyrate (PHB), poly(hydroxyl valerate) (PHV), and their copolymers are such examples and they can be enzymatically produced from certain bacteria by feeding them sugar or other type of nutrition (alcohols, alkanes, alkenes, etc.). Several companies are producing such polymers commercially by microbial fermentation. However, their cost is quite high owing to difficulties in extracting and purifying the polymer from microorganisms.

Today high-molecular-weight polyesters applicable for practical purposes, such as poly(butylene succinate) (PBS), poly(butylene succinate/adipate) (PBSA) and poly(lactic acid) (PLA), can be prepared and commercialized as biodegradable plastics [Okada, 2002].

Besides conventional condensation polymerization technique, some other methods have been developed to synthesize aliphatic polyesters, such as ring-opening polymerization of cyclic esters, solid-state polymerization, and the addition of chain extenders. Catalysts also play an important role in molecular weight increase during polymerization.

1.2.1 Synthesis

Aliphatic polyesters can be synthesized through polycondensation of di-functional monomers such as the self-condensation of hydroxy acids, di carboxylic acids with diols, diacid chlorides with diols or through ester interchange reaction of diesters and diols, or by ring-opening polymerization (ROP) of lactones and lactides [Nair & Laurencin, 2007]. The early studies on polycondensation reaction revealed the

formation, in addition to the desired high molar mass linear polymers, also of low molar mass cyclic side products. Some of these, for example ε-caprolactone, were then isolated, purified, and used by Carothers [Van Natta et al., 1934] as monomers in the ROP, eventually providing linear aliphatic polyesters. However, it was necessary to wait for another 40 years before the procedure of controlled polymerization of cyclic esters was established. Nowadays, commercially available biodegradable polyesters are produced by both these methods. Polycondensation can be applicable for a variety of combinations of diols and diacids, but it requires, in general, higher temperature, longer reaction time and removal of reaction byproducts to obtain high molecular weight polymers. In addition, polymers obtained do not have controlled chain lengths and polydispersity index (PDI) is usually around two. In contrast, ring-opening polymerization has a restriction on monomer type, but it can be carried out under milder conditions (lower temperatures and atmospheric pressure) to produce high molecular weight polymers in shorter time and does not produce any by-product, such as water or methanol.

Furthermore, recent progress in catalyst and initiators for living polymerization has enabled us to obtain polyesters of controlled chain lengths [Okada, 2002]. Recently, the use of enzymes as catalysts in organic syntheses has been deeply investigated. In general, enzymatic reactions can be carried out under moderate conditions. More important, enzymes can easily realize high regiospecificity as well as high stereospecificity, that conventional catalysts never achieve [Okada, 2002]. For polymer synthesis, in vitro enzyme-catalyzed polymerization has been developed as an effective method to synthesize environmentally benign polymers. Lipases catalyze the ring-opening polymerization of lactones (small to large rings) and cyclic diesters (lactides) to produce polyesters. The condensation polymerization of hydroxy acid and diacids with diols is also catalyzed by lipase. Lipase catalyzed polymerization is an eco-friendly technique for the preparation of useful polyesters by polycondensation as well as polyaddition (ring opening) reactions [Varma et al., 2005; Albertsson, 2008; Gross et al., 2010].

1.2.1.1 Polycondensation

Melt polycondensation is the most used technological method of aliphatic-aromatic polyesters production, such as poly(alkylene terephthalate)s, but also fully aliphatic polyesters, such as PBS or PBSA, are industrially synthesized at large scale by polycondensation too. Moreover, this synthetic route is used in the alternative method of polylactic acid (PLA) industrial production.

Polyesterification may be based on two different methods: homo-polycondensation of hydroxycarboxylic acid (Eqn. [1)]) or hetero-polycondensation of a diol with a dicarboxylic acid (Eqn. [2]):

$$n\ HO\text{-}R\text{-}COOH \leftrightarrow HO\text{-}(RCOO)n\text{-}H + (n\text{-}1)\ H_2O \quad \textbf{[1]}$$

$$n\ HO\text{-}R^1\text{-}OH + n\ HOOC\text{-}R^2\text{-}COOH \leftrightarrow HO\text{-}(R^1COOR^2COO)n\text{-}H + (2n\text{-}1)\ H_2O \quad \textbf{[2]}$$

where R, R^1, and R^2 denote alkylene groups. Polycondensation is a reversible process, and in order to prepare a high molar mass polymer the condensation equilibrium constant (K_C) has to be high enough. As reported by Carothers [Carothers 1936], generally in the polycondensation of alcohols with carboxylic acids, the equilibrium constant is not sufficiently high (typically $K_C \leq 10$), the condensation side products (usually water or methanol) must be removed from the reaction mixture in order to obtain a reasonably high degree of polymerization (DP_n). This number is related to K_C by a simple equation:

$$DP_n = K_C^{0.5} + 1 \quad \textbf{[3]}$$

Since generally $K_C \approx 10$ for a majority of condensations of simple aliphatic alcohols with carboxylic acids, the number average degree of polymerization $DP_n \approx 4$ would result in the equilibrium polymerization. On the other hand:

$$DP_n = 1/(1 - p) \quad \textbf{[4]}$$

where p is a degree of conversion of the reactive groups [Carothers 1936]. This means that for $K_C = 10$, only 76% of hydroxyl and carboxylic group would react until an equilibrium is reached. For majority of polyesters, $DP_n \geq 100$ is needed in order to obtain the required physical properties; this corresponds to degree of conversion not less than 0.99 and in turn would require $K_C \geq 10^4$. K_C of this level are observed when acid

chlorides (Schotten-Baumann reaction), acid anhydrides or activated carboxylic acids are used.

Shifting the equilibrium to the side of a high molar mass polyester is realized, as mentioned above, by removing from the reaction mixture the low molar mass byproduct of esterification. Eqn. [5], which is derived from Eqn. [3] by assuming $K_C >> 1$, provides a dependence of the degree of polymerization on the extent of removal of the byproduct (q):

$$DP_n = (K_C / q) \cdot 0.5 \quad \textbf{[5]}$$

where $q = N_e/N_0$, i.e., the ratio of the concentration of the byproduct at a given equilibrium to its hypothetical concentration resulting from reactive groups conversion degree related to the required DP_n. For example, in order to prepare polyester having $DP_n = 10^2$, it is necessary to keep K_C/q above 10^4. If $K_C = 10$, then q should be below 10^{-3}. This means that only 0.1% of the byproduct of its "normal" equilibrium concentration is allowed to be left in the reacting mixture. Such a situation creates one of the practical limitations in the syntheses of various polyesters, including PLA, directly by polycondensation. In addition, high viscosity of the system at higher degrees of conversion hampers removal of the low molar mass byproduct, such as water.

Another important factor is related to the stoichiometry of the substrates. Dependence of the number average degree of polymerization of the polyester formed in hetero-polycondensation on the stoichiometric imbalance parameter r is given by:

$$DP_n = (1 + r) / (1 + r - 2p) \quad \textbf{[6]}$$

where $r = N_{OH}/N_{COOH}$ for $N_{OH} < N_{COOH}$ or N_{COOH}/N_{OH} for $N_{OH} > N_{COOH}$ (N_{OH} and N_{COOH} stand for the concentrations of hydroxyl and carboxylic groups, respectively). Thus, for example at $p = 0.99$, and $DP_n = 100$ for the exactly equimolar reacting mixture ($r = 1$), it is sufficient to introduce only 1.0 mol% of imbalance ($r = 0.99$) to reduce DP_n to the value of 67. Even if in the feed the 1:1 stoichiometry is secured, one of the components may be partially lost during the polycondensation process, either because of volatilization, since high reaction temperatures are often used, or reactant losses by side reactions. Therefore, even in the case of homo-polycondensation the internally supplied equimolar stoichiometry may be distorted. In order to minimize this type of difficulty, modification of polycondensation was introduced based on transesterification. At least in one known instance transesterification is at the basis of

the large-scale industrial process, i.e. the twostep synthesis of poly(ethylene terephthalate).

The rate of polycondensation only very seldom agrees with simple kinetic expressions throughout the entire polycondensation process. Changes in the reaction mixture properties, such as viscosity or dielectric constant, influence the course of the reaction, even if the most fundamental assumption of equal reactivities of functional groups, independently on the material chain length is obeyed. It is mostly obeyed indeed, because even if at high viscosities the "diffusion in" is slowed down, it is believed to be compensated by equally slowing down of the "diffusion out" (Rabinovitch, 1937).

Polycondensation may be accompanied by the appearance of a certain fraction of macrocyclic products. In polyesterification, two reactions giving eventually cyclic (macro)molecules must be distinguished: back-biting and end-to-end condensation.

However for the processes conducted in bulk and under reversibility governing conditions.cyclization can be considered as a side reaction of a minor importance because critical concentrations of macrocycles (in terms of repeating units) are well below 1 g/l [Duda et al; 2002].

1.2.1.2 Ring opening polymerization

Although polycondensation in general is still the most widely used method for the synthesis of polyester, ring-opening polymerization (ROP) of cyclic esters is the preferred preparation route to obtain well-defined high molar mass aliphatic polyesters. High molecular weight polyesters can be easily prepared under mild conditions from lactones and lactides of different ring-size, substituted or not by functional groups [Jérôme & Lecomte, 2008].

Upon the choice of polymerization conditions (temperature, solvent, initiator, and catalyst), ROP can be a "living" process, i.e, without any irreversible transfer and termination reactions, affording a good control over the molecular parameters of polymeric chains (predetermination of the molecular weight by the monomer-to-initiator molar ratio and a narrow molecular weight distribution) and the topology of the as-synthesized polymer [Albertsson and Varma, 2003].

Alternate architectural structures (e.g., linear random or block copolyesters) have been investigated for improving the mechanical properties, hydrophilicity and degradability of these polyesters.

The polymerization of lactones is generally carried out in bulk or in solution (THF, dioxane, toluene, etc.), emulsion, or dispersion. The temperature of bulk polymerization is generally in the range of 100-170 °C, whereas in solution polymerization, low temperatures have been used (0-25 °C) to minimize side reactions (inter- and intramolecular transesterfication) [Albertsson and Varma, 2003]. Few lactones polymerize spontaneously on standing or on heating. Most do so in the presence of catalysts or initiators.

Many organometallic compounds, such as oxides, carboxylates, and alkoxides are effective initiators for the controlled synthesis of polyesters using ROP of lactones. Generally speaking, ionic initiators are much reactive and, in case of polyesters, are responsible for detrimental inter- and intra-molecular transesterification reactions lowering the molecular weight and broadening the molecular weight distribution of the polymer. Many organometallic derivatives of metals, such as Al, Sn, Nd, Y, Yb, Sm, La, Fe, Zn, Zr, Ca, Ti and Mg, are imparting control to the polymerization in contrast to their anionic counterpart. In the more favorable cases, the ring-opening polymerization of lactones and lactides is a living/controlled process that leads to polyesters of narrow molecular weight distribution with a molecular weight predetermined by the monomer-to-initiator molar ratio.

The ROP proceeds mainly via two major polymerization mechanisms depending on the used organometallics. Some of them act as catalysts, and activate the monomer by complexation with the carbonyl group. Polymerization is then initiated by any nucleophile, e.g., water or alcohol, present in the polymerization medium as impurities or as compound added on purpose. In the second mechanism, the organometallic plays the role of initiator and the polymerization proceeds through an ‘insertion–coordination’ mechanism. Metal alkoxides are typical initiators, which first coordinates the carbonyl of the monomer, followed by the cleavage of the acyl–oxygen bond of the monomer and simultaneous insertion into the metal alkoxide bond. An example of ring opening polymerization of lactide is reported on Figure 1.7.

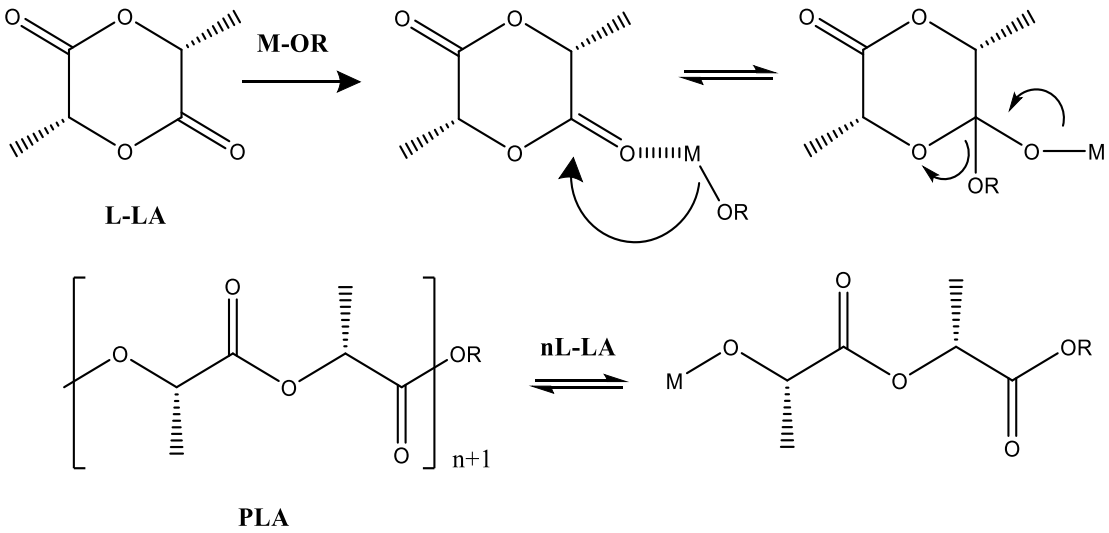

Figure 1.7: ROP of L-lactide.

Depending on the nature of catalysts and initiators, ROP can proceed through different mechanisms: cationic, anionic (nucleophilic), or coordination type [Endo 2009]. For industrial implementation, $Sn(Oct)_2$ is preferentially used due to the FDA approval (US Food and Drug Administration); it has good efficiency toward the synthesis of high molecular weights within short reaction times via a "coordination-insertion" mechanism [Kowalski et al., 2008]. In the most likely proposed polymerization mechanism, $Sn(Oct)_2$ is converted into tin alkoxide, the actual initiator, by reaction with alcohols or other protic impurities.

$$Sn(Oct)2 + ROH \rightarrow Oct–Sn–OR + OctH \quad [7]$$

$$Oct–Sn–OR + ROH \rightarrow Sn(OR)2 + OctH \quad [8]$$

As a consequence, the polymerization involves a coordination–insertion mechanism.

Again, the deliberate addition of a predetermined amount of alcohol to the polymerization medium is an effective way to control the molecular weight by the monomer-to-alcohol molar ratio. Tin octanoate is also efficient in copolymerization of various lactones. Playing on the composition of such copolymers allows tailoring their properties.

High volumes of PLA are produced via ROP under the name Natureworks™ by the joint venture between Dow and Cargill in a plant built in North America with a capacity of 0.14 million tonnes/year, mainly for commodity market [Jérôme and Lecomte, 2008].

1.2.2 Blending

The practice of blending polymers is as old as the polymer industry itself with early examples involving natural rubber.

In the first half of the twentieth century, the greatest progress in the industry regarded the development of a wide range of different polymers. In the 70s, on the contrary, most of the economically convenient monomers had already been exploited, and consequently polymer industry moved towards two additional directions over the last forty. On one hand, new homopolymers and copolymers based on monomers used much earlier were manufactured. On the other hand, polymer blending underwent a remarkable development.

A polymer blend is a mixture of two or more polymers in order to create a new material with different physical properties.

While most monomers cannot be easily copolymerized to gain intermediate properties, their polymers could be economically melt blended.

Polymer blending has attracted much attention as an easy and cost-effective method of developing polymeric materials that have versatility for commercial applications. In other words, the properties of the blends can be manipulated according to their end use by correct selection of the component polymers [Paul, 1989].

Generally, polymer blends are classified into either homogeneous (miscible on a molecular level) or heterogeneous (immiscible) blends. Miscible blends involve thermodynamic solubility and are characterized by the presence of one phase and a single glass transition temperature. Their properties can often be predicted being intermediate between those of the individual components and depending on blend composition. On the other hand, immiscible blends are phase separated, exhibiting the glass transition temperatures and/or the melting temperatures of each blend component. Their overall performance depends on the properties of the individual components, but significantly also on the morphology of the blends and the interfacial properties between the blend phases [Jiang et al.1991; George et al., 2013]. Performance is not easy predictable. Only few polymer pairs form miscible blends, while most blends are immiscible and have poor physical properties compared to their components. This problem is rooted in the lack of favorable interactions between blend phases.

This leads to a large interfacial tension between the components in the blend melt, which renders difficult to deform the dispersed phase of a blend during mixing and to resist phase coalescence during subsequent processing. It also leads to poor interfacial adhesion in the solid state, which frequently causes premature mechanical failure, depending on the nature of the applied stress. The key to make successful blends of this kind is the use of compatibilizers to control morphology. Compatibilization is the result of a process or technique for improving blend performance by making blend components less immiscible. Compatabilizers are generally molecules characterized by hydrophobic and hydrophilic parts that can be aligned along the interfaces between the two polymer phases, causing the interfacial tension to be reduced and the compatibility of the polymer blends to be increased. Compatibility results in a reduction of the dispersed particle size, an enhanced phase stability, and increased mechanical properties [Chen and White, 1993].

Compatible blends constitute the majority of commercially important blends. The compatibility of these blends may vary widely from one system to another. There are several methods of compatibilizing immiscible blends, such as: compatibilization by the introduction of non-reactive graft or block copolymers, nonbonding specific interactions, low molecular weight coupling agents and reactive polymers. Suitable block and graft copolymers can be used as compatibilizer for polymer blends. A suitable block or graft copolymer contains a segment miscible with one blend component and another segment with the other blend component. The copolymer segments are not necessarily identical with the respective blend components. Significant amounts of the copolymer are expected to locate at the interface between immiscible blend phases, reducing the interfacial tension between blend components, reducing the resistance to minor phase breakup during melt mixing thus reducing the size of the dispersed phase, and stabilizing the dispersion against coalescence. Non-bonding specific interactions like hydrogen bonding, ion-dipole, dipole-dipole, donor-acceptor, and π-electron interactions are useful for enhancing the compatibility of polymer blends. Generally, however, these specific interactions are weak and high concentrations, e.g. one interacting group per repeating unit, are often required for effective compatibilization. Addition of low molecular weight reactive compound may serve the purpose of compatibilization of polymer blends through copolymer formation.

Graft or block polymers acting as compatibilizers for polymer blends can be formed in situ through covalent or ionic bonding during the melt blending of suitably functionalized polymers. In situ reactive compatibilization has already been implemented in a number of commercial products and, in many instances, appears to be the method of choice for compatibilization.

A required reactive group can be incorporated into a polymer by:

a. incorporation into the backbone, side chain, and at chain ends as a natural result of polymerization;

b. copolymerization of monomers contained the desired reactive groups;

c. chemical modification of a preformed polymer through a variety of chemical reactions.

1.2.3 Copolymerization

Copolymers are macromolecules derived from two or more different species of monomer. The behavior of monomers in copolymerization reactions is especially useful for studying the effect of chemical structure on reactivity. Copolymerization is also very important from the technological viewpoint. It greatly increases the ability of the polymer scientist to tailor-make a polymer product with specifically desired properties. Polymerization of a single monomer is relatively limited as to the number of different possible products. Copolymerization allows the synthesis of an almost unlimited number of different products by variations in the nature and relative amounts of the two monomer units in the copolymer product. Most commercial copolymers are designed to present synergistic improvements with respect to their parent homopolymers, including better processability, higher mechanical properties and better chemical resistance. In fact, the final properties of the copolymers can be favourably modified, depending on the kind, relative amount and distribution of the comonomeric units along the polymeric chain.

To better understand the structure of copolymers, different parameters have to be taken into consideration, calculating them on different kinetic and statistical models. These last permit to describe the comonomeric units linking process and their distribution along the polymer chain. Copolymers classification can be made on the basis of the

arrangement along the polymeric chain of the monomeric units (represented to simplify by the symbols ■ and ●). In particular, we can have:

- alternating copolymers with regular alternating of ■ and ● units:

  ■-●-■-●-■-●-■-●-■-●-■-●

- periodic copolymers with ■ and ● units arranged in a repeating sequence:

  (■-●-■-●-●-■-■-■-■-●-●-●)

- statistical or random copolymers in which the sequence distribution of monomeric units follows Bernoullian statistics:

  ■-●-■-■-●-●-■-●-■-■-●-■

- block copolymers with two or more homopolymer subunits linked by covalent bonds. Block copolymers with two or three distinct blocks are called diblock copolymers and triblock copolymers, respectively:

  ■-■-■-●-●-●-■-■-■-●-●-●

Copolymers may also be described in terms of the existence of branches in the structure. Linear copolymers consist of a single main chain whereas branched copolymers consist of a single main chain with one or more polymeric side chains. Graft copolymers are a special type of branched copolymers in which the side chains are structurally distinct from the main chain: usually main chain and side chains are composed of two distinct homopolymers. However, the individual chains of a graft copolymer may be homopolymers or copolymers; moreover, different copolymer sequencing is sufficient to define a structural difference, thus an ■-● diblock copolymer with ■-● alternating copolymer side chains is properly called a graft copolymer. Other special types of branched copolymers include star copolymers, brush copolymers, and comb copolymers.

In the following, the present work will focus on random and block copolymers, i.e. the two copolymer types synthesized during the experimental research.

1.2.3.1 Random copolymers.

In amorphous random copolymers, Tg is usually a monotonic function of composition and the most common relationship used to predict Tg as a function of comonomer content is the Fox equation:

$$1/T_g = \omega_A/T_{g,A} + \omega_B/T_{g,B} \quad \textbf{[9]}$$

where $T_{g,A}$ and $T_{g,B}$ are the glass transition temperatures of the pure homopolymers and ω_A and ω_B the respective weight fractions.

A random copolymer can potentially crystallize in two extreme ways. It can form a two phase system in which the crystalline phase is composed entirely of A units and is in equilibrium with a mixed amorphous phase of A units and non crystallizable comonomer B units (comonomer exclusion). Alternatively, the copolymer may form a two phase system in which the crystalline phase is a solid solution of A and B units; the comonomer B units produce defects in the crystalline A lattice and both phases have the same composition (comonomer inclusion). Real copolymer crystals may exhibit a morphology intermediate to the two extremes [Sanchez and Eby, 1973].

The case of comonomer exclusion in thermodynamic equilibrium was first described by Flory [Flory, 1947], who calculated the upper bound of the copolymer melting temperature, i.e., the melting temperature of crystals built up from "infinitely long" homopolymer sequences of units A in the copolymer. Starting with the general equation:

$$\Delta G = \Delta G^\circ + RT \ln(\alpha) \quad \textbf{[10]}$$

where α is the activity of the crystallizing copolymer, Flory found the melting temperature equation:

$$1/T_m^\circ - 1/(T_m(X_B)) = (R / H_m^\circ) \ln(1-X_B) \quad \textbf{[11]}$$

where X_B is the concentration of B units in the polymer and $\ln(1-X_B)$ equals the collective activities of A sequences in the limit of the upper bound of the melting temperature. Tm° and Hm° denote the homopolymer equilibrium melting temperature and heat of fusion and R is the gas constant.

The drawback of this model is Flory's assumption that these homopolymer sequences of infinite length build up unfolded crystals of the length of A sequences, an assumption that is unrealistic for polymers.

Attempts to overcome this drawback treat copolymer crystals as a "pseudo-eutectic" system, where the homopolymer sequences of length ξ may only be included into crystals of lamellar thickness corresponding to that length. The activity of a sequence of length ξ is then related to the mean sequence length $\langle\xi\rangle$ as follows:

$$\Delta G = \Delta G^\circ + (RT / \xi) \ln(X_{A\xi} / f_{A\xi}) \quad \textbf{[12]}$$

$X_{A\xi}$ is the concentration and $f_{A\xi}$ is the activity coefficient for crystallizing sequences of length ξ. Baur (Baur, 1966) used the activity coefficient:

$$f_{A\xi} = (\xi / \langle\xi\rangle) e^{-[(\xi / \langle\xi\rangle) - 1]} \quad \textbf{[13]}$$

The melting point of infinitely long homopolymer sequences is then given by:

$$1/ T_m^\circ - 1/ (Tm(X_B)) = (R / H_m^\circ)[\ln(1 - X_B) - \langle\xi\rangle^{-1}] \quad \textbf{[14]}$$

where $\langle\xi\rangle = [2X_B(1-X_B)]^{-1}$ is the average length of homopolymer sequences in the melt. This model, while incorporating finite crystal thickness and concomitant depression in the melting point, still neglects the fact that the homopolymer sequences are invariably fixed in chains due to bond connectivity; the eutectic equilibrium, which requires total separation into the "components" (the homopolymer sequences of same length ξ) is unrealistic. However, it was shown by several investigations [Baur, 1966; Helfland & Lauritzen, 1973; Sanchez & Eby, 1975; Windle et al., 1985; Allegra et al., 1992; Yoshie et al., 1994; Wendling & Suter, 1998] that the Baur model fits experimental data much better than the Flory equation. Inspection of experimental data shows readily that comonomer exclusion alone cannot account for the observed melting point depression in many cases; hence, comonomer inclusion is to be considered in the melting point prediction. The case of comonomers B that are included into the crystal of A where they act as defects was considered by Helfand and Lauritzen [Helfland & Lauritzen, 1973] and later in a more general way by Sanchez and Eby [Sanchez & Eby, 1975]. In this model, the melting temperature is then given by:

$$1/(T_m(X_B)) - 1/T_m^\circ = (R/Hm^\circ)\{(\varepsilon X_{CB})/(RT_m) + (1-X_{CB}) \ln[(1 - X_{CB})/(1-X_B)] + X_{CB}\ln(X_{CB}/X_B)\} \quad \textbf{[15]}$$

This equation (Eqn. [15]) holds for any concentration X_{CB}, including two limits: when $X_{CB} = X_B$, uniform inclusion takes place and Eqn. [15] reduces to:

$$T_m(X_B) = T_m^\circ [1 - \varepsilon X_B / H_m^\circ] \quad \textbf{[16]}$$

For the equilibrium state, the concentration of B units in the cocrystal is given by:

$$X_{CB}eq = (X_B e^{-\varepsilon / RT}) / (1 - X_B + X_B e^{-\varepsilon / RT}) \quad \textbf{[17]}$$

and the equilibrium melting point is derived from Eqn. [15] as:

$$1/T_m° - 1/(T_m(X_B)) = (R/H_m°)\ln(1 - X_B + X_B e^{-\varepsilon / RT}) \textbf{ [18]}$$

This equation is similar to the Flory equation (Eqn. [11]) but includes the equilibrium fraction $XBe^{-\varepsilon / RT}$ of repeat units B that are able to crystallize. It is obvious that Eqn. [18] reduces to the Flory model for the case of high defect free energies, and one might not be surprised that it also overestimates the melting temperatures for $\varepsilon \gg 0$ or, in the general application of this model, underestimates the defect free energy. The temperatures derived by Eqn. [18] can be taken as an upper bound of the melting temperature. The behavior at $\varepsilon \gg 0$ is the principal shortcoming of the Sanchez-Eby model: when ε is too high to allow cocrystallization, Eqn. [18] reduces to the Flory model (Eqn. [11]), but it should preferentially converge to the Baur model, (Eqn. [14]).

The model recently proposed by Wendling and Suter [Wendling & Suter, 1998], equals Eqn. [18] and Eqn. [12] in the limits of high and low defect free energies.

Accordingly to this method, the melting temperature is given by:

$$1/(T_m(X_B)) - 1/T_m° = (R/H_m°)\{(\varepsilon X_{CB})/(RT_m) + (1 - X_{CB})\ln[(1 - X_{CB}) / (1 - X_B)] + X_{CB}\ln(X_{CB}/X_B) + \langle\xi\rangle^{-1}\} \textbf{ [19]}$$

Assuming equilibrium comonomer inclusion, Eqn. [18], Eqn. [19] reduces to:

$$1/T_m° - 1/(T_m(X_B)) = (R/H_m°)\{\ln(1 - X_B + X_B e^{-\varepsilon / RT}) - \langle\xi\rangle^{-1}\} \textbf{ [20]}$$

$$\text{where: } \langle\xi\rangle^{-1} = 2(X_B - X_B e^{-\varepsilon / RT})((1 - X_B + X_B e^{-\varepsilon / RT}) \textbf{ [21]}$$

Both the inclusion and exclusion models predict a depression of the crystalline melting point. For the inclusion model the melting point depression is caused by a defective heat of fusion that accompanies the crystallization, whereas for the exclusion model, the depression is caused by the fact that preferential ordering of the copolymer chains is required for crystallization which raises the entropy of fusion. However, careful crystallinity studies combined with calorimetric determinations of heats of fusion can ascertain which model is more appropriate for a given random copolymer system.

1.2.3.2 Block copolymers

The phase behaviour of block copolymers depends on two competitive self-organizing mechanisms: microphase separation and crystallization. In general, diblock copolymer are formed by an amorphous block, the other one being crystalline. A distinct situation arises in block copolymers where both blocks are able to crystallize. As it is expected, the crystallization behaviour of crystalline-crystalline block copolymers is more complicated; for instance, when the copolymers are quenched from a microphase-

separated melt to a temperature below the melting temperatures of the corresponding blocks, various situations can be observed. When the melting temperatures of both blocks are close enough, a simultaneous crystallization of both blocks occurs by quenching. On the other hand, when the melting temperature of one block is far from the other, one block crystallizes in advance and produces a specific morphology, which can or cannot be modified upon crystallization of the other block. Such modification depends, among other controlling parameters, on segregation strength, crystallization temperature and molecular weight of the block components [Muller *et al.*, 2007].

There are different ways to synthesize a block polymer. In the present work, the research was focused on an innovative synthetic route carried out through a chain extension reaction of two hydroxyl-terminated low molecular weight subunits (homo- or copolymers).

Chain extension is a well-established synthetic strategy, which can help to obtain high molecular weight polymers. In particular, the use of diisocyanates has been deeply investigated [Shirahama *et al.*, 2001; Cohn *et al.*, 2006; Chen *et al.*, 2011]. By reacting diisocyanates with hydroxyl-terminated polyesters, high molecular weight poly(ester urethane)s (PEU) can be easily achieved. Moreover, by selecting the number, chemical structure and relative amount of the hydroxyl-terminated polyesters, it is possible to synthesize a wide plethora of new materials with tailored and more functional properties, according to the intended final use.

A polymer like poly(butylene succinate) could be chosen as semicrystalline segment, as it displays $T_g < T_{room} < T_m$. On the other hand, the second subunit should be characterized by a $T_g > T_{room}$ to confer rigidity to the new material or a T_g well below T_{room} and T_m close to T_{room} to increase its flexibility. Finally, a small amount of diisocyanate (in general below 5 wt%) is used with the purpose of coupling together the OH-terminated polyesters and of achieving higher molecular weights. According to these motivations, by changing the properties of hydroxyl-terminated polyesters is possible obtain final high weight copolymers with modulated properties depending on the application field.

1.2.4 Physical properties

The physical properties of aliphatic polyesters depend on several factors, such as the chemical structure of the repeating units, flexibility of the chain, presence of polar groups, molecular mass, degree of branching, crystallinity, orientation, etc. Short chain branches reduce the degree of crystallinity of polymers while long chain branches lower the melt viscosity and impart elongational viscosity with tension-stiffening behavior. Aliphatic polyesters showing x,y $\geq$ 2 (Figure 1.6) are characterized by a high crystallinity degree, T_m usually in the range 40-90°C (in most cases it is well below 100°C) and T_g between –70 and –30°C. In general, the lower the ratio between methylene and carboxylic groups in the polymer chain, the higher the melting temperature: e.g. poly(butylene adipate) T_m is equal to 47°C, while poly(butylene succinate) shows T_m = 116°C [Soccio, Lotti et al., 2012; Gigli, Fabbri et al.,2016]. As far as mechanical properties are concerned, polyesters containing ether-linkages display enhanced flexibility, e.g. poly(1,4-dioxan-2-one) properties are similar to those of the human tissues [Albertsson & Varma, 2002, Gigli, Lotti et al., 2012; Gigli, Lotti et al., 2013 (a); Gigli, Negroni et al., 2013 (b)] . The properties of these materials can further be tailored by blending and copolymerization or by changing the macromolecular architecture (e.g. hyper-branched polymers, starshaped or dendrimers, etc.).

1.2.5 Degradation

Polymer degradation and erosion play a crucial role for all plastics. The distinction between degradable and non-degradable polymers is, therefore, not clean-cut and is in fact arbitrary, as all polymers can in principle degrade. What makes the difference between degradable and non-degradable polymers is the relation between the time-scale of degradation and the time-scale of the application. We usually assign the attribute “degradable” to materials, which degrade during their application, or immediately after it. Non-degradable polymers are those that require a substantially longer time to degrade than the duration of their application [Gopferich, 1996]. Polymer degradation takes place mostly through scission of the main chains or side-chains of polymer molecules, induced by thermal or mechanical activation, oxidation, photolysis, radiolysis, or hydrolysis. Some polymers undergo degradation in biological environments when living

cells or microorganisms are present. Such environments include soils, seas, rivers, and lakes on the earth as well as the human body. Such polymers are called biodegradable polymers. Concerning the solid environments under which the biodegradable polymers biodegrade, the two main categories considered in the technical literature, in the norms and in the market are: (a) the materials that biodegrade under composting conditions (compostable materials; the composting conditions may vary) and (b) the materials which biodegrade in soil (biodegradable in soil materials).

Only the polymers able to degrade in these biological environments through enzymatic hydrolysis are considered biodegradable ones, not those subjected to thermal oxidation, photolysis, or radiolysis. In a strict sense, a polymer that loses its weight over time in a living body should be defined as absorbable, resorbable or bioabsorbable, regardless of its degradation occurs by chemical or enzymatic hydrolysis; in conclusion, the term biodegradable should be used only for those polymers developed according to the protection of earth environments from plastic wastes [Ikada, 2000].

The processes involved in the biodegradation of a polymer, and specifically in the case of polyesters, are complicated. As mentioned above, they can be divided into chemical and enzymatic hydrolysis, in both cases being water involved in the process.

Which degradation mechanism dominates depends on both the structure of the polyester and the environment.

Aliphatic polyesters have ester bonds, which, due to their mobility, can be cleaved by enzymes such as lipases, with the generated chain fragments finally dissolving in the surrounding water phase. The degradation proceeds either at the surface (homogeneous) or within the bulk (heterogeneous) and is controlled by a wide variety of compositional and property variables, for example, matrix morphology, chain orientation, chemical strucutre, stereochemical structure, sequence distribution, molecular weight and distribution, presence of residual monomers, oligomers and other low-molecular-weight products, size and shape of the specimen, and degradation environment, (humidity %, oxygen, microorganisms, enzymes, pH, and temperature) [Hakkarainen, 2002]. Hydrophilicity and crystallinity degree of the polymer play an important role in determining its degradability, affecting significantly polymer surface accessibility. The crystalline regions a polymer limit the accessibility of water and confined the

degradation in the amorphous phase, although highly crystalline starch and bacterial polyester have been reported to hydrolyse rapidly [Van der Zee 1997].

1.2.5.1 Chemical hydrolysis

To be degraded by water the polymer must contain hydrolysable covalent bonds, such as esters, orthoesters, ethers, anhydrides, amides, carbamides (ureas), ester amides (urethanes) and so forth [Lucas et al., 2008].

The type of bonds in the polymer backbone determine the rate of hydrolysis: anhydride and orthoester bonds are the most reactive ones, followed by esters and amides. In the same way, hydrophobic polymers cannot take up large quantities of water and therefore are characterized by low degradation rate. Hydrophilic polymers, in contrast, take up large quantities of water and consequently degrade quite fast [Gopferich, 1996]. The uptake of water is especially important in drug delivery systems. Hydrogels, for example, may undergo substantial swelling, which is a key parameter for controlling the release of drugs, and may be more important than polymer degradation.

There are two principal pathways by which polymer bonds can be cleaved: i) bulk erosion, if the diffusion of water into the polymer is faster than the degradation of polymer bonds, and ii) degradation confined to the polymer surface, when the degradation of the polymer bonds is faster than the diffusion of water [Von Burkersroda *et al.*, 2002]. For aliphatic polyesters the hydrolytic degradation occurs in bulk: the intrusion of water triggers the chemical polymer degradation, leading to the creation of oligomers and monomers [Gopferich, 1996]. Several phenomena are involved: water absorption, ester bond cleavage, neutralization of carboxyl end groups at the surface, autocatalysis inside, diffusion and solubilisation of oligomers [Li, 2006]. The reaction is:

$$RCOOR^1 + H_2O \leftrightarrow RCOOH + R^1OH \quad \textbf{[22]}$$

The chemical hydrolysis reaction is catalyzed by acid or basic compounds. The acid byproduct, RCOOH, is able to accelerate the hydrolysis by autocatalysis. From a macroscopic point of view, this hydrolysis occurs in two steps: firstly, a random cleavage of polymer chain backbone with a concomitant substantial decrease in molecular weight occurs, leading to a decrease in mechanical properties such as tensile strength, ultimate elongation and impact strength, while weight losses are negligible

[Mochizuki and Hirami, 1997]. In the intermediate to the last stage of degradation, the molecular fragments are solubilized and weight losses are measured [Grima *et al.*, 2000].

1.2.5.2 Enzymatic hydrolysis

The biological hydrolysis reaction, differently to the chemical hydrolysis, is catalyzed by enzymes. A large number of different enzymes are involved, depending of the type of bond to be hydrolyzed. In general, they are called depolymerases. Glycosidic bonds, peptide bonds, and ester bonds are affected by this kind of reaction. It is well known that the ester bond of aliphatic polyesters is cleaved by lipases and PHA-depolymerases [Suyama *et al.*, 1998]. The reaction products of an enzymatic hydrolysis or a chemical hydrolysis are the same.

In a biological system when enzyme fits the stereochemical conformation of the substrate molecule the biodegradation is effective. This action is described as analogous to a key fitting into a lock (Figure 1.8), and each enzyme performs one chemical function.

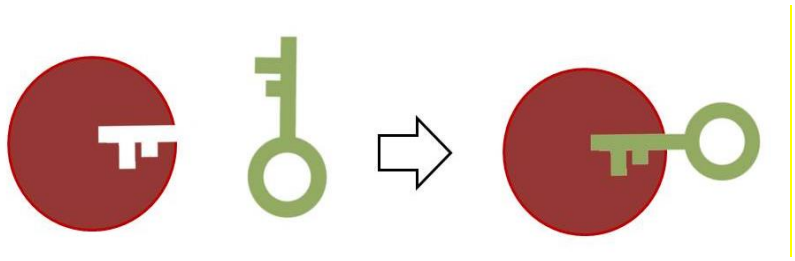

Figure 1.8 Key-lock mechanism of enzyme-substrate fitting.

Enzymatic degradation proceeds only on the surface of the solid substrate accompanying both the surface erosion and weight loss, because the enzyme cannot penetrate polymer matrix. Thus, with an enzymatic hydrolysis, the polymer weight decreases and molar mass and molecular weight distribution barely changes, differently from chemical hydrolysis [Grima *et al.*, 2000]. The low molecular weight degradation products are removed from the substrate by solubilization in the surrounding aqueous medium.

Homogeneous enzymatic reactions obey to Michaelis–Menten type-equation. In the case of heterogeneous system a completely different mechanism takes place: the

enzymes have a hydrophobic domain acting as a binding site to adhere to the hydrophobic substrates as well as a catalytic domain as an active site. A new kinetic model has been proposed and its usefulness has been confirmed experimentally [Mukai *et al.*, 1993]. The heterogeneous enzymatic degradation takes place via the two steps of adsorption and hydrolysis. There are two types of degradation process: cleavage occurs i) randomly along the polymer chain (endo-type degradation) or ii) at the ends of the polymer chain (exo-type degradation). Lipases or PHA depolymerases primarily work with the endo-type scissions, and thus are not dependent on the molecular weight and molecular weight distribution. A very common feature of depolymerases is a reaction mechanism that uses three aminoacids residues: aspartate, histidine and serine. Aspartate interacts with the histidine ring to form a hydrogen bond. The ring of histidine is thus oriented to interact with serine. Histidine acts as a base, deprotonating the serine to generate a very nucleophilic alkoxide group (-O-). This group attacks the ester bond (the alkoxide group is in fact a stronger nucleophile than the alcohol group) leading to the formation of an alcohol end group and an acyl-enzyme complex. Subsequently, water attacks the acyl-enzyme bond to produce a carboxyl end group and free enzyme. This arrangement of serine, histidine and aspartate is defined as catalytic triad [Lucas *et al.*, 2008].

1.2.5.3 Composting

According to the standard specifications (ASTM D6400, ASTM D6868 , ASTMD 7081, or EN13432), biodegradability is defined as the capability of a material to undergo decomposition into carbon dioxide, methane, water, inorganic compounds, and biomass, in which the predominant mechanisms are the hydrolysis and the enzymatic action of microorganisms [Bastioli, 2005]. Biodegradation catalyzed by microorganisms, which can occur in the presence of oxygen (aerobically) or in its absence (anaerobically), ultimately leads to the formation of carbon dioxide, water and new biomass (Figure 1.9). The chemical process can be summarized by the following equations:

Aerobic conditions (C = carbon):

$$C_{polymer} + O_2 \rightarrow CO_2 + H_2O + C_{residue} + C_{biomass} + \text{salts} \quad \textbf{[23]}$$

Anaerobic conditions:

$$C_{polymer} \rightarrow CO_2 + CH_4 + H_2O + C_{residue} + C_{biomass} + \text{salts}$$ **[24]**

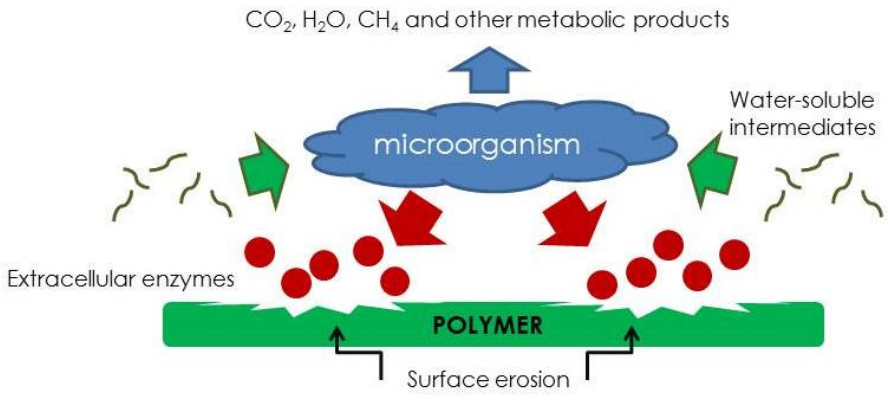

Figure 1.9: Polymer biodegradation catalyzed by microorganisms

Complete biodegradation (or mineralization) occurs when no residue remains, i.e. when the original product is completely converted into gaseous products and salts [Grima, 2000].

Compostability represents the biodegradability of a material buried in a compost medium where moisture, temperature, and aerobic environment are controlled. The difference between biodegradable and compostable polymers lies in additional requirements related to the latter. Besides biodegradation into carbon dioxide, water, inorganic compounds, and biomass, compostable polymers must fulfil other criteria such as compatibility with the composting process, no negative effect on quality of compost and degradation rates consistent with other known composting materials.

Various worldwide standardized tests have been developed to assess "biodegradable" labels. Nowadays, ISO and ASTM standards exist describing in detail the purposes of "biodegradable" and "compostable".

For instance, ASTM D6400 standard establishes the requirements for the labelling of materials and products, including packaging made from plastics, as "compostable in municipal and industrial composting facilities":

- conversion to carbon dioxide, biomass, and water under micro-bacterial action on the test polymer material in powder, film, or granule form;

- ninety percent of conversion to carbon dioxide and less than 10% of tested material with a size of 2 mm or less;
- same rate of biodegradation as natural materials (leaves, papers, grass, and food scraps);
- time of biodegradation less than 180 days;
- nontoxicity to the environment of the resulting compost.

ASTM standards [ASTM D 6400-04; ASTM D 6002-96) define composting as" a managed process that controls the biological decomposition and transformation of biodegradable materials into a humus-like substance called compost: the aerobic mesophilic and thermophilic degradation of organic matter to make compost, the transformation of biologically decomposable material through a controlled process of biooxidation that proceeds through mesophilic and thermophilic phases and results in the production of carbon dioxide, water, minerals and stabilized organic matter (compost or humus)". Composting requires special conditions, particularly of temperature, moisture, aeration, pH and carbon to nitrogen (C/N) ratio, related to optimum biological activity in the various stages of the process [www.compost.org].

According to ASTM standard, degradation of the waste in compost proceeds in three phases [www.compost.org; Dorsch et al. 2002]:

1. **The first mesophilic phase**

At the beginning of composting, mesophilic bacteria and fungi degrade soluble and easily degradable compounds of organic matter, such as monosaccharides, starch, and lipids. Bacteria produce organic acids, and pH decreases to 5–5.5. Temperature starts to rise spontaneously as heat is released from exothermic degradation reactions. The degradation of proteins leads to release of ammonia, and pH rises rapidly to 8–9. This phase lasts from a few hours to a few days.

2. **Thermophilic phase**

The compost enters the thermophilic phase when the temperature reaches 40ºC. Thermophilic bacteria and fungi take over, and the degradation rate of the waste increases. If the temperature exceeds 55–60ºC, microbial activity and diversity decrease dramatically. After peak heating, the pH stabilizes to a neutral level. The thermophilic phase can last from a few days to several months.

3. **Cooling and maturation phase**

After the easily degradable carbon sources have been consumed, the compost starts to cool. After cooling, the compost is stable. Mesophilic bacteria and fungi reappear, and the maturation phase follows. However, most of the species are different from the species of the first mesophilic phase. Actinomycetes often grow extensively during this phase, and some protists and a wide range of macroorganisms are usually present. The biological processes are now slow, but the compost is further humified and becomes mature.

The duration of the phases depends on the composition of the organic matter and the efficiency of the process, which can be determined by oxygen consumption [Rudnik, 2008].

The polymers degradation in compost can be monitored by measuring molecular weight changes, due to bond cleavage, or by measuring weight loss, due to depletion of low molecular weight material [Albertsson and Varma, 2003]. Besides loss of molecular weight, other parameters have been proposed as a measure for degradation, like loss of mechanical strength, complete degradation into monomers or monomer release.

1.2.6 Applications

The abundance of monomers employed in polyester synthesis allows the preparation of a wide spectrum of materials possessing specific characteristics for a wide range of applications.

Thanks to their mechanical performance, biocompatibility and biodegradability, aliphatic polyesters are used, for example, for the manufacturing of different medical devices, such as prosthetics, artificial skin, dental implants, vascular grafts, pins, bone screws, stents, and plates for temporary internal fracture fixation [Diaz et al., 2014; Sokolsky-Papkov et al., 2007]. Because they are to be used for a limited time period, all these systems require degradable polymers to fulfill the criterion of elimination after use. They also have to fulfill many other requirements related to the respect of the human body and specific regulations.

In addition to biomedical sector, aliphatic polyesters are also used for, the so-called, environmental applications. Indeed, applications such as packaging, mulching films, agricultural staples, coatings to protect seeds, chewing gums, cigarette filters, cartridge and cartridge wax, and so forth, can be compared with biomedical implants [Vert,

2005]. In this field too, the materials are used for a limited period of time, and after use generate wastes. In addition, traditional polymers are not biorecyclable and accumulate in the environment. For this reason, degradable polymers are basically necessary to many applications. For example, in agronomy are used polymeric systems to deliver pesticides, insecticides, fertilizers, and so forth (higher relative efficiency; lower overall toxicity; localization, time, and rate control of the delivery; etc.). Unfortunately, the available materials themselves cannot provide solutions to the listed potential applications. Consequently, polymer scientists and industrials are going to develop sciences and technologies to take advantage of the outstanding possibility offered by polymeric systems to match material properties and application requirements, namely, copolymerization and formulation with additives [Vert, 2005].

1.3 Packaging

Packaging represents the largest plastic application segment covering alone almost 40% of the European converter demand [Plastics Europe, 2015].

Currently, petrochemical-based plastics, such as polyethylene terephthalate (PET), polyvinylchloride (PVC), polyethylene, polypropylene (PP), polystyrene (PS) and polyamide (PA) have been increasingly used as packaging materials because of their large availability at relatively low cost and their good mechanical performance such as tensile and tear strength, good barrier to oxygen, carbon dioxide, anhydride and aroma compound, heat sealability, and so on [Siracusa et al., 2008]. In recent years, their use has been restricted because they are not completely recyclable and/or not biodegradable so they pose serious ecological problems. New bio-based materials for food packaging have been designed in order to replace their non-degradable counterparts [De Azeredo, 2009]. It is well-known that high production costs of biodegradable materials are a stumbling block, being an important disadvantage against synthetic ones. However, eco-friendly materials development is justified since they guarantee environmental preservation. This implies to protect non-renewable sources as well as to avoid pollution problems related to the final disposition of non-degradable materials [Davis & Song, 2006].

Moreover, safer and nutritious and high quality food with prolonged shelf life are bring to the development of specific performant packages [Sorrentino, et al. 2007]. Even a

thin plastic film packaging only few micron thick can increase the shelf life of products, reducing food waste and decreasing energy consumption and greenhouse gas emissions at the same time. In order to perform these functions food packages should have tailored properties such as mechanical, optical, and barrier ones that depend on the structure of the polymeric packaging material. Materials must be tough and flexible enough to guarantee their manipulation without any food product damage. In addition, other relevant issue is package tightness related to barrier properties since food organoleptic and microbial qualities depend on package's effectiveness to control gases exchange. Specific barrier requirement of a package system depends on food characteristics and intended end-use applications [Siracusa, 2012]. Water vapor and oxygen are two of the main gases studied as permeants in packaging applications; they diffuse through the film modifying product quality and shelf-life. Water vapor barrier property of film packaging is important for products whose physical and chemical deteriorations are related to moisture content [Siracusa, 2012]. As to oxygen gas, a low gas transmission rate is fundamental, since this gas promotes several food degradation mechanisms, such as corrosive phenomena, oxidations, and organoleptic properties modifications [Lopez et al.2015].

As to fresh fruits and vegetables, the major problems limiting their shelf-life are the high respiration rate, off-flavors production, acidification, loss in firmness and discoloration, high ethylene production, and microbial spoilage [Amanatidou et al., 2000; Barry-Ryan and Beirne, 2000;. Barry-Ryan et al., 2000; Sandhya, 2010].

Reducing the rate of respiration by limiting O_2 prolongs the shelf life of fruits and vegetables by delaying the oxidative breakdown of the complex substrates, which make up the product. O_2 concentrations below 8% reduce the production of ethylene, a key component of the ripening and maturation process [Russo, Simon, & Incarnato, 2006].

Modern food packaging technologies include modified atmosphere packaging (MAP), active packaging, and smart packaging, designed to enhance food safety and quality, in a way as natural as possible [Hotchkiss, 1995]. Under controlled conditions, the atmosphere is modified on respect to the ambient atmosphere, and these conditions are maintained throughout storage. This technique desirably generates an atmosphere low in O_2 and high in CO_2, which influences the metabolism of packed product or the activity

of microorganisms that cause food spoilage, which ultimately results in increased storability and shelf-life [Pasha et al., 2014]

MAP hinders spoilage mechanisms, as well as reduces respiration, delays ripening, decreases ethylene production and sensitivity, retards textural softening, reduces chlorophyll degradation, and alleviates physiological disorders by using different oxygen (O_2), nitrogen (N_2), and carbon dioxide (CO_2) concentrations [Ohlsson and Bengtsson, 2002; Farber et al., 2003; Xing et al., 2010].

In addition, it is important to study the change that can occur on the characteristics of the plastics during the time of interaction with the food [Scott, 2000]. Last but not least, the compatibility with the food plays a crucial role in this kind of application; as a matter of fact, it has been recognized as a potential source of loss in food quality properties [Halek, 1988]. The field of application of biodegradable polymers in food-contact articles includes disposable cutlery, drinking cups, salad cups, plates, overwrap and lamination film, straws, stirrers, lids and cups, plates and containers for food dispensed at delicatessen and fast-food establishments. These articles will be in contact with aqueous, acidic and fatty foods that are dispensed or maintained at or below room temperature, or dispensed at temperatures as high as 60°C and then allowed to cool to room temperature or below [Conn *et al*., 1995]. For all these reasons, up to now, only a limited amount of biodegradable polymers have suitable properties and can be used for food packaging application. More solutions have been found for other packaging types.

Depending on the production process and on the source, biopolymers can have properties similar to traditional ones. They can be generally divided into two main groups: starch-based polymer and polyesters.

1.3.1 Starch-based polymers and blends

Starch is one of the naturally occurring biopolymers, inexpensive biodegradable resource, annually derived from corn and other crops. Of late, starch has received extensive attention in packaging industries, for producing commercial thermoplastic polymers [Zhang and Liu, 2008; Chang et al., 2010]. Starch-based packaging could be used for fresh cut beef steaks (Cannarsi, et Al., 2005) or whole fresh celery and is already used for milk chocolates and organic tomatoes [Highlights in bioplastics, 2006].

The biodegradation of starch products recycles atmospheric CO_2 trapped by starch producing plants. Depending on the type of the thermoplastic starch materials, they can degrade in 5 days in aqueous aerobic environment, in 45 days in controlled compost and in water [Siracusa et al., 2008].

All starches contain amylose and amylopectin, at ratios that vary with the starch source (figure 1.10)

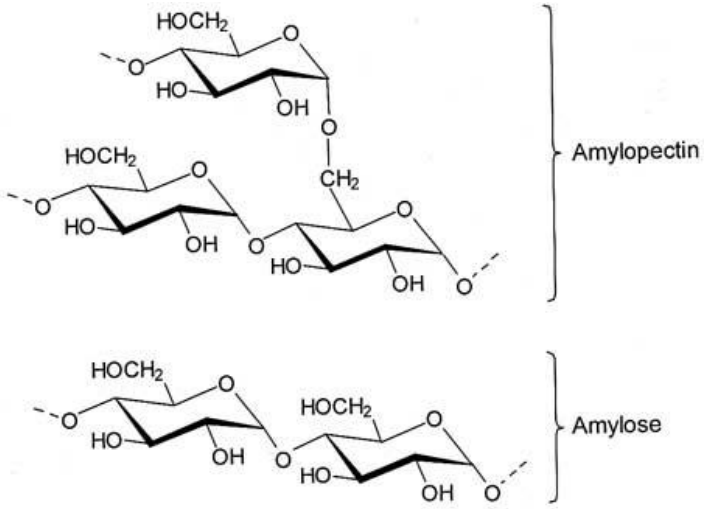

Figure 1.10: Chemical structures of Amylopectin and Amylose

Amylose forms a colloidal dispersion in hot water whereas amylopectin is completely insoluble.

The physical properties of starch are influenced by the amylose/amylopectin ratio. During gelatinization, the starch granules swell and form gel particles. In general, the swollen granules are enriched in amylopectin, while the linear amylose diffuses out of the swollen granules and makes up the continuous phase outside the granules.

In general, a starch granule degrades before it melts under applied heat because its molecular structure possesses strong inter- and intra-molecular hydrogen bonds which result in high glass transition (215–238 ◦C) and melting temperatures (267–277 ◦C) [Yokesahachart & Yoksan, 2011].

Although starch shows a high capacity to form homogeneous films with excellent oxygen barrier properties, they exhibit some drawbacks, such as poor mechanical properties, and high water vapor sensitivity which leads to high water vapor permeability [Averous & Boquillon, 2004; Ghanbarzadeh, et al, 2011], and retrogradation. This consists of a slow recoiling of gelatinized amylose and amylopectin

molecules, which back into their native helical arrangements or into a new single helix conformation. The retrogradation is undesirable as it increases crystallinity and reduces film elongation over time. This limits their potential to be used as a basic raw material for developing biodegradable packaging materials.

In order to improve the starch film properties, blends with other components, such as plasticizers, crosslinking agents or other polymers have been studied. Glycerol can be added as a plasticizer to enhance the mechanical properties of the film, increasing its flexibility [Vieira et al. 2011] The addition of other thermoplastic polymers to form blend starch films can modulate the films properties in order to improve their functionality. Among all commercially available biodegradable polymeric materials, hydrophobic synthetic polymers, such as aliphatic polyesters, could offer adequate solutions if blended with thermoplastic starch (TPS), destructurized starch that is noncrystalline, produced by the application of heat and work in presence of a plasticizer [Di Franco et al. 2004; Ortega-Toro 2015].

The greater difficulty in making starch//Polyester blends is the deficient interfacial adhesion between the hydrophilic starch and the hydrophobic polyester. To address this issue, multifunctional substances, such as maleic anhydride (MA) and citric acid (CA), are added to promote esterification/transesterification reactions (crosslinking) at the interface between polymeric chains to improve their compatibility. This fact, according to literature [Zhang & Sun, 2004;Olivato et al., 2012] has been effective for the morphology control in several polymeric systems.

By varying the synthetic polymer component the properties can be regulated easily and efficiently, playing also on blend morphology. In 1993, LDPE-starch blends were commercialized under the trade name Ecostar®. Other commercial trade names are Bioplast® (from Biotec GmbH), NOVON® (from NOVON International) and Mater-Bi® (from Novamont). All these materials are mainly processed into films and sheets. Blends with more than 85% starch are used for foaming and injection molding. The foams can be used as loose-fill in place of polystyrene; the starch-based loose fills have an average density of 6 to 8 kg/m^3, compared with 4 kg/m^3 for expanded polystyrene loose fill. The commercial trade names are Biopur® (from Biotec GmbH), Eco-Foam® (from National Starch & Chemical) and Envirofill® (from Norel). Loose-fill materials from starch are generally water sensitive. This is a problem if the packaging material is

exposed to water, but an advantage when down-the-drain disposal is desired. By mixing thermoplastic starch with cellulose derivatives, rigid and dimensionally stable injection-molded articles result. Chemically modified plant cellulose is used in a remarkably diverse set of applications. For example, cellulose acetate is employed in many common applications, including toothbrush handles and adhesive tape backing. Eastman Chemical Company has developed very promising fully biodegradable cellulose acetates.

1.3.2 Polyesters

Among the biodegradable polymers, aliphatic polyesters undoubtedly represent one of the most promising classes for packaging applications, as they combine interesting properties with proven biodegradability and acceptable production costs.

.At present, unfortunately, biopolymers must compete head-to-head in cost and performance with existing familiar and inexpensive products. This is extremely difficult because new processes require intensive research and large capital expenses and must be scaled-up to be economically competitive. On the basis of both economic and environmental considerations, the commercialization of biodegradable plastics will continue to increase especially in those markets where products have a relatively short-use lifetime. Several biodegradable polyesters are actually on the market or at an advanced stage of development.

1.3.2.1 Long chain aliphatic polyesters

As already stated above, the most commonly employed polymers in packaging application are synthetic polymers, produced from petrochemical resources. The most widely used in these applications is undoubtedly polyethylene (low density (LDPE), linear low density (LLDPE), and high density (HDPE))

Their great success is due to their low cost and excellent physic-mechanical properties.

Unfortunately, as it is well-known, these materials are not readily degraded in the environments where they are disposed once their function has ended.

For this reason, since 80s, both academic and industrial researchers devoted their efforts to the design of biodegradable polymers with chemical and physical properties very similar to PE or other polyolefins.

Long chain aliphatic polyesters well mimic the Poly(Ethylene) backbone, due to the large number of methylene units along the macromolecular chain. The PE-like polyesters can be synthesized through polycondensation of long-chain diols and long-chain diacids.

Recently, different studies have focused on the synthesis and characterization of aliphatic long chain polyesters, whose properties have been also compared to HDPE and LDPE [Cai et al., 2010; Liu et al 2011;Pepes et al., 2013;Menges et al., 2007; Stempfle et al. 2013; Trzaskowski et al. 2011; Vilela et al., 2012].

Unfortunately, due to the low amount of hydrolysable ester bonds along the polymeric chains, the biodegradation rate of these polymers, remains anyway very low.

1.3.2.2 Poly(buthylene succinate) PBS

Among bioplastics, poly(butylene succinate) (PBS) [Chrissafis et al., 2005] and its copolymers, represent a family of biodegradable polyesters useful in a wide range of applications [Mochizuki et al., 1997; Gan et al., 2001; Tserki,et al., 2006; Papageorgiou & Bikiaris, 2007; Lee & Kim, 2010].

Since the very early work of Carothers and his group in the early '30s [Carothers, 1931], many efforts have been directed to the realization of industrially relevant aliphatic polyesters. Among other successful cases, PBS is commercially available since 1993 [http://www.showa-denko.com]. It is produced under the tradename BionolleTM by Showa-Denko [http://www.showa-denko.com] and by Mitsubishi Chemical Corporation under the tradename GS PlaTM [http://www.m-kagaku.co.jp]. Its main uses regard environmental purposes, such as mulching films, compostable bags, nonwoven sheets & textiles, catering products and foams [http://www.showa-denko.com; http://www.m-kagaku.co.jp.]. The monomers employed in the PBS synthesis are succinic acid (SA) and 1,4-butanediol (BD) (Fig. 3.1 chap. 3), which are commonly obtained from fossil resources and are readily available on the market. Interestingly, both SA and BD can be also obtained through fermentation. In the last years, various microorganisms have been screened and tested for the production of

succinic acid via biotechnological processes, with good yields [Bechthold et al., 2008]. The so-obtained SA can then be converted into 1,4-butanediol through hydrogenation [Varadarjan, & Miller, 1999]. This would lead to a complete bio-based PBS. Various companies such as Succinity (a joint venture between BASF and Purac), Reverdia, BioAmber and Myriant are operating in the production of biosuccinic acid at industrial scale.

The success of PBS as thermoplastic materials is strictly due to its properties. As a matter of fact, PBS is a semicrystalline polymer with high crystallization ability (vc = 35–45%) [Soccio et al., 2008] and its melting temperature is one of the highest among poly(alkylene dicarboxylate)s [Yoo & Im, 1999; Xu & Guo, 2010]. The glass transition temperature is well below room temperature, therefore PBS possesses a broad processability range, which allows its processing through extrusion, injection molding and thermoforming [Miyata, & Masuko, 1998; Papageorgiou &Bikiaris, 2005; Fabbri et al., 2014]. As to the mechanical properties, they are strictly dependent on the presence of small amounts of diisocyanates, typically hexamethylene diisocyanate, used as chain extenders. High molecular weight PBS synthesized without chain extenders shows a brittle behaviur, with very short elongation at break [Gigli et al., 2012], while the use of isocyanates significantly improves its elongation [M. Fabbri et al., 2014], up to values comparable to those of polyolefins. [Fujimaki, 1998].

Unfortunately, the use of PBS in those applications where fast degradation rate and flexibility are required, is limited because of its high crystallinity degree and rigidity.

1.3.2.3 Poly(lactic acid) (PLA)

PLA is one of the most promising bio-based polymer, being biodegradable, recyclable and biocompatible, requiring low manufacturing energy, having good processability, high transparency and water solubility resistance [Gupta et al., 2007; Rasal et al., 2010; Siracusa et al, 2008]. Such properties coupled with a competitive market price have made it one of the first commercially available biopolymers widely used in the packaging of fresh produce. Today, companies around the world such a s Mitsui Chemicals Inc. (Japan), NatureWorks Llc (USA), or Futerro (Belgium) produce PLA on large scale.

The manufacture of polyester from lactic acid was pioneered by Carothers in 1932 and further developed by Dupont and Ethicon [Gross & Kalra, 2002]. Prohibitive production costs restricted the applicability of this polymer outside the medical field until the late 1980s. Since then, major breakthroughs in process technology, coupled with decreased costs of biologically produced lactic acid, have led to the commercial-scale production of plastics from lactic acid for nonmedical applications. This integration of biotechnology and chemistry is an important strategy, crucial for the improvements in many other chemical processes in future years.

Two chemical routes have been developped to convert lactic acid to high molecular weight PLA. Cargill Dow LLC uses a solvent-free continuous process and a novel distillation method [Lunt, 1998]. In contrast, Mitsui Toatsu [Lunt, 1998] converts lactic acid directly to high molecular weight PLA by a solvent based process with the azeotropic (where vapor and liquid have the same composition at some point in distillation) removal of water by distillation.

The chemical synthesis of the monomer has based on the hydrolysis of lacto-nitrile by strong acid, giving rise to the racemic mixture of D- and L-lactic acid. Other synthetic strategies could be the catalyzed degradation of sugars, the oxidation of propylene glycol, the reaction of acetaldehyde, carbon monoxide and water at high temperature and pressure, the hydrolysis of chloro-propionic acid and the nitric acid oxidation of propylene.

In order to use renewable resources instead of petrochemical ones, and in order to obtain an environmentally friendly monomer, the interest in the microbial fermentative production of lactic acid has increased. The carbon source for microbial production of lactic acid could be sugar in pure form (glucose, sucrose, lactose) or sugar-containing materials like whey, sugar cane bagasse and cassava bagasse, potato, tapioca, wheat, barley, and so on. In order to restrain the cost of the raw material, food/agro industrial by-products or residues could be used as cheaper alternative, by using selected microorganisms [Madhavan, Nampoothiri et al., 2010]. Thanks to the fact that both a hydroxyl and a carboxylic group are present in the lactic monomer, a direct polycondensation reaction could be employed to obtain the corresponding polyester. In this case, in order to obtain high molecular weights and reduce the polymerization time

and temperature, the addition of acidic catalysts is necessary. Nevertheless, a moderate yield of relatively high molecular weight PLA is obtained.

A good alternative is the step-growth polymerization, starting from lactic acid or by ring-opening polymerization (ROP) of lactide (LA), that is, the ring-formed dimer from lactic acid [Auras et al., 2004 (a)]

Because of the chiral nature of Lactic acid , LA exists in three different forms, L,L-LA, D,D-LA, and D,L-LA (*meso*lactide) as well as a 50/50 mixture of L,L-LA and D,D-LA referred to as *racemic lactide* (Figure 1.11).

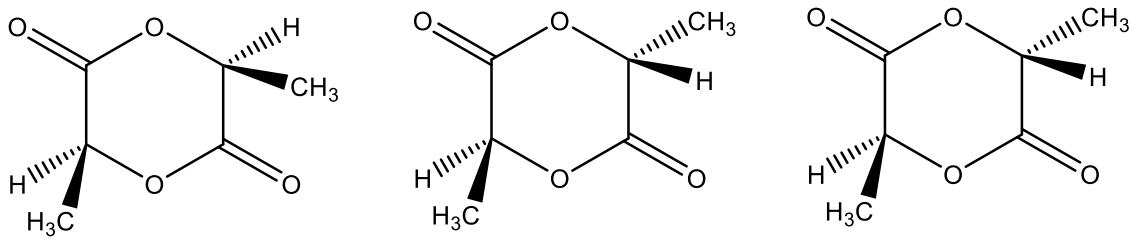

Figure 1.11: Chemical structures of LL-, meso- and DD-Lactides (m.p. is melting point)

PLA material properties depend upon the isomer type (D-, L-, DL-lactide), processing temperature, annealing time and molecular weight. The stereochemical composition has a strong effect upon the melting point and on the polymer crystallization ability [Chen, & Patel, 2012]. PLLA has a crystallinity around 37%, a glass transition temperature between 50 and 80 °C and a melting temperature between 173 and 178 °C. The introduction of stereochemical defects (meso-lactide or D-lactide) into PLLA reduces these parameters but has a little effect on the glass transition temperature [Drumright et al., 2000]. Similar effects are observed when D-lactide is copolymerised with L-lactide. By varying the crystallinity degree of the polymers, it is possible to modulate its degradation rate. The higher the crystallinity percentage, the lower the biodegradation rate. Further, degradation has been found to be dependent upon a range of factors, such as molecular weight, purity, temperature, pH, presence of terminal carboxyl or hydroxyl group, water permeability, plasticizer and additives [Ingrao, 2015].

Upon disposal, PLA degrades primarily by hydrolysis, not microbial attack [Gross & Kalra, 2002]. Hence, even at high humidity, it is uncommon to encounter contamination of high molecular weight PLA by fungi, mold, or other microbes. This unusual characteristic of a bioplastic is attractive for applications in which they are in direct contact with foods for extended time periods. For these reasons, PLA is currently used in packaging (film, thermoformed containers, and short-shelf life bottles).

PLA's certified compostability and compliance with the food contact safety regulations [Auras et al., 2004 (b)] makes it attractive as packaging material, since it meets the compostability requirements of EN13432 for packaging [EN 13.432, 2005], thus alleviating the plastic wastes problem.

Although PLA can be considered a valid substitute for many non-biodegradable polymers, its application is limited, due to its brittleness and barrier properties [Chaiwong et al., 2010; Rasal et al., 2010; Pankaj, 2014].

Nevertheless, it is possible to manipulate its physical, mechanical and barrier properties by changing its chemical composition and varying its molecular characteristics. It is also possible to blend PLA with other polymers, making it a good biodegradable alternative to traditional polymers for use in plastic packaging.

1.3.2.4 Poly(alkylene 1,4-cyclohexanedicarboxilate)s

Within the polyester class, poly(alkylene 1,4-cyclohexanedicarboxilate)s offer different advantages: the introduction of cycloaliphatic ring to the main chain of the polymer can be a way to increase the rigidity of the macromolecular chains, enables the material to have good thermal stability, even higher than the aromatic counterparts, [Berti et al., 2008 (b)] to show interesting mechanical properties and to maintain the biodegradability [Gigli et al., 2014 (a)]. Moreover, conformational transitions of cyclohexylene rings in the backbone originate secondary relaxations in dynamical mechanical spectrum, which contribute to improve the performances of the materials [Berti et al., 2008 (b)].

Both *trans* and *cis* configurations of the aliphatic ring are possible; it has been observed that stereochemistry strongly influences the final properties of the material. In particular, the *trans* stereoisomer is less flexible and more symmetrical than the *cis* favoring chain packing, and consequently the capacity of the polymer to crystallize with

increment also of the crystal perfection. [Berti et al., 2008 (a); Berti et al., 2008 (b)]. On the other hand, if the *trans* content is decreased, these properties are significantly reduced. For example, for the fully (100%) *trans* PBCE the crystallization temperature measured during the cooling scan at 20 °C/min from the melt (T_c) is 140 °C and the enthalpy about 40 J/g; on the other hand, a *trans* percentage of 72% is sufficient to cause a decrement of T_c of about 55 °C and to reduce the crystallization enthalpy by half, whereas a *trans* content of 52% completely prevents PBCE crystallization [Berti et al., 2008 (b)].

The synthesis and properties of polyesters and copolyesters containing these cycloaliphatic rings were studied at the beginning of the eighties by Eastman Chemical Company, interested to develop materials with excellent tensile strength, stiffness and impact properties as well as materials to be used as improved hot melt adhesives.

Although 1,4-cyclohexane dicarboxylic acid is now obtained from petroleum resources, however, it can be prepared from bio-based terephthalic acid, starting from limonene and other terpenes [Berti et al.. US 2010]. Therefore, polymers derived, for example, from 1,4-cyclohexane dicarboxylic acid and a diol obtainable from biomass (as 1,3-propanediol, obtainable by renewable feedstocks, such as corn) can be considered fully sustainable materials.

Moreover, the presence of the 1,4-cyclohexylene units along a macromolecule does not hinder the attack of microorganisms.[Gigli et al., 2013; Gigli et al., 2014 (a); Gigli et al., 2014 b)]. Therefore, the polyesters containing the 1,4-cyclohexylene rings can be considered biodegradable materials and are very promising environmentally friendly polyesters.

Anyway, as previously pointed out for the polyesters described above, poly(alkylene 1,4-cyclohexanedicarboxilate) homopolymers are not suitable for any applications. Again, blending and copolymerization can be efficient tools to improve unsatisfactory performances without compromising those already good.

2.

AIM OF THE WORK

2 AIM OF THE WORK

There is no larger market segment in the plastics industry than the packaging segment. More than a third of all plastics are converted into packaging, that is approximately 100 million tonnes worldwide and more than 20 million tonnes in the EU. In Western industrial countries, 50 percent of all goods are packaged in plastics [Plastics – the Facts 2015]. Food packaging accounts for almost two-thirds of total packaging waste by volume and is approximately 50% (by weight) of total packaging sales.

Until now, petrochemical-based plastics have been extensively used as packaging materials thanks to their low cost and excellent physic-mechanical properties. Unfortunately, as it is well-known, these materials are not readily degraded in the environments where they are disposed once their function has ended. [Mecking, 2004; Ali Shah et al 2008; Zheng, et al 2005; Arutchelvi, et al. 2008]. Although recycling of these materials increased during the last decade, only a small part of the generated amount of plastic waste is finally recycled due to the contamination with organic matter [Themelis et al., 2011].

As a consequence, thousands of tons of plastic packaging are disposed in landfills every year, causing a continuous pollution increment, besides various municipal waste management problems.

Therefore, replacing non-degradable conventional plastics based on fossil oil with sustainable bio-based biodegradable materials for short time applications is of great environmental importance. Biodegradable polymers have attracted much interest all over the world and various bio-based plastics satisfying the requirement of degradability, compatibility with the disposed environment and release of low-toxicity degradation products have been already studied as possible alternatives to conventional packaging materials [Siracusa et al., 2008].

The recent technological advances offer great promise towards achieving biodegradability with less pollutants and greenhouse emissions. Linking performance with cost is a tremendous task, which needs imaginative steps in the selection of materials, processes, product structures and production schedules.

Nowadays, several biobased and biodegradable plastic packaging materials can be or are already used for short shelf-life applications. Among them one of the most economically competitive polymer class is represented by aliphatic polyesters, [Tserki

et al., 2006] that have attracted considerable attention in last decades as they combine the afore mentioned features with interesting physical and chemical properties.

Poly(Lactic acid) is one of the most promising bio-based aliphatic polyester: it is biodegradable, recyclable and biocompatible, and combines low manufacturing energy, with good processability, high transparency and water solubility resistance. Such properties coupled with a competitive market price have made it one of the first commercially available biopolymers widely used in the packaging of fresh food. [Pankaj et al. 2014].

In recent years, poly(butylene succinate) (PBS) as well has attracted considerable attention thanks to its good mechanical properties and thermal stability, although it exhibits a slow biodegradation rate due to its high crystallinity degree [Papageorgiou and Bikiaris, 2007]. It can be produced from renewable feedstocks and is already commercialized by Mitsubishi and Showa Denko, under the trademark Bionolle®.

Although not yet commercialized, poly(alkylene 1,4 cyclohexanedicarboxilate)s are very interesting members of aliphatic polyester family. The presence of the aliphatic ring along the polymer backbone enables the material to have high melting point, good thermal stability, even higher than aromatic counterparts [Berti et al., 2008b], interesting mechanical properties and to be biodegradable [Berti et al., 2010]. Moreover, aliphatic ring containing polyesters are characterized by good resistance to weather, heat, light and moisture [Berti et al., 2008a]. Actually 1,4-cyclohexane dicarboxylic acid is obtained from petroleum resources, but it can be prepared from bio-based terephthalic acid, starting from limonene and other terpenes [Berti and Binassi. 2010]. Therefore, polymers derived from 1,4-cyclohexane dicarboxylic acid and a diol obtainable from biomass (1,3-propanediol from corn, to cite one example) can be considered fully sustainable materials.

Despite the availability of the above mentioned materials on the market and considering their interesting performance in food packaging applications, they do not fulfill all the requirements for a wide range of possible uses. In this view, copolymerization represents undoubtedly an interesting tool to design novel materials, which display the right combination of properties for the desired application.

Through copolymerization, it is also possible to obtain classes of new polymers with a broad range of properties depending on the kind, relative amount and distribution of the

comonomeric units along the polymer chain. Lastly, copolymerization represents also an efficacious way of promoting the biodegradability of a polymer, which is basically attributed to the limited copolymer crystallinity [Rizzarelli et al., 2004].

In this framework, the present research work focused on the modification of some interesting aliphatic polyesters, in order to prepare new materials, which guarantee full compostability and offer suitable characteristics specially in terms of mechanical and barrier properties to be used in food packaging applications.

In particular, five different copolyester systems have been synthesized and deeply characterized:

- ✓ Long chain Polyethylene-like random aliphatic copolyesters containing ether linkages
- ✓ Random aliphatic copolyesters based on poly(butylene succinate) containing thioether-linkages.
- ✓ Poly(lactic acid) based A-B-A triblock copolymers
- ✓ 1,4 cyclohexane dicarboxylic acid-based random copolyesters and multiblock poly(ester urethanes)

Simple, ecofriendly, cost-effective synthetic strategies have been employed to obtain the designed materials:

- ✓ Two stage melt polycondesation (to obtain random copolyesters),
- ✓ Ring opening copolymerization of L-lactide using an *ad-hoc* hydroxyl-terminated random pre-polymer as initiator (to obtain Poly(lactic acid) based A-B-A triblock copolymers) followed by chain extention reaction.
- ✓ Chain extension reaction of hydroxyl terminated prepolymers (to obtain multiblock poly(ester urethane) copolymers)

All the obtained materials have been deeply characterized by the molecular, thermal and mechanical point of view. Moreover, their barrier properties have been studied to prove their suitability for packaging applications. Lastly, lab-scale composting experiments have been carried out, in order to check their potential compostability.

More specifically, in all cases the choice of comonomeric unit employed to chemically modified the parent homopolymer was dictated by the need to improve the mechanical properties, accelerate the degradation process and possibly improve or at least not worse the barrier properties.

The research activity here presented consisted of the following steps:

- careful bibliographic research to get the state of the art on the subject;
- synthesis of the polymers under investigation with optimization of the reaction conditions;
- molecular, physico-chemical and mechanical characterization of the synthesized polymers;
- analysis of the barrier properties
- analysis of the biodegradability under composting.

Lastly, the properties of the materials under investigation have been correlated to polymer chemical structure in order to establish structure-property correlations, which are fundamental to be able to design an *ad-hoc* material to fit a specific application.

3.
MATERIALS AND METHODS

3 MATERIALS AND METHODS

3.1 Materials

The chemical structures of the reagents employed in the syntheses are collected in Figure 3.1: 1,12-dodecanedioic acid (DA), 1,6-hexanediol (HD), triethylene glycol (TEG); dimethylsuccinate (DMS), thiodiethylene glycol (TDG), 1,4-butanediol (1,4-BD), 1,3-propanediol (1,3-PD), neopenthyl glycol (NPG), diglycolic acid (DGA), titanium tetrabutoxide ($Ti(OBu)_4$) and Sn(II)-2 ethylhexanoate ($Sn(Oct)_2$) were purchased from Sigma Aldrich (Milan, Italy) whereas trans-cyclohexane-1,4-dicarboxylic acid (CHDA) containing 99% of trans isomer, was purchase by TCI Europe (Zwijndrecht, Belgium), glycerin vegetal (Gly) was purchased from Alfa Aesar (Karlsruhe, Germany) and L-lactide (L-LAC, Chiral purity >99%) has been provided by Purac (Amsterdam, The Netherlands). All the used chemicals were reagent grade products and used without any further purification. The catalysts employed for polycondensation synthesis, titanium tetrabutoxide ($Ti(OBu)_4$), was on the contrary distilled before use.

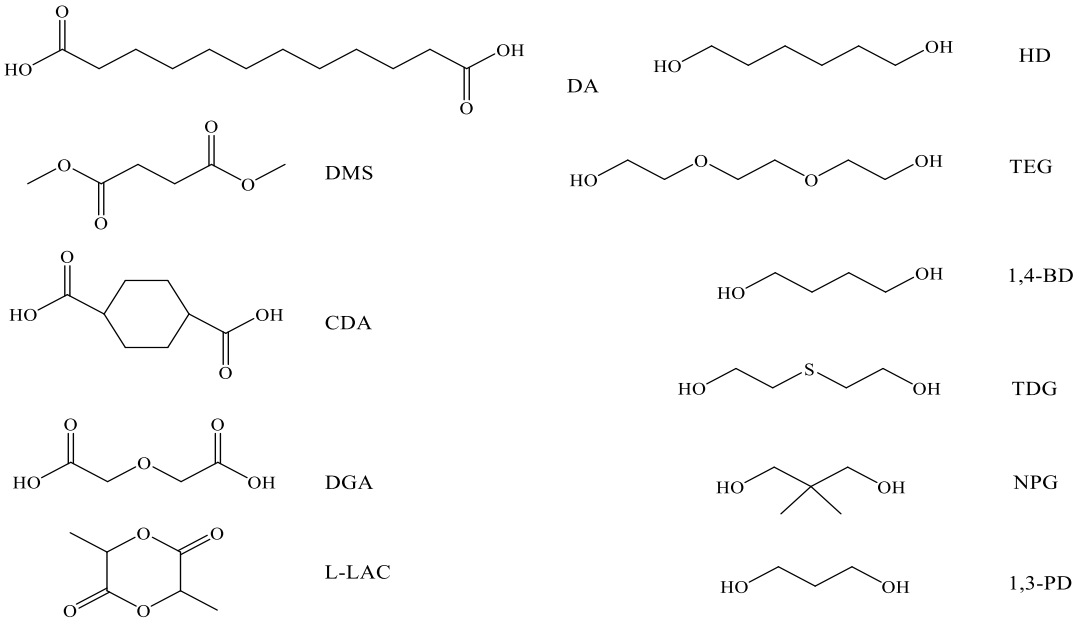

Figure 3.1: chemical structures of the reagents

3.2 Synthesis

Different synthetic strategies have been followed to obtain the designed materials:

- ✓ Two stage melt polycondesation

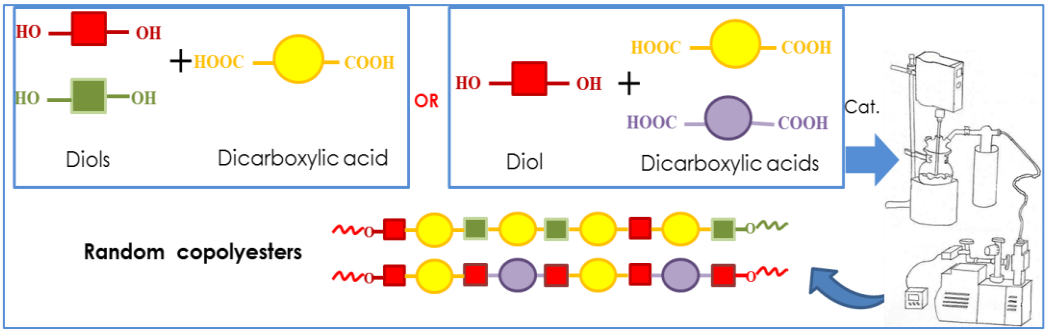

Figure 3.2: Schematic representation of Polycondensation reaction.

Through this synthetic approach, homopolymers as well as random copolyesters have been synthesized, with both high or low molecular weight (hydroxyl - terminated pre-polymers). The seconds were subsequently chain extended to obtain high weight homo- and copolymers.

✓ Ring opening copolymerization (ROP) of L-lactide using an hydroxyl-terminated random pre-polymer, synthesized ad-hoc, as initiator.

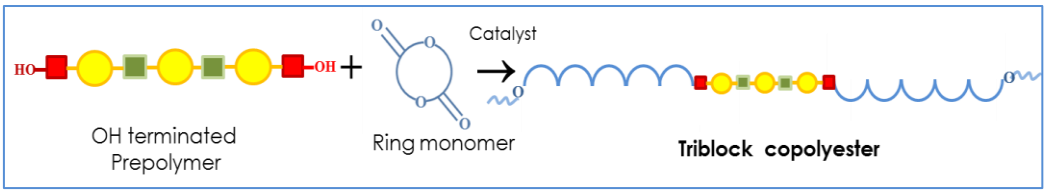

Figure 3.3: Schematic representation of Ring Opening Polymerization (ROP)

ROP was employed to obtain Poly(lactic acid) based A-B-A *soft-hard* triblock copolymers.

✓ Chain extension reaction of hydroxyl-terminated random prepolymers using hexamethylene diisocyanate (HDI) as chain extender.

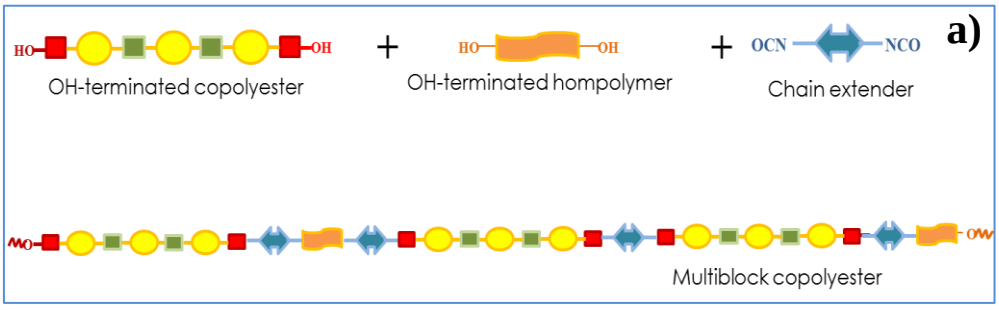

b)

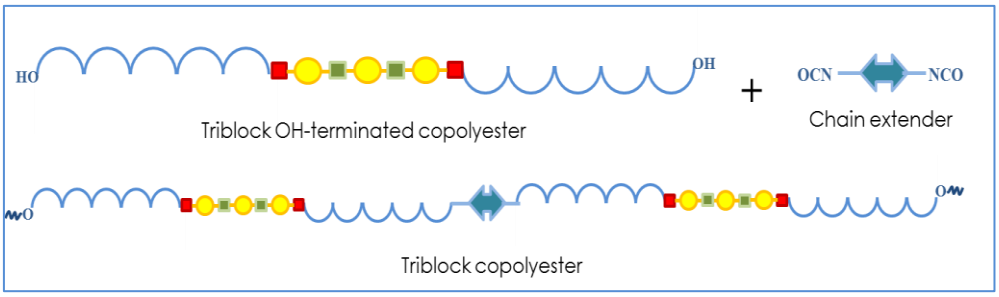

Figure3.4: Schematic representation of chain extension reactions: a) to obtain multiblock copolymers; b) to obtain high molecular weight A-B-A triblock copolymers.

Chain extension reactions were employed to obtain multiblock poly(ester urethane) copolymers with random distribution of the co-units (figure 3.4a) or to promote the growth of the molecular weight of A-B-A *soft-hard* triblock copolymers previously synthesized by ROP (figure 3.4b).

3.2.1 Homopolymers

High molecular weight homopolymers were synthesized in bulk starting from the appropriate monomers (using from 20% to 40% mol excess of the glycol with respect to dimethylester or dicarboxylic acid), employing $Ti(OBu)_4$ as catalyst (about 150 ppm of Ti/g of theoretical polymer). The syntheses were carried out in a 250 mL stirred glass reactor, with a thermostatted silicon oil bath; temperature and torque were continuously recorded during the polymerization

The polymers were prepared according to the usual two-stage polymerization procedure. In the first stage, under pure nitrogen flow, the temperature was raised to 180°C and maintained there for until more than 90% of the theoretical amount of methanol was distilled off (about 2 hours). In the second stage the pressure was gradually reduced to about 0.08 mbar, in order to facilitate the removal of the glycol in excess and the temperature was risen to 230-250°C (see table 3.1); the polymerization was carried out until a torque constant value was measured.

Table 3.1: Reagents and operating conditions employed for homopolymers syntheses

Polymer	Dicarboxylic acid/ester	Glycol	T1st Stage (°C)	T2nd Stage (°C)
Poly(hexane dodecanoate) (PHD)	DA	HD	180	250
Poly(triethylene dodecanoate) (PTED)	DA	TEG	180	250
Poly(butylene succinate) (PBS)	DMS	1,3-PD	180	230
Poly(propylene cyclohexanedicarboxylate) (PPCE)	CHDA	1,3-PD	180	240
Poly(neopenthyl glycol cyclohexanedicarboxylate) (PNCE)	CHDA	NPG	180	240
Poly(butylene cyclohexanedicarboxylate) (PBCE)	CHDA	1,4-BD	190	250

Chemical structures of the synthesized homopolymers are collected in figure 3.5.

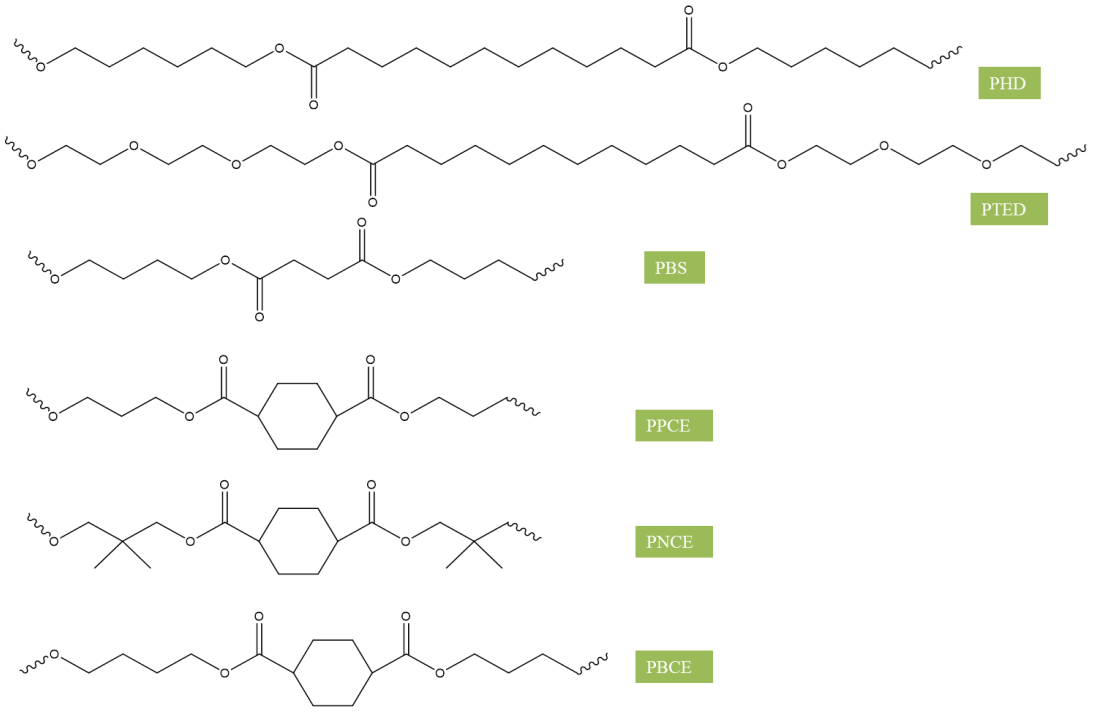

Figure 3.5: Chemical structures of synthesized high molecular weight homopolymers

3.2.2 Hydroxyl-terminated homopolymer

Poly (butylene cyclohexane dicarboxylate) (PBCE) hydroxyl-terminated homopolymer was synthesized starting from 1,4-trans cyclohexane dicarboxylic acid and 1,4-buthane diol. To ensure the obtaining of an OH-terminated polyesters, a glycol excess of 60%, compared to the dicarboxylic acid, was used.

The polycondensations reaction were carried out in bulk employing $Ti(OBu)_4$ as catalyst (about 150 ppm of Ti/g of polymer) in a 250 ml stilled glass reactor, with a thermostated silicon oil bath; temperature and torque were continuously recorded during the polymerization. The prepolymer was obtained according to the usual two-stage polymerization procedure (following the procedure described in par. 3.2.1) To obtain an hydroxyl-terminated prepolymer, the syntheses were carried out for two hours during the second stage (the torque value increased of 2–3 N·cm with respect to that measured at the beginning of the second stage).

The prepolymers obtained were carefully purified by dissolution in chloroform and precipitation in methanol. The samples were then kept under vacuum at room temperature for at least one week to remove the residual solvent.

3.2.3 Random copolymers

3.2.3.1 High molecular weight random copolymers

Random copolymers were synthesized by polycondensation in bulk starting from the appropriate monomers (using from 20% to 40 % mol excess of the glycol with respect to dimethylester or dicarboxylic acid), employing $Ti(OBu)_4$ as catalyst (about 150 ppm of Ti/g of theoretical polymer). The syntheses were carried according to the procedure described above for homopolymers (Chapter 3.2.1). Depending on the synthesized copolymers, different ratios of the two diols or dimethylesters/dicarboxylic acids have been employed in order to obtain copolymers of variable compositions.

Three different classes of random copolymers were synthesized:

- Poly(hexane/triethylene glycol dodecanoate) (P(HDxTEDy))
- Poly(butylene/thiodiethylene glycol succinate) (P(BSxTDGSy))
- Poly(propylene/neopenthyl glycol cyclohexanedicarboxylate) (P(PCExNCEy))

where x and y represent the mol% of the two different comonomeric units. The details on operative conditions of copolymers are reported in Table 3.2 while the chemical structures are reported in Figure 3.6

Table 3.2: Reagents and operating conditions employed for random copolymers syntheses

Polymer	Dicarboxylic acid/esters	Glycols		T1st Stage (°C)	T2nd Stage (°C)
		1	2		
P(HDxTEDy)	DA	HD	TEG	180	250
P(BSxTDGSy)	DMS	1,4-BD	TDG	180	230
P(PCExNCEy)	CHDA	1,3-PD	NPG	180	240

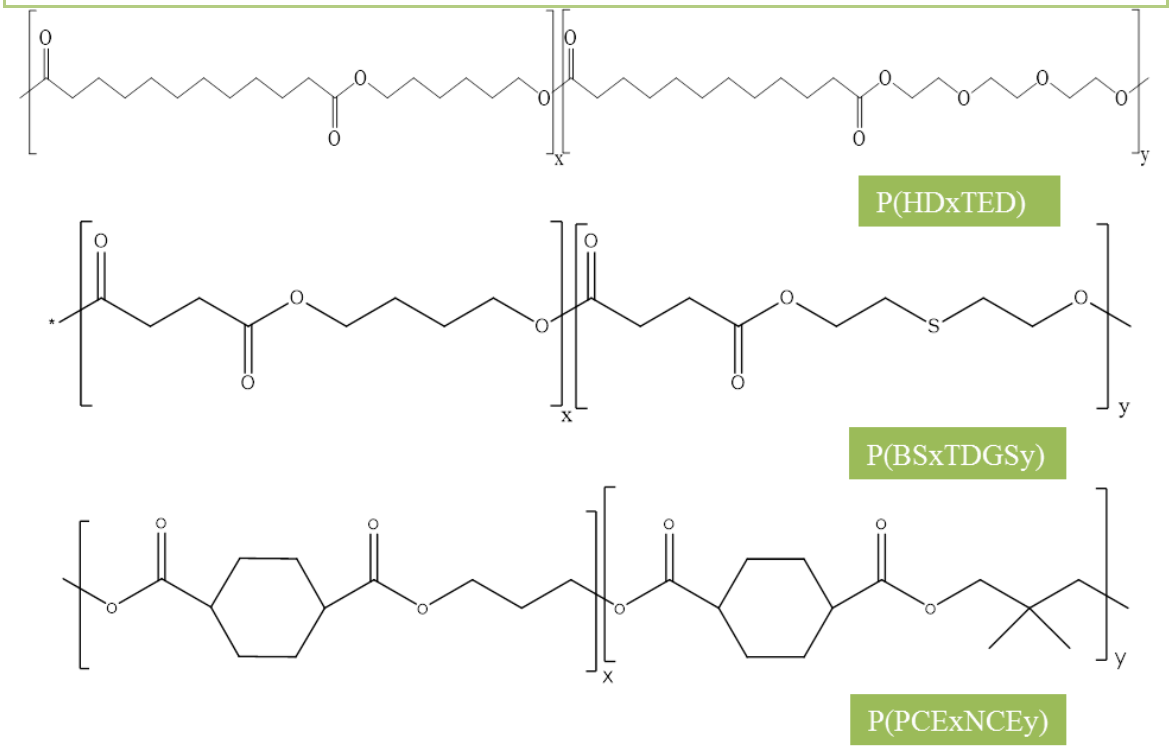

Figure 3.6: chemical structures of synthesized high molecular weight random copolymers.

3.2.3.2Hydroxyl-terminated random copolymers

Hydroxyl-terminated random copolymers were synthesized by polycondensation in bulk starting from the appropriate monomers (using 50-80% mol excess of the glycol with

respect to dimethylester/dicarboxylic acid), employing $Ti(OBu)_4$ as catalyst (about 150 ppm of Ti/g of theoretical polymer). The syntheses were carried according to the procedure described above for hydroxyl-terminated homopolymers (Chapter 4.1.2). Depending on the synthesized copolymers, different ratios of the two diols or dimethylesters/dicarboxylic acids have been employed in order to obtain copolymers of variable compositions.

Two different classes of OH-terminated random copolymers were synthesized:

- poly(propylene/neopentyl glycol succinate) (P(PS80NS20)-OH);
- poly(butylene succinate/diglycolate) (P(BSxBDGy)-OH);

where x and y represent the mol% of the two different comonomeric units. The details on operative conditions of copolymers are reported in Table 3.3, while the chemical structures are reported in Figure 3.7.

Table 3.3: Reagents and operating conditions employed for homopolymers syntheses

Polymer	Dicarboxylic acid/esters		Glycols		T1st Stage (°C)	T2nd Stage (°C)
	1	2	1	2		
P(PS80NS20)-OH	DMS	/	1,3-PD	NPG	180	240
P(BSxBDGy)-OH	DMS	DGA	1,4-BD	/	180	230

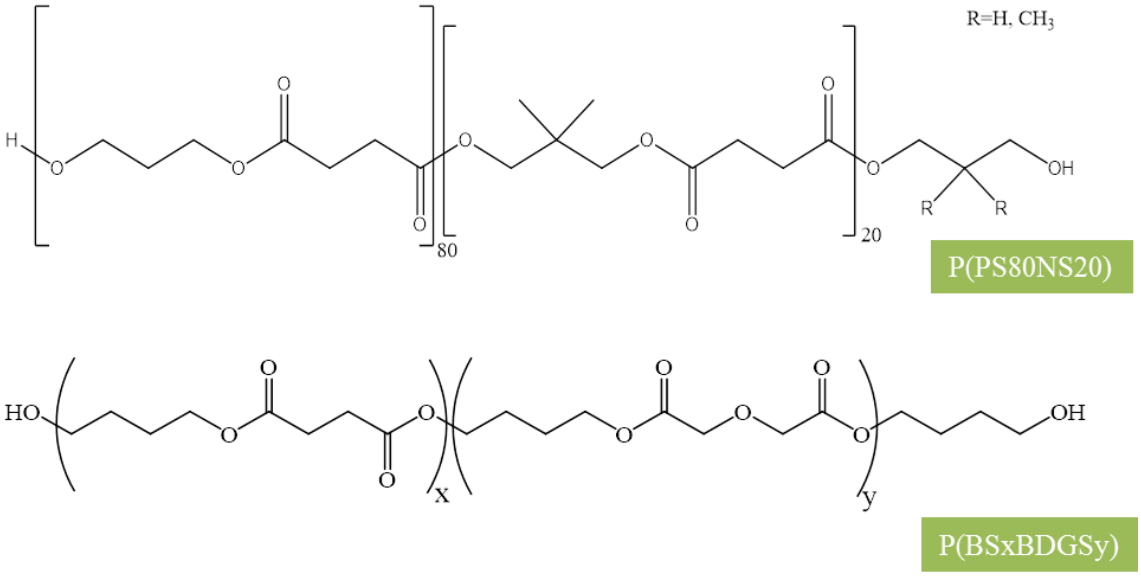

Figure 3.7 : Chemical structures of Hydroxyl-terminated random copolymers

3.2.4 Poly(ester-urethane)'s

3.2.4.1 Triblock copolymers by ROP

An innovative synthetic approach of triblock copolymers A-B-A, where A indicates PLLA blocks (*hard* segments) and B refers to P(PS80NS20) blocks (*soft* segments), was studied. Such new synthetic route involves two stages.

In the first step, P(PS80NS20) prepolymer previously synthesized and purified, was charged into the polymerization reactor, heated to 170 °C and held under inert atmosphere. Once the desired temperature is reached, the indicated amount of L-lactide is added together with the catalyst Sn(II)-2-ethylhexanoate, this latter in an amount of 100 ppm per gram of polymer. During the first phase, which lasts about 3 hours, the *in situ* ring opening polymerization (ROP) of L-lactide by the terminal OH groups of the central P(PS80NS20) takes place, with the consequent formation of PLLA based tri-blocks.

In the second stage, to promote the growth of the molecular weight, hexamethylene diisocyanate (HDI) has been employed as a chain extender. Isocyanate groups of HDI react with terminal hydroxyl groups of PLLA leading to the formation of copoly(esters-urethanes) (PEUs). An equimolar amount of HDI with respect to the -OH groups was used. Their amount was determined by NMR analysis on the prepolymer. During the chain extension stage a sudden increase of the torque value was detected, demonstrating

the formation of urethane links between the triblocks. There were no traces of unreacted HDI after 45 min. After the chain extension process, the PEUs have been purified by dissolution in chloroform and precipitation in methanol. The structure of the final copoly(ester-urethane)s ($PLLA_mP(PS80NS20)_n$) is reported in Figure 3.8.

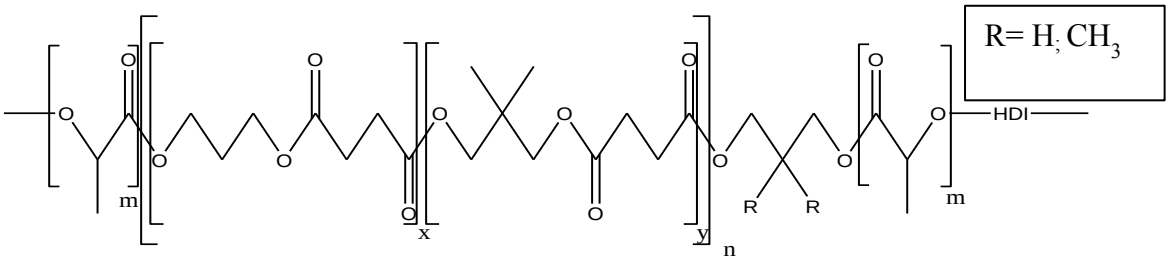

Figure 3.8 Chemical structure of $PLLA_mP(PS80NS20)_n$ triblock copolymers

3.2.4.2 Multiblock copolymers

Multiblock copolymers were synthesized by chain extending PBCE-OH with different amounts of hydroxyl-terminated random copolymers (P(BSxBDGy)-OH).

Chain extension reactions were accomplished in bulk at 170°C, under nitrogen atmosphere, by adding hexamethylene diisocyanate (HDI) to the molten prepolymers. The reactions were carried out until a constant torque was measured (about 45 minutes). An equimolar amount of isocyanate groups with respect to the OH-terminal groups concentration in the prepolymers was considered. During the chain extension stage a sudden increase of the torque value was detected, demonstrating the formation of urethane links between the blocks. There were no traces of unreacted HDI after 45 min. After the chain extension process, the PEUs have been purified by dissolution in chloroform and precipitation in methanol.

Chain extended PBCE homopolymer was also considered for sake of comparison. The structure of multiblock copolymers obtained is reported in Figure 3.9.

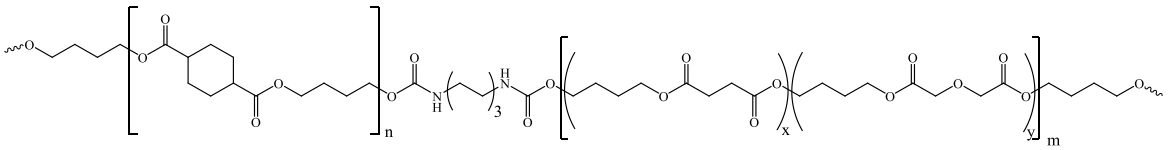

Figure 3.9 Chemical structure of $PBCE_m(PBSxPBDGy)_n$ multiblock copolymers

3.3 Film preparation and thickness determination

Films were obtained by hot pressing the polymers between Teflon sheets in a Carver press for 2 minutes at a temperature T equal to T_m + 40°C. The films were cooled to room temperature in press by using running water. Prior to analyses, the films were stored at room temperature for at least two weeks in order to attain equilibrium crystallinity.

The film thickness was determined using the Sample Thickness Tester DM-G, consisting of a digital indicator (Digital Dial Indicator) connected to a computer. The reading was made twice per second (the tool automatically performs at least three readings), measuring a minimum, a maximum and the average value. The reported results represent the mean value thickness of three experimental tests run at 10 different points on the polymer film surface at room temperature.

3.4 Molecular characterization

3.4.1 Nuclear magnetic resonance (NMR)

The polymer structure and actual copolymer composition were determined by means of ^{1}H-NMR spectroscopy, whereas the distribution of the comonomeric sequences along the polymer chain was evaluated by means of ^{13}C-NMR spectroscopy. The samples were dissolved in chloroform-d solvent with 0.03% (v/v) tetramethylsilane (TMS) added as an internal standard. ^{1}H-NMR spectra were recorded at room temperature for solutions with a polymer concentration of 0.5 wt% (a relaxation delay of 1 s, an acquisition time of 1 s and up to 64 repetitions). ^{13}C-NMR spectra were obtained using 5 wt% solutions and a full decoupling mode with a NOE effect (a relaxation delay of 2 s, an acquisition time of 1 s and up to 512 repetitions). A Varian INOVA 400 MHz instrument was employed for the measurements. Information on the arrangement of the comonomeric units in the main chain of copolymers can be deduced by the degree of randomness b, which has been determined by ^{13}C-NMR spectroscopy. It has to be emphasized that b is equal to 1 for random copolymers, equal to 2 for alternate copolymers, closed to zero for physical blends and between 0 and 1 for block copolymers.

The calculation of b has been carried out taking into consideration the resonance peaks of the carbon atoms of the common subunit between the two comonomeric units (X and Y), so it can be expressed:

$$b = P_{X-Y} + P_{Y-X} \quad \textbf{[25]}$$

where P_{X-Y} and P_{Y-X} are the probability of finding a X unit next to a Y unit and the probability of finding a Y unit next to a Xunit, respectively. The two probabilities can be expressed as:

$$P_{X-Y} = \frac{(I_{X-Y} + I_{Y-X})/2}{(I_{X-Y} + I_{Y-X})/2 + I_{X-X}} \quad [\mathbf{26}]$$

$$P_{Y-X} = \frac{(I_{Y-X} + I_{X-Y})/2}{(I_{Y-X} + I_{X-Y})/2 + I_{Y-Y}} \quad [\mathbf{27}]$$

where I_{X-Y}, I_{Y-X}, I_{X-X} and I_{Y-Y} represent the integrated intensities of the resonance signals of X-Y, Y-X, X-X, and Y-Y sequences, respectively. Additionally, the average length of the sequences of the two different comonomeric units are defined as:

$$L_X = \frac{1}{P_{X-Y}} \quad [\mathbf{28}]$$

$$L_Y = \frac{1}{P_{Y-X}} \quad [\mathbf{29}]$$

3.4.2 Gel permeation chromatography (GPC)

Molecular weight data were obtained by gel-permeation chromatography (GPC) at 30°C using a 1100 Hewlett Packard system equipped with a PL gel 5m MiniMIX-C column (250 mm/4.6 mm length/i.d.) and a refractive index detector. In all cases, chloroform was used as eluent with a 0.3 mL min-1 flow and sample concentrations of about 2 mg mL^{-1} were applied. Polystyrene standards in the range of molecular weight 2000–100000 were used.

3.5 Thermal characterization

3.5.1 Differential scanning calorimetry (DSC)

Calorimetric measurements were carried out by means of a Perkin Elmer DSC7 instrument equipped with a liquid sub ambient accessory and calibrated with high purity standards (indium and cyclohexane). With the aim of measuring the glass transition and the melting temperatures of the polymers under investigation, the external block temperature control was set at -70°C and weighed samples of c.a. 10 mg were encapsulated in aluminum pans and heated to about 40°C above fusion temperature at a rate of 20°C/min (first scan), held there for 3 min, and then rapidly quenched (about 100°C/min) to -70°C. Finally, they were reheated from -70°C to a temperature well above the melting point of the sample at a heating rate of 20°C/min (second scan). The glass-transition temperature Tg was taken as the midpoint of the heat capacity increment ΔCp associated with the glass-to-rubber transition. The melting temperature ™ and the crystallization temperature (Tc) were determined as the peak value of the endothermal and the exothermal phenomena in the DSC curve, respectively. When multiple endotherms were observed, the highest peak temperature was taken as Tm. The specific heat increment Δcp, associated with the glass transition of the amorphous phase, was calculated from the vertical distance between the two extrapolated baselines at the glass transition temperature. The heat of fusion (ΔHm) and the heat of crystallization (ΔHc) of the crystal phase were calculated from the total areas of the DSC endotherm and exotherm, respectively. In order to determine the crystallization rate under non-isothermal conditions, the samples were heated at 20°C/min to about 40°C above fusion temperature, kept there for 3 min and then cooled at 5°C/min. The temperature corresponding to the maximum of the exothermic peak in the DSC cooling-curve (Tcc) can be correlated to the crystallization rate. At least five replicates were run for each sample.

3.5.2 Thermogravimetric Analysis (TGA)

Thermogravimetric analysis was carried out both in air and under nitrogen atmosphere using a Perkin Elmer TGA7 apparatus (gas flow: 30 mL/min) at 10°C/min heating rate up to 900 °C. The procedure suggested by the supplier was followed for the temperature

calibration of equipment. This method is based on the change of the magnetic properties of two metal samples (Nickel and Perkalloy) at their Curie points (354.0 and 596.0°C, respectively).

3.5.3 Dynamic Mechanical Thermal Analysis (DMTA)

Suitable specimens for dynamic mechanical measurements were obtained by injection moulding in a Mini Max Molder (Custom Scientific Instruments), supplied with a rectangular mould (30x8x1.6 mm). Immediately after moulding, samples were quenched in liquid nitrogen and then stored in a desiccator under vacuum for 1 month prior analysis.

Dynamic mechanical measurements were performed with a dynamic mechanical thermal analyser (Rheometric Scientific, DMTA IV), operated in the dual cantilever bending mode, at a frequency of 3Hz and a heating rate of 3°C/min, over a temperature range from -150 to T_{final}, which changes according to the polyester analysed.

3.6 Structural characterization

X-ray diffraction patterns were obtained with CuK_α radiation in reflection mode by means of an X'Pert PANalytical diffractometer equipped with a fast X' Celerator detector, 0.1° step, 100s /step. The samples were 65nalysed in form of films. The indices of crystallinity (χ_c) were calculated from the X-ray diffraction profiles by the ratio between the crystalline diffraction area (A_c) and the total area of the diffraction profile (A_t), $X_c = A_c/A_t$. The crystalline diffraction area was obtained from the total area of the diffraction profile by subtracting the amorphous halo. The incoherent scattering was taken into consideration. The length of the coherent domains along the *b*-axis (L_{020}) was evaluated from the line broadening of the 0 2 0 reflection from the widths at half maximum intensity ($b_{1/2}$) by using the Scherrer equation [Klug & Alexander, 1974]: $L_{020} = K\lambda / b_{1/2}\cos\theta$ where λ is the wavelength, θ the diffraction angle and K a constant depending on crystal habit (chosen as 1.0). The silicon standard peak 111 was used to evaluate the instrumental broadening.

3.7 Surface wettability

Static contact angle measurements were performed on polymer films by using a KSV CAM101 instrument (Helsinki, Finland) at ambient conditions by recording the side profiles of deionized water drops for image analysis. Eight drops were observed on different areas for each film and contact angles were reported as the average value ± standard deviation. Each drop was deposited on the films by placing it in contact with the polymeric surface using the syringe needle and then withdrawing this last. The data were recorded after 5 second from the deposition of the drop upon the polymer surface.

3.8 Mechanical characterization

The tensile testing of the copolymers was performed on rectangular films (5 mm wide and 0.2 mm thick) with a crosshead speed of 50 mm/min by using a Zwick Roell Texture machine mod. Z2.5, equipped with a rubber grip and a 500 N load cell. A preload of 1 Mpa (preload speed: 5 mm/min, waiting time at preload: 30 s) was applied to the specimen before testing. At least five replicates were run for each sample and the results were provided as the average ± standard deviation.

Cycling loading was performed under the same experimental conditions. Film samples were strained to 50%. Tests were run in two steps. First, 25 cycles were made, followed by 48 h of recovery. After this time, 5 more cycles were carried out.

3.9 Dielectric characterization

Complex dielectric permittivity measurements ($\varepsilon^* = \varepsilon' - i\varepsilon''$) were performed over a frequency range of $10^{-1} < F < 10^{7}$ Hz in a temperature range from T= -150 to T_{final}, which changes according to the polyester analysed.

A Novocontrol system integrating an ALPHA dielectric interface was employed. The temperature was controlled by means of a nitrogen gas jet (QUATRO from Novocontrol) with a temperature error of (0.1 during every single sweep in frequency). P(PCExNCEy) films were sandwiched between the two metallic electrodes of the spectrometer. No gold evaporated/sputtered electrodes were used in order to eliminate the risk of damaging the sample.

The dielectric relaxations were empirical described in terms of the Havriliak-Negami (HN) equation:

$$\varepsilon^* = \varepsilon_\infty + \frac{\varepsilon_0 - \varepsilon_\infty}{\left[1+(i\omega\tau)^b\right]^c} \qquad \textbf{[30]}$$

Where ε_0 and ε_∞ are the relaxed (ω = 0) and unrelaxed (ω = ∞) dielectric constant values, τ is the central relaxation time of the relaxation time distribution function, and b and c ($0 < b, c < 1$) are shape parameters which describe the symmetric and the asymmetric broadening of the relaxation time distribution function, respectively [Havriliak & Negami, 1967]. An additional contribution of the conductivity process was taken into account by adding a term $-i(\sigma/(\varepsilon_{vac}\omega))^s$ to equation 30. Conductivity is usually associated with generation and transport of polarization-induced charges through the polymer under the action of an electric field. Here σ is related to the direct current electrical conductivity, ε_{vac} is the dielectric constant of vacuum, and the value of the coefficient $0 < s < 1$ depends on the conduction mechanism [Kremer & Schonhals, 2002].

More precisely, the experimental data were analysed using different approaches depending on the studied temperature range. Under the T_g, the relaxation spectrum was interpreted as due to local modes (β processes), in this view we have employed the Cole-Cole (CC) analysis (Equation 1 with $c = 1$). When the α relaxation appears in the experimental frequency window ($T > T_g$), the dielectric loss spectrum is described as a superposition of one CC function (β relaxation) to one HN (α relaxation).

3.10 Barrier properties evaluation

Barrier properties evaluation of the polymers investigated in the present work has been conducted in the labs of Agri-food Science and Technology Department, University of Bologna, thanks to the scientific cooperation with Prof. Valentina Siracusa. The permeability determination was performed by a manometric method using a Permeance Testing Device type GDP-C (Brugger Feinmechanik GmbH), according to ASTM 1434-82 (Standard test Method for Determining Gas Permeability Characteristics of Plastic Film and Sheeting), DIN 53 536 in compliance with ISO/DIS 15 105-1 and

according to Gas Permeability Testing Manual, Registergericht München HRB 77020, Brugger Feinmechanik GmbH. The equipment consists of two chambers between which the film is placed. The chamber on the film is filled with the gas used in the test (CO_2, O_2, N_2, N_2O, C_2H_4) at a pressure of 1 atm. A pressure transducer, set in the chamber below the film, records the increasing of gas pressure as a function of the time. From pressure/time plot the software automatically calculates permeation which, known the film thickness, can be converted in permeability. The film sample was placed between the top and the bottom of the permeation cell. The gas transmission rate (GTR), i.e. the value of the film permeability to gas, was determined considering the increase in pressure in relation to the time and the volume of the device. The pressure is given by the instrument in bar units. To obtain the data value in kPa, the primary SI units, it is necessary to use the following correction factor: 1 bar = 10 kPa, according to NIST special publication 811 [Thompson &Taylor, 2008]. Time lag (t_L), diffusion coefficient (D), and solubility (S) of the tested gases were measured according to the mathematical relations reported in literature [Mrkic *et al*., 2006;]. Fluctuation of the ambient temperature during the test was controlled by special software with an automatic temperature compensation, which minimizes gas transmission rate (GTR) deviations. All the measurements have been carried out at 23 °C, with a relative humidity (RH) of 26%. The operative conditions were: gas stream of 100 $cm^3 \cdot min^{-1}$; 0% gas RH; sample area of 11.34 cm^2. The sample temperature was set by an external thermostat HAAKE-Circulator DC10-K15 type (Thermoscientific, Selangor Darul Ehsan, Malaysia). Method A was employed in the analysis, as just reported in the literature with evacuation of top/bottom chambers [Siracusa et al., 2012; Gas Permeability Testing Manual, Registergericht Munchen HRB 77020, Brugger Feinmechanik GmbH, 2008]. Permeability measurements were performed at least in triplicate and the mean value plus standard deviation is presented.

3.11 Photo and thermo ageing

The samples were exposed to thermal and photo degradation, simulating respectively the ageing process and the exposition to supermarket light.

Thermal ageing was performed by a Constant Climate Chambers with Peltier Technology, model HPP 108/749 (Memmert GmbH + Co. KG, Schwabach, Germany),

at 40°C and 50% of relative humidity (RH). The photo degradation was carried out by exposing the polymer film sample to a Philips fluorescent Tube TL-D 18W/33-640 1SL cool white (4100 K color temperature, 63 Ra8 CRI Index, 1200 Lumen) at 23 °C (ambient temperature) and 50% of relative humidity. The light exposer is a homemade instrument, inclusive of a temperature and light manual controller. Times of exposition ranged from 0 to 40 days. Film samples were exposed at a distance of about 30 cm.

3.12 Interaction with food simulant fluids

The food contact simulation was performed in accordance with Regulation (EC) No 1935/2004 of the European parliament and of the council of 27 October 2004 on materials and articles intended to come into contact with food and in accordance with the Union Guidelines Regulation (EU) No 10/2011 on plastic materials and articles intended to come into contact with food [Regulation (EC) No 1935/2004; Regulation (EU) No 10/2011]. Four substances were used as food simulants:

- ✓ Simulant A, distilled water, at 40°C for 10 days (DW);
- ✓ Simulant B, Acetic Acid 3%v/v, at 40°C for 10 days (AA);
- ✓ Simulant C, Ethanol 10% v/v, at 40°C for 10 days (EtOH);
- ✓ Simulant D, Isooctane at 20°C for 2 days (i-O).

The test time simulated the extreme contact conditions between the packaging and the product. The measurement was made by total immersion of film specimen of about 8x8 cm. 100 ml of simulant was placed into 150 ml glass flasks containing the specimens; the flasks were then covered with caps. At the end of the test, the samples were removed from the flasks, washed with distilled water two times and dried with blotting paper. Before analysis, the films were kept in dry ambient at room temperature for at least two weeks in order to attain equilibrium crystallinity. All the experiments were run in triplicate.

3.13 Composting experiments

Degradation tests were performed at different temperatures, depending on the thermal behavior of the analyzed polymers. Each polyester film (diameter of 16 mm, 0.2 mm thick) was placed in darkened vessels and sandwiched between two layers of compost (20 g each). Finally, 10 ml of deionized water were added.

Home-made compost was prepared (to test P(HDxTEDy) and P(BSxTDGSy) copolymers) by means of an automatic composter (NatureMill, San Francisco, CA): organic waste fraction was collected, cultured in the composter for three weeks, and then transferred in the cure chamber for at least four weeks prior to use.

The compost used to test $PLLA_mP(PS80NS20)_n$ and $PBCE_mP(BSxBDGy)_n$ degradation rate was kindly provided by "Nuova Geovis S.p.A." (HERA group, Sant'Agata Bolognese). Three different variety of compost, have been used for the study of $PLLA_mP(PS80NS20)_n$ system: food craps, mature food scraps and mature compost; while PBCEmP(BSxBDGy)n system was tested directly in mature compost.

3.13.1 Film weight loss analyses

Prior to degradation experiments, each specimen was immersed in a 70% ethanol solution for 10 min, washed repeatedly with deionized water and placed over P_2O_5 under vacuum at room temperature to constant weight (at least 24 h). Lastly, each sample was weighed to obtain the initial mass. At different time intervals, duplicate sacrificial specimens of each sample were recovered from the compost and washed according to the following procedure to remove microbial cells adhered on the film:

- ✓ immersion in a 2% SDS solution at 50°C for 2 h;
- ✓ repeated washing with 70% ethanol (3x);
- ✓ immersion in 70% ethanol and stirring at 120 rpm, then storing at RT for 10 min;
- ✓ repeated washing with deionized water (3x);
- ✓ drying over P_2O_5 under vacuum for 2 days to constant weight.

The mass loss was then gravimetrically determined by comparing the residual dry weight with the initial value.

3.13.2 Scanning electron microscopy (SEM)

SEM images were acquired on a desktop Phenom microscope on metal sputtered film samples glued with carbon tape on aluminum stabs.

4.

RESULTS AND DISCUSSION

4. RESULTS AND DISCUSSION

4.1 Biodegradable Long Chain Aliphatic Polyesters Containing Ether Linkages

Poly(hexane dodecanoate) (PHD) based random copolyesters containing ether-linkages (P(HDxTEDy)) have been synthesized and characterized from the molecular and thermomechanical point of view. Gas permeability and biodegradability in compost have been also evaluated.

Moreover, in order to get a better understanding on the possible application of these novel materials for food packaging applications, deeper analysis have been here performed. The contact with food has been simulated by the use of four liquids, in accordance with international regulations [Regulation (EC) No 1935/2004; Regulation (EU) No 10/2011]. In addition, a stressed treatment, by thermal and photo exposition, has been carried out. The temperatures selected for the ageing experiments are those suggested in the literature, as the most suitable for accelerated tests on food [Robertson, 2006]. The relative humidity was chosen as an average of the values recorded inside a supermarket within a solar year [Robertson, 2006], and as the value with less influence on food oxidation rate [Lu & Xu, 2009].

Physic/mechanical and barrier properties of the polymers under investigation have been analyzed before and after the treatments to verify possible decays of the materials' characteristics. In particular, the gas transmission behavior is of crucial interest. Barrier properties to different gases (O_2 and CO_2) have been evaluated, and the relations binding the diffusion coefficients (D) and solubility (S) with copolymer composition have been investigated..

4.1.1 Synthesis and molecular characterization

PHD and PTED random homopolymers and their copolymers have been synthetized following the procedure described in paragraph 3.2.1 and 3.2.3.1 respectively. At room temperature, all the synthesized polyesters appear as semicrystalline light yellow solids. The chemical structures of the two parent homopolymers are reported in Figure 4.1; on other hand Table 4.1 collects the data of molecular characterization of PHD, PTED and P(HDxTEDy) copolymers.

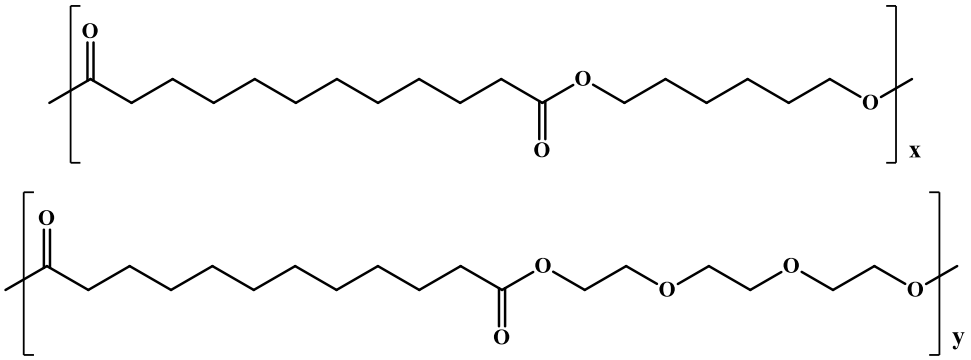

Figure 4.1. Chemical structures of PHD (above) and PTED (below).

All the polyesters under investigation are characterized by relatively high and similar molecular weights, indicating that appropriate synthesis conditions and a good polymerization control were achieved. ^{1}H-NMR analysis confirmed the awaited structures (see as an example the ^{1}H-NMR spectrum of P(HD55TED45) shown in Figure 4.2).

Table 4.1. Molecular characterization data and film thickness of PHD, PTED and P(HDxTEDy) copolymers.

Polymer	M_n	D	TED (mol %) ^{1}H-NMR	Thickness (μm)
PHD	47900	2.1	0	144±19
P(HD85TED15)	58900	2.1	13	185±6
P(HD70TED30)	58500	2.4	30	192±45
P(HD55TED45)	52200	2.4	45	148±19
PTED	50200	2.5	100	167±13

The copolymer composition, calculated from the relative areas of the ^{1}H-NMR resonance peak of the d aliphatic protons of the hexanediol subunit located at 4.06 ppm and of the g protons of the methylene groups of the triethylene glycol subunit at 4.23 ppm, is close to the feed one (see Table 4.1).

Because of the high temperature adopted in the polycondensation process and of the catalyst employed ($Ti(OBu)_4$), which both favour the transesterification reactions, the arrangement of the comonomeric units along the chain follows a random distribution.

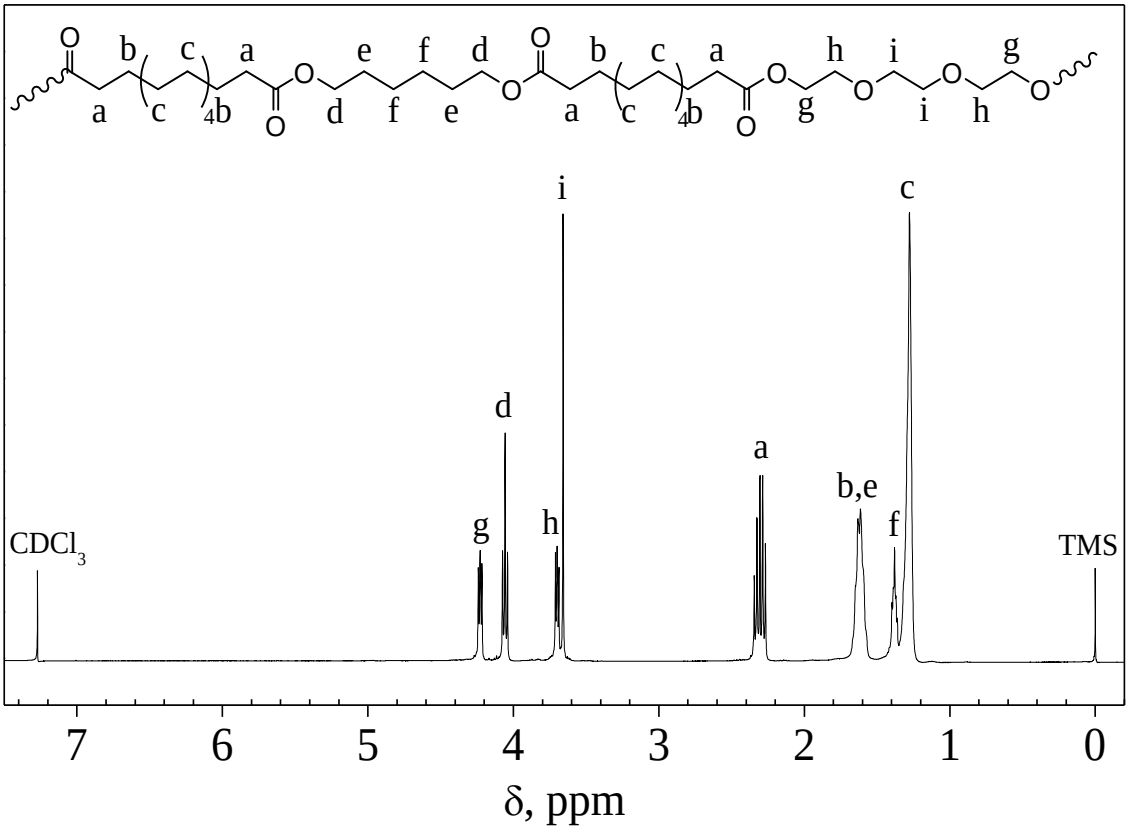

Figure 4.2. ^{1}H-NMR spectra of P(HD55TED45) with resonance assignments.

4.1.2 Thermal and structural characterization

The synthesized polyesters have been subjected to thermogravimetric analysis, and the temperature corresponding to 5% weight loss ($T_{5\%\ w.loss}$) and the temperature corresponding to the maximum weight loss rate (T_{max}) were determined and collected in Table 4.2.

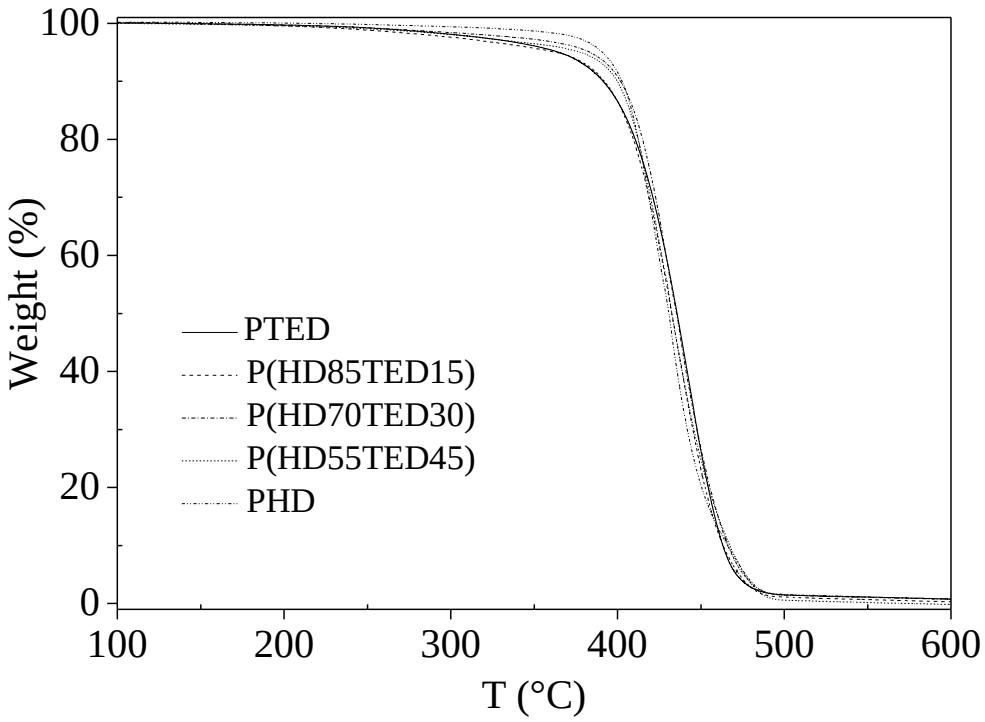

Figure 4.3. Thermogravimetric curves of PHD, PTED and P(HDxTEDy) copolymers under nitrogen atmosphere.

As can be evicted from Figure 4.3, the weight loss took place in one step, and all the synthesized polymers are characterized by a good thermal stability ($T_{5\%\ w.loss}$ ranges from 365 to 391°C), which clearly correlates with the copolymer composition (see Table 4.2): as a matter of fact, the thermal stability regularly decreases with the increase of TED unit content. The trend observed is in agreement with the data reported in the literature [Zimmermann, 1984]: in fact, as it is well known, ether linkages can favor thermo-oxidative degradation processes.

It is well established that the melting behaviour of a polymer is affected by its previous thermal history; therefore, as mentioned above, in order to provide the same heat treatments to all the samples investigated, prior to thermal analysis each film was kept at room temperature for two weeks. DSC traces of so-treated samples are reported in Figure 4.4a and the data obtained in Table 4.2.

Table 4.2. Thermal and diffractometric characterization data and water contact angles for PHD, PTED and P(HDxTEDy) copolymers.

Polymer	$T_{5\%\ w.loss}$ (°C)	T_{max} (°C)	T_m (°C)	ΔH_m (J/g)	T_{cc} (°C)	χ_c (%)	L_{max} (nm)	WCA (°)
PHD	391	432	76	79	59	55±2	24	88±2
P(HD85TED15)	383	433	71	75	53	50±3	28	86±2
P(HD70TED30)	378	435	59	71	44	45±3	28	84±3
P(HD55TED45)	363	437	54	66	35	40±2	30	80±3
PTED	365	443	43	55	26	37±2	9	78±2

All the polymers under investigation are characterized by the same phase behaviour: in particular, all of them are semicrystalline, being the corresponding calorimetric traces characterized by a conspicuous melting endotherm (see Table 4.2). Anyway, the T_m of PTED (T_m = 43°C) is much lower than that of PHD (T_m = 76°C). As far as the P(HDxTEDy) copolymers are concerned, the peak location appears to depend on copolymer composition and, as expected, the higher the TED unit content in the copolymers, the lower the melting temperature and the heat of fusion (see Table 4.2). Such trend can be explained on the basis of the significant reduction of the perfection of crystalline phase, which is strongly affected by the regularity of the polymeric chain, that is drastically reduced in P(HDxTEDy) copolymers, and above all in PTED, by the introduction of ether-oxygen atoms along the PHD polymer chains (van der Waals volume of oxygen atom, 7.36 $Å^3$, is indeed significantly lower than that of the neighbor $–CH_2–$ groups, 16.27 $Å^3$).

To confirm that in the copolymers the tendency to crystallize decreases as the content of TED co-units is increased (up to 100% in the case of PTED homopolymer), non-isothermal experiments were carried out, subjecting the samples to a controlled cooling rate from the melt. It is worth remembering that the half-time of primary crystallization in isothermal experiments correlates with the temperature of the maximum of the crystallization peaks in non-isothermal experiments (T_{cc}), [Legras et al., 1986] being this latter more easily obtainable. The exothermic crystallization peaks of the samples under investigation are shown in Figure 4b. It can be observed that the temperature of the maximum of the exothermal crystallization peak regularly decreases as the TED unit content is increased (Table 4.2). This fact indicates a decrement of the overall

crystallization rate of PHD, due to the presence of co-units which act as obstacles in the regular packing of polymer chains.

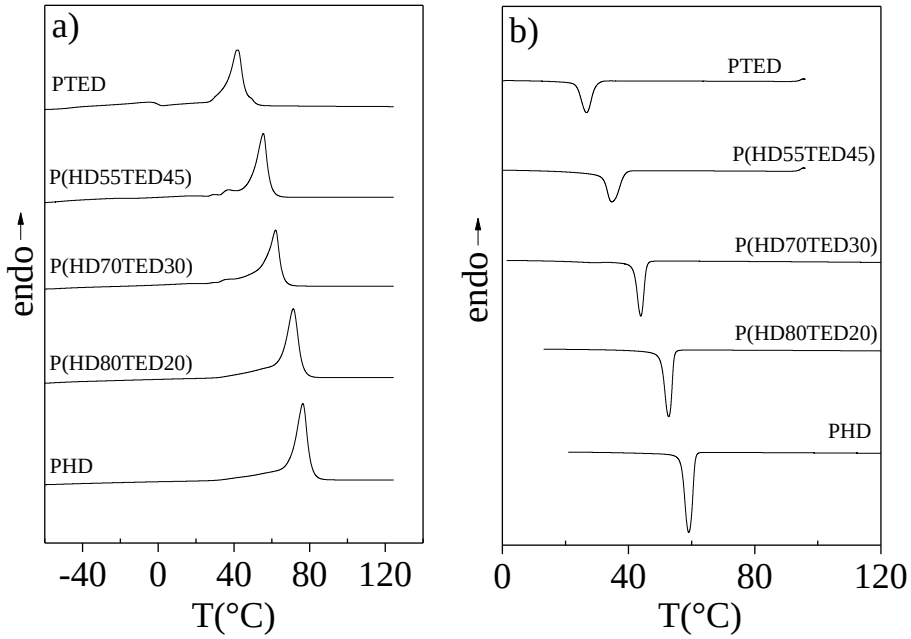

Figure 4.4. Calorimetric curves of PHD, PTED and P(HDxTEDy) copolymers: (a) 1st scan, (b) cooling from the melt.

As to the T_g, the endothermal baseline shift related to the glass transition phenomenon is not well observable, due to the high amount of crystal phase present in the samples, even after melt quenching, conducted in order to limit their crystallinity degree (results not shown).

To better understand the nature of the crystalline phase present in the polymers under investigation, the structural characterization was carried out by X-ray diffraction. The patterns are reported in Figure 4.5 (curves A-E). The profile of PHD shows two intense peaks at 21.3° and 24.2° (2θ) and less intense others at 30.0, 35.3, 40.8 and 43.3°; two broad reflections of low intensity are present at 8.9 and 7.4°. On the other hand, PTED showed a different pattern with broader reflections, the most intense being at 21.3 and 24.3°, others at 25.2, 30.0° and in the small angle region at 4.2 and 7.7° (see Figure 4.5b). The profiles of the two homopolymers are different enough to state they belong to two different crystal structures.

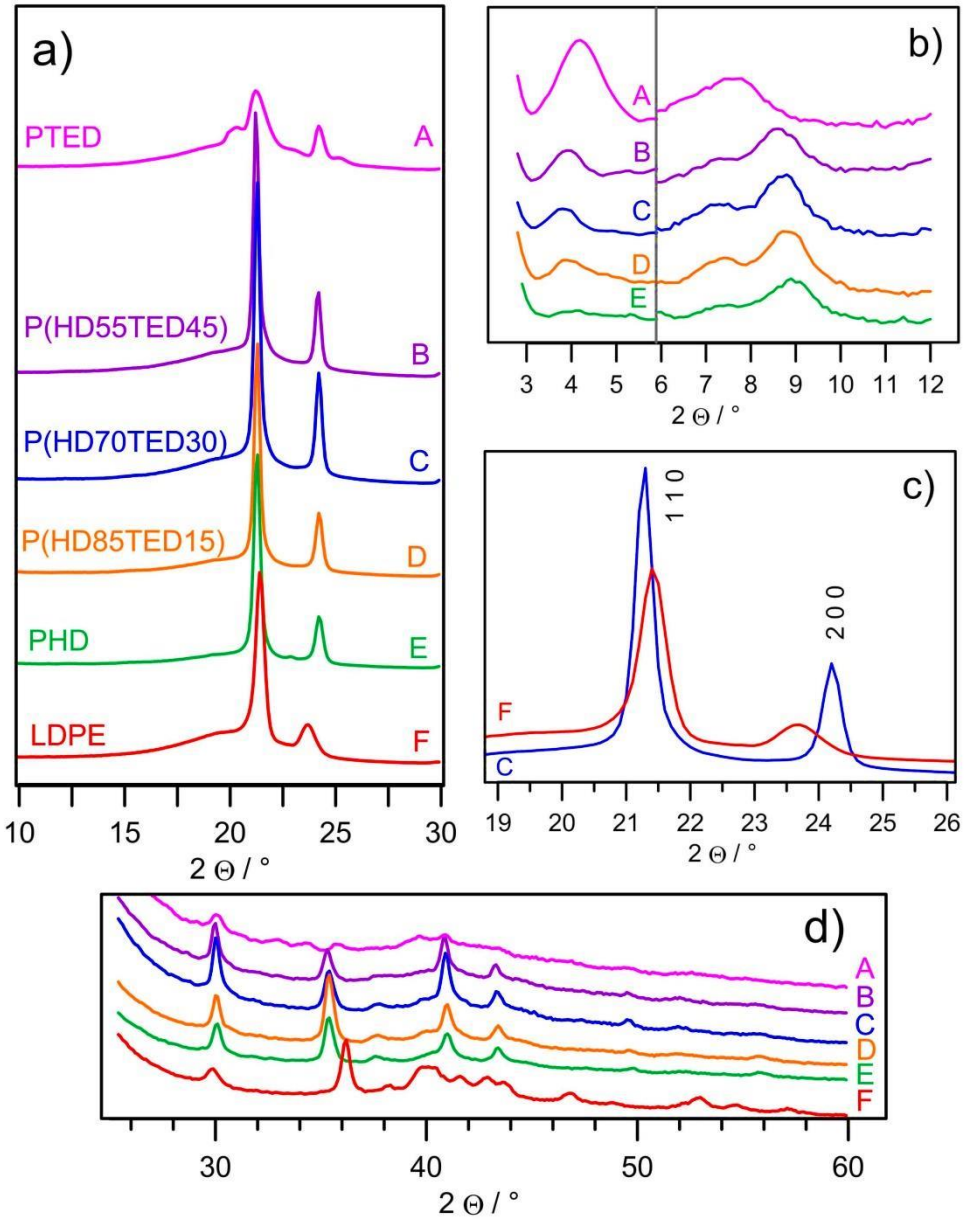

Figure 4.5. X-ray diffraction patterns of PHD, PTED, P(HDxTEDy) copolymers and LDPE. a) and d) show wide angle regions, in d) the intensities are 11 times magnified. b) displays the small angle region; different experimental setups were used in the two sides of the d) picture in order to enhance small angle reflections.

All the copolymers showed patterns very similar to the PHD one, but with the addition of a low intense small angle reflection. No changes in the reflection positions were observed as a function of the composition. In addition, the wide angle patterns of PHD and P(HDxTEDy) copolymers resemble very much the LDPE one (Figure 4.5, curve F). Taking this consideration into account, it is possible to hypothesize that the macromolecular chains are in a 'all trans' conformation with a lateral packing as in

orthorhombic polyethylene, as previously reported for several aliphatic polyesters [Chatani et al., 1970; Gazzano et al., 2003]. As a consequence, the two main reflections can be indexed as *1 1 0* and *2 0 0*, and the cell parameters in the plane perpendicular to chain axis, calculated over the position of several peaks, are: *a*=7.506Å, *b*=4.966Å and *a*=7.346Å, *b*=5.066Å for LDPE and P(HDxTEDy) copolymers, respectively. A little mismatch in the cell dimensions, due to the different directions of peak shifts, is present; however, the product, that is the area of the cell section perpendicular to the chain axis, remains constant. As an example, Figure 4.5c shows an enlarged view of the P(HD70TED30) and LDPE patterns: by comparing the two profiles it is clearly visible that the LDPE *1 1 0* reflection moves toward higher angular values (shorter distances), while *2 0 0* shifts in the opposite direction. The measured parameters values are slightly bigger than those reported for high crystalline PE, but well fit those of polyesters packing in a PE-like manner [Gazzano et al., 2003].

The intensity of the small angle reflection at 4.2° (d= 2.1 nm) in PTED and at 3.9° (d= 2.3 nm) in the copolymeric samples, reduces and slightly shifts to bigger distance with the increasing of the HD molar%. This behavior suggests that a certain degree of disorder is introduced in the chain repetition by the presence of HD counits, which lower the chain regularity along the main axis.

The extimated length of the PTED repeating unit is around 2.9 nm. Morevoer, the presence of the reflection at a shorter distance value suggests the inclination of the macromolecular chains cell axis with respect to the *ab* plane.

As reported in Table 4.2, the crystallinity of the samples decreases as the content of TED units increases, but the average domain size (L_{max}), estimated from the width of the main diffraction peak, is larger in the copolymers with respect to the PHD.

4.1.3 Wettability and mechanical properties

In order to investigate the relative hydrophilicity of polymeric films under study, water contact angle (WCA) measurements have been performed. It has to be pointed out that surface wettability reflects surface hydrophilicity but, in the present case, it cannot be directly correlated with bulk material hydrophilicity. Table 4.2 reports the contact angle values for each polymer. Data showed that PHD was the most hydrophobic material (WCA = 88°) while PTED displayed the highest hydrophilicity (WCA = 78°): this

result can be explained on the basis of the the presence along the polymeric chain of PTED of highly electronegative ether-oxygen atoms.

In addition, the copolymer wettability, in all cases between those of the two homopolymers, seems to be affected by the copolymer composition: a slight increase of hydrophilicity can be observed with the increasing of the TED mol%. In Figure 4.6 the water drops deposited on some of the polymeric films under study are reported as an example.

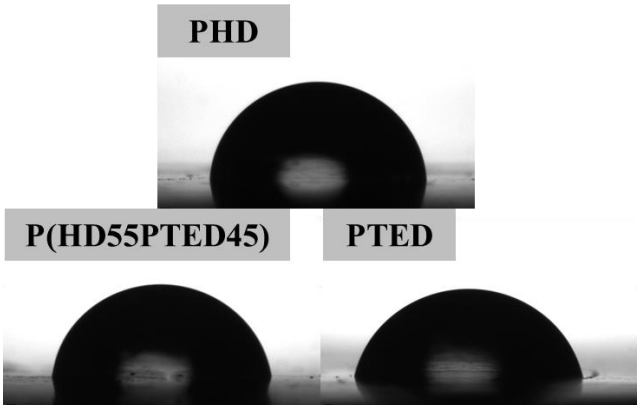

Figure 4.6. Water drops on the polymeric film surface of PHD, P(HD55TED45) and PTED.

The mechanical properties of PHD, PTED and P(HDxTEDy) copolymers were investigated subjecting the samples to stress-strain measurements. Table 4.3 reports their corresponding mechanical data: elastic modulus (E), stress and deformation at yield (σ_y and ε_y, respectively) and stress and deformation at break (σ_b and ε_b, respectively).

Table 4.3. Mechanical characterization data of PHD, PTED and P(HDxTEDy) copolymers.

Polymer	E (MPa)	σ_y (MPa)	ε_y (%)	σ_b (MPa)	ε_b (%)
PHD	400 ± 21	17.2 ± 0.5	12 ± 1	15.8 ± 0.7	80 ± 6
P(HD85TED15)	361 ± 6	18.0 ± 0.9	12 ± 1	15.6 ± 0.9	742 ± 67
P(HD70TED30)	246 ± 13	10.5 ± 0.7	14 ± 2	13.9 ± 0.2	907 ± 56
P(HD55TED45)	222 ±9	9.6 ± 0.5	15 ± 2	10.0 ± 0.4	842 ± 23
PTED	201 ± 7	13.6 ± 0.5	16 ± 1	19.8 ± 1.5	856 ± 81

Among the synthesized polyesters, the elastic modulus is strictly dependent on the copolymer composition: as a matter of fact elastic modulus regularly decreases as TED

unit content is increased, from the maximum of 400 MPa (PHD) to a minimum of 200 MPa in the case of PTED (see inset of Figure 4.7). In all the polymers under investigation, the yield phenomenon is present, and with the exception of PHD, all the polyesters showed very high elongation to break, above 700% (Table 4.3 and Figure 4.7).

Since all the investigated polymers display a soft amorphous phase (T_g values are well below room temperature), the observed trend can be ascribed to two effects: changes in copolymer composition and in crystallinity degree (see Table 4.2). In conclusion, PHD is the stiffest materials among those under study, while the mechanical properties of the copolymers render them really promising for the realization of packaging flexible films.

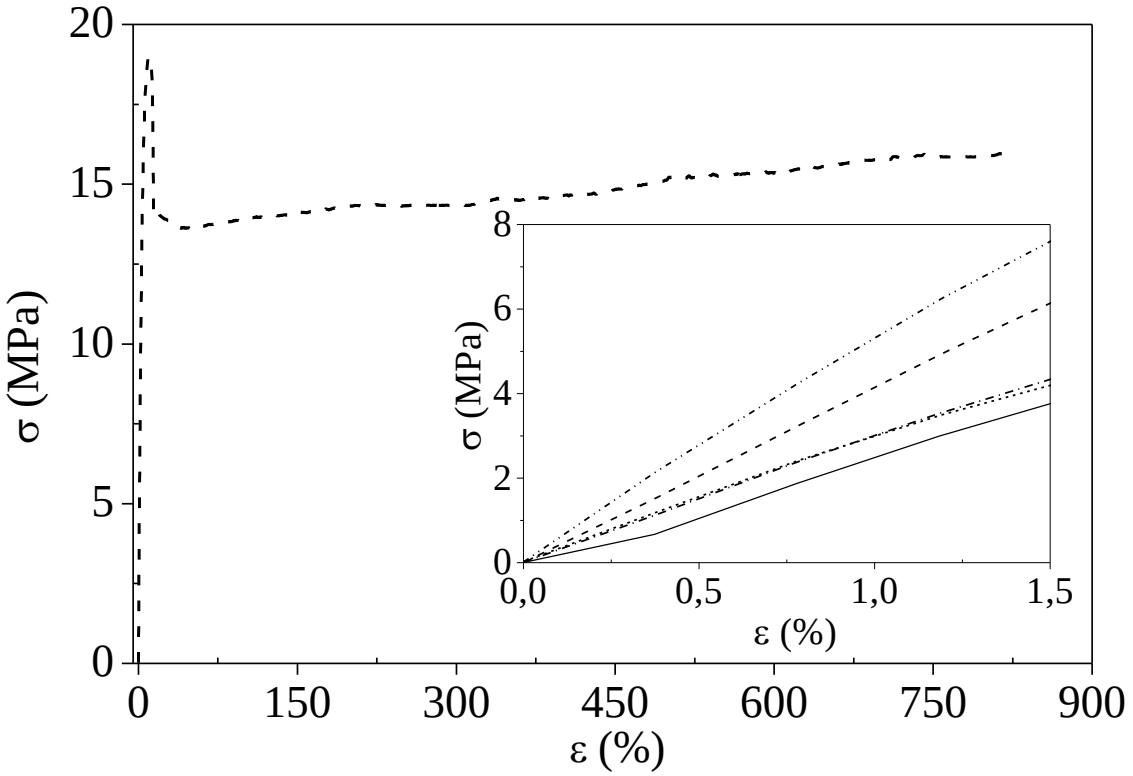

Figure 4.7. Stress-strain curve of P(HD85TED15). In the inset: enlarged zone of the initial linear portion of the stress-strain curve: PHD, dash dot dot; P(HD85TED15), dash; P(HD70TED30), dash dot; P(HD55TED45), short dash; PTED, solid.

4.1.4 Barrier properties

Carbon dioxide and oxygen are the main permeating agents studied in packaging applications because they may transfer from or to the environment through the polymer package wall, continuously influencing the product quality and durability.

The gas permeation through a polymer is described by a diffusion model, by means of Henry and Fick's laws. The Transmission Rate (TR) of the material can be deduced from [31]:

$$TR = Q / At \quad \textbf{[31]}$$

where Q is the amount of permeant passing through the film (cm^3), A is the sample area (cm^2) and *t* is the time (days).

Permeability measurements were carried out on the polymeric films of a measured thickness. Gas Transmission Rate (GTR), time Lag (t_L), Diffusion coefficient (*D*) and Solubility (*S*), reported in Table 4.4 and Table 4.5 for O_2 and CO_2 pure gas, respectively are well described in the literature [Robertson 1993; Mrkic et al., 2006; Lee and al., 2008].

Another interesting parameter is the permeability ratio (also called selectivity ratio) between O_2 and CO_2 gases: it permits to determine the permeability on respect to a gas knowing the permeability behavior on respect to the other one under the same experimental conditions.

Although molecular size of permeating species could affect the transmission speed, in the case of O_2 and CO_2 there is no relationship between gas molecular size and permeability behavior. In fact, CO_2 is more permeable with respect to O_2, despite its molecular diameter (3.4 Å) is greater than that of oxygen molecules (3.1 Å) [Gigli et al., 2013 (b)].

High crystalline polymers usually possess low permeability to both O_2 and CO_2 gas; moreover, a high dependence of the permeability behavior on the crystalline/amorphous ratio can be expected. This is because, as already reported [Kofinas et al., 1994], gas molecules are unable to permeate the polymer crystallites, being insoluble into the material. The gas permeation into semicrystalline polymers is then confined to the amorphous regions. Theoretically, the permeability increment is therefore proportional with the volume fraction of the amorphous phase.

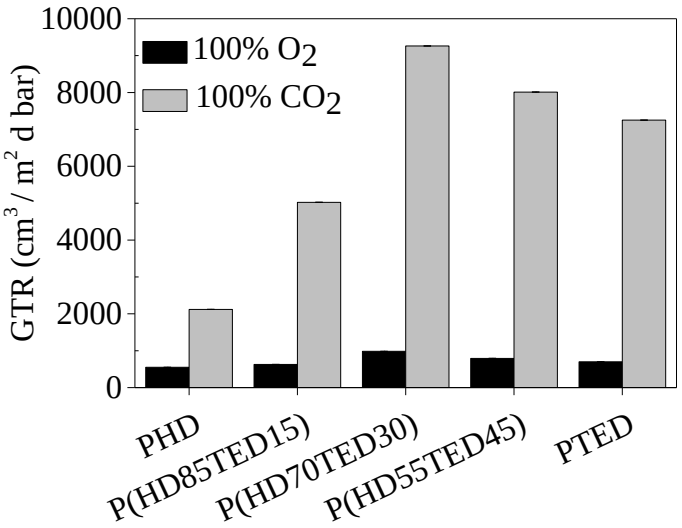

Figure 4.8. Gas transmission rate of O_2 and CO_2 for PHD, PTED, P(HDxTEDy) copolymers.

In real cases, anyway, the permeation process does not show a Fickian behavior, where a linear relationship is obtained; many other factors can in fact influence the barrier properties, such as the interaction between permeate and polymer, which is correlated to the polymer chemical structure [Siracusa, 2012].

Table 4.4. t_L, *GTR*, *D* and *S* for O_2 gas.

Polymer	t_L (s)	GTR ($cm^3m^{-2}d^{-1}bar^{-1}$)	S ($cm^3cm^{-2}bar^{-1}$)	D (cm^2sec^{-1})
PHD	26±1	551±2	$7.13\cdot10^{-3}\pm1\cdot10^{-5}$	$1.24\cdot10^{-6}\pm4\cdot10^{-8}$
P(HD85TED15)	102±1	628±2	$2.43\cdot10^{-2}\pm2\cdot10^{-5}$	$5.63\cdot10^{-7}\pm3\cdot10^{-9}$
P(HD70TED30)	87±1	984±1	$3.10\cdot10^{-2}\pm1\cdot10^{-5}$	$7.10\cdot10^{-7}\pm2\cdot10^{-9}$
P(HD55TED45)	46±2	792±1	$1.72\cdot10^{-2}\pm3\cdot10^{-5}$	$7.93\cdot10^{-7}\pm2\cdot10^{-9}$
PTED	52±2	699±1	$1.53\cdot10^{-2}\pm1\cdot10^{-5}$	$8.94\cdot10^{-7}\pm1\cdot10^{-9}$

It is worth noticing that the chemical structure of PHD and PTED differs for the presence of two additional ether-oxygens atoms per repeating unit: these lasts cause two different competing effects. On one hand, an increased chain mobility, and therefore higher permeability, due to the greater flexibility of C-O bonds with respect to C-C ones (as already observed in other aliphatic copolymeric systems) [Gigli et al., 2014 (a)]; on the other hand, stronger interchain interactions which give rise to a decrease in the chain mobility, and therefore to an increasing difficulty to the film crossing by the gas molecules. Three factors are then present in the polyesters under

study, whose contribution varies according to the copolymer composition (i.e. TED content): the decrease in the crystallinity degree and the enhanced flexibility, which increases the permeability, and the stronger interchain interactions, which, on the contrary, are expected to increase the barrier performances.

By a comparison of the PHD and PTED experimental results, it can be observed that the crystallinity degree plays the major role: as a matter of fact, PHD possesses lower GTR with respect to PTED for both tested gases.

Table 4.5. t_L, *GTR*, *D*, *S* for CO_2 gas and selectivity ratio GTR_{CO2}/GTR_{O2}.

Polymer	t_L (s)	GTR ($cm^3m^{-2}d^{-1}bar^{-1}$)	S ($cm^3cm^{-2}bar^{-1}$)	$D \cdot 10^7$ (cm^2sec^{-1})	GTR_{CO2}/GTR_{O2}
PHD	542±2	2120±2	0.554±0.003	0.637±0.004	3.9
P(HD85TED15)	161±2	5024±3	0.309±0.005	3.64±0.05	8.0
P(HD70TED30)	119±1	9261±3	0.391±0.003	5.14±0.03	9.4
P(HD55TED45)	136±1	8012±2	0.509±0.002	2.70±0.02	10.1
PTED	257±2	7251±3	0.772±0.007	1.75±0.05	10.4

As regards the copolymers, the following trend can be deduced: up to a TED unit content of 30 mol%, the decrease in the crystallinity degree together with the greater flexibility prevail, with an increase in the gas permeability; then, a decrease in the GTR has been recorded, due to the increased number of ether linkages and therefore to stronger interchain interactions. The higher permeability of the CO_2 molecules with respect to the O_2 molecules was confirmed in all cases.

The diffusivity and solubility data, which perfectly correlate to each other, highlighted however a different trend for the two tested gases. For O_2, the homopolymers showed the lowest solubility and the highest diffusivity among the polymers under investigation. On the other hand, in the case of CO_2, the opposite trend can be observed: PHD and PTED displayed the highest solubility and the lowest diffusivity. This means that in the case of CO_2, the gas molecule diffusion is hampered by the high crystallinity degree (PHD) or the strong interchain interactions (PTED); the O_2 molecules are on the contrary not affected by these factors. Therefore, the two gases differently interact with the polymer matrix.

The time lag very well fitted the diffusion data: the higher the solubility (interaction between gas and matrix), the higher the time lag (time required to reach the steady-state). The behavior was confirmed for both gases.

As to the selectivity ratio, the CO_2/O_2 increased with the increasing of the TED mol%, showing a high dependence on the copolymer composition.

Finally, from the data collected, it has been observed that the permeability of the polyesters can be nicely tailored with respect to the desired application, by just varying the copolymer composition.

4.1.5 Composting

The biodegradability of PHD, PTED and P(HDxTEDy) copolymers was monitored by subjecting them to composting. Biodegradation rate was investigated by weight loss measurements.

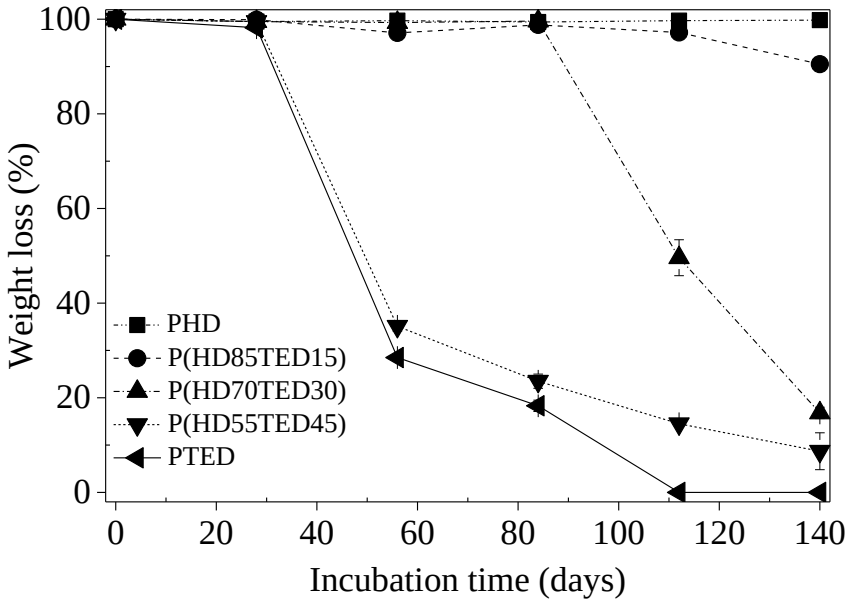

Figure 4.9. Weight losses as a function of incubation time for PHD, PTED and P(HDxTEDy) copolymers.

The degradation rate was found to be strictly affected by the presence of ether-oxygen atoms along the polymeric chain (Figure 4.9). In fact, PHD displayed negligible weight loss, while PTED film disappeared after 112 days of incubation (100% weight loss). In the case of copolymers, biodegradability appeared to be correlated to copolymer composition, being the weight loss higher the higher the TED mol% (Figure 4.9).

The observed trend can be explained on the basis of the differences in the crystallinity degree and surface wettability, both being well known factors influencing the biodegradation rate of a polymer [Gigli, Negroni et al., 2012; Gigli, Negroni et al., 2013 (a); Gigli, Negroni et al., 2013 (b);]: the higher the crystallinity degree and the surface hydrophobicity, the lower the biodegradation rate.

The morphology of the polymeric films under study was analysed by SEM. Their micrographs are reported in Figure 4.10 together with some visuals of PTED degraded films.

As it can be seen, the polymeric specimens underwent fragmentation during incubation (Figure 4.10, top image). Polymer biodegradation is considered to be a two-step process: the first one is characterized by the material fragmentation carried out by heat, moisture, sunlight and/or enzymes; the second stage is on the contrary considered to occur only if the fragmented residues are totally consumed by microorganisms as a food and energy source and if this happens within a reasonable time frame [Roy et al., 2011].

Fragmentation can be observed in the so-called biodegradable polymers as well as in the recalcitrant ones (e.g. PE), especially when pro-degradants are added. If this phenomenon is anyway beneficial in the case of biodegradable polymers, because the smaller particles are more readily available to the microorganisms responsible of degradation, fragmentation does not represent a solution when it occurs in the case biostable plastics [Feuilloley et al., 2005].

As to SEM images, all polymers showed a smooth and homogeneous surface before incubation (as reported in Figure 4.10 for PTED, as an example).

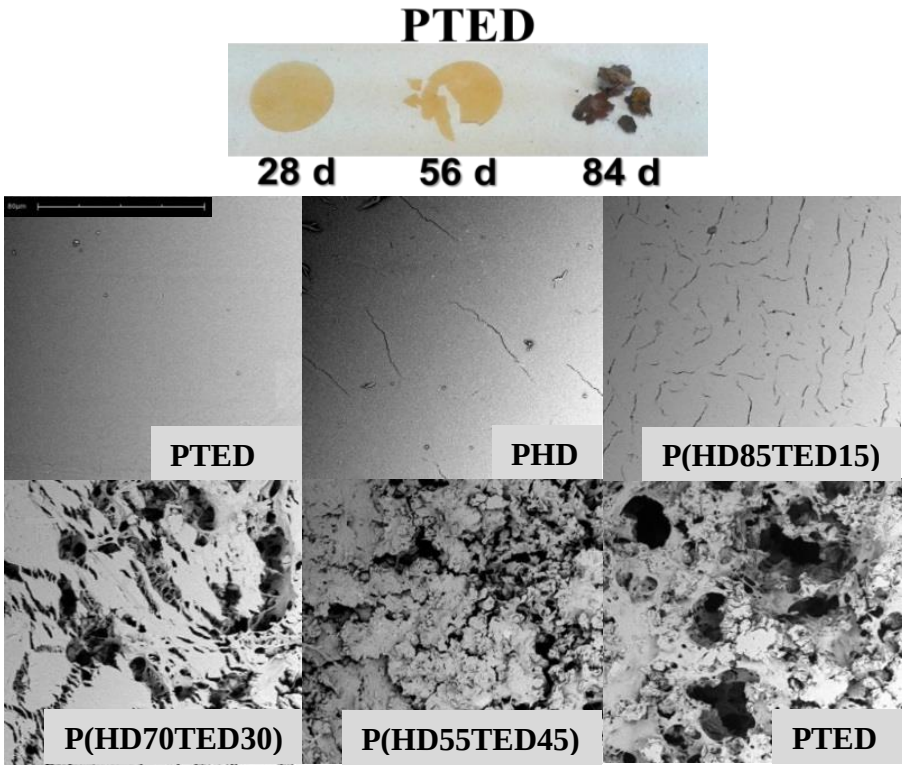

Figure 4.10. Photographs of degraded PTED films and SEM micrographs of incubated samples, 1500×. PHD and P(HD85TED15) at 140 d, P(HD70TED30) at 112 d and P(HD55TED45) and PTED at 84 d.

SEM analyses of partially degraded films are in perfect agreement with weight losses: PHD and P(HD85TED15) films were characterized by the presence of cracks on the polymeric surface, whose number was higher in the case of P(HD85TED15), while in the other copolymers large damaged areas appeared, which were more evident with the increase of TED co-unit content. The P(HD55TED45) and PTED film surfaces were completely affected by the erosion phenomenon already after 84 days of incubation, with the appearance of deep channels and holes.

4.1.6 Ageing treatments and food simulant interactions

In order to get a better understanding on the possible application of these novel materials for food packaging, deeper analysis have been performed.

The contact with food has been simulated by the use of four liquids (see paragraph 3.13), in accordance with international regulations [Regulation (EC) No 1935/2004 ; Regulation (EU) No 10/2011].

In addition, a stressed treatment, by thermal and photo exposition, has been carried out (see paragraph 3.12). The polymeric films, after the contact with simulant liquids and the ageing processes, were subjected to molecular, thermal, mechanical and barrier properties evaluation. The results have been then compared to those obtained before the treatments. LDPE was also considered for sake of comparison.

4.1.6.1 Photo and thermo oxidative treatments

4.1.6.1.1 Variation of Molecular weight

The polymer molecular weight has been determined after thermal and photo ageing. The results have been reported in Figure 4.11 as a function of the treatment time.

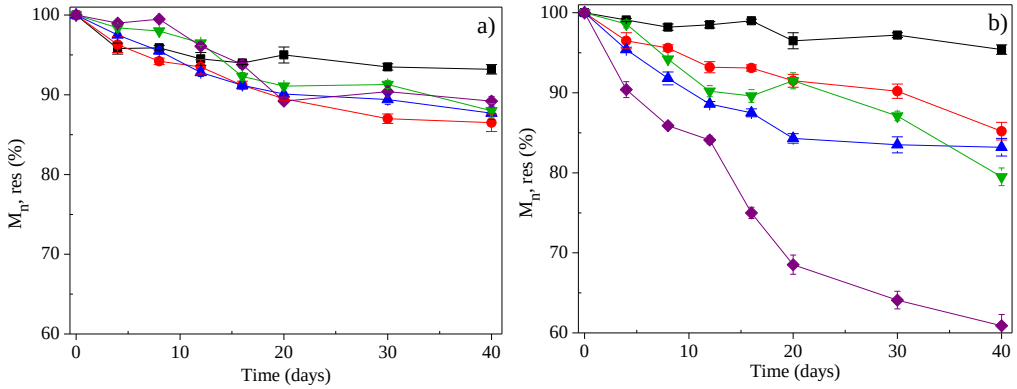

Figure 4.11. Residual M_n (%) as a function of incubation time after thermal (a) and photo-ageing (b). ■ PHD; ● P(HD85TED15); ▲ P(HD70TED30); ▼ P(HD55TED45); ♦ PTED.

As can be evicted from Figure 4.11a, the thermal treatment caused a decrease of molecular weight in all the polyesters under investigation. PHD homopolymer lost about 8% of the initial M_n, while the copolymers and PTED homopolymer degraded to a higher extent (10-13%). On the other hand, photo ageing produced a greater effect (Figure 4.11b), with the exception of PHD, whose degradation profile was similar for both treatments. As a matter of fact, the higher the amount of TED co-unit, the higher the degradation rate, up to the PTED homopolymer, whose residual M_n was about 60%. The results can be explained on the basis of the different chemical structure of the polymers under investigation. The presence of ether-oxygen atoms, could in fact

promote the degradation of the macromolecular chains, as already reported in the literature [Genovese et al., 2014].

4.1.6.1.2 Variation of Thermal properties

Calorimetric studies carried out on the polymers after ageing evidenced a variation of the melting endotherm with respect to the values before treatment. The data obtained have been collected in Table 4.6.

Table 4.6. Thermal data after ageing treatments.

Samples	**ΔH_m (J/g)**				
	0 days	**20 days**		**40 days**	
	standard	**photo**	**thermal**	**photo**	**thermal**
PHD	79 ± 1	82 ± 1	81 ± 1	82 ± 1	84 ± 2
P(HD85TED15)	75 ± 2	74 ± 2	72 ± 1	73 ± 2	73 ± 1
P(HD70TED30)	71 ± 1	78 ± 2	77 ± 2	81 ± 1	78 ± 2
P(HD55TED45)	66 ± 3	73 ± 3	79 ± 3	71 ± 2	83 ± 4
PTED	55 ± 2	60 ± 1	66 ± 2	59 ± 4	65 ± 3
LDPE	37 ± 1	42 ± 2	38 ± 2	41 ± 2	41 ± 2

The ageing experiments contributed to increase the crystallinity degree of the polymers under study (Table 4.6), even though some differences can be highlighted. In particular, LDPE, PHD and P(HD85TED15) underwent only a small variation, while for the copolymers and PTED homopolymer an higher increase was observed. This effect was even more evident in the case of thermal treatment. The results can be explained on the basis of annealing phenomena that occur when a polymer is placed at a temperature between its T_g and its T_m. For PTED and P(HD55TED45) the temperature of the test (40°C) is much closer to the melting (43°C and 54°C, respectively), thus the macromolecular chains possessed an increased mobility which allowed a better reorganization into crystalline domains.

4.1.6.1.3 Variation of Mechanical properties

In order to investigate the possible modification of the mechanical behavior, tensile tests were carried out on the polymer samples after ageing treatments. As to the neat polymers, the mechanical properties were found strictly dependent on the chemical composition and on the crystallinity degree. It is in fact well known [Halpi & Kardos

1972; Dusunceli & Colak 2008] that the crystallinity degree has a considerable effect on the mechanical properties of a polymer. In particular, high Xc results in harder, stiffer and less ductile behavior. Therefore, as expected, the elastic modulus gradually decreased with the increase of the TED co-unit content as a consequence of the Xc decrease. On the other hand, besides PHD that displayed a ε_b of about 80%, all the other polymers under study displayed elongation to break above 700% [Genovese et al., 2014].

Table 4.7a) Mechanical data after thermal ageing treatments.

Polymer	Untreated		Thermal			
	0 days		20 days		40 days	
	E (MPa)	ε_b (%)	E (MPa)	ε_b (%)	E (MPa)	ε_b (%)
PHD	400±21	80±6	430±20	9±1	420±4	9±1
P(HD85TED15)	361±6	740±70	432±45	129±20	440±9	90±28
P(HD70TED30)	250±10	910±60	246±18	817±58	306±14	696±54
P(HD55TED45)	222±9	840±20	190±13	527±55	253±13	310±8
PTED	201±7	860±80	226±14	8±1	343±25	10±1
LDPE	135±6	820±40	149±6	728±42	237±10	205±43

Table 4.7b) Mechanical data after photo-ageing treatments.

Polymer	Untreated		Photo			
	0 days		20 days		40 days	
	E (MPa)	ε_b (%)	E (MPa)	ε_b (%)	E (MPa)	ε_b (%)
PHD	400±21	80±6	418±8	8±1	425±5	8±2
P(HD85TED15)	361±6	740±70	430±25	354±65	448±33	230±38
P(HD70TED30)	250±10	910±60	279±17	736±65	315±13	708±45
P(HD55TED45)	222±9	840±20	207±16	682±53	295±8	12±1
PTED	201±7	860±80	212±49	5±1	250±15	6±1
LDPE	135±6	820±40	158±7	612±28	258±29	342±51

Data recorded after ageing treatments (at day 20 and at the end of the experiment) are reported in Table 4.7a) and b). A gradual decrease of the elongation at break was evidenced for all polymers, including LDPE: the longer the time of the test the lower the ε_b. In general, thermal treatment caused a stronger effect with respect to the photo ageing. Once again, PTED homopolymer suffered the biggest worsening of the mechanical properties, as the film broke very easily during handling revealing a significant degradation.

A general increase of the elastic modulus, was on the contrary observed, because of the enhanced crystallinity degree (Table 4.7a) and b)).

4.1.6.1.4 Variation of Barrier properties

Gas transmission rate (GTR), solubility (S), diffusivity (D) and time lag (t_L) of the samples have been evaluated after the ageing treatments and compared with those of the neat polymers, previously recorded [Genovese et al., 2014].

Thermal and photo ageing have been conducted to simulate an accelerate degradation process and the supermarket exposition, respectively. The thermal treatment carried out corresponded to an ageing of 0.6-6.06 solar years, calculated accordingly to studies conducted on polyethylene films previously reported [Jakubowicz, 2003; Koutny et al., 2006].

CO_2 GTR values recorded after thermal and photo ageing treatments are reported in Figure 4.12, while Table S1 contains the GTR increment/decrement (%) with respect to the untreated materials.

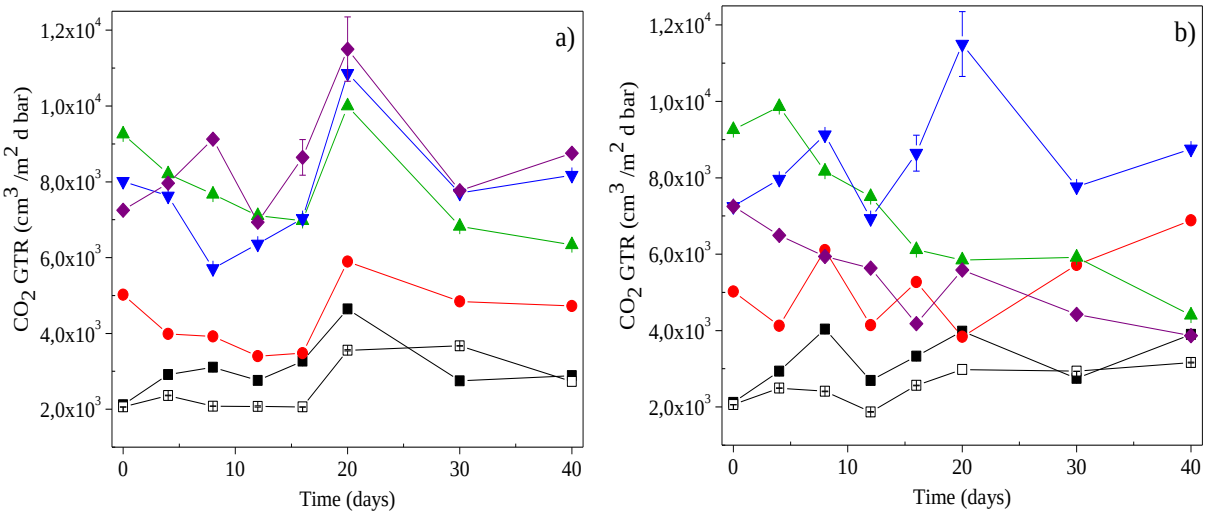

Figure 4.12 CO_2 GTR data after ageing: ■ PHD; ● P(HD85TED15); ▲ P(HD70TED30); ▼ P(HD55TED45); ♦ PTED; □ LDPE. a) thermal ageing at 40°C, 50% RH, air ventilated; b) photo-ageing at 23°C, D65 Neon light, 50% RH, air ventilated.

Thermal ageing caused an increase in the CO_2 permeability, but the trends observed, although not linear, confirmed that the higher the amount of TED co-units, the higher

the GTR. On the other hand, PHD and LDPE displayed a similar behavior, converging to the same permeability at the end of the experiment (Figure 4.12a).

As to the photo ageing, a different behavior of the polymers under investigation can be highlighted. PHD and LDPE showed similar and high barrier properties, but PTED and P(HDxTEDy) copolymers underwent different modifications of the permeability with respect to the thermal ageing. As it can be observed, photo treatment of P(HD70TED30) and PTED produced a linear decrease of the GTR: at day 40 similar barrier properties of PHD have been achieved (Figure 4.12b). On the contrary, P(HD85TED15) exhibited a more fluctuant behavior, even though a general increase of the permeability could be noticed (Figure 4.12b).

To explain the results observed, it is worth noting that the polymers underwent significant changes, above all decrease of the molecular weight and crystallinity degree increase, due to the ageing treatments: the longer the exposure the greater the modifications. The ΔH_m increase was more significant for polymers rich in TED co-units.

On the basis of the above mentioned information, two different trends can be detected. For LDPE, PHD and P(HD85TED15), although a higher crystallinity degree was achieved after the treatments, and therefore better barrier properties could be expected, the decrease in molecular weight promoted the formation of smaller and less perfect crystallites that facilitated the gas crossing. This explains the increase of GTR.

On the other hand, in the case of P(HD70TED30), P(HD55TED55) and PTED a higher increase of crystallinity degree during treatment was achieved. The much greater amount of crystallites, countered their lower perfection, causing a smaller variation (and in some cases a decrease) of the GTR during ageing with respect to the values recorded for the untreated corresponding samples.

The GTR is correlated to the quantitative evaluation of the gas transmission through the polymer wall. On the other hand, the solution-diffusion process, associated to S and D coefficients, describe the material behavior regarding the gas-polymer interaction, during the gas barrier study. The calculation of the gas permeation behavior is based on four assumptions: i) the diffusion process occurs under steady-state conditions; ii) the gas concentration-distance relationship through the polymer is linear; iii) diffusion takes place only in one direction; iv) S and D are independent from the gas concentration.

However, the above mentioned hypotheses are valid only in an ideal case [Robertson, 2006]. When materials are exposed to stressing environments, considerable interactions between the polymer and the permeants could take place. As a consequence, S and D will show a different behavior than the theoretical one and are no longer independent from the gas concentration.

An important consideration must be made also regarding the steady state. Although steady state is normally reached in a few hours (within the food shelf life period), with larger gas molecules (like CO_2) the steady state could be reached in a longer time (sometimes exceeding the food shelf-life), once more promoting the polymer/permeate interaction.

S and D data recorded after thermal and photo ageing are reported in Figure 4.13 and Figure 4.14, respectively.

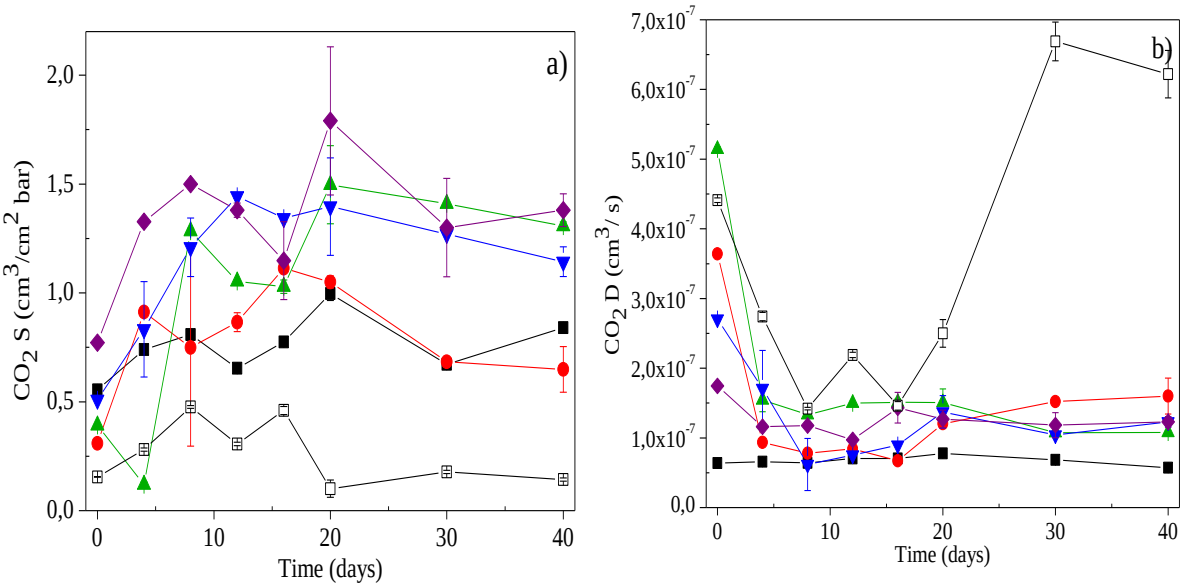

Figure 4.13 S (a) and D (b) coefficients, after thermal ageing, at 40°C, 50% RH, air ventilated.

■ PHD; ● P(HD85TED15); ▲P(HD70TED30); ▼P(HD55TED45); ♦ PTED; □ LDPE.

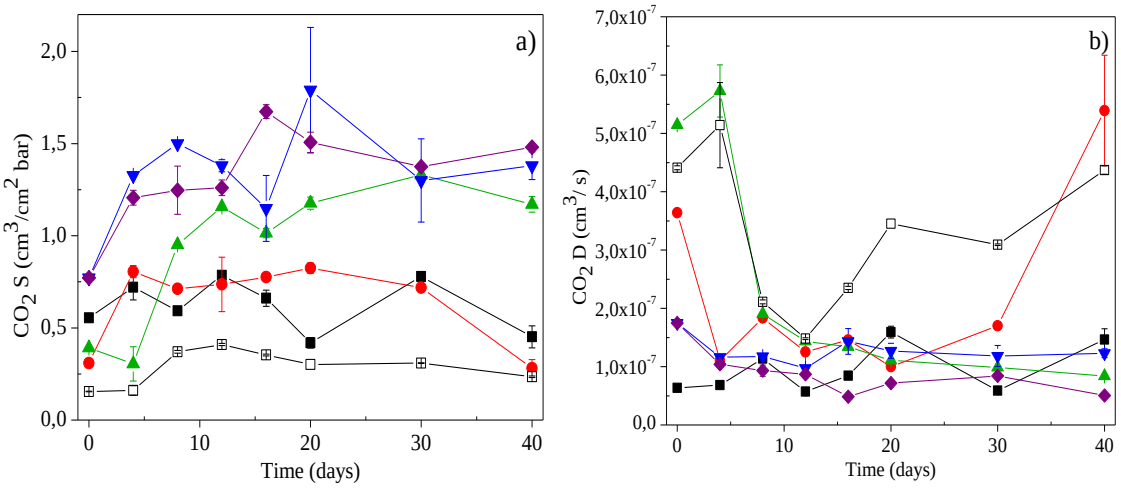

Figure 4.14. S (a) and D (b) coefficients, after photo ageing at 23°C, D65 Neon light, 50% RH, air ventilated. ■ PHD; ● P(HD85TED15); ▲ P(HD70TED30); ▼ P(HD55TED45); ♦ PTED; □ LDPE.

Both the thermal and photo ageing results display a good correlation between S and D: to S increase corresponded a D decrease and vice versa. From day 0 to day 20 of exposure an increment of S was recorded, while from day 20 till the end of the experiment S slowly decreased.

Consequently, D rapidly decreased during the first days of treatment, then increased very smoothly, with the exception of LDPE that displayed a sudden rise of D after 15 days of incubation. The increase of solubility means a better interaction and solubilization of the gas molecules inside the polymer, with a resulting slower diffusion. Lastly, the time lag data are reported in Figure 4.15.

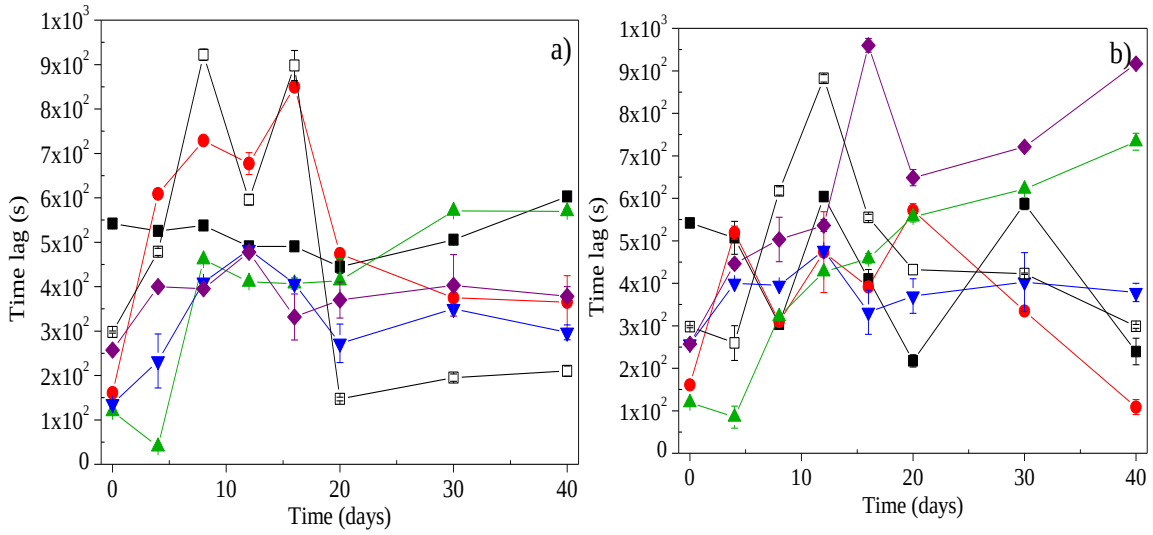

Figure 4.15. t_L coefficients, after a) thermal ageing and b) photo ageing. ■ PHD; ● P(HD85TED15); ▲ P(HD70TED30); ▼ P(HD55TED45); ♦ PTED; □ LDPE.

As it can be noticed, although fluctuations are present, the reaching of the steady state can be observed after 20 days of thermal treatment, while for the photo ageing only P(HD55TED45) reached the steady state in the time scale explored.

4.1.6.2 Food simulants interactions

4.1.6.2.1 Variation of Molecular weight

The polymers under study have been subjected to molecular weight determination after the contact with four different food simulants: iso-octane (i-Oct); ethanol (EtOH); distilled water (DW); acetic acid (AA) and the results have been reported in Figure 4.16.

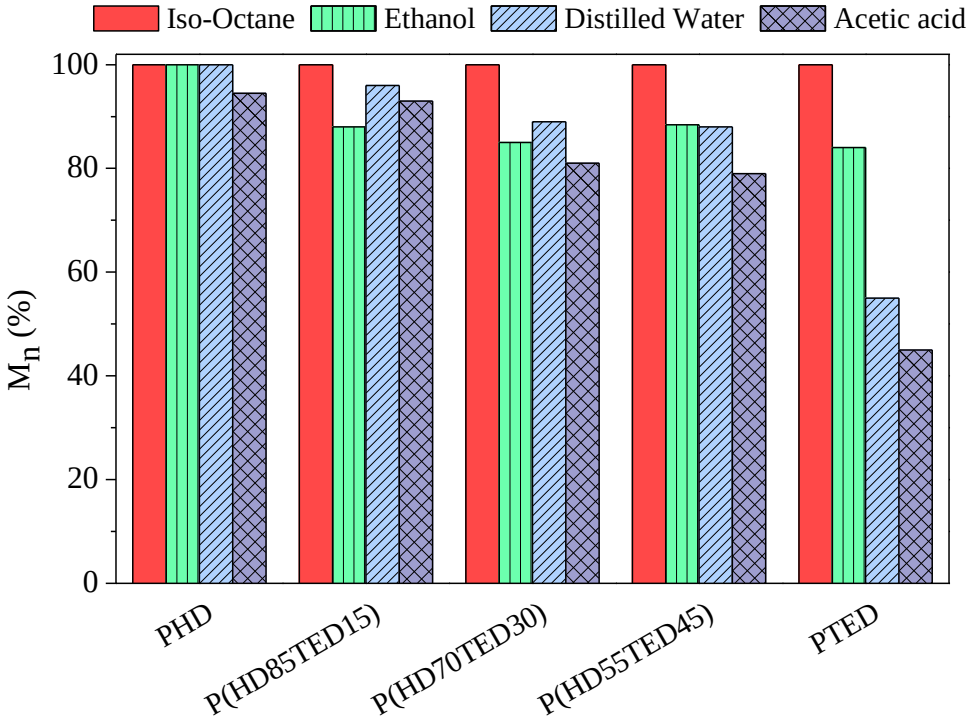

Figure 4.16. Residual M_n (%) as a function of incubation time after the treatment with food simulants.

It can be observed that the treatment with iso-octane did not influence the polymer molecular weight, while the polymers appreciably degraded when in contact with the other simulant liquids. In general, the higher the amount of TED co-units the higher the degradation. Greater effects have been observed when the films were treated with AA, probably due to the acidic environment.

4.1.6.2.2 Variation of Thermal properties

Calorimetric studies carried out on the polymers after contact with simulant liquids evidenced a variation of the melting endotherm with respect to the values before treatment.

Table 4.8. Thermal data after contact with food simulants

Polymer	**ΔH_m (J/g)**				
	Standard	**DW**	**AA**	**EtOH**	**i-O**
PHD	79 ± 1	85 ± 2	80 ± 3	82 ± 2	87 ± 1
P(HD85TED15)	75 ± 2	81 ± 1	80 ± 1	75 ± 2	81 ± 1
P(HD70TED30)	71 ± 1	61 ± 1	69 ± 2	54 ± 1	76 ± 3
P(HD55TED45)	66 ± 3	75 ± 3	78 ± 2	72 ± 3	81 ± 3
PTED	55 ± 2	84 ± 3	86 ± 4	90 ± 3	73 ± 2
LDPE	37 ± 1	37 ± 2	43 ± 1	40 ± 2	44 ± 3

As it is possible to see from data collected in table 4.8, an increase of the ΔH_m (J/g) has

been generally recorded, with the exception of P(HD70TED30), for which a significant decrease in the crystallinity degree was found when put in contact with distilled water and ethanol. PTED displayed the most conspicuous variation of melting endotherm. This can be ascribed to annealing processes, which occurred during treatment, as the sample melting temperature (43°C) is very close to the treatment one. Moreover, at the end of the experiment in water, PTED was found to be completely dissolved. This phenomenon has been probably induced by the hydrophilicity of this sample combined with the temperature of the experiment, close to the T_m. The highest increase in the ΔH_m was detected when the polymers were in contact with isooctane. As already reported in the literature[Mrkić et al., 2006; Zhu et al., 2014] , the aggregation structure of the film, including the crystalline structure, plays an important role on migration plasticizers through the polymer matrix. Moreover, the migration of the food simulant was affected by the affinity (intense or weak interaction) of the chemical compound with the polymeric film.

4.1.6.2.3 Variation of Mechanical properties

Figure 4.17 a) and b) report, respectively, the elastic modulus (E) and the elongation at break (ε_b) after the contact with simulant liquids (data are reported in table S2).

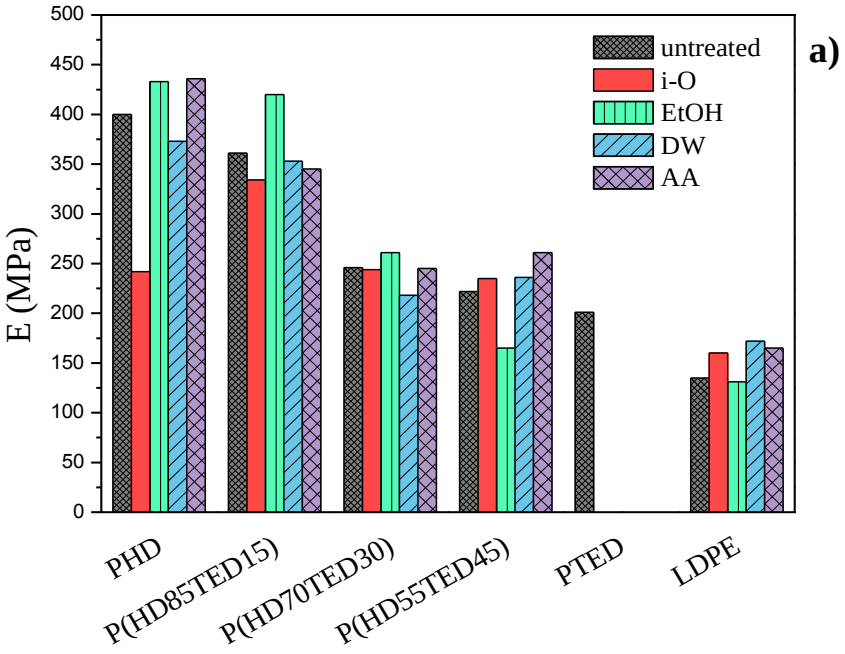

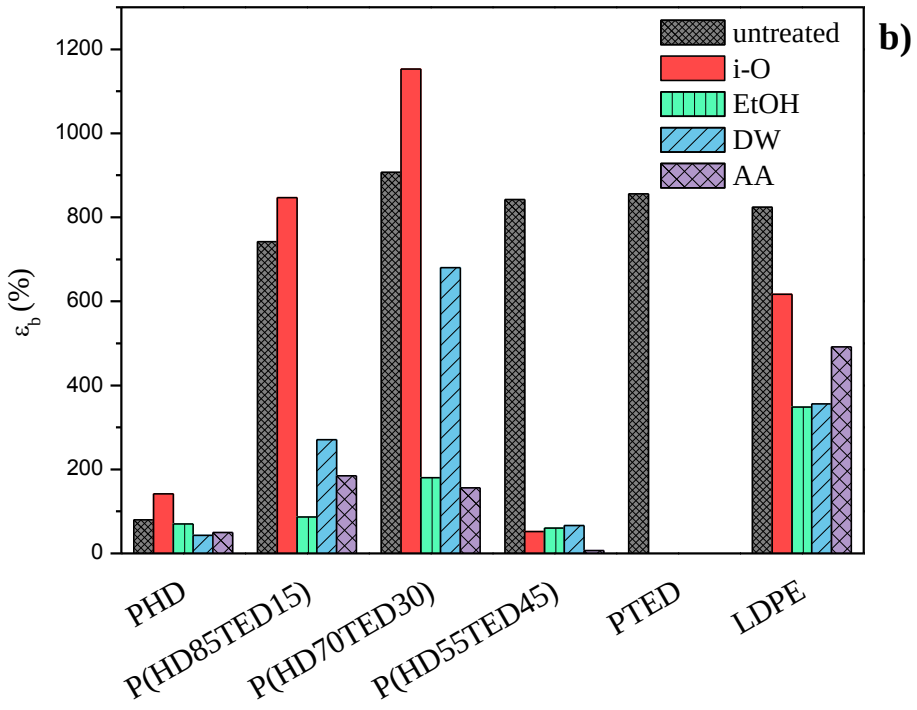

Figure 4.17: Elastic modulus (E) and elongation at brak (ε_b) after interaction with food simulants.

A general worsening of the elongation at break was observed in all polymers whatever the liquid, probably due to a partial degradation induced by the treatment; this was even more evident in P(HD55TED45) and PTED. LDPE also displayed a decrease in the elongation at break. As to E, only slight variations could be detected. Interestingly, PHD, P(HD85TED15) and P(HD70TED30), after the treatment in isooctane evidenced a greater elongation to break, which can be ascribed to a plasticizing effect of this organic compound, confirmed, in the case of PHD, by a significant reduction of the elastic modulus.

4.1.6.2.4 Variation of Barrier properties

CO_2 GTR data recorded after contact with food simulants are reported in Table 4.9, while the corresponding percentage of GTR increment /decrement (+/-, %) with respect to the untreated (standard) values [Genovese et al., 2014], can be found in Table S3. O_2

GTR values can be calculated by using the relative selectivity ratio previously determined and reported in Table S3 for sake of simplicity.

In the case of the untreated samples, the chemical structure played an important role. As a matter of fact, PHD behavior was comparable to LDPE, while PTED displayed a much higher permeability. This is because of the lower crystallinity degree and the enhanced flexibility of this sample, due to the presence of ether linkages, notwithstanding the stronger interchain interactions, which gave rise to a decrease in the chain mobility (and therefore an increase in the barrier performances).

As to the treated samples, few points need to be underlined. The contact with different liquids can change the polymer surroundings, therefore affecting in a different manner the permeability behavior. In fact, it is well known that polymer/permeant and permeant/permeant interactions affect more the gas transmission process than the polymer/polymer interactions [Robertson et al., 2006].

In addition, materials that are good barriers when dry, can perform badly when tested in a different environment, like for example in water. In the case of low barrier film, the medium reduces the gas permeation, while for the highest barrier materials, for example poly(vinylidene-chloride) (PVDC), the medium's influence on permeation is almost undetectable [Galić & Ciković, 2001]. Finally, it is important to notice that according to the literature [De Leiris, 1986], under the action of water the polymer swells and changes its structure making the diffusion of gases easier.

Concerning the D, S and t_L coefficients, different behaviors were recorded depending on the food simulant and on the polymer under analysis. In general, if GTR value decreases, a decrement of S is recorded, due to a lower compatibility between the polymer and gas molecules (less amount of permeant in the polymer). On the contrary, D increases, because the gas molecules diffuse more rapidly through the film, and less time is needed to reach the steady-state of the permeability process and t_L decreases.

Table 4.9. GTR, S, D and t_L data after contact with food simulants.

Permeability parameters	Untreated	DW	AA	EtOH	i-O
			PHD		
GTR	2120±2	2871±1 (>)	1961±1 (<)	3900±8 (>)	1831±2 (<)
S	0.6 ±0.1	0.3±0.1(<)	0.2±0.1(<)	1.2±0.1(>)	0.2±0.1(<)
$D \cdot 10^8$	6.40±0.04	31±2 (>)	31±3 (>)	11.3±0.1 (>)	28±3 (<)
t_L	542±2	530±30 (<)	520±50 (<)	1430±20 (>)	590±60 (>)
			P(HD85TED15)		
GTR	5024±3	4570±1 (<)	6273±9 (>)	5557±5 (>)	3223 ±5 (<)
S	0.3±0. 1	1.0 ±0.1 (>)	1.5±0.1 (>)	0.6 ±0.1(>)	0.4±0.1 (>)
$D \cdot 10^8$	36±1	17±1 (<)	15±1 (<)	35±3 (<)	36±1 (=)
t_L	161±2	1014±6 (>)	1110±20 (>)	480±40 (>)	550±80 (>)
			P(HD70TED30)		
GTR	9261±3	14100±1 (>)	6230±8 (<)	6587±5 (<)	10700±1 (>)
S	0.4±0.1	1.7±0.1 (>)	0.4±0.1 (=)	0.7±0.1 (>)	0.5±0.1 (>)
$D \cdot 10^8$	51±1	23±1 (<)	46 ±10 (<)	29 ±4 (<)	58 ±8.3 (>)
t_L	119±1	428±8 (>)	220±40 (>)	340±40 (>)	170±20 (>)
			P(HD55TED45)		
GTR	8012±2	6827±5 (<)	6333±5 (<)	6507±5 (<)	2898±2 (<)
S	0.5±0.1	1.4 ±0.1 (<)	0.4±0.1 (<)	1.3±0.1 (>)	0.5±0.1 (<)
$D \cdot 10^8$	27±1	13 ±1 (<)	46 ±1(>)	13 ±2 (<)	15±1.2 (<)
t_L	136 ±18	620±20 (>)	200±60 (>)	610±70 (>)	540±40 (>)
			PTED		
GTR	7251±3	--	--	7007±5 (<)	4857±5 (<)
S	0.8±0.1	--	--	1.2±0.1 (>)	1.3±0.1 (>)
$D \cdot 10^8$	18±1	--	--	14±1 (<)	9±1 (<)
t_L	257 ±2	--	--	490 ±20 (>)	770±10 (>)
			LDPE		
GTR	2061±2	3875±2 (>)	3553±9 (>)	2788±3 (>)	2233±2 (>)
S	0.2±0.1	0.4±0.1 (>)	0.7±0.1 (>)	0.6 ±0.1 (>)	0.3±0.1 (>)
$D \cdot 10^8$	44±1	40±4 (<)	18±1(<)	16 ±1 (<)	30±2 (<)
t_L	298 ±3	430±50 (>)	920±20 (>)	1010±70 (>)	550±30 (>)

DW: Distilled Water, AA: Acetic Acid, EtOH: Ethanol, i-O: iso-Octane
GTR (cm^3/cm^2 d bar), S (cm^3/cm^2 bar), D (cm^2/s), t_L (s)

Several factors can influence the diffusion and solubility coefficients, as pressure of the diffusing gas, sorption of the permeant molecules into the polymer matrix and temperature [Galić & Ciković, 2001; Mrkić et al., 2006]. These factors are well described in literature for ideal behavior (pressure < of 1 atm, and very low solubility of the permeant gases in the polymer matrix) [Robertson, 2006], but under real and stresses conditions (such as the use of food simulants) the expected behavior can be modified, as reported in Table 4.9.

PHD homopolymer showed a slight improvement of the barrier properties after contact with AA and i-O, On the contrary, a significant worsening of the barrier behavior was observed after treatment with distilled water and especially with ethanol. The solubility decreased for AA and DW, with an increase of the diffusion. For EtOH, both S and D were enhanced by the treatment; the opposite occurred with i-O.

PTED displayed a lower GTR after contact with i-O, while no significant effect was observed after immersion in ethanol. In both cases, solubility displayed similar and higher values while D decreased with respect to the untreated polymer. The PTED films after immersion in water and acetic acid broke during handling, revealing a significant degradation.

In the case of LDPE, all the simulant liquids caused a decrease of the barrier properties, most evident in the case of DW and AA. S increased and D decreased whatever the food simulant liquid.

Interestingly, PHD revealed a higher resistance to simulant fluids than LDPE, highlighting a good suitability for the production of biodegradable packaging.

As far as the P(HDxTEDy) copolymers are concerned, it is known that the permeability of polymeric materials can be influenced in different ways. As reported in literature, the magnitude of such effect is directly correlated with the chemical composition of the matrix [Robertson, 2006]. Qualitatively, any agent that increases the number or size of cavities in a polymer, or the mobility of chain segments, increases the rate of gases diffusion. This effect was observed with the introduction of TED co-units in the PHD macromolecular backbone.

P(HD85TED15) evidenced an improvement of the barrier performances after immersion in DW and i-O. On the other hand, a decrease was detected after contact with ethanol and acetic acid. Independently of the food simulant, an increase of the solubility and a lowering of the D coefficient was recorded.

Both P(HD70TED30) and P(HD55TED45) displayed a similar and improved barrier behavior after treatment with EtOH and AA. On the contrary, the immersion in distilled water and i-O caused diverse effects: the distilled water generated a worsening of the P(HD70TED30) performances and an improvement of those of P(HD55TED45), while in the case of isooctane the polymers behaved the opposite.

The solubility for P(HD70PTED30) increased when the film was treated with DW, EtOH and i-O, while remained constant after the treatment with AA. The diffusivity coefficient, was lower after the contact with water, acetic acid and ethanol and increased in the case of iso-octane.

Lastly, as to the P(HD55TED45), S decreased in all cases with the exception of EtOH. D was enhanced by the treatment with AA, and was reduced in all the other cases.

In conclusion, the values of S, D and tL resulted strictly dependent on the chemical composition of the polymer and the food simulant used and no general trends could be highlighted.

4.1.7 Conclusions

A new class of ether-linkages containing aliphatic polyesters based on 1,12-dodecanedioic acid has been studied and characterized with respect to packaging applications. The copolymerization strategy allowed us to successfully introduce TED sequences into PHD backbone. This modification had different effects on the physical characteristics of this homopolymer; among all, a decrease in the crystallinity degree and in the melting point, because of the reduced chain symmetry, and an improved hydrophilicity, due to the presence of highly electronegative ether-oxygen atoms, were observed. Both χc and WCA are strictly linked to the copolymer composition: the higher the TED unit content, the lower χc and WCA. Moreover, the resulting copolymers highlighted improved mechanical properties with respect to PHD: a decrease in the elastic modulus, which was found to depend on the copolymer composition, and a significant increase in the toughness were achieved. In addition, the biodegradation rate of the P(HDxPTEDy) copolymers resulted remarkably higher than that PHD, this last being almost undegraded under the adopted composting conditions. On the other hand, the lower crystallinity degree resulted in a decrease in the barrier properties of the copolyesters, more evident in the case of the CO_2 gas.

Molecular, thermal, mechanical and barrier properties have been evaluated after contact with food simulant liquids and after thermal and photo ageing treatments. The results have been compared to LDPE films. All the polymers, including LDPE, underwent a modification of the physic/chemical and mechanical properties after the treatments. A decrease of the molecular weight and an increase of the crystallinity degree were observed. Moreover, a general rise of the elastic modulus, due to the higher crystallinity

degree, and a worsening of the elongation at break have been detected. However, the samples, with the exception of PTED homopolymer, did not show sever damage at the end of the experiments.

The above mentioned variations of the polymer properties had a significant influence on the permeability behavior, which was strictly correlated also to their chemical structure.

The GTR of the untreated samples was dependent on the chemical composition: the higher the amount of TED co-units, the higher the permeability. As to the treated polymers, different trends have been found and explained on the basis of the changes occurred in the crystallinity/amorphous ratio and on the crystal perfection and size.

Moreover, due to the presence of various amounts of highly electronegative ether-oxygen atoms, different interactions with the environment were recorded: as a matter of fact, PTED homopolymer showed the greatest differences on permeability behavior, being more influenced by the environment. On the contrary, PHD homopolymer displayed a similar or better response to the treatments with respect to LDPE, confirming its suitability for packaging uses.

By tailoring the chemical composition of the synthesized polymers, it could be therefore possible to obtain a material displaying the best combination of properties with respect to the intended application.

Lastly, the study conducted permitted to evidence the response of a new class of materials to different experiments simulating real working conditions, and allowed a better understanding of how the chemistry influences the physic/mechanical and barrier properties of log chain aliphatic polyesters when employed as food packages in supermarkets.

4.2 Novel biodegradable aliphatic copolyesters based on poly(butylene succinate) containing thioether-linkages

A new class of Poly(butylene succinate) PBS based random copolymers was synthesized. The new copolyesters contain thioether linkages, whose introduction in polymeric chains can remarkably affect crystallinity degree and chain flexibility. The structural, thermal and mechanical properties, together with surface wettability have been investigated. In addition, the permeability to oxygen and carbon dioxide and the biodegradation rate in compost medium have been evaluated.

4.2.1 Synthesis and molecular characterization

Poly(butylene succinate) random homopolymer and Poly(butylene/thiodiethylene glycol succinate) random copolyesters (P(BSxTDGSy)) have been synthesized following the synthetic procedure explained in paragraphs 3.2.1 and 3.2.3.1, respectively.

At room temperature all the synthesized polyesters appear as semicrystalline light yellow solids. Figure 4.18 shows the chemical structures of the two comonomeric units present in the copolymers under study: as it can be observed, butylene succinate (BS) and thiodiethylene glycol succinate (TDGS) units have a very similar structure with two ester groups along a saturated aliphatic chain, the only difference being the presence, in the TDGS one of a sulphur atom, absent in the BS unit.

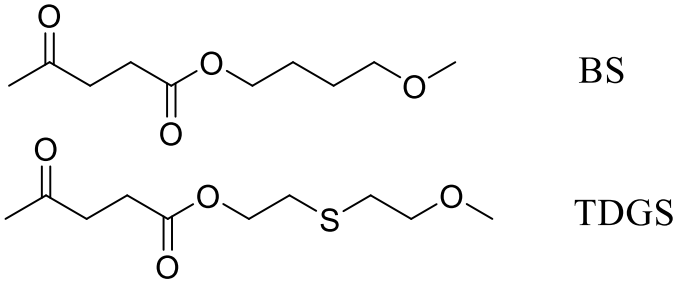

Figure 4.18. Chemical structures of BS (above) and TDGS (below) comonomeric units.

Data of molecular characterization of parent homopolymer PBS and P(BSxTDGSy) copolymers are collected in Table 4.10. As revealed by relatively high and similar sample molecular weights, appropriate synthesis conditions were used and a good polymerization control was achieved. The ^{1}H-NMR spectra confirmed the awaited

molecular structures (figure 4.19 shows, as an example, the ^{1}H-NMR spectrum of P(BS60TDGS40) copolymer).

Table 4.10. Data of molecular characterization: molecular weight (**M_n**), polydispersity degree index (**PDI**), sample composition (**TDGS (mol %)**), contact angle (**WCA**), film thickness.

Polymer	M_n	PDI	TDGS (mol %) by ^{1}H-NMR	WCA (°)	*Thickness (μm)*
PBS	51000	2.7	0	90 ± 2	192 ± 4
P(BS90TDGS10)	59000	2.7	8	84 ± 2	304± 21
P(BS80TDGS20)	54000	2.8	20	83 ± 3	231± 20
P(BS70TDGS30)	50000	3.2	30	82 ± 2	243± 23
P(BS60TDGS40)	51000	2.8	36	80 ± 2	291±7

The real copolymer composition was calculated from the relative areas of the ^{1}H-NMR resonance peak of the aliphatic proton of the butanediol subunit located at 4.11 ppm (**b** labelled protons) and of the protons of the methylene groups of the thiodiethylene diol subunit at 4.25 ppm (**d** labelled protons). The calculated molar composition is, in all cases, closed to the feed one (see Table 4.10).

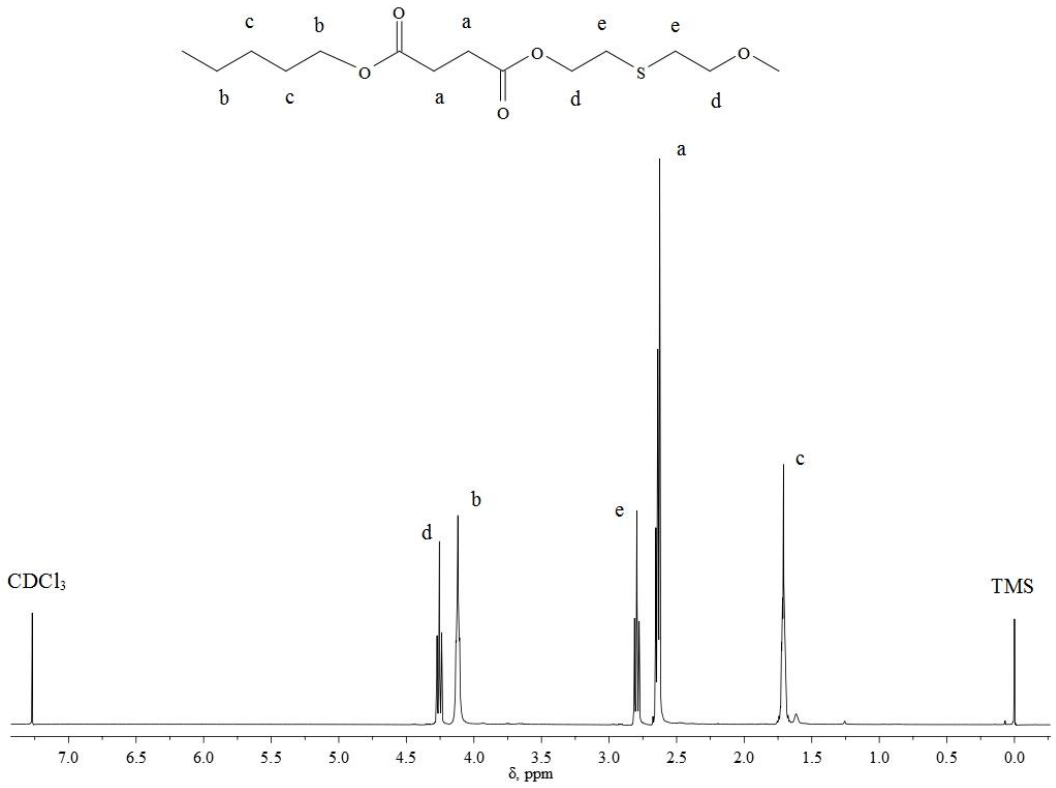

Figure 4.19. ^{1}H-NMR spectra of P(BS60TDGS40) with resonance assignments.

Water contact angle (WCA) measurements were performed in order to investigate the polymers films hydrophilicity. From data reported in Table 4.10 it can be noticed that PBS is the most hydrophobic material and that the introduction of a sulphur atom per repeat unit leads to increased material hydrophilicity: as a matter of fact, the random copolymers are characterized by a lower WCA value respect to PBS, which slightly decreases as the TDGS co-unit content is increased. Therefore, the introduction along PBS macromolecular chain of TDGS units permits to obtain a new class of random copolymers with enhanced hydrophilicity thanks to the introduction, along the polymer chain, of sulphur atoms.

4.2.2 Thermal properties and crystallization ability

The thermal stability of the synthesized copolyesters was studied by thermogravimetric analysis. Table 4.11 collects the temperatures corresponding to 5% weight loss ($T_{5\%w.loss}$) and to the maximum weight loss rate (T_{max}), determined from the thermogravimetric curves (figure 4.20).

Table 4.11. Thermal characterization data for PBS and its random copolymers.

		1st scan				2nd scan					
Polymer	$T_{5\%\ w.loss}$	T_{max}	T_m	ΔH_m	T_g	ΔC_p	T_m	ΔH_m	T_c	ΔH_c	T_{cc}
PBS	336	411	114	81	-34	0.105	114	83	-	-	78
P(BS90TDGS10)	328	407	105	68	-34	0.419	105	72	-	-	68
P(BS80TDGS20)	328	407	94	52	-34	0.375	94	63	-	-	47
P(BS70TDGS30)	321	400	86	45	-36	0.524	86	51	9	22	36
P(BS60TDGS40)	315	389	72	12	-38	0.548	72	24	15	24	10

T= °C; ΔH= J/g; ΔC_p=J/°C·g

As evidenced in Figure 4.20, the weight loss takes place in all cases in one-step and is 100%. The thermal stability of the copolymers was found to be good, even if it however decreases with TDGS co-unit content. This is due as to the lower energy of C-S bonds with respect to C-C ones.

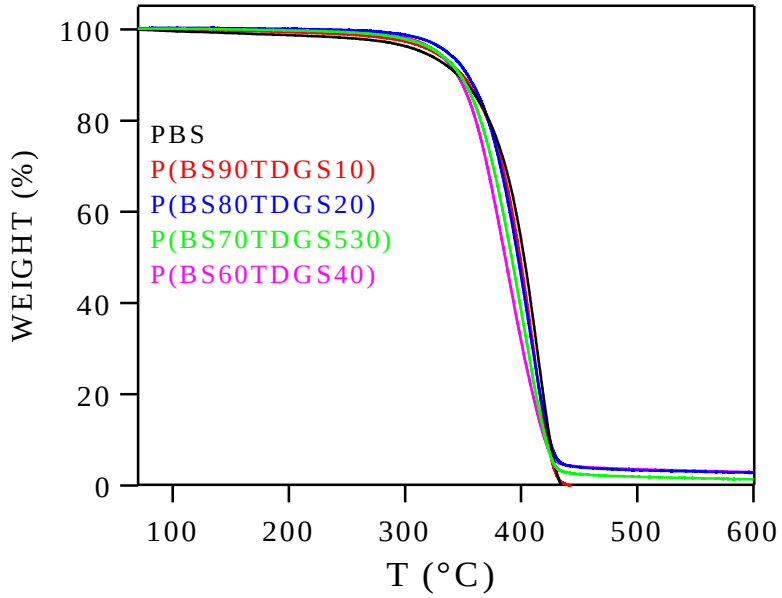

Figure 4.20 Thermogravimetric curves of PBS and its random copolymers under nitrogen atmosphere (heating rate: 10 °C/min).

In order to provide the same heat treatments to all the investigated samples, prior to thermal analysis each film was kept at room temperature for 14 days. Figure 21a shows the DSC scans, for the so-treated samples, whereas Table 4.11 collects the thermal data.

As evidenced in Figure 4.21a, all P(BSxTDGSy) copolymers presented a glass transition and a melting endotherm. As to the melting process, the calorimetric results indicate that with the increasing TDGS molar percentage, both the melting temperature and the heat of fusion decrease (see data in Table 4.11), as previously found in random copolymers with the comonomeric units present in minor extent completely rejected from the crystalline phase or partially assimilated in it [Soccio et al., 2013; Ichikawa et al., 2001].

Furthermore, the presence of a larger distribution of crystallites with different degree of perfection is suggested by the presence of a broader endotherm region in the copolymers with respect to the homopolymer. P(BS60TDGS40) sample shows multiple melting peaks, which can be ascribed to melt-recrystallization processes occurring during the DSC scan [Halpi &Kardos 1972].

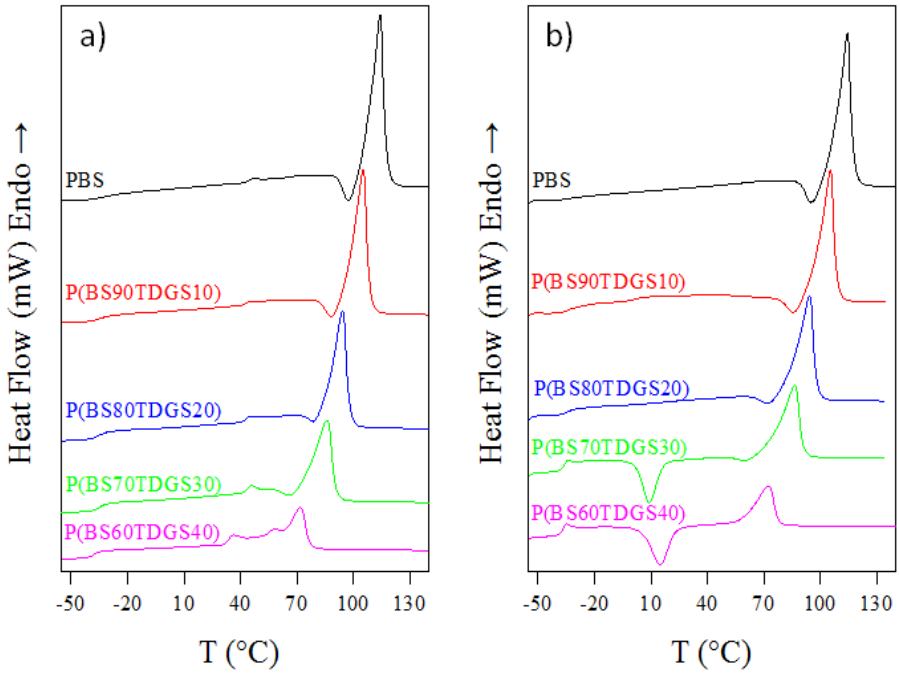

Figure 4.21 Calorimetric curves of PBS and P(BSxTDGSy) copolymers: (a) 1st scan, (b) 2nd scan after melt quenching.

X-ray diffraction (XRD) measurements were performed to study the nature of the crystalline phase present in P(BSxTDGSy) copolymers. The patterns are showed in Figure 4.22, together with that of PBS added for sake of comparison. The PBS sample

shows three main reflections at 2θ values of 19.6°, 21.9°, 22.6° attributable respectively to 020, 021 and 110 planes of α-crystal form [Dusunceli & Colak, 2008].

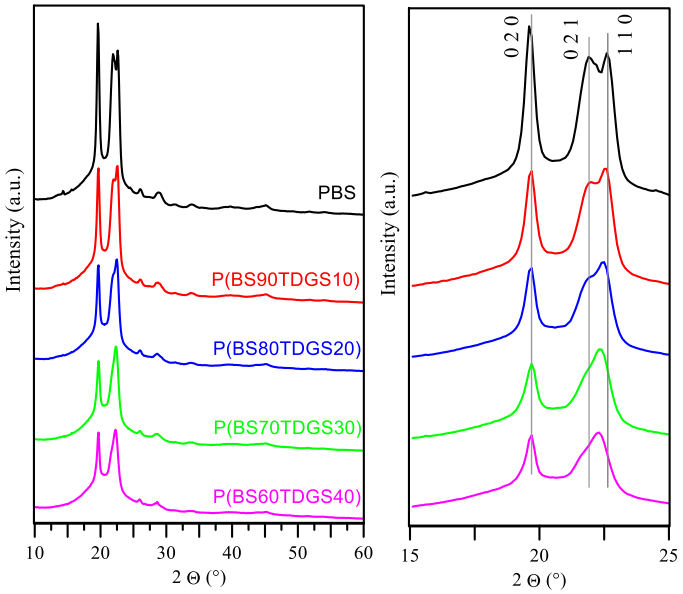

Figure 4.22 X-ray diffraction profiles of PBS and P(BSxTDGy) copolymers (left). An enlarged view (right); vertical lines are reference for the reader.

The copolymer samples are characterized by the same kind of pattern, i.e. the same crystal phase. However, the reflections appeared to be progressively broader and less intense as the TDGS content increased, indicating the presence of smaller crystal size and lower crystallinity amount (see Table 4.12).

Table 4.12 Crystal sizes in the direction perpendicular to 0 2 0 planes (L_{020}) and crystallinity index (X_c).

Polymer	L_{020} (nm)*	X_c (%)#
PBS	20	45 (4)
P(BS90TDGS10)	19	41 (4)
P(BS80TDGS20)	17	36 (3)
P(BS70TDGS30)	16	33 (3)
P(BS60TDGS40)	15	31 (3)

* e.s.d. < 1 nm # e.s.d. in parentheses

As can be seen from the zoomed view in Figure 4.22, the position of the 021 and 110 reflections slightly shifted towards smaller angles (longer distances) as the amount of TDGS co-units increased, while the position of the 020 reflection did not change. This could be due to a distortion in the *α*-PBS unit cell caused by the presence of the longer TDGS co-unit, in line with a modest increase in the *c*-axis (chain axis) length as well as along the *a*-axis.

It has to be pointed out that the distortion is different from that observed for the P(BSxPBDGy) system, previously investigated by some of us [Gigli et al., 2013 (a)]. In this case, the position of 110 reflection remained constant, while those of the 0 2 0 and 0 2 1 reflections shifted in the expansion direction (see Figure 4.23). Although the cocrystallization of TDGS or BDG units inside *α*-PBS phase can be excluded, in both cases the disorder caused by the presence of the ethero atom containing co-units affects the position of *hkl* reflections containing a *l*≠0 index (i.e. along those related with chain length). Nevertheless, for BDG also the *k*≠0 reflections are influenced, being the C=O groups of the diglycolate unit in a planar zig-zag conformation oriented in the *b*-axis direction.

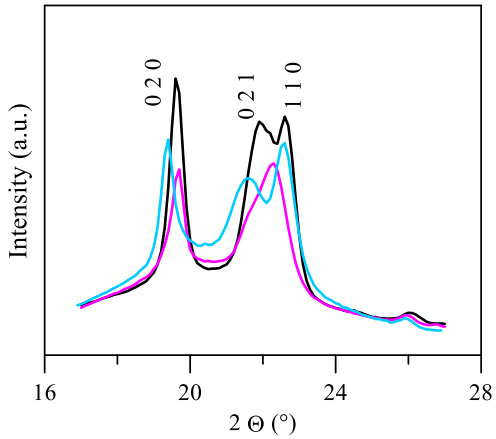

Figure 4.23 Comparison of XRD patterns of PBS (black), P(BS60TDGS40) (pink) and P(BS60BDG40) (light blue).

In order to confirm X-ray results about the complete exclusion of the TDGS comonomer units from the PBS crystal lattice, the applicability of the Baur's model [Baur, 1966] proposed in the literature to describe the dependence of T_m on composition (see chapter 1.2.3.1) was verified.

The melting temperatures of synthesized copolymers together with the data related to random copolymers poly(butylene succinate/diglycolate) (P(BSxBDGy)) previously investigated in our laboratories [Gigli et al., 2013 (a)] were plotted as a function of buthylene succinate molar fraction in Figure 4.24a. As can be observed, T_m of both the copolymeric systems examined appeared to lie on the same curve, decreasing with the increasing of the co-unit content. As T_m depends exclusively on the molar fraction of BS and not on the specific chemical characteristics of the co-units, the total exclusion of these last from the crystalline lattice of PBS was confirmed, as well as the random nature of the copolymers investigated.

On the basis of Baur's equation [Baur, 1966], which is applicable in the case of comonomer exclusion, the $T_{m,co}$ were reciprocally plotted against $-[lnx_c - 2x_c\,(1-x_c)]$ in Figure 4.24b and the equilibrium melting temperature (T_m^0) and the heat of fusion (ΔH_m^0) for the completely crystalline PBS were extrapolated. As can be noted, a good linear extrapolation is obtained. This result can be considered a further proof of the random nature of the copolymers investigated as well as of the exclusion of the co-units from the crystalline lattice of PBS. The estimated T_m^0 and ΔH_m^0 were found to be 128°C and 114 J/g respectively, in good agreement with the values reported in the literature [Gigli et al., 2013 (a); Baur, 1966; Halpi &Kardos 1972].

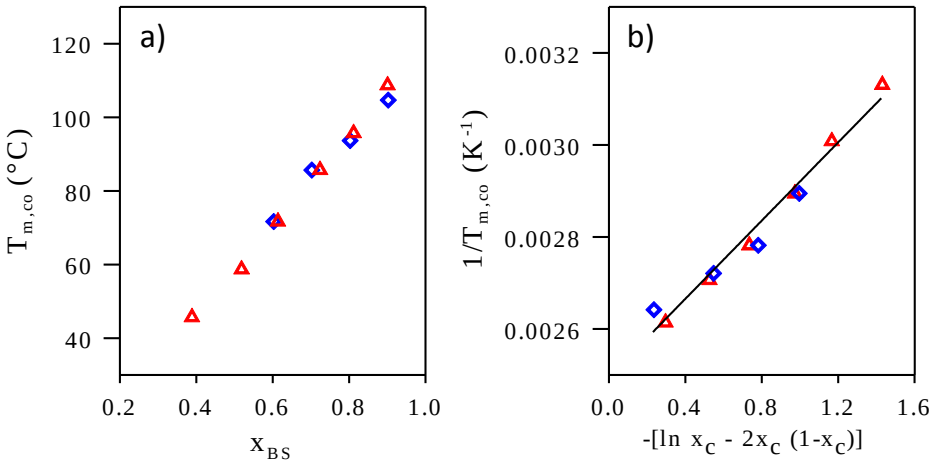

Figure 4.24 a) $T_{m,co}$ – X_{BS} molar fraction plot and b) $1/T_{m,co}$ – composition plot according to Baur's equation: ◇ P(BSxTDGSy) copolymers, △ P(BSxBDGy) copolymers[Gigli et al., 2013 (a)].

Figure 4.21b) shows the DSC curves after rapid cooling (quenching) from the melt: the calorimetric curves of PBS and P(BSxTDGSy) copolymers containing up to 20 mol % of TDGS units showed a melting endotherm phenomenon, indicating the partially crystalline nature of these samples.

P(BS70TDGS30) and P(BS60TDGS40) displayed a glass transition followed by an exothermal "cold crystallization" peak and a melting endotherm at higher temperature. In the case of P(BS70TDGS30), the enthalpy associated with the crystallization phenomenon is lower than that of the fusion endotherm, indicating that this sample cannot be frozen into a completely amorphous state by quenching. The DSC scan of such sample is therefore typical of semi-crystalline polymers. Lastly, P(BS60TDGS40) has proved to be completely amorphous since the enthalpy of crystallization very well compares with the corresponding heat of fusion.

Regarding the glass transition phenomenon, it has to be noted that no effect of copolymer composition was observed, being the T_gs of the two homopolymers very similar [Siracusa et al., 2015].

To evaluate the tendency of PBS to crystallize in the copolymers under study, non-isothermal experiments were carried out, subjecting the samples to a controlled cooling rate from the melt (see Figure 4.25).

As it can be observed in figure 4.25, the temperature of the maximum of the exothermal crystallization peak regularly decreased as the TDGS molar percentage was increased. The decrease of the exothermal crystallization temperatures reveals a decrement of the overall crystallization rate of PBS, due to the presence of the co-unit, which acts as obstacle in the regular packing of polymer chains.

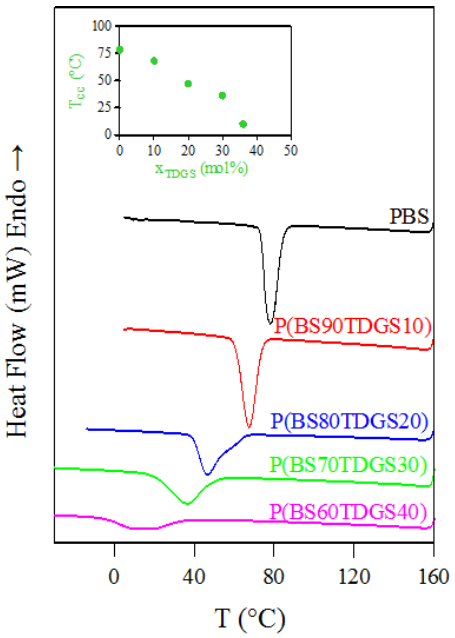

Figure 4.25 DSC crystallization exotherms of PBS and P(BSxTDGSy) random copolymers cooled from the melt at 5°C/min. In the inset: T_{cc} as a function of TDGS unit content.

4.2.3 Mechanical characterization

The study of the mechanical properties of the synthesized polymers is very significant for the potential application of the materials. Therefore, P(BSxTDGSy) copolymers were subjected to stress-strain measurements. In Table 4.13 are reported the values of elastic modulus (E), stress at break (σ_b), and deformation at break (ε_b), together with the data of PBS added for sake of comparison.

Table 4.13 Mechanical characterization data of PBS and P(BSxTDGSy) copolymers.

Polymer	E (MPa)	σ_b (MPa)	ε_b (%)
PBS	440±30	32±3	17±2
P(BS90TDGS10)	360±10	29±1	290±30
P(BS80TDGS20)	260±10	23±3	580±70
P(BS70TDGS30)	230±20	29±2	870±40
P(BS60TDGS40)	160±3	21±2	810±20

As to the homopolymer, it is worth noting that the measured E is 24% higher than that previously determined by us. The difference is due to the presence in the PBS under

study of glycerol, which creates more entanglements, making more difficult the polymer chain slipping past.

As far as the copolymers are concerned, it can be observed that the elastic modulus gradually decreased with increasing TDGS contents; on the contrary, the elongation at break shows an opposite trend and increases with the increasing of the molar amount of TDGS co-unit.

Moreover, it is worth mentioning that the copolymers P(BS70TDGS30) and P(BS60TDGS40) are characterized by an elastomeric behavior.

Since all the investigated polymers display a soft amorphous phase (T_g values are in all cases well below room temperature), the observed trend can be ascribed to the crystallinity degree (Table 4.12) and to the higher copolymer chain flexibility due to the presence of longer C-S bonds with respect to C-C ones.

It is in fact well known [Van Krevelen, 1977; Dusunceli & Colak, 2008] that crystallinity degree has a remarkable effect on the mechanical properties of a polymer: in particular high X_c results in harder, stiffer and less ductile behavior. As therefore expected, the higher the BS content, the higher the elastic modulus and the stress at break and the lower the elongation ability of the investigated polymers.

In conclusion, by just varying the molar composition of the copolymers, it is possible to obtain new materials that can be used for different packaging applications, from rigid plastic containers to soft wrapping films.

4.2.4 Barrier properties

Gas transmission rate (GTR) values of the synthesized polymers, with respect to the two analyzed gases are collected in figure 4.25.

Time lag (t_L), solubility (S), and diffusivity (D) are reported in Tables 4.14 and 4.15 for O_2 and CO_2 pure gas, respectively.

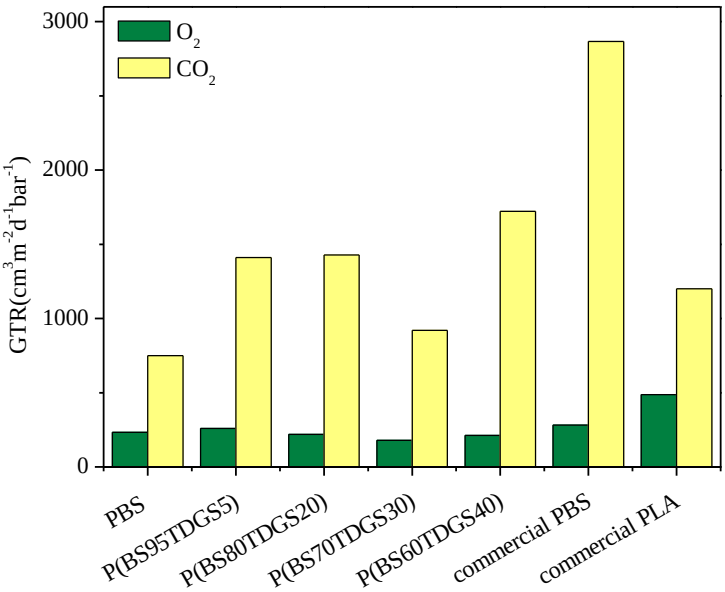

Figure 4.25: GTR values for O_2 and CO_2 gases of P(BSxTDGSy) copolymers

Table 4.14. Permeability coefficients: t_L *(s)*, S *($cm^3 cm^{-2} bar^{-1}$)* and D *($cm^2 sec^{-1}$)* for O_2 gas of P(BSxTDGSy) copolymers.

Polymer	t_L	$S \cdot 10^3$	$D \cdot 10^8$
PBS	110±10	4.35±2.76	88.6±0.1
P(BS90TDGS10)	80 ±10	6.95±0.56	89.1±7.4
P(BS80TDGS20)	90±4	7.22±0.02	71.2±0.1
P(BS70TDGS30)	1400±5	72.5±2.5	6.95±0.23
P(BS60TDGS40)	1400 ±10	70.6±0.7	10.1±0.1
PBS*	50±10	4.48±2.76	67.4±9.9
PLA***	/	/	/

Table 4.15 Permeability coefficients: : t_L *(s)*, S *($cm^3 cm^{-2} bar^{-1}$)* and D *($cm^2 sec^{-1}$)* for CO_2 gas and selectivity ratio CO_2/O_2 of P(BSxTDGSy) copolymers.

Polymer	t_L	S	$D \cdot 10^8$	CO_2/O_2
PBS	4400±500	1.18±0.14	1.43±0.19	3.21
P(BS90TDGS10)	1300±200	0.68±0.12	4.74±0.81	5.44
P(BS80TDGS20)	2300±100	0.99±0.05	3.90±0.22	6.49
P(BS70TDGS30)	4800±100	1.78±0.04	1.45±0.03	5.14
P(BS60TDGS40)	6800±100	0.97±0.13	6.13±0.93	8.10
PBS*	810±20	1.10±0.06	4.34±0.12	10.20
PLA*	/	/	/	2.46

From data collected in figure 4.25, it can be observed that copolymers show a different permeability behavior, depending on the gas used. Using O_2 gas test, the highest GTR value was recorded for P(BS90TDGS10) sample, while the lowest for the P(BS70TDGS30) one. Interestingly, this trend is not correlated with the crystallinity degree, which decreased with the increasing of TDGS mol %. It can be on the contrary explained on the basis of polymer molecular weight: in P(BS90TDGS10) the low chain mobility, due to the high polymer molecular weight, allows the O_2 molecules to move faster across the polymer matrix, without obstacle.

On the contrary, for P(BS70TDGS30) sample the lowest GTR value is due to the high flexibility and mobility of the lower molecular weight polymer chains, which gives rise to a more tortuous path across the matrix. As reported from Jamshidian et al. [Jamshidian et al., 2012], in some cases crystallinity leads to a higher permeability because of the phenomenon of de-densification of the amorphous phase, which counteracts the decrease of the quantity of permeable amorphous phase due to crystallization [Siracusa, 2012]. With CO_2 gas test, the GTR values are higher and increase with the increment of the TDGS mol %. In particular, the samples under investigation follow a standard trend, well correlated both to molecular weight and percentage of crystallinity with the exception of P(BS70TDGS30). As a matter of fact, the samples with lowest molecular weight and lowest crystallinity degree showed the highest permeability, in agreement with data[Gigli; Negroni et al., 2012]. The P(BS70TDGS30) copolymer is characterized by a peculiar and different behavior. Its permeability appeared to be the lowest to both gases.

As is well known, factors affecting the permeability coefficients of a polymer may be divided into those associated with the polymer itself and those influencing the diffusion coefficient D and the solubility coefficient S. In this case, the factors correlated to chemical structure are prevalent and determine its permeability behavior. This could be explained taking into account the polymer molecular weight and the polydispersity index (PDI).

As can be noted from the data reported on Table 4.10, this copolymer sample is characterized by the lowest molecular weight and by the highest degree of polydispersity, among the polymers synthesized. The gas molecule motion is more tortuous due to the short polymer length chain and consequently the associated

permeability coefficients change: in particular, GTR decreases, S increases, D decreases and t_L increases, more significantly for CO_2 than for O_2 gas, as expected.

As far as the perm-selectivity ratio between the two gases is concerned, it increases with the increasing of TDGS mol % (see Table 4.15). The presence of the C-S bonds facilitates the CO_2 gas crossing, due to the lower chain mobility, confirming the higher tendency of this gas to cross the polymer wall. With O_2, gas transmission on the contrary shows an opposite trend, decreasing even though slightly with increasing TDGS unit mol %. Despite the high crystallinity degree decrement, the large atomic radius of S atoms (the volume of S atom is similar to that of CH_2 group) and as a consequence, the longer C-S bond (1.81-2.55 Å) with respect to the C-C (1.54-1.20 Å) and C-O ones (1.43-2.15 Å) [Siracusa, 2012], lead to a major steric obstacle to the gas molecules crossing, giving rise to a decrement of the corresponding O_2 GTR. Further, as can be observed from the data reported, experimental perm-selectivity ratios are very different from those reported in literature (CO_2/O_2 average ratio of 6.32 is considered for all polymer matrix). This is a further evidence that the perm-selectivity ratio of the two gases is not relatively constant and independent on polymer type [George and Thomas, 2001]. In the case of CO_2, the highest GTR value was recorded, beside the greater molecular dimension, due to the low diffusion coefficient D and the very high solubility coefficient S (much greater than that of the other gas). As it can be evicted from the data reported in Tables 4.14.and 4.15, O_2 D values are higher than CO_2 D ones, O_2 S values are lower than CO_2 S ones and consequently O_2 t_L values are lower than CO_2 t_L ones. This last permeability coefficient indicates that the carbon dioxide molecules spend more time to distribute on the polymer film surface than O_2 ones, due to their faster and very chaotic motion.

Gas transmission results here presented are of particular relevance if we compare the permeability behavior of the P(BSxTDGSy) copolymers with that of commercial PBS and PLA films, investigated under the same conditions [Siracusa et al., 2012; Blanco & Siracusa, 2013]. As it can be observed in figure 4.25, the copolyesters under investigation show lower permeability, and therefore improved barrier properties, to both CO_2 and O_2 gases, especially with respect to Poly (lactic acid) that is, as a matter of fact, the most extensively used polyester in the production of biodegradable packaging films.

4.2.5 Composting

Biodegradation rate has been evaluated by determining the weight losses of PBS and P(BSxTDGSy) copolymers during compost incubation.

The degradation rate was found to be strictly affected by the presence of sulphur atoms along the polymeric chain (Figure 4.26). In fact, PBS displayed negligible weight loss, while in the case of copolymers, biodegradability appeared to be correlated to copolymer composition, being the weight loss higher the higher the TDGS mol% (Figure 4.26).

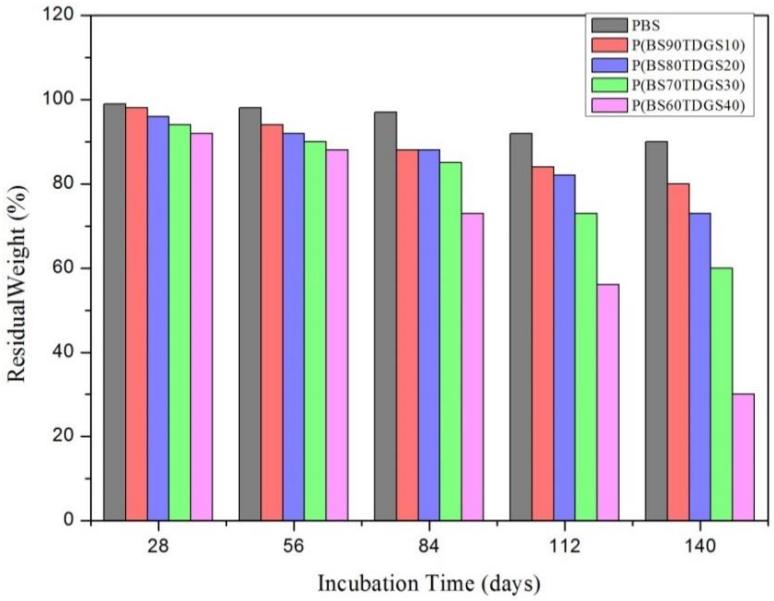

Figure 4.26 Residual weight % as a function of incubation time of PBS and P(BSxTDGSy) random copolymers.

The observed trend can be explained on the basis of the differences in the crystallinity degree and surface wettability: both factors can influence the biodegradation rate of a polymer, the higher the crystallinity degree and the surface hydrophobicity, the lower the biodegradation rate [Gigli, Negroni et al., 2012; Gigli, Negroni et al., 2013 (a)].

The morphology of the polyesters films was studied by Scanning Electron Microscopy. As an example, micrographs of PBS, P(BS90TDGS10) and P(BS60TDGS40) films are reported in Figure 4.27. All the copolymers showed a smooth and homogenous surface before incubation. After composting, SEM analyses highlighted results in agreement with weight loss measurements: the films were characterized by the presence of cracks

and holes on the polymeric surface, whose number and dimensions increased with incubation time and with TDGS unit content. The P(BS60TDGS40) copolymer displayed large damaged areas, of about 50% of the total surface after 140 days of incubation, with numerous cracks, channels and large holes.

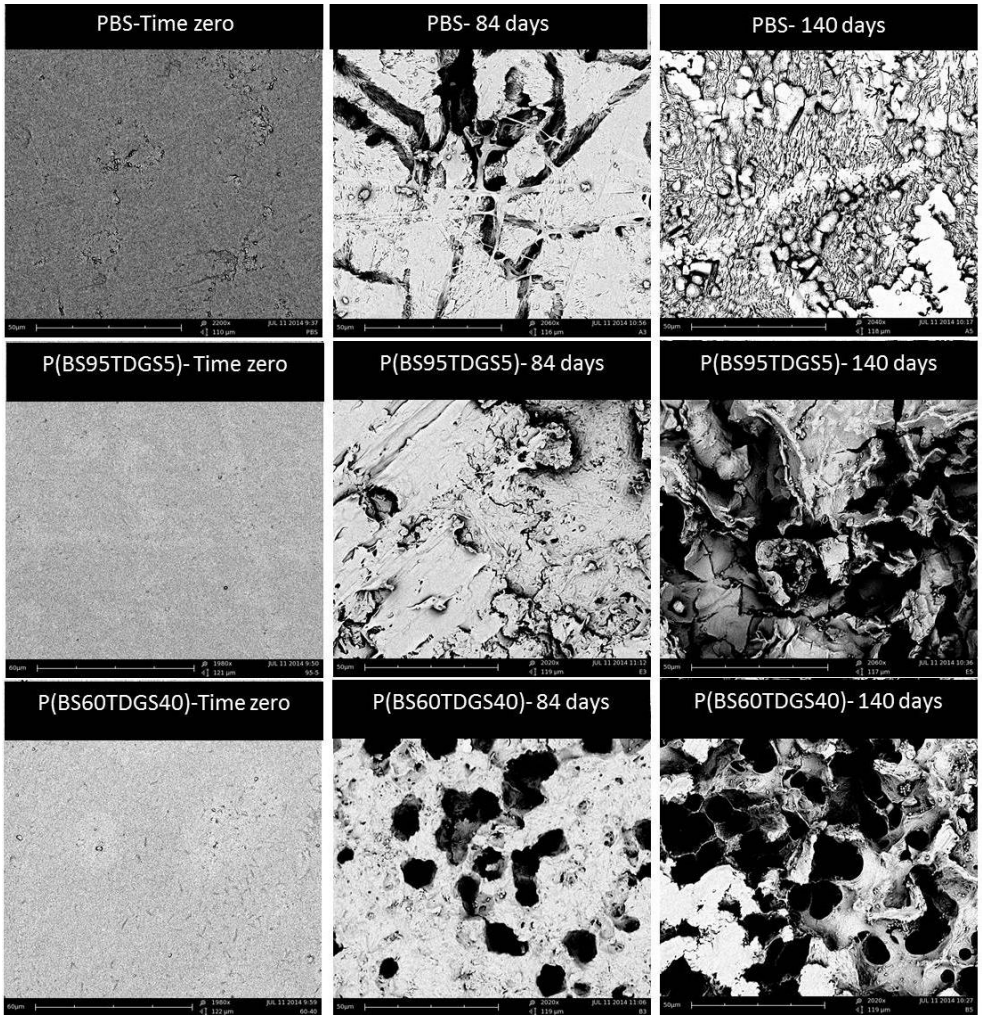

Figure 4.27 SEM micrographs of PBS, P(BS90TDGS10) and P(BS60TDGS40) at different incubation times.

4.2.6 Conclusions

Poly(butylene succinate) has been chemically modified by copolymerizing it with different amounts thiodiethylene glycol to obtain fully aliphatic copolyesters. This easy, solvent free, synthetic way allowed the preparation of a new class of copolymers with improved properties with respect to the parent homopolymer which can be effectively tuned simply varying the copolymer composition.

As expected, the introduction of thioether-linkages resulted in a decrease of the crystallinity degree and melting point, due to a decrement of chain symmetry and regularity, and in slightly increase of the surface hydrophilicity. The higher the molar content of TDGS co-units, the greater the effect on these properties. As a consequence, the mechanical and barrier properties and the biodegradation rate turned out to be deeply influenced by the copolymer composition. It has been observed that the mechanical properties of the copolymers are controllable and tunable, and the copolymers can be ranged from rigid plastics to soft elastomers with increasing TDGS molar content.

As to the barrier properties, a modulation of the permeability behavior to CO_2 and O_2, depending on the copolymer composition of the copolymers, has been noticed. It is worth noting that P(BSxTDGSy) copolymers displayed better barrier properties to both gases with respect to commercial Poly-lactic acid. Moreover, the copolyesters presents a higher biodegradation rate in compost with respect to the homopolymer, once again related to the copolymer composition: the higher the TDGS mol%, the higher the weight losses of the copolymers under study.

In conclusion, copolymerization of PBS with TDGS units permits a fine modulation of the properties of the final material: in particular, P(BS70TDGS30) copolymer can be considered the best candidate for sustainable food packaging applications, being characterized by good mechanical properties, excellent gas barrier features and good biodegradation rate.

4.3 Biodegradable PLLA-based triblock copolymers

A novel poly(lactic acid)-based copoly(ester-urethane) system has been synthesized. The system is composed of a series of A-B-A triblock copolymers, where A, the *hard block*, is poly(lactic acid) and B, the *soft block*, is a random aliphatic copolyester poly(propylene/neopentyl glycol succinate), characterized by low crystallinity and high flexibility. Triblock units are joined by hexamethylene diisocyanate, known chain extender, that allows to obtain polymers with high molecular weights and good mechanical properties.

With the aim of improving the functional performance of poly(lactic acid) for food packaging applications, we studied the effect of copolymerization on its mechanical and barrier properties and compostability. A detailed molecular, thermal and structural characterization of the samples under investigation was also carried out.

4.3.1 Synthesis and Molecular Characterization

After the purification process (see chapter 3.2.3.2 for synthetic and purification procedures), the OH-terminated P(PS80NS20) random copolymer appeared as a light yellow coloured rubber. The chemical structure, the composition and the molecular weight of P(PS80NS20) prepolymer have been determined by ^{1}H-NMR spectroscopy. Figure 4.28 shows the ^{1}H-NMR spectrum of P(PS80NS20), together with the chemical shift assignments. The spectrum was found to be consistent with the expected structure. In particular, the methylene protons, *b* and *d*, of the propylene subunit are located at δ 4.19 ppm and δ 1.98 ppm, respectively, while the protons of neopentyl glycolic unit, *c* and *e*, are located at δ 3.91 ppm and δ 0.97 ppm, respectively. The singlet *a* of the acid subunit is situated at δ 2.63 ppm. Besides the signals of the aliphatic protons of the inner repetitive units, the peaks due to the outer subunits can also be detected: the triplets *b*', *b*'' and *d*' for propanediol and the singlets *c*', *c*'' and *e*' for neopentyl glycol.

The copolymer composition was calculated from the relative areas of the ^{1}H-NMR resonance peaks related to *b*, *b*' and *b*'' protons of the propanediol subunit and *c*, *c*' and *c*'' aliphatic protons associated to neopentyl glycol subunit. The actual molar composition is very close to the feed one.

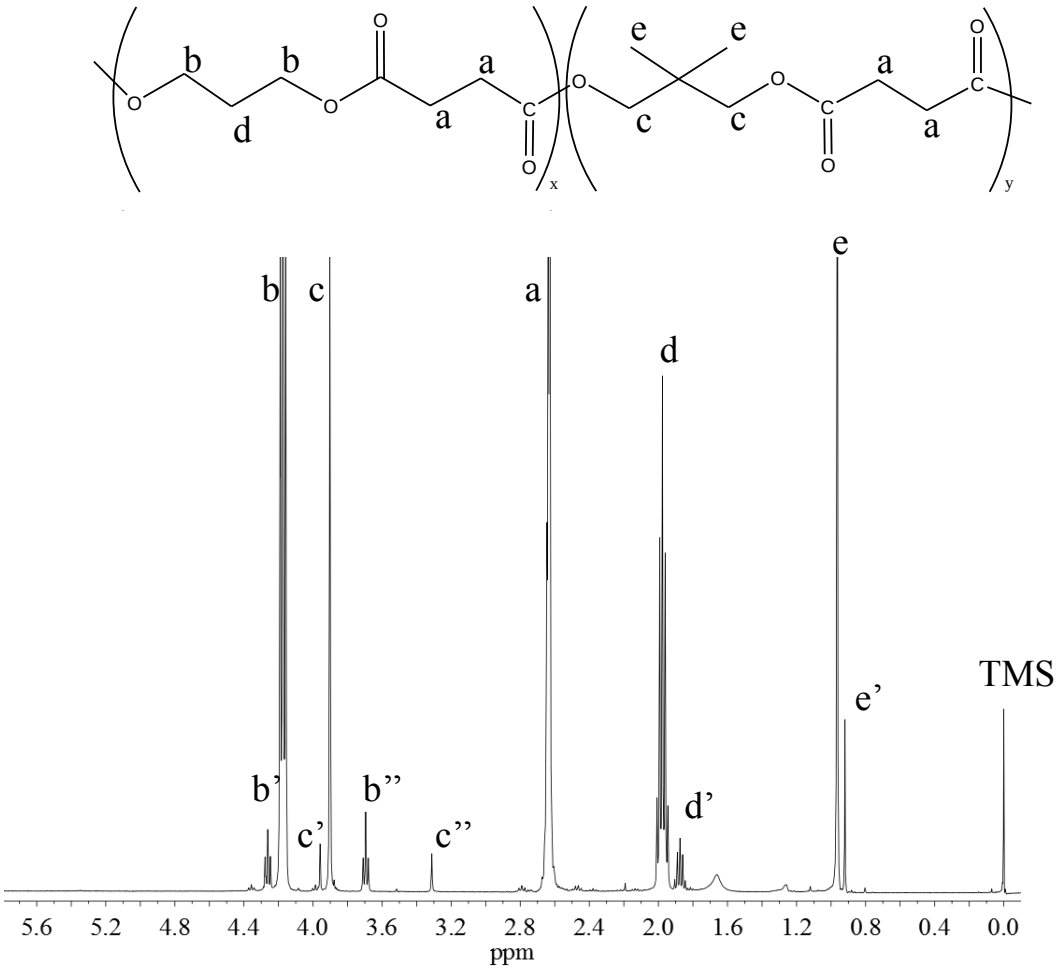

Figure 4.28: ^{1}H-NMR spectrum of the low molecular weight random copolymer P(PS80NS20) with resonance assignments.

The copolymer degree of polymerization (DP) has been calculated from the relative areas of *b* and *c* protons of central propanediol and neopentyl glycol, respectively (I_b and I_c) and *b*' and *c*' protons of terminal propanediol and neopentyl glycol, respectively ($I_{b'}$ and $I_{c'}$) as follows:

$$DP = \frac{I_b + I_c + 2 * (I_{b'} + I_{c'})}{I_{b'} + I_{c'}} \qquad [32]$$

The copolymer molecular weight (M_n) has been obtained according to the following formula:

$$M_n = DP * (M_w^{PS} * X_{PS} + M_w^{NS} * X_{NS}) \qquad [33]$$

where:

M_w^{PS} is the molecular weight of the propanediol succinate repetitive unit; M_w^{NS} is the molecular weight of the neopentyl glycol succinate repetitive unit; X_{PS} is the actual propanediol succinate molar fraction; X_{NS} is the actual neopentyl glycol succinate molar fraction.

M_n calculated by this procedure turns out to be 4300 g/mol.

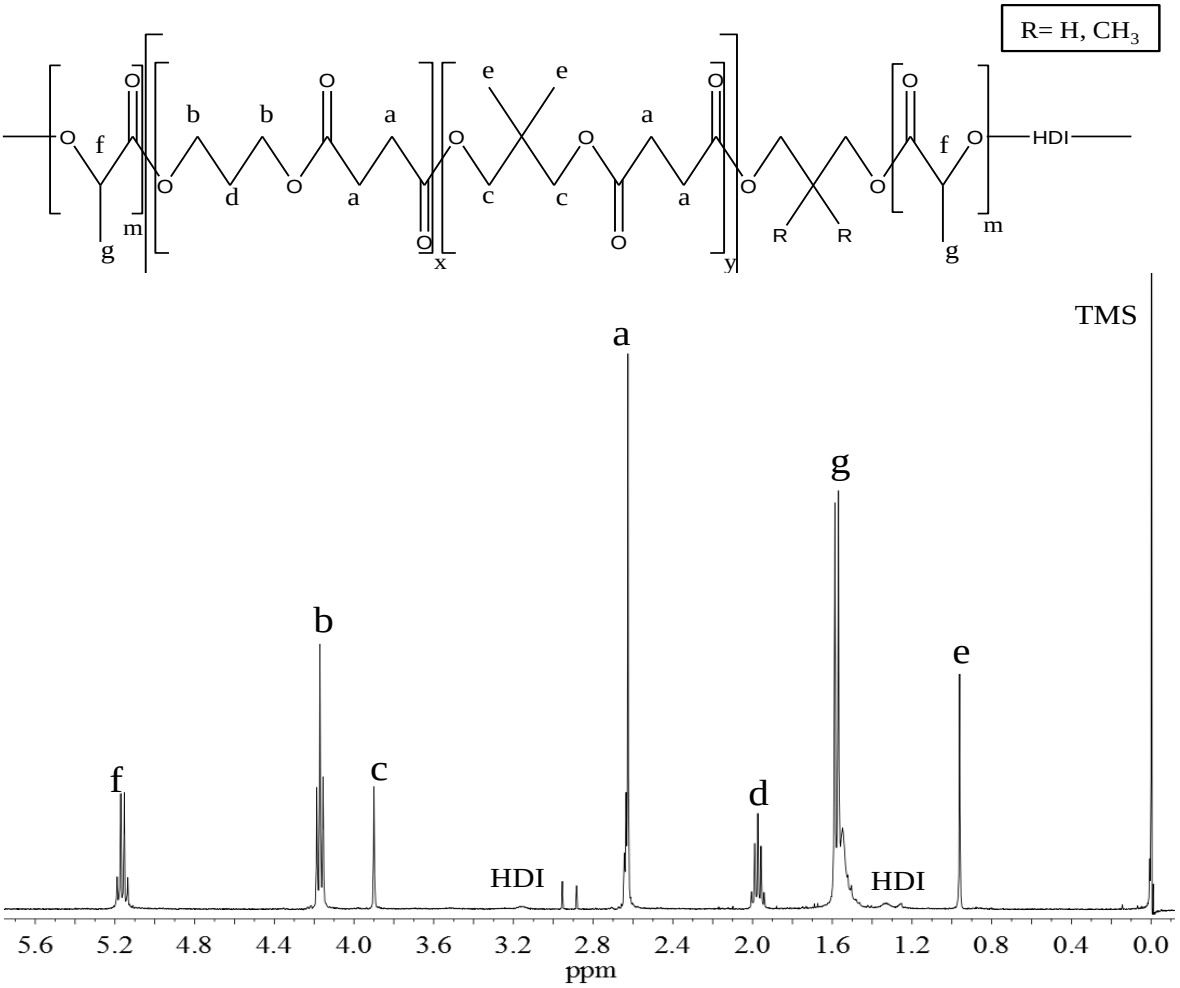

Figure 4.29: ^{1}H-NMR spectrum of $PLLA_{30}P(PS80NS20)_{70}$ triblock copolymer with the corresponding resonance assignments.

The triblock copolymers have been obtained by *in situ* ring opening polymerization (ROP) of L-lactide by OH-terminated P(PS80NS20) and subsequently, by chain extension process, adding an equimolar amount of HDI with respect to the OH groups of the molten prepolymer. Similarly, chain extended PLLA has also been synthesized, by using low amount of propanediol as initiator (see chapter 3.2.4.1).

Chain extended PLLA and triblock copolymers appeared as semicrystalline solids,

white and light yellow coloured respectively.

No unreacted HDI was detected by NMR analysis after 1 hour of reaction. As an example, the ^{1}H-NMR spectrum of $PLLA_{30}P(PS80NS20)_{70}$ triblock copolymer is reported in Figure 4.29: with *h*, *i* and *j* indicate the protons of the chain extender located at δ 3.18 ppm, 1.34 ppm and 1.25 ppm, respectively. All the spectra are consistent with the expected structure. The actual composition, calculated by the relative areas of protons *a* of the succinic unit (2.62 ppm) and the proton *f* of the lactic unit (5.18 ppm), resulted very close to the feed one (Table 4.16). The HDI content was in all the cases below 5%.

Table 4.16 reports also the molecular weight data (M_n) obtained by GPC. As expected, the samples show a molecular weight higher than that of prepolymer. Moreover, a pretty narrow polydispersity (D) was found, indicating a good control over both the ring opening polymerization and the chain extension process.

Table 4.16. Molecular characterization data of the synthesized copoly(ester-urethane)s system.

Samples	wt% PLA (feed)	wt% PLA (^{1}H-NMR)	M_n (g/mol) (GPC)	D (GPC)
$PLLA_{16}P(PS80NS20)_{84}$	20	16	18300	2,5
$PLLA_{24}P(PS80NS20)_{76}$	30	24	15600	2,9
$PLLA_{43}P(PS80NS20)_{57}$	45	43	21100	1,4
$PLLA_{45}P(PS80NS20)_{55}$	50	45	41000	1,2
$PLLA_{46}P(PS80NS20)_{54}$	50	46	15000	1,7
$PLLA_{67}P(PS80NS20)_{33}$	70	67	12100	1,6
PLLA	100	100	33000	2,2

4.3.2 Thermal and Structural Characterization.

The synthesized triblock copolymers have been subjected to thermogravimetric analysis under dry nitrogen atmosphere (TGA). The calorimetric curves are reported in Figure 4.30and the temperature corresponding to 5% weight loss ($T_{5\%loss}$) for all the samples analysed is collected in Table 4.17. As shown in Figure 4.30, PLLA homopolymer is less thermally stable with respect to P(PS80NS20) prepolymer. This effect could be due to the higher ester groups density per repeating unit in the PLLA chains with respect to the P(PS80NS20) ones. Regarding the triblock copolymers, the thermal degradation

took place in two steps. The relative height of the two steps clearly depends on the composition. The higher is the PLLA content, the more intense is the first weight loss step. Anyway, the thermal stability in the PLLA-based copolymers is comparable to that of the homopolymer: with the increasing of B-block content, the thermal degradation process starts at slightly lower temperatures (lower $T_{5\%loss}$).

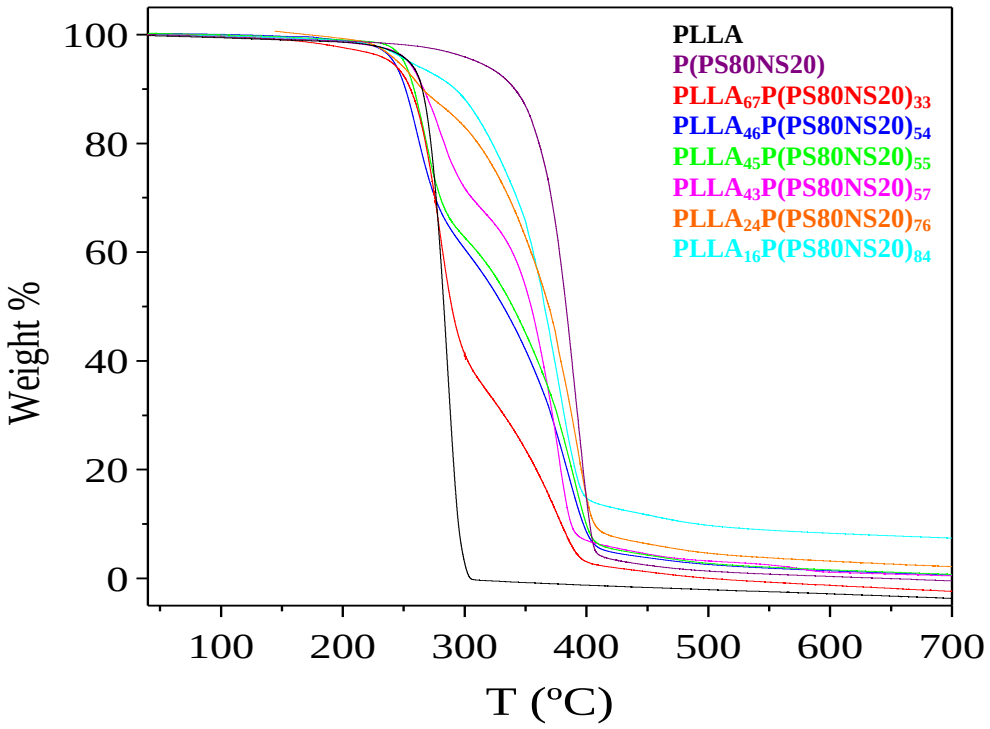

Figure 4.30: Thermogravimetric curves of PLLA, P(PS80NS20) and the corresponding $PLLA_mP(PS80NS20)_n$ under nitrogen atmosphere and at a heating rate of 10°C/min.

Prior to further characterization, the compression moulded polymers films (see section 3.4) have been stored at room temperature for one month in order to attain equilibrium crystallinity. In fact, as shown in Figure 4.31 for $PLLA_{67}P(PS80NS20)_{33}$, the thermal behaviour clearly depends on the storage time at room temperature. The just prepared film presents one wide glass transition and a melting peak at 135° C; after 14 days, two T_gs can be detected in the calorimetric curve together with a double melting peak; after 30 days, the DSC curve still presents two T_gs but a single endothermic peak at 141°C and, in between, a crystallization peak at 75°C.

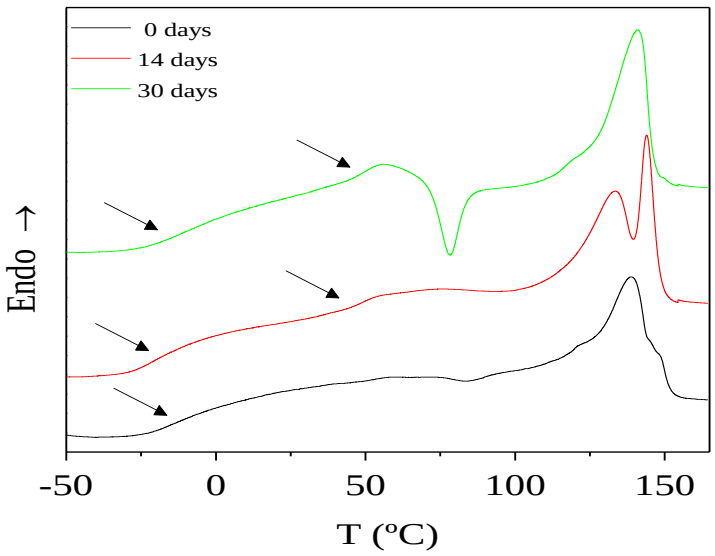

Figure 4.31 Calorimetric curves of $PLLA_{67}P(PS80NS20)_{33}$: 1st scan at different storage times.

The DSC curve of the compression moulded polymer film (0 days) indicates that, after the melting and cooling to room temperature, an amorphous and a semicrystalline phase are present in the material. The presence of one wide glass transition phenomenon suggests that the two comonomeric units are miscible in the amorphous phase. On the other hand, the endotherm at higher temperature points out that PLLA segments have crystallized during the cooling of the compression moulded film. After 14 days, a phase separation in the amorphous state occurs, generating a PLLA-rich phase and a P(PS80NS20)-rich one, each with own T_g. The melting peak also suffers a change suggesting the mobility of PLLA segments at 25° C. After one month, the calorimetric curve, besides the two glass transition phenomena and the melting peak, also evidenced an exothermic peak, due to the crystallization of the remaining amorphous PLLA segments formed because of the further phase separation, which are long enough to fold. No further changes have been detected for longer storage times (data not shown).
Therefore, a period of 30 days has proven to be appropriate for making uniform the thermal history and reaching the equilibrium crystallinity. DSC traces of the films stored for 1 month are reported in Figure 4.32 and the data obtained in Table 4.17 and 4.18.

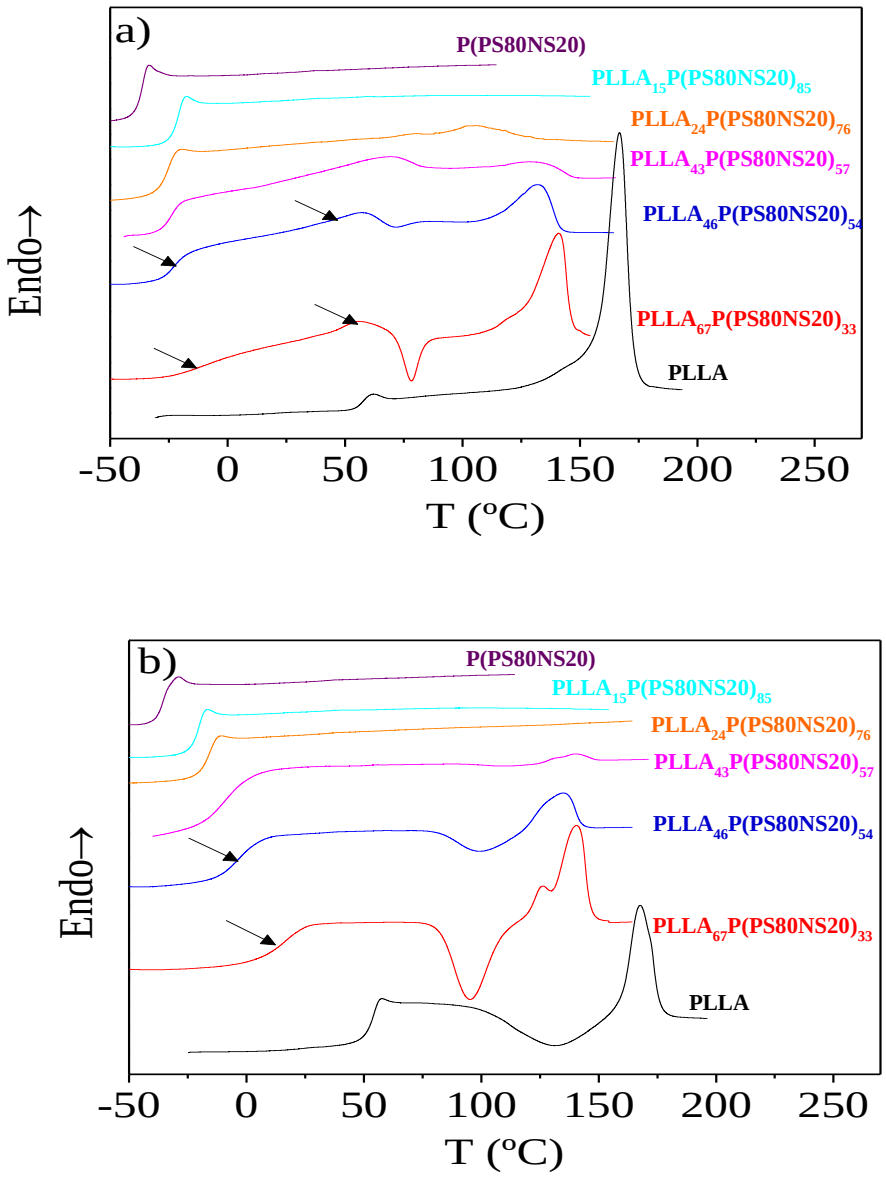

Figure 4.32: Calorimetric curves of chain extended PLLA and $PLLA_mP(PS80NS20)_n$ triblock copolymers: a) 1st scan; b) 2nd scan after melt quenching.

In Figure 4.32a are reported the first scan DSC traces of PLLA, P(PS80NS20) and their copoly(ester urethane)s ($PLLA_mP(PS80NS20)_n$). The calorimetric curves of the system under investigation evidence that the thermal behaviour of $PLLA_mP(PS80NS20)_n$ copolymers deeply depends on the weight ratio between the *hard* and the *soft* blocks. The triblock copolymer with PLLA weight content equal to 24% shows at low temperature the step associated with the glass transition followed by a melting endotherm at higher temperature. For PLLA weight amounts ≥ 43%, two glass

transitions can be detected: the low temperature T_g, related to the P(PS80NS20)-rich phase and the higher temperature T_g associated with the PLLA-rich phase. Moreover, the samples with weight contents of PLLA ≥ 46%, after passing T_g, are able to crystallize during the temperature scan. Nevertheless, as one can see from the data collected in Table 4.17, the corresponding crystallization heat is significantly lower than the melting enthalpy indicating these copolymers are semicrystalline. On the other hand, the DSC traces of the random prepolymer P(PS80NS20) and $PLLA_{16}P(PS80NS20)_{84}$ are exclusively characterized by a endothermic baseline deviation associated with the glass transition.

Concerning the melting phenomenon, in the case of PLLA homopolymer, the melting peak is located at high temperature (167 °C) and the heat of fusion associated is consistent, while the semicrystalline copolymers show melting temperatures and melting heats lower than PLLA. In particular, as the amount of *soft* segment increases, the melting peak shifts towards lower temperatures. In fact, higher content of P(PS80NS20) block leads to the formation of crystals with a lower degree of perfection. Simultaneously, the decrease of the *hard* phase (PLLA) also causes a reduction in the melting enthalpy value due to a lowering of the crystallinity degree. Anyway, the reduction of the melting temperature is not so consistent because of the structural regularity associated to the triblock architecture.

Table 4.17 Thermal characterization data by TGA and DSC (first scan) analysis.

Samples	$T_{5\%loss}$ (°C)	T_c (°C)	ΔH_c (J/g)	T_m (°C)	ΔH_m (J/g)	T_g (°C)	Δc_p (J/°Cg)
PS80NS20	319	-	-	-	-	-37	0,485
$PLLA_{16}P(PS80NS20)_{84}$	248	-	-	-	-	-22	0,465
$PLLA_{24}P(PS80NS20)_{76}$	251	-	-	103	2	-26	0,483
$PLLA_{43}P(PS80NS20)_{57}$	253	-	-	113	4	45	0,125
						-22	0.363
$PLLA_{45}P(PS80NS20)_{55}$	252	71	1	132	11	45	0,117
						-22	0,319
$PLLA_{46}P(PS80NS20)_{54}$	244	67	1	126	13	44	0,110
						-21	0,370
$PLLA_{67}P(PS80NS20)_{33}$	243	78	5	141	19	49	0,112
						-6	0,171
PLLA	265	-	-	167	40	56	0,389

Table 4.18 Thermal characterization data by DSC analysis (second scan, after melt quenching).

Samples	T_c (°C)	ΔH_c (J/g)	T_m (°C)	ΔH_m (J/g)	T_g (°C)	Δc_p (J/°Cg)
PS80NS20	-	-	-	-	-36	0,464
$PLLA_{16}P(PS80NS20)_{84}$	-	-	-	-	-21	0,475
$PLLA_{24}P(PS80NS20)_{76}$	-	-	-	-	-17	0,471
$PLLA_{43}P(PS80NS20)_{57}$	96	1	123	1	-7	0,616
$PLLA_{45}P(PS80NS20)_{55}$	99	7	135	8	-3	0,505
$PLLA_{46}P(PS80NS20)_{54}$	103	4	131	4	-2	0,576
$PLLA_{67}P(PS80NS20)_{33}$	96	17	140	17	16	0,437
PLLA	116	39	168	43	53	0,476

Wide angle X-ray scattering analysis was carried out in order to investigate the crystalline phase present in PLLA and in the semicrystalline copoly(ester urethane)s. The X-ray spectra are reported in Figure 4.33, while the cristallinty degree together with the 110 interplanar spacing are collected in Table 4.19. The diffractometric profiles are typical of semicrystalline materials showing well defined reflections, characteristic of the ordered portion of the material, superimposed over a bell-shaped baseline due to the amorphous component. As one can see from Figure 4.33, all the samples present a X-ray spectrum similar to the α crystalline phase of PLLA that is characterized by the peaks at 16.7° (110/200) and 19.1° (203/113) and by the intense reflections at 12.3° (103/004), 14.8° (011) and 22.3° (211), together with other less intense peaks. This evidence allows us to confirm that in all the semicrystalline copolymers under investigation, the crystalline phase detected by DSC is the α phase of PLLA. Copolymerization does not affect the position of the reflections, confirming the total exclusion of the amorphous *soft* segments from the PLLA crystals. However, the copolymer diffractometric spectra show a broadening of the reflections and an increase in the interplanar distances evidenced by the decrease in the 110 interplanar spacing (see Table 4.19), due to the difficulty of rejecting the comonomer units out of the PLLA crystal lattice. The reduction of the perfection of the crystal cell is also suggested by the decrease of the peaks intensity and the disappearance of some reflections, i.e. 021. In conclusion, the samples containing higher percentages of *soft* block are characterized by lower crystallinity degrees (see Table 4.19), in agreement with calorimetric results.

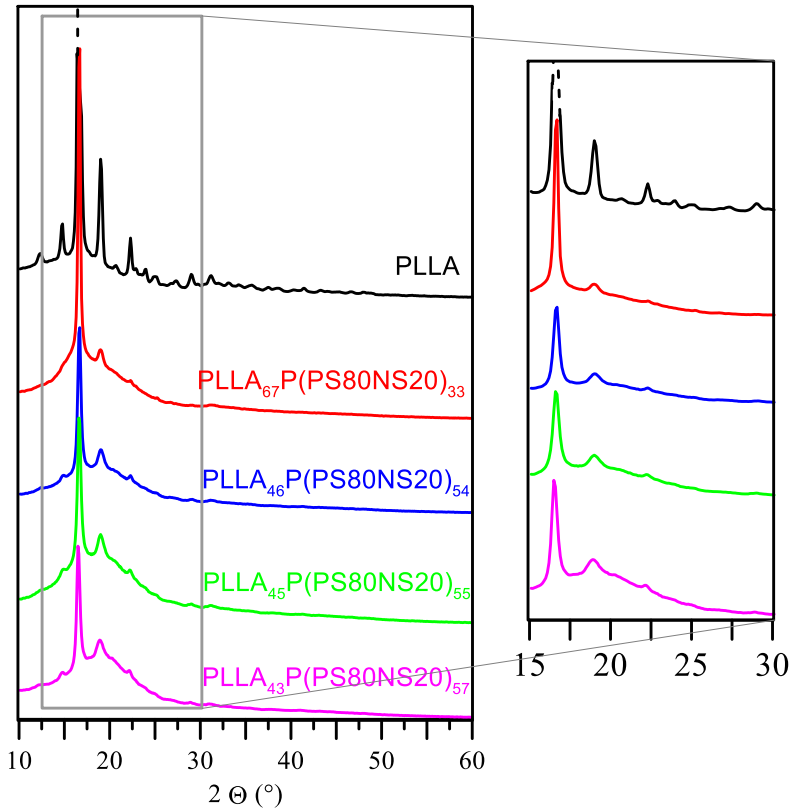

Figure 4.33: X-Ray diffraction patterns of PLLA and its $PLLA_mP(PS80NS20)_n$ copolymers.

Table 4.19 Diffractometric characterization data: crystallinity degree (X_c) and 110 interplanar spacing (L_{110}) of PLLA and its semicrystalline copoly(ester urethane)s.

Samples	X_c (%)	L_{110} nm *
PLLA	30	28
$PLLA_{67}P(PS80NS20)_{33}$	23	22
$PLLA_{45}P(PS80NS20)_{55}$	18	20
$PLLA_{46}P(PS80NS20)_{54}$	17	18
$PLLA_{43}P(PS80NS20)_{57}$	13	21

*estimated from the most intense reflex

Miscibility of the two components in the amorphous phase has been further investigated by analysing the thermal behaviour after melt quenching. In fact, with a cooling rate higher than the crystallization rate, it is possible to avoid crystallization during the cooling process obtaining reasonably an amorphous material. If the sample cannot be

quenched in a completely amorphous state, the amorphous phase will be however more abundant than in the semicrystalline sample, giving rise to a more intense glass transition step. As well known, the glass transition phenomenon in a partially crystalline polymer is different than in the analogous amorphous material. Although in literature, different results have been reported, it is commonly accepted that crystallinity acts like crosslinking points reducing the mobility of the amorphous polymer chains and consequently increasing the T_g value. Figure 4.32b shows the calorimetric curves after melt quenching. For all the samples under study, this treatment allows to obtain totally amorphous materials: the macromolecular chains of the samples containing an amount of *hard* block PLLA ≥ 43% in weight, once passed T_g, acquire adequate energy and mobility to crystallize during the temperature scan. Nevertheless, being $\Delta H_c \approx \Delta H_m$ (Table 4.18), we can assert the samples have been totally vitrified in the amorphous state by rapid cooling from the melt. As one can see from Figure 4.32b and from the results collected in Table 4.18, all the copolymers present a single T_g in an intermediate position with respect to those of the two blocks. The presence of one T_g for all the copolymers in the second scan indicates that the permanence in the molten state for few minutes favours the miscibility of the two blocks. The glass transition temperature value depends on the ratio between *soft* and *hard* segments in the chain. In particular, as expected, the copolymers with a higher percentage of *soft* block present lower T_gs.

4.3.3 Mechanical Properties

To provide insight into the mechanical response of the copolymers synthesized, tensile measurements have been carried out.

The results of tensile testing (the elastic modulus *E*, the yield strength σ^y and the yield strain ε^y, the stress at break σ^B and the strain at break ε^B), are summarized in Table 4.20 while in Figure 4.34 are reported the stress-strain curve recorded for PLLA45P(PS80NS20)55as an example and in the the inset, an enlargement of the initial portion of the stress-strain curve for PLLA and $PLLA_mP(PS80NS20)_n$ triblock copolymers.

Table 4.20: Mechanical characterization data of PLLA and $PLLA_mP(PS80NS20)_n$ triblock copolymers.

Polymers	E (MPa)	σ^y (MPa)	ε^y (%)	σ^b (MPa)	ε^b (%)
PLLA	1812±122	-	-	37±4	2.7±0.2
$PLLA_{67}P(PS80NS20)_{33}$	310±23	14±2	11±2	9±1	20±3
$PLLA_{46}P(PS80NS20)_{54}$	77±10	6±0.5	24±6	3±0.4	51±4
$PLLA_{45}P(PS80NS20)_{55}$	87±7	7±0.8	27±13	9±1	709±79
$PLLA_{43}P(PS80NS20)_{57}$	25±2	2±0.2	25±7	2±0.2	25±9

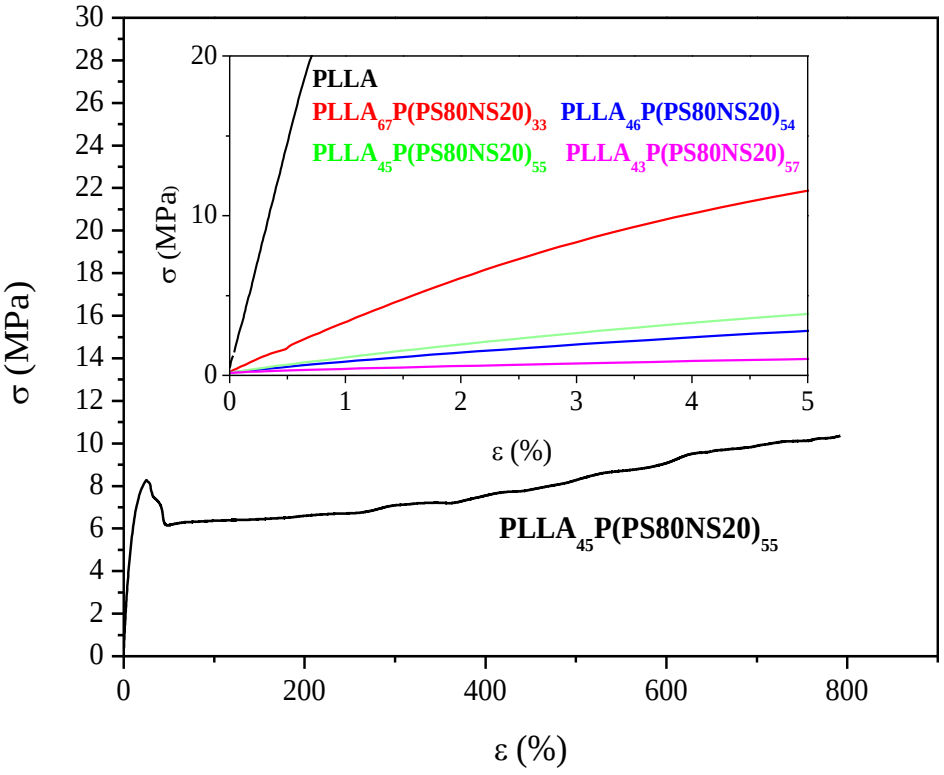

Figure 4.34. Stress-strain curve of PLLA45P(PS80NS20)55; In the inset, an enlargement of the initial portion of the stress-strain curve of PLLA and of $PLLA_mP(PS80NS20)_n$ triblock copoly(ester urethane)s.

It can be noted that PLLA shows a very high *E* value, confirming the remarkable stiffness of this homopolymer. On the other hand, the copolymers have a significantly different mechanical response. The introduction of the *soft* P(PS80NS20) segments

along the *hard* PLLA chain causes a huge decrease of *E*. Even in the copolymer containing only 33 wt% of the *soft* block, the elastic modulus is six times lower than *E* of the neat PLLA. This reduction reaches almost two order of magnitude in the case of $PLLA_{43}P(PS80NS20)_{57}$. As one can see by comparing the tensile results with the diffractometric data reported in Table 4.19, the trend observed is directly related to the crystallinity degree and to the glass transition temperature of the samples under investigation. In fact, the copolymers with higher *soft* block content show lower crystallinity degree and T_gs. Moreover, the amorphous P(PS80NS20)-rich phase is in the rubbery state at room temperature allowing higher chain mobility with consequent *E* reduction.

A progressive improvement of the elongation at break ε^B, that reaches a value of ≈700% for the sample $PLLA_{45}P(PS80NS20)_{55}$, and a decrease of the break strength σ^B have been also observed. This result can be explained taking into account X_c and T_gs values, and the molecular weight M_n. It is worth emphasizing the importance of M_n for the final mechanical response, by comparing the two copoly(ester urethane)s characterized by the same *hard*/*soft* block ratio, and consequently identical crystallinity degree and T_gs, but different molecular weights: 15000 and 41000 Da for $PLLA_{46}P(PS80NS20)_{54}$ and $PLLA_{45}P(PS80NS20)_{55}$, respectively (Table 4.16). In the linear elastic range, the two samples show a very similar behaviour in terms of *E*, σ^y and ε^y. On the contrary, they show a quite different behaviour in the plastic range. The main difference is the strain at break, 51% for $PLLA_{46}P(PS80NS20)_{54}$ and 709% for $PLLA_{45}P(PS80NS20)_{55}$. The worst mechanical response of $PLLA_{46}P(PS80NS20)_{54}$ is due to its significantly lower molecular weight.

All the stress-strain curves of the copolymers under study show a yield point that moves toward lower σ^y and higher ε^y, as the *soft* block amount increases.

In conclusion, the copolymer $PLLA_{45}P(PS80NS20)_{55}$ turns out to be very interesting, since it is characterized by the best compromise between strength, imparted by 45% in weight of the *hard*-block PLLA, and elasticity, conferred by the *soft*-block P(PS80NS20).

4.3.4 Barrier Properties

In order to verify the possible use of the synthesized materials for food packaging applications, the films obtained were subject to gas permeability tests (see experimental procedure paragraph 3.11).

Table 4.21: Gas transmission rate (GTR) to O_2, CO_2, N_2 and N_2O gases for PLLA and its semicrystalline triblock copolymers.

GTR (cm^3/m^2 d bar)	**O_2**	**CO_2**	**N_2**	**N_2O**
Commercial PLLA	500±1	1013±12	80±0.5	1253±12
PLLA	98±1	240±1	39±1	251±1
$PLLA_{67}(PS80NS20)_{33}$	168±1	1061±1	67±0	1090±0
$PLLA_{46}(PS80NS20)_{54}$	227±1	1523 ±5	74±0.5	1752±2
$PLLA_{45}(PS80NS20)_{55}$	195±1	1440±1	70±0.5	1470±0.5

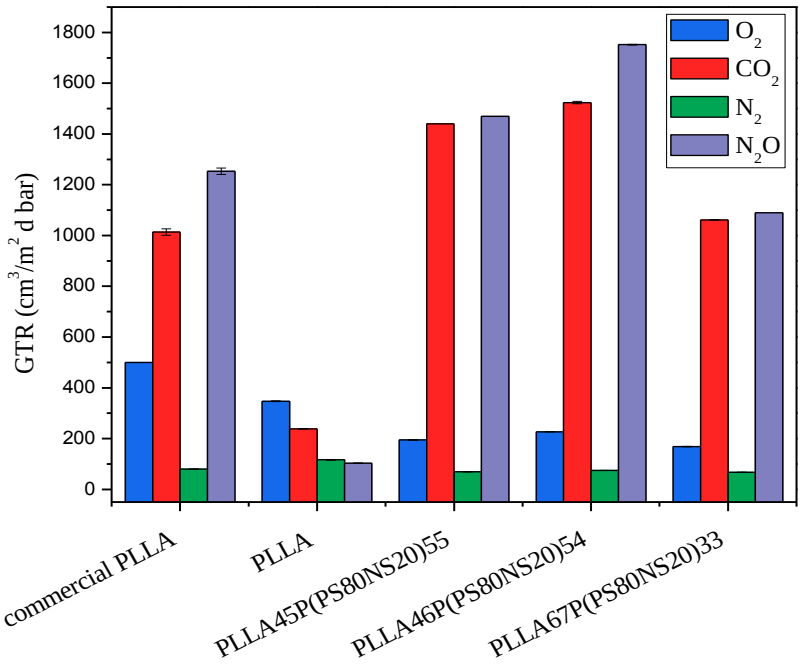

Figure 4.35: Gas transmission rate (GTR) to O_2, CO_2, N_2 and N_2O gases for PLLA and its semicrystalline triblock copolymers. GTRs for a commercial PLLA are also reported.

Figure 4.35 and Table 4.21 show the values of gas transmission rate (GTR) of O_2, CO_2, N_2 and N_2O for PLLA and its semicrystalline copolymers $PLLA_mP(PS80NS20)_n$. It was not possible to perform permeability measurements on the other block copolymers, as their amorphous nature and the low value of the glass transition temperature prevent the obtaining of films useful for practical purposes. For the sake of comparison, in Figure 4.35 and Table 4.21, the permeability data, measured under the same experimental conditions, of a commercial PLLA have been also added for sake of comparison.

As one can see from the graph of Figure 4.35, PLLA synthesized at our laboratories presents lower GTR values against O_2, CO_2 and N_2O than the trade PLLA. On the contrary, the behaviour with respect to the gas test N_2 is comparable for the two homopolymers. The differences can be related to the presence of additves in the commercial PLLA.

As regards the triblock copolymers $PLLA_mP(PS80NS20)_n$, at a first sight, their permeability data are not very different from those of the trade PLLA. Nevertheless, a more detailed analysis of the data revealed that the values of GTR against O_2 for all the copolymers are even better than both PLLA homopolymers. This result is definitely a positive point since makes the materials under investigation interesting candidates for food packaging under modified atmosphere (MAP). Typically, oxygen gives rise to oxidation processes, with consequent deterioration of the chemical-physical and organoleptic properties of the packaged food. Low GTR values hinder the process of diffusion of the gas through the polymer membrane. On the other hand, barrier properties against N_2 gas are very similar for all the samples. In particular, GTR values are lower than the data recorded with O_2, as reported in the literature for materials suitable for food packaging [Siracusa et al., 2015].

As far as CO_2 and N_2O gas test are concerned, the copolymers under investigation are characterized by higher GTR values with respect to both PLLA synthesized by us and commercial PLLA. Such result can be explained as due to the reduction of X_c, together with the increase of the polymer chains mobility, with respect to the reference sample PLLA. In particular, as *hard*-block content decreases, the polymeric chains hinder to a lesser extent the passage of gas molecules through the film. The fact that permeability does not increase proportionally with the *soft*-block amount can be related to the different molecular weight of the samples under investigation. $PLLA_{46}P(PS80NS20)_{54}$

shows GTR values higher than $PLLA_{45}P\ (PS80NS20)_{55}$. In fact, these two samples practically have the same composition, but a considerable difference in molecular weights (M_n = 15000 and M_n = 41000, respectively). This result evidences that chain length also plays an important role for the barrier properties.

4.3.5 Composting

As mentioned in the Introduction section, both academic and industrial researchers are interested to develop new biodegradable materials for food packaging applications. In this view, a preliminary assessment of the degradability of the copolymers $PLLA_nP(PS80NS20)_m$ by composting tests was performed (see experimental procedure paragraph 3.14). PLLA homopolymer has been subjected, for comparison, to the same treatment. The biodegradation process was monitored by measuring the weight loss, the molecular weight variation and the molecular structure evolution, after 21, 36 and 52 days of incubation. Except for PLLA, all the samples are significantly degraded: as an example, in Figure 4.36 the virgin and the incubated films of the sample $PLLA_{67}P(PS80NS20)_{33}$ are shown.

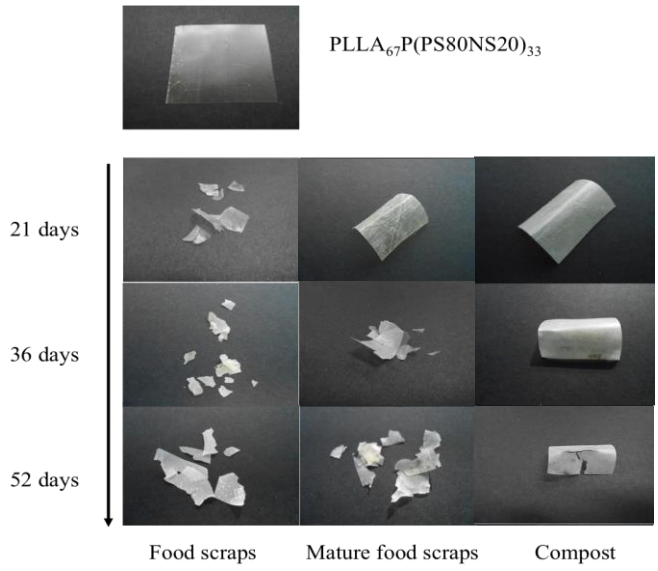

Figure 4.36. $PLA_{67}P(PS80NS20)_{33}$ after 21, 36 and 52 days in composts with different maturation degree.

As one can see, the not incubated film is characterized by a smooth and homogeneous surface, while the incubated material shows an extensive fragmentation just after only 21 days of incubation in food scraps. From a comparison of the images of the sample

incubated in three different composts, it emerges that the degradation activity is much higher in the food scraps, followed by the mature food scraps, while the final compost appears to be less active. In this case, in fact, the sample shows signs of degradation on the surface only after 52 days of incubation.

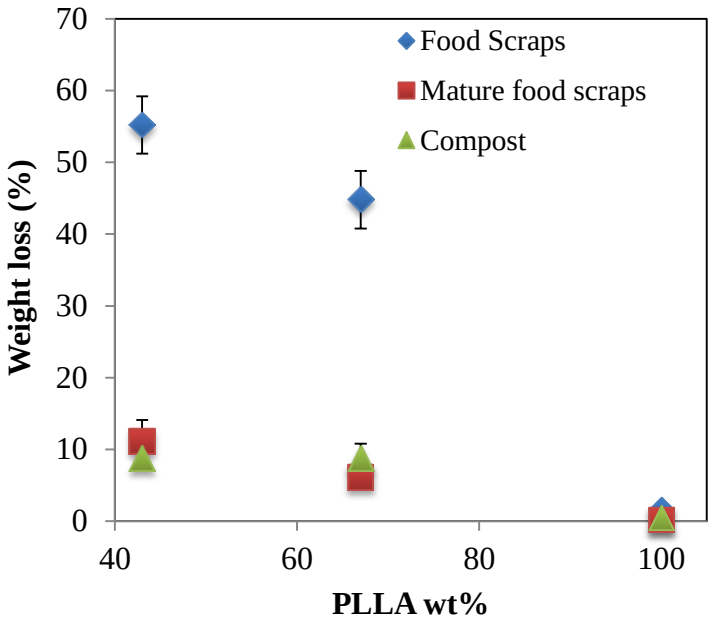

Figure 4.37: Weight loss (%) as a function of PLLA wt% for PLLA and its triblock copolymers after 21 days of incubation in the three different compost matrices.

Figure 4.37 shows the gravimetric weight losses of the system under investigation as a function of composition, for the three different composts. The results confirm that the degradation rate of the fresh compost is much higher than both mature food scraps and compost, having these latter a quite similar behaviour. It is also interesting to note that the biodegradation rate is significantly influenced by the composition of the copolymer, decreasing significantly as the *hard*-block content (PLLA) increases. This trend can be explained on the basis of the different degree of crystallinity of the samples, in fact, X_C increases with the content of PLLA and, as known from the literature, the biodegradation rate is inversely proportional to the degree of crystallinity. The enzymes secreted by the microorganisms attach preferentially the amorphous areas of the material, which are more accessible. To shed light on the mechanism of biodegradation, the partially biodegraded samples were subjected to ^{1}H-NMR spectroscopy and GPC measurements. As an example, in Figure 4.38 the spectrum of $PLLA_{45}P(PS80NS20)_{55}$ incubated for 36 days in food scraps is reported. In addition to the peaks characteristic

of the molecular structure of the neat copolymer, the appearance of peaks related to the end groups of the central *soft*-block can be evidenced at δ = 3.75 and 4.40 ppm. This indicates that the *soft*-block P(PS80NS20) is preferentially degraded. As confirmation of that, a change in the copolymer composition has also been detected. PLLA content increases from 45wt% in the virgin copolymer to 52 wt% in the sample incubated in food scraps for 52 days. The result can be explained taking into account the central block P(PS80NS20) is completely amorphous and therefore degraded first by the microorganisms.

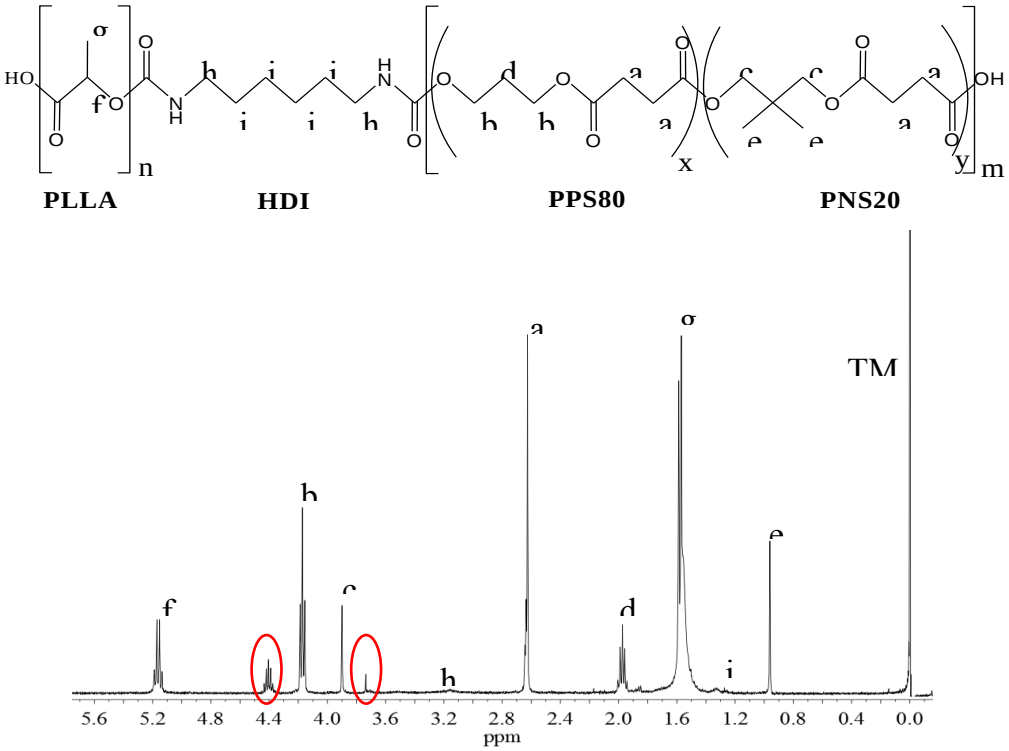

Figure 4.38: ^{1}H-NMR spectrum of $PLLA_{45}P(PS80NS20)_{55}$ triblock copolymer after 36 days of incubation in food scraps with the corresponding resonance assignments. The red circles indicate the end groups of the central *soft*-block P(PS80NS20).

A measurement of the molecular weight of the samples incubated in the three different types of compost confirmed their different degradation activity. Figure 4.39 shows the M_n variation concerning the copolymer $PLLA_{45}P(PS80NS20)_{55}$. The sample incubated in the food scraps, in just 21 days of incubation, presents a molecular weight almost halved with respect to the initial value, confirming that the material suffers an important microbial attack.

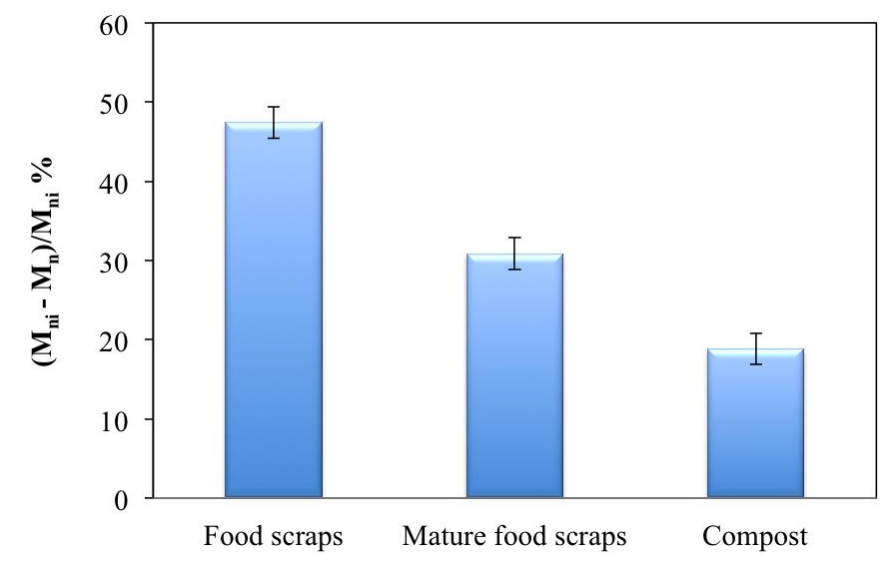

Figure 4.39: Molecular weight decrease % for $PLLA_{45}P(PS80NS20)_{55}$ incubated for 21 days in the three different compost matrices.

4.3.6 Conclusions

A new class of poly(ester urethane)s has been successfully synthesized by a simple and solvent-free synthetic approach, that permits to realize copolymers with a A-B-A triblock controlled architecture. The central B sequences are soft, whereas A sequences are formed by the rigid PLLA. Through this strategy, it has been possible to synthesize high molecular weight semicrystalline polymers.

The results obtained, show that copolymerization leads to better mechanical response without compromising the good barrier properties of poly(lactic) acid homopolymer. Moreover, the presence of the *soft* block in the main polymer chain facilitates the process of compostability.

Last but not least, the final polymer properties can be finely tuned simple playing on *soft*/*hard* ratio.

The new class of PEUs here presented displayed therefore a good versatility that makes them suitable for a wide range of possible applications in packaging.

4.4 Random copolyesters based on poly(propylene cyclohexanedicarboxylate)

Poly(propylene cyclohexanedicarboxylate) (PPCE), Poly(neopentyl glycol cyclohexanedicarboxylate) (PNCE), and a series of new fully aliphatic (P(PCExNCEy)) random copolymers, have been synthesized and characterized in terms of molecular and solid-state properties. In order to better understand the role of the methyl groups incorporated in the polymeric chain and establish structure-dynamics relationships, the polymers have been investigated by means of X-ray scattering and dielectric loss spectroscopy experiments too. Moreover, to deeply understand the nature of the subglass processes of the homopolymers, dielectric data have been compared with those of Poly(propylene terephthalate) (PPT) and Poly(neopentyl terephthalate) (PNT) previously synthesized in our laboratories [Soccio et al., 2008 (b and c); Soccio, Nogales et al., 2012].

In addition, biodegradability studies in compost have been conducted.

4.4.1 Synthesis, molecular and thermal characterization

At room temperature the as-synthesized polyesters are opaque light yellow colored solids. Their solubility was checked in various solvents: all the samples showed a good solubility at room temperature in the most common organic solvents, i.e. chloroform, tetrachloroethane, methylene chloride, etc. The polymers are listed in Table 4.22, which also collects the data of molecular characterization: as it can be seen, the polymers were characterized by relatively high and comparable molecular weights, indicating that appropriate synthesis conditions and a good polymerization control were achieved. In order to have an understanding into their chemical structure, the ^{1}H-NMR investigation was performed. The analysis confirmed the awaited structures (see as an example the ^{1}H-NMR spectrum of P(BCE70TECE30) shown in Figure 4.40).

The copolymer composition was calculated from the relative areas of the ^{1}H-NMR resonance peak of the **3** aliphatic proton of the propylene diol subunit located at 4.15 ppm and of the **5** protons of the methylene groups of the neopentyl diol subunit at 3.87 ppm. From the data of Table 4.22, it can be seen that in all cases the actual molar composition is close to the feed one.

Table 4.22: Molecular characterization data of PPCE and P(PCExNCEy) random copolymers.

Polymer	M_n[a]	D[b]	NCE (mol %)[c]	Thickness (µm)
PPCE	36398	2.2	0	246±22
P(PCE95NCE5)	29549	2.9	5	292±31
P(PCE90NCE10)	31124	2.2	10	268±18
P(PCE85NCE15)	27522	2.6	15	238±33
P(PCE80NCE20)	25386	2.4	20	308±10

[a] number average molecular weight calculated by GPC analysis
[b] polydispersity index calculated by GPC analysis
[c] real copolymer composition calculated by ^{1}H-NMR

Previous studies [Soccio et al., 2007; Gigli, Negroni et al., 2013 (b)] reported that the 1,4-cyclohexylene ring present in DMCE can isomerize during polymer synthesis, due to the high temperatures employed for long times, moving toward the thermodynamically stable *cis/trans* ratio of 34-66%. Therefore, ^{1}H-NMR analysis has been also used to calculate the *trans* percentage in the polymers under study: in particular, the ratio of the areas of the signals centred at 2.28 ppm (*trans* isomer) and 2.44 ppm (*cis* isomer) has been considered (Figure 4.40). From the data obtained, it can be evicted that no significant isomerization from the *trans* form to the *cis* one occurred during polymerization, the *cis* content being in all cases less than 5%.

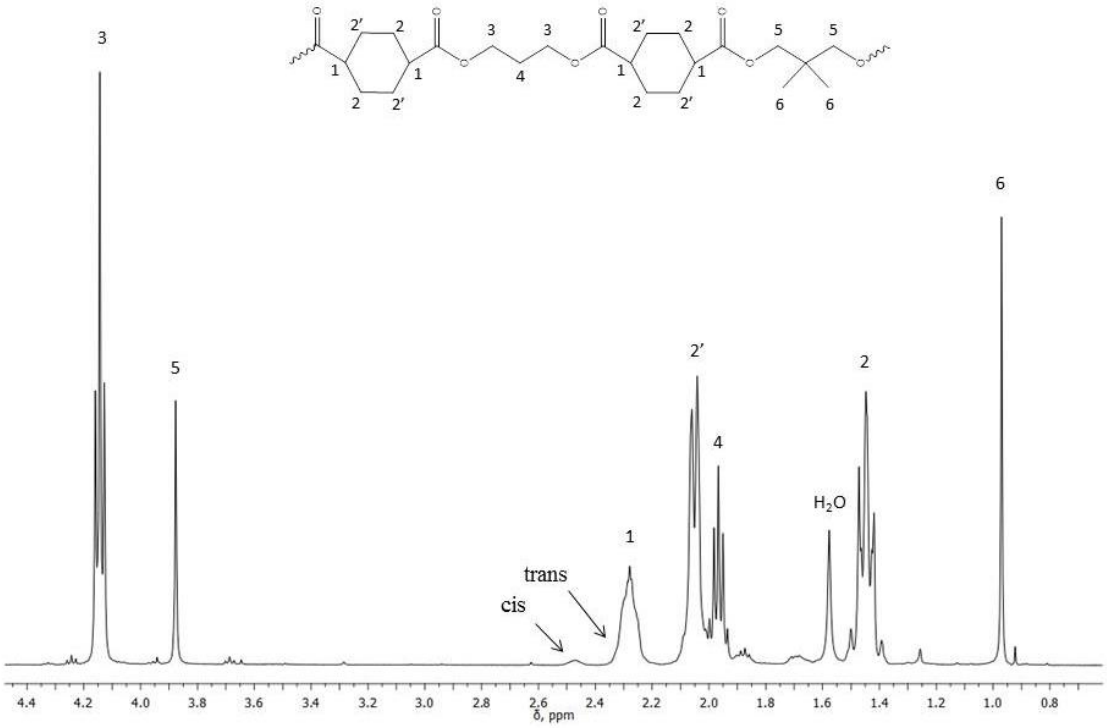

Figure 4.40 ^{1}H NMR spectra of P(PCE80NCE20) with resonance assignments.

Subsequently, the polymers were subjected to thermogravimetric analysis and the temperature corresponding to 5% weight loss ($T_{5\%\ w.loss}$) has been determined and collected in Table 4.23. As evidenced in Figure 4.41, where the thermogravimetric curves of the parent homopolymer and of the synthesized copolyesters are reported, the weight loss takes place in all cases in one-step.

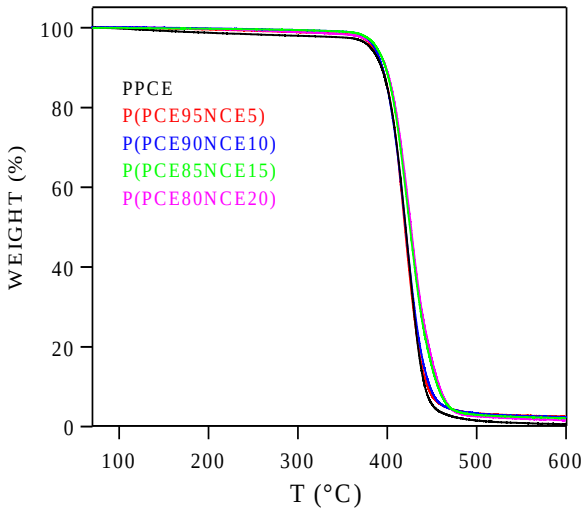

Figure 4.41 Thermogravimetric curves of PPCE and P(PCExNCEy) copolymers under nitrogen atmosphere (heating rate: 10 °C/min).

All the copolyesters showed a high thermal stability, comparable with that of PPCE. This is due to the presence of bulky and thermally stable cyclohexylene groups, which render the polymer even more thermally stable than the corresponding aromatic polyester, i.e. PPT as well as to neopentyl glycol sub-unit [Soccio et al., 2007; Soccio et al., 2008 (b)]. The result demonstrated that the introduction of NCE co-units along the PPCE macromolecular chain did not have any detrimental effect on thermal stability, which, as well known, is crucial during polymer processing.

Table 4.23 Thermal and diffractometric characterization data for PPCE and P(PCExNCEy) copolymers.

	1st scan					2nd scan					
Polymer	**$T_{5\%\ w.loss}$ (°C)**	**T_m (°C)**	**ΔH_m (J/g)**	**T_g (°C)**	**ΔC_p (J/°C g)**	**T_m (°C)**	**ΔH_m (J/g)**	**T_c (°C)**	**ΔH_c (J/g)**	**T_{cc} (°C)**	**X_c [#] (°C)**
PPCE	381	148	58	9	0.132	148	31	63	17	91	29 (4)
P(PCE95NCE5)	385	142	49	11	0.183	143	26	90	26	75	26 (3)
P(PCE90NCE10)	386	135	43	12	0.189	135	13	97	13	-	25 (2)
P(PCE85NCE15)	387	125	42	13	0.262	-	-	-	-	-	25 (2)
P(PCE80NCE20)	388	119	39	13	0.236	-	-	-	-	-	24 (2)

[#] Estimated standard deviation (e.s.d.) in parentheses

In order to provide the same heat treatments to all the investigated samples, prior to thermal analysis each film was kept at room temperature for two weeks. DSC traces of so-treated samples are reported in Figure 4.42 and the data obtained in Table 4.23.

As evidenced in Figure 4.42, all P(PCExNCEy) copolymers presented a glass transition and a melting endotherm. The glass transition phenomenon is always not so evident, due to the high amount of crystalline phase present in these samples.

As to the melting process, the samples showed a premelting peak at low temperature (around 50°C), whose heat of fusion regularly increased as the NCE unit content is increased, which can be ascribed to the fusion of crystals with a poor degree of perfection. At much higher temperature, the main melting peak can be observed. The calorimetric results indicate that an increase in the amount of the comonomer NCE leads to a reduction in the samples both of the melting temperature and the heat of fusion, as usually found in random copolymers with the comonomeric units present in

minor amount completely rejected from the crystalline phase or partially incorporated in it (see Table 4.23) [Mandelkern 1954; Mandelkern, 1989]. Furthermore, in the copolymers, the endotherm region is broader, suggesting the presence of a larger distribution of crystallites with different degree of perfection.

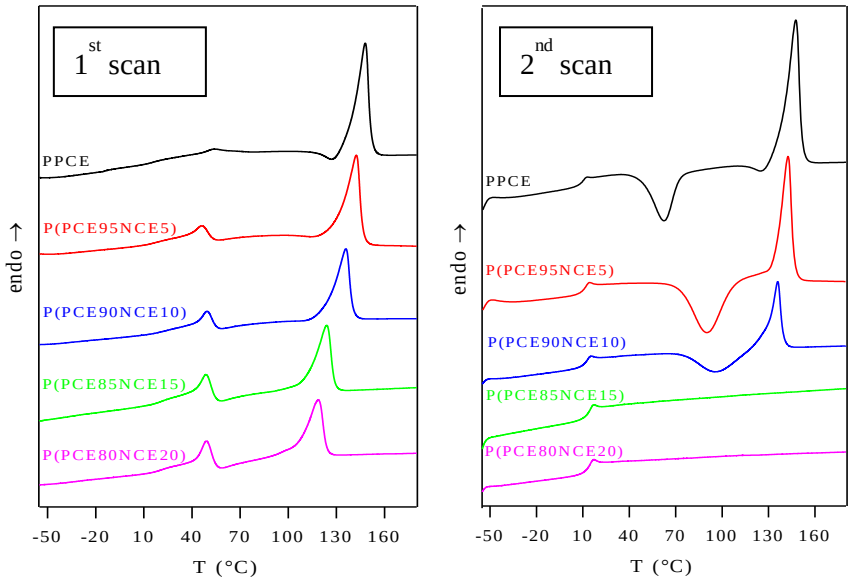

Figure 4.42. Calorimetric curves of PPCE and P(PCExNCEy) copolymers: 1st scan, 2nd scan after melt quenching.

To better understand the nature of the crystalline phase present in the polymers under investigation, the structural characterization of P(PCExNCEy) copolymers was carried out by X-ray diffraction (XRD). The patterns are reported in Figure 4.43, together with that of PPCE added for sake of comparison. The PPCE sample shows the main reflections at 2θ values of 16.7°, 17.5°, 19.5°, 23.3°.

As far as the copolymers are concerned, the corresponding WAXD patterns appear to be characterized by relatively intense diffraction peaks over the whole composition range.

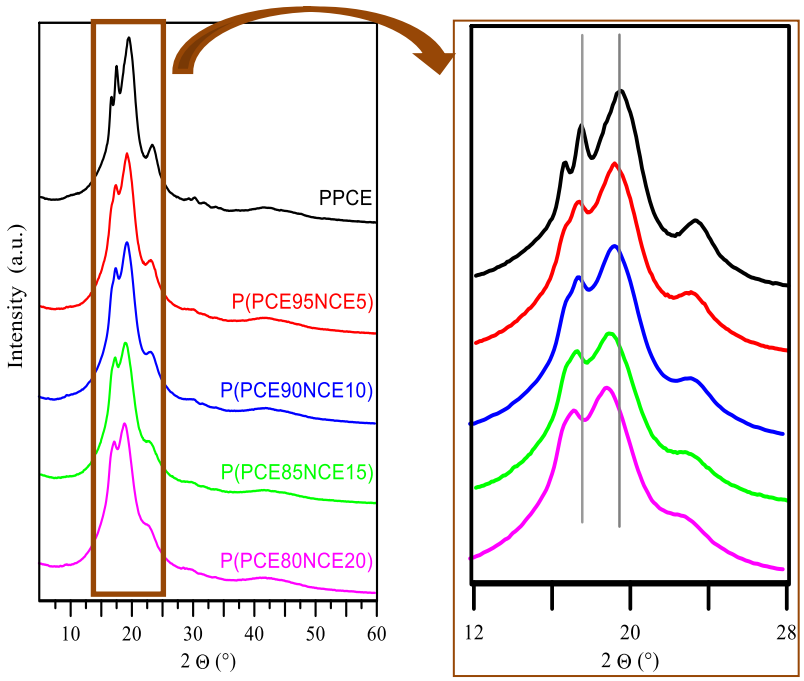

Figure 4.43 X-ray diffraction profiles of PPCE and P(PCExNCEy) copolymers (left). An enlarged view (right); vertical line are reference for the reader.

The copolymer samples are characterized by the same XRD pattern of PPCE, indicating that the crystal structure which develops in these copolymers has the characteristics of PPCE lattice.

Nevertheless, the presence of NCE units causes the collapse of the two reflections at 16.7° and 17.5° and the reflections seems be shifted towards lower angles (higher distances, see Figure 4.43, right panel), the shifting being higher as the content of NCE units increases.

Such increases of the interplanar distances could be caused by the insertion of bigger NCE units into the PPCE crystal cell. Cocrystallization is supported by the modest decrease of crystallinity degree with copolymer composition (see Table 4.23), which is lower than the value expected on the basis of the complete rejection of the "foreign" units from the crystalline phase present in the sample. In conclusion, it can be plausible that at least a certain amount of comonomeric units enter into the crystal lattice.

It is well known that a partially crystalline material usually exhibits a different glass transition behavior than the completely amorphous analogous. In fact, although some conflicting results are reported in the literature [Bolyer, 1963], crystallinity usually acts

like crosslinking and raises T_g through its restrictive effect on the segmental motion of amorphous polymer chains. Therefore, in order to study the influence of chemical structure on the glass transition of random copolymers, the phenomenon should be examined in the total absence of crystallinity. In this view, all the samples under investigation were subjected to rapid cooling (quenching) from the melt. The DSC curves after melt quenching are shown in Figure 4.42: the calorimetric traces of PPCE and P(PCExNCEy) copolymers containing up to 10 mol % of NCE units showed a glass transition followed by an exothermal "cold crystallization" peak and a melting endotherm at higher temperature. In particular, as concern PPCE, the enthalpy associated with the crystallization phenomenon is lower than that of the fusion endotherm, indicating that this sample cannot be frozen into a completely amorphous state by quenching. Nevertheless, a portion of amorphous material, once T_g is exceeded, acquires enough mobility to rearrange and crystallize. The DSC curves of such sample is therefore typical of partially crystalline polymers. In the case of P(PCE95NCE5) and P(PCE90NCE10) copolymers, the enthalpy of crystallization very well compares with the corresponding heat of fusion, indicating that these polymers are completely amorphous. As regards the calorimetric curves of copolymers containing from 15 to 20 mol % of NCE units, only an intense endothermal baseline deviation associated with the glass transition is observed. Therefore, the DSC scans indicate that the phase behavior of PPCE changed even for small amount of neopentyl glycol sub-units (5 mol%). On the other hand, no effect of copolymer composition on material phase behavior was observed.

As can be seen from the data collected in Table 4.23, the glass transition temperature is slightly influenced by the presence of NCE units in the chain, the T_g copolymer values being higher than that of PPCE and increasing with the molar content of NCE units. As is well known, the second-order transition temperature is affected by several factors, such as chain flexibility, steric effects, molar mass, branching and crosslinking. For high molecular weight polymers, the flexibility of the chain is undoubtedly the most important factor influencing T_g. This latter is a measure of the ability of a chain to rotate, and therefore the more flexible chains are, the lower the T_g. The increase in the glass transition temperature on introducing the two methyl side groups into the

polymeric chain of PPCE can be explained as due to the steric effect of these two groups which hinder the rotation, imposing restrictions.

To evaluate the tendency of PPCE to crystallize in the copolymers under study, non-isothermal experiments were carried out, subjecting the samples to a controlled cooling rate from the melt. The temperatures of the maximum of the exothermal crystallization peak (T_{cc}) of the samples under investigation, which can be correlated to the isothermal melt crystallization rate, are collected in Table 4.23. As it can be observed, the crystallization rate of P(PCE95NCE5) is significantly lower than that of parent homopolymer. Moreover, amounts of NCE co-units ≥ 10 mol % completely undone the PPCE ability of crystallizing, indicating that the co-units act as obstacles in the regular packing of polymer chains. This result is in agreement with those obtained previously by some of us in investigating other copolymeric systems containing neopentyl glycol sub-unit [Soccio et al., 2007; Soccio et al., 2008 (c)].

4.4.2 Dynamic mechanical characterization

The dynamical mechanical spectra of the samples under investigation are shown in Figure 4.44.

The upper curve of each polymer refers to the sample stored at room temperature: in the temperature range -150/100°C, all the polymers exhibits three relaxations regions denoted as γ, β and α in order of increasing temperature. In all cases, the γ relaxation detected in the range -150/-100°C at 3 Hz, has small intensity and is rather broad. The β relaxation is approximately located at about -75°C and has a small intensity too. On the other hand, the α relaxation, detected around 40°C, has higher intensity and a certain asymmetry, being steeper on the low-temperature side and broader on the high-temperature one. Looking into more detail to the high-temperature side of α relaxation, one can see a shoulder, denoted as α'. As regards the storage modulus E', at low temperature it exhibits values typical of the glassy state (*ca.* 10^{10} Pa) and decreases slightly with increasing temperature due to thermal expansion. In correspondence with α relaxation the modulus shows a steep decrease of about two orders of magnitude.

Table 4.24. Dynamical mechanical data of PPCE and its random copolymers at 3Hz (heating rate: 3°C/min).

Polymer	1st scan			2nd scan[a)]		
	T_α (°C)	**T_β (°C)**	**T_γ (°C)**	**T_α (°C)**	**T_β (°C)**	**T_γ (°C)**
PPCE	40	-74	-130	23	-73	-125
P(PCE95NCE5)	40	-76	-133	27	-75	-123
P(PCE90NCE10)	42	-78	-132	29	-76	-125
P(PCE85NCE15)	43	-78	-133	32	-77	-123
P(PCE80NCE20)	46	-79	-131	40	-75	-123

[a)] 2nd scan after cooling from high temperature under nitrogen flow

As regards the assignment of these relaxations, α relaxation is confidently assigned to the glass-to-rubber transition, its temperature location being in good agreement with the calorimetric T_g. The small intensity of the peak and the high value of the modulus above the relaxation evidence the partially crystalline character of the polymer, in agreement with the calorimetric results. The location of the main relaxation shifts toward higher temperature values as the NCE unit content is increased (see Table 4.24), in agreement with calorimetric results. This can be explained on the basis of the progressive decrease in chain flexibility as the amount of NCE units increases. The α' process can be related to a rigid confined amorphous phase, analogously to another similar copolymeric systems previously investigated by some of us [Soccio, Nogales et al., 2012].

Concerning the identification of the molecular origin of the γ relaxation, it can be traditionally associated with restricted motions of the chain in polymers with aliphatic sequences: in particular, the relaxation is generally attributed to rotations of the methylene units of glycol sub-unit which is the flexible part of the repeating unit [Berti et al., 2008 (b)].

As regards the attribution of the β relaxation to a molecular motion, as reported in the literature [Berti et al., 2008 (b)], this relaxation originates from the chair-boat-chair conformational transition of the cyclohexylene ring. Indeed, the cyclohexylene rings in chair conformations can transform from chair to chair via an intermediate twist boat conformation [Vanhaecht et al., 2002].

In the second scan after cooling from high temperature under dry nitrogen gas, the shoulder α' disappeared, the α peak keeping anyway a certain asymmetry. Moreover, α intensity decreases indicating that during the cooling crystallization occurs in the

samples under investigation. Surprisingly, however, the α relaxation moves to lower temperature: taking into account that α' shoulder disappears, such result can be explained as due to a significant improving of crystal phase perfection that reduces significantly the rigid-amorphous phase fraction.

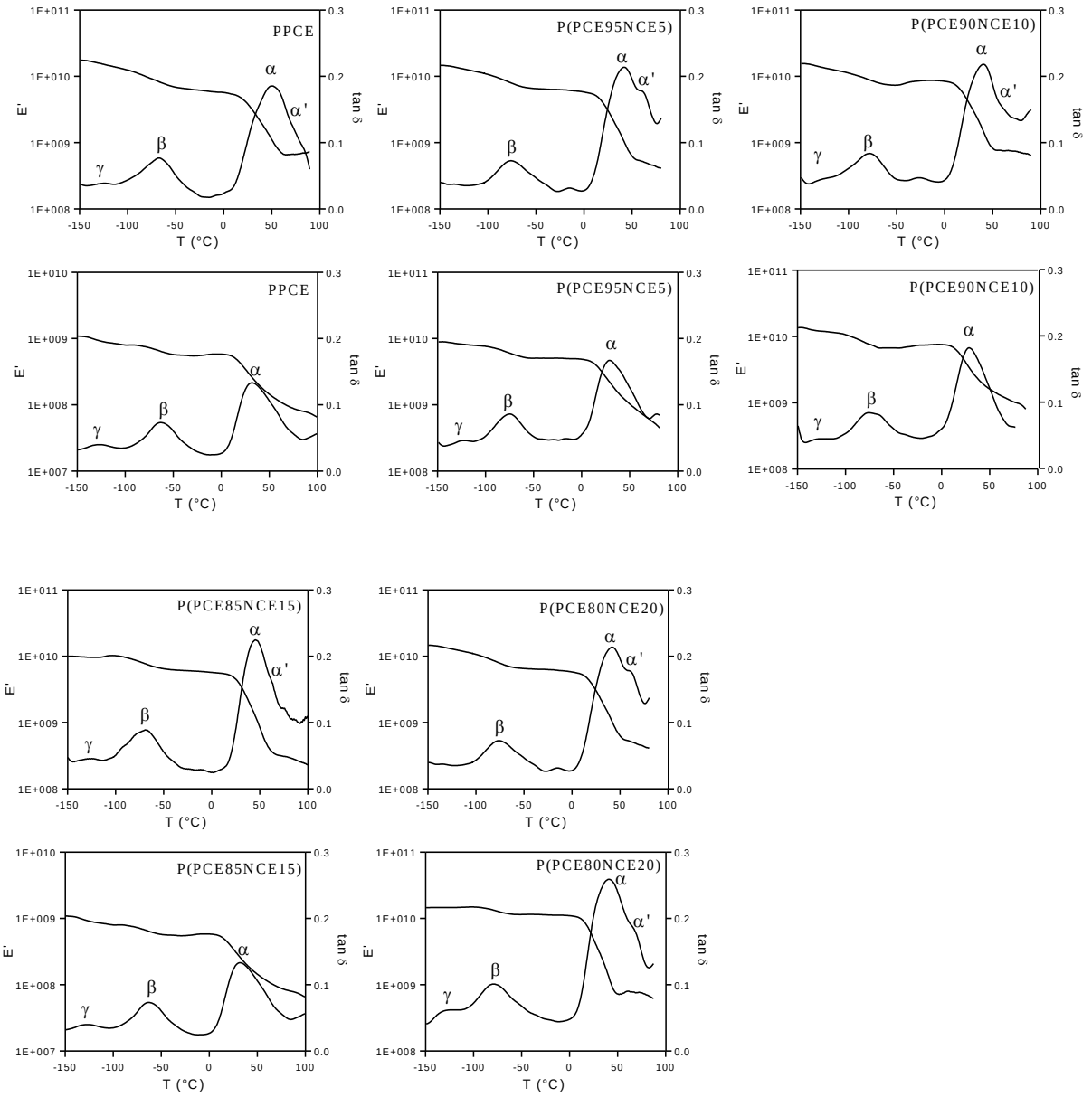

Figure 4.44. Dynamical mechanical curves at 3 Hz: for each sample, top row room stored sample; bottom row after cooling from high temperature under dry nitrogen flow.

The copolymer with the highest content of NCE co-unit, P(PCE80NCE20), is characterized by a different behavior: as a matter of fact, the α' relaxation does not

disappear in 2nd scan after cooling from high temperature under dry nitrogen flow and the intensity of α relaxation doesn't decrease in magnitude. This last result clearly indicates that no significant crystallization occurred on cooling, due to slow crystallization kinetic of this copolymer. As it is well known, the amount of rigid amorphous phase depend upon the area of the crystalline-amorphous boundary, the degree of irregularity of the crystalline phase and the molecular mobility [Soccio et al., 2008 (b)]. In the case of P(PCE80NCE20), the non-crystallizable comonomer hinders significantly the crystallization process, leading to small and imperfect crystallites. The crystalline phase turns out to be highly dispersed, and the increase in crystal surface results into extensive constraints on the amorphous phase.

As to elastic modulus E' in second scan, also the steepness and intensity of the modulus drop in the α transition region show a great reduction as the crystallinity increases, reflecting the typical behavior of partially crystalline polymers [Mc Crum et al., 1967].

4.4.3 Mechanical characterization

In an application perspective, the analysis of the mechanical properties of the polymers under study is of primary importance. Therefore, P(PCExNCEy) copolymers were subjected to stress-strain measurements. In Table 4.25 their elastic modulus (E), stress at break (σ_b), and deformation at break (ε_b) are shown, together with the data of PPCE and PPT added for sake of comparison.

Table 4.25. Mechanical characterization data of PPCE and P(PCExNCEy) copolymers.

Polymer	E (MPa)	σ_b (MPa)	ε_b (%)
PPCE	435±26	15±2	11±1
P(PCE95NCE5)	381±29	20±1	150±14
P(PCE90NCE10)	338±20	12±1	190±32
P(PCE85NCE15)	248±12	12±2	332±32
P(PCE80NCE20)	232±20	20±1	559±18
PPT	942±85	42±5	5±1

As it can be seen, the elastic modulus regularly decreased as NCE unit content was increased; on the contrary, the elongation at break, increased with the increasing of the molar amount of NCE co-unit. Since all the investigated polymers display a soft

amorphous phase (T_g values are in all cases below room temperature), the observed trend can be ascribed to crystallinity degree (Table 4.23).

It is in fact well known [Van Krevelen, 1977; Dusunceli & Colak, 2008] that crystallinity degree has a considerable effect on the mechanical properties of a polymer: in particular high X_c results in harder, stiffer and less ductile behavior. As therefore expected, the higher the PCE content, the higher the elastic modulus and the lower the elongation ability of the investigated polymers. Moreover, it is worth emphasizing that the copolymer containing the 20 mol% of NCE is characterized by an elastomeric behavior.

In conclusion, a new class of aliphatic polyesters with tunable mechanical properties has been here presented. Indeed, by just varying the molar composition of the copolymers, even for modest changes of crystallinity degree, it is possible to synthesize a new material which can be used for rigid plastic containers or soft wrapping films.

Last but not least, substituting the aromatic ring with the aliphatic one, the modulus changes dramatically (see Table 4.25): it is lower in aliphatic sample. In particular, PPT, due to the presence of the aromatic ring, has a very high modulus and a brittle behavior.

4.4.4 Composting

The biodegradability of P(PCExNCEy) copolymers was monitored by subjecting them to composting, which is a particularly useful technique to biodegrade a polymeric material which has been contaminated by organic matter. Biodegradation rate was investigated by weight loss measurements.

After 140 days of incubation the highest weight loss value was of 11%, measured for P(PCE80NCE20). Degradation rate was found dependent on composition: the higher the NCE content, the higher the weight loss. As a matter of fact, weight losses were equal to 3, 4, 6 and 8% for PPCE, P(PCE95NCE5), P(PCE90NCE10) and P(PCE85NCE15), respectively.

As expected, the higher the crystallinity degree of the polymers under study, the lower the biodegradation rate in compost; in fact it is a well known factor influencing the biodegradation rate of a polymer [Gigli, Negroni, 2012; Gigli, Negroni, 2013 (a and b)].

The morphology of the polymer films was analyzed by SEM. As an example, micrographs of PPCE and P(PCExNCEy) films after 140 days of incubation in compost are reported in Figure 4.45.

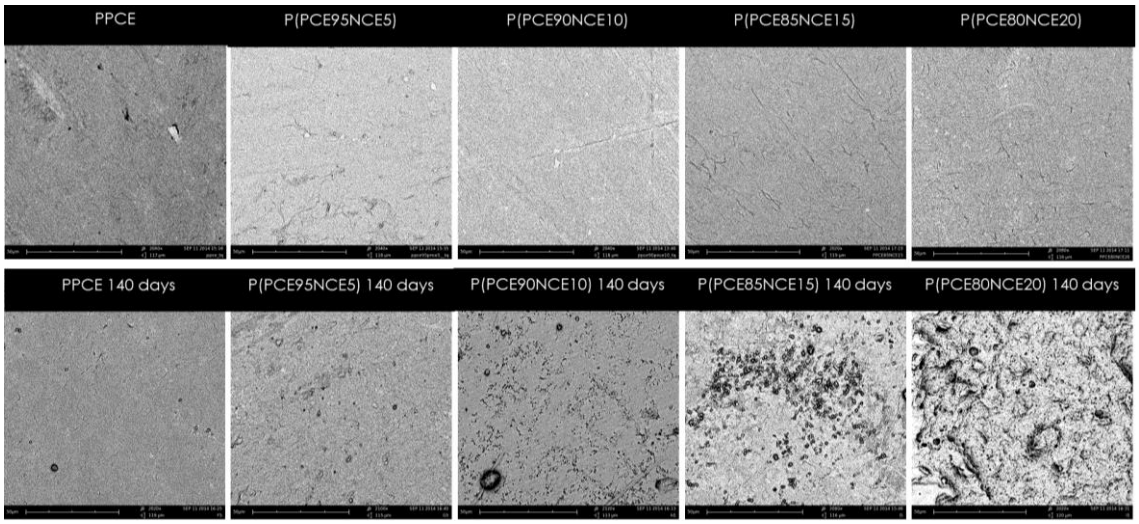

Figure 4.45. SEM micrographs of PPCE and P(PCExNCEy) before composting (top) and after 140 days of incubation (bottom).

All the samples under investigation showed a smooth and homogenous surface before incubation. After incubation, SEM analyses highlighted results in agreement with weight loss measurements: PPCE film presented only a surface roughening after 140 days of incubation in compost, while in the copolymers large damaged areas appeared, with numerous cracks and channels, whose intensity depended on the degree of degradation.

4.4.5 Dielectric spectroscopy

In order to better understand the origin of the subglass relaxations observed in DMTA spectra, dielectric loss spectroscopy experiments were performed on the polymers under study. Such measurments were carried out during the stage at IEM-CSIC in Madrid as visiting PhD-student under the supervion of Prof. T. Ezquerra.

In order to establish structure-dynamics relationships Poly(neopentyl glycol cyclohexanedicarboxylate) (PNCE) homopolymer has been synthesized and characterized by the molecular and thermal point of view (Table 4.26).

Table 4.26: Molecular and thermal characterization of PNCE homopolymer

	I Scan		II Scan							
Polymer	T_m (°C)	ΔH_m (J/g)	T_g (°C)	ΔC_p (J/°C g)	T_m (°C)	ΔH_m (J/g)	T_c (°C)	ΔH_c (J/g)	Mn	D
PNCE	196	29	33	0.193	195	29	111	29	17300	2.3

Figure 4.45 shows, as an example, the dielectric loss values as a function of temperature and frequency for PPCE (top) and PNCE (bottom). At lower temperatures, both polymers exhibit a broad maximum of the dielectric loss labelled as β process. The β relaxation process observed below T_g and moving towards higher frequencies as temperature increases, can be related to the local chain dynamics, observed in aliphatic [Soccio, Nogales et al., 2007]] as well in aromatic polyesters [Soccio, Nogales et al., 2012; Soccio, Nogales et al., 2008].

Then, above T_g, a strong increase in ε" values is observed which can be associated to the α process appearing as due to the segmental dynamics. P(PCExNCEy) random copolymers present a dielectric spectra very similar to that of PPCE.

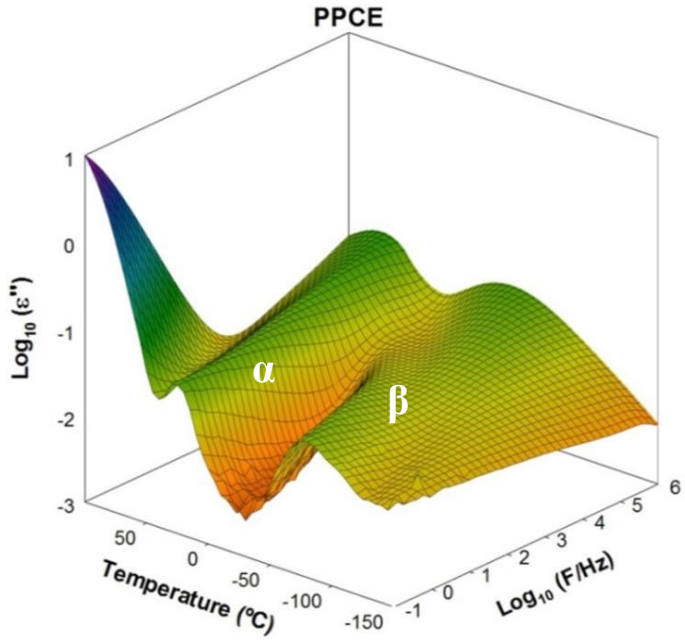

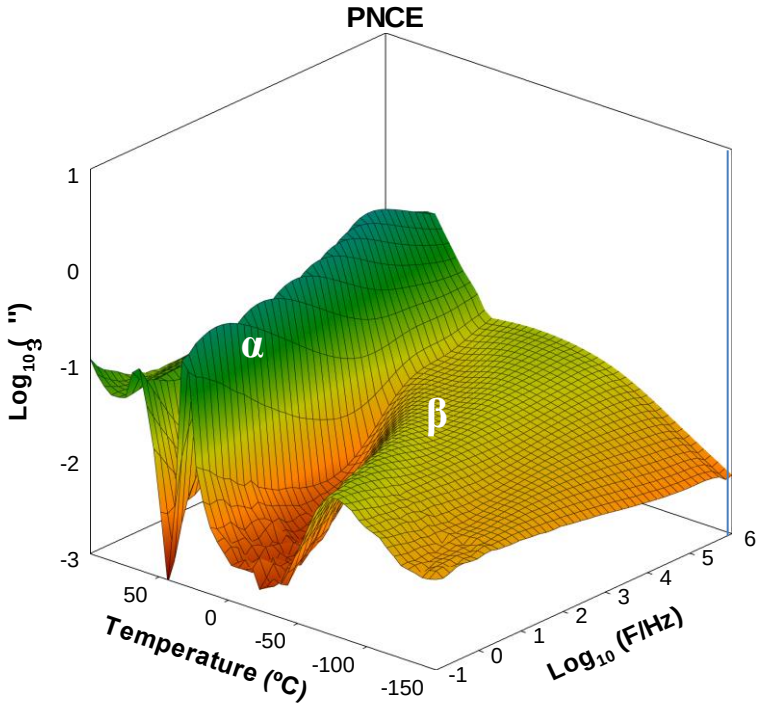

Figure 4.45: Dielectric loss values as a function of temperature and frequency for the two homopolymers of the series: PPCE (top) and PNCE(bottom).

PNCE shows a very similar 3D spectrum except for the alpha that is much more intense. This effect is due to the amorphous nature of PNCE homopolymer with respect to PPCE and P(PCExNCEy) copolymers that, having lower T_g values, at room temperature are able to develop a crystalline phase.

4.4.5.1 β Relaxation

Figure 4.46(a) shows isothermal dielectric loss data for PPCE at different temperatures below T_g. In these plots the subglass relaxation turns out to be composed of two contributions, labeled as β_1 and β_2, appearing well resolved in the frequency range. Figure 4.46(b) shows the dielectric loss values for PNCE in a similar representation. The comparison between PPCE and PNCE reveals this latter presents and additional contribution, labelled as β_3, located at intermediate frequencies with respect to β_1 and β_2 processes.

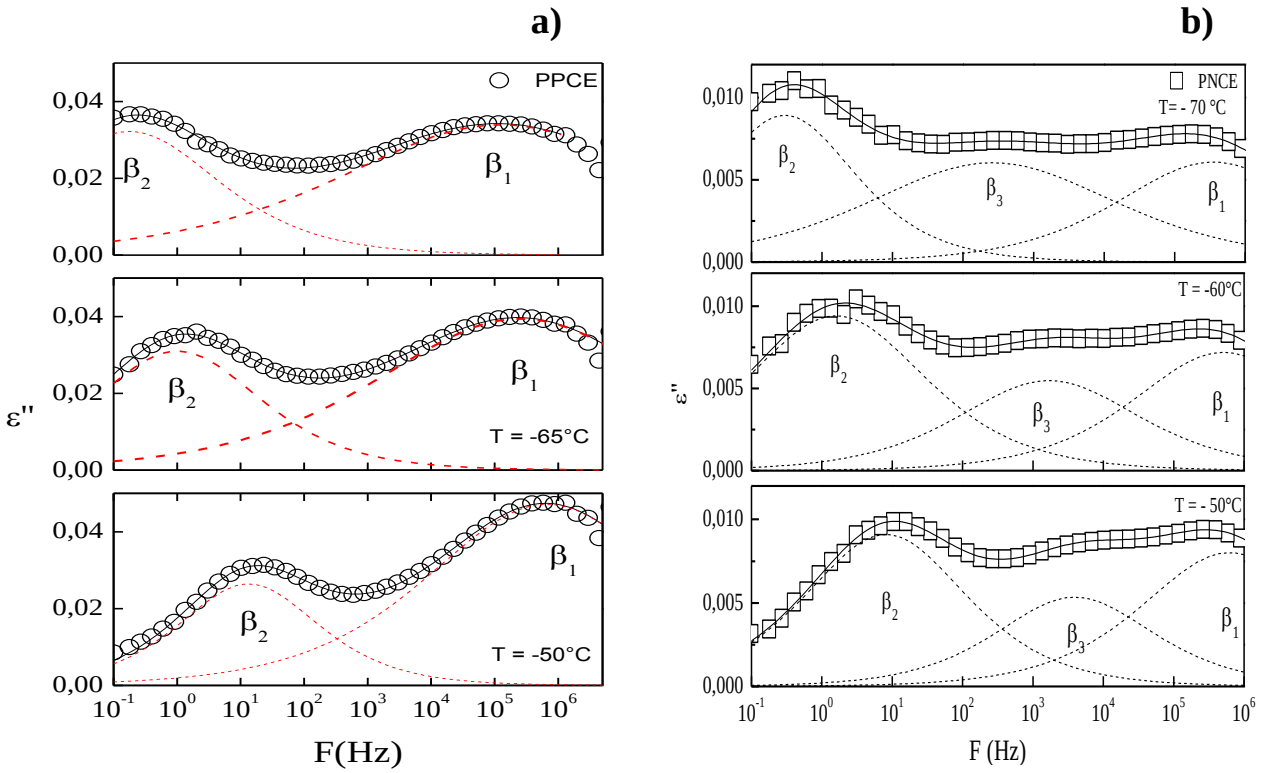

Figure 4.46. Isothermal dielectric loss values as a function of frequency at different temperatures for the two homopolymers of the series: PPCE (a) and PNCE(b). Continuous lines represent best fits according to CC equation, dashed lines show the separated contribution of the different relaxation processes.

For the P(PCExNCEy) random copolymers the subglass relaxation behavior is closer to that exhibited by PPCE, however for the P(PCE80NCE20) the presence of the intermediate β_3 process can be hypothesised (see figure 4.47).

The relaxation data in this temperature region can be well described by a superposition of three Cole-Cole functions (eq. 30 paragraph 3.10 with c=1). Some examples of these fittings are shown in Fig.4.46 by the dashed lines.

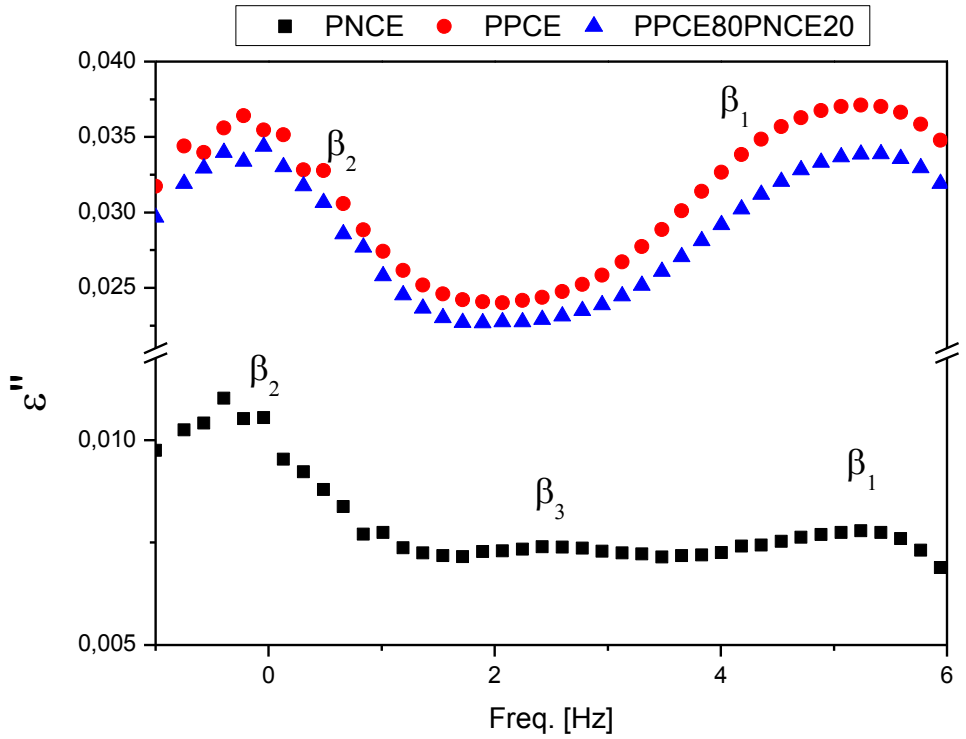

Figure 4.47 Subglass relaxations of PPCE(●) , PNCE (■) and P(PCE80NCE20) (▲) at T= -70°C.

In these cases the relaxation time, τ_{HN}, coincides with τ_{max} which is the one associated to the frequency of maximum loss [Kremer & Schonhals, 2002].

Figure 4.48 shows the τ_{max} values as a function of the reciprocal temperature for PPCE, PNCE and for P(PCE80NCE20) random copolymer. In such a representation, β_1 β_2 and β_3 processes follow an Arrhenius behavior. This is characteristic of sub-glass relaxation processes. From the slope of the τ_{max} it is possible to obtain the activation energy (E_a) of the processes considering the Arrhenius equation:

$$\tau_{max} = Aexp\left({E_a}/{RT}\right) \qquad \textbf{[31]}$$

where A is a pre-exponential factor and R is the ideal gas constant.

As regards the β_1 relaxation, the activation energy varies from 35 kJ/mol for PPCE and PNCE to 37 kJ/mol for P(PCE80NCE20), while the activation energy calculated for the β_2 process keeps almost a constant value with a value of ≈ 62 kJ/mol, as the NCE unit

content is increased. The β_3 process, evidenced in PNCE, exhibits the highest E_a value: 69 kJ/mol.

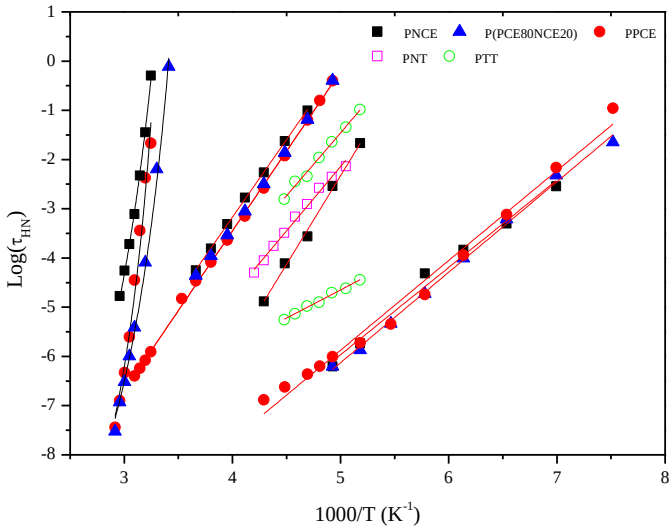

Figure 4.48: Relaxation time as a function of the reciprocal temperature for the α relaxation and for the local processes β_1 and β_2 for PPCE(●), PNCE(■) and P(PCE80NCE20)(▲). Thick continuous lines correspond to best linear fits for β relaxations and best fits to the VFT equation.

In order to deeply understand the nature of the subglass processes of the polymers under study, dielectric data have been compared with those of Poly(trimethylene terephthalate) (PTT) and Poly(neopenthyl terephthalate) (PNT) previously synthesized in our laboratories and investigated by means of dielectric spectroscopy [Soccio, Lotti, et al., 2008 (b); Soccio, Nogales et al., 2012], whose chemical structure is shown in Figure 4.49.

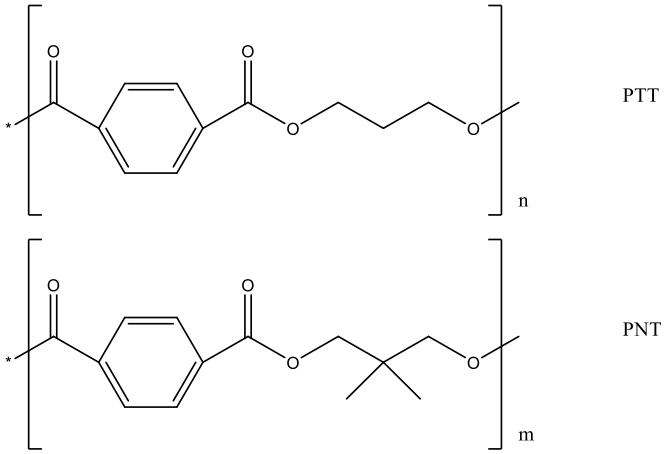

Figure 4.49: Chemical structure of PTT and PNT

As it can be observed, PPT and PNT present a chemical structure very similar to that of PPCE and PNCE, respectively. The only difference is given by aromatic ring present in PTT and PNT.

Figure 4.50 shows the comparison between the relaxation processes in the subglass region between PPCE and PTT (Fig. 4.50a) and PNCE and PNT (Fig. 4.50b).

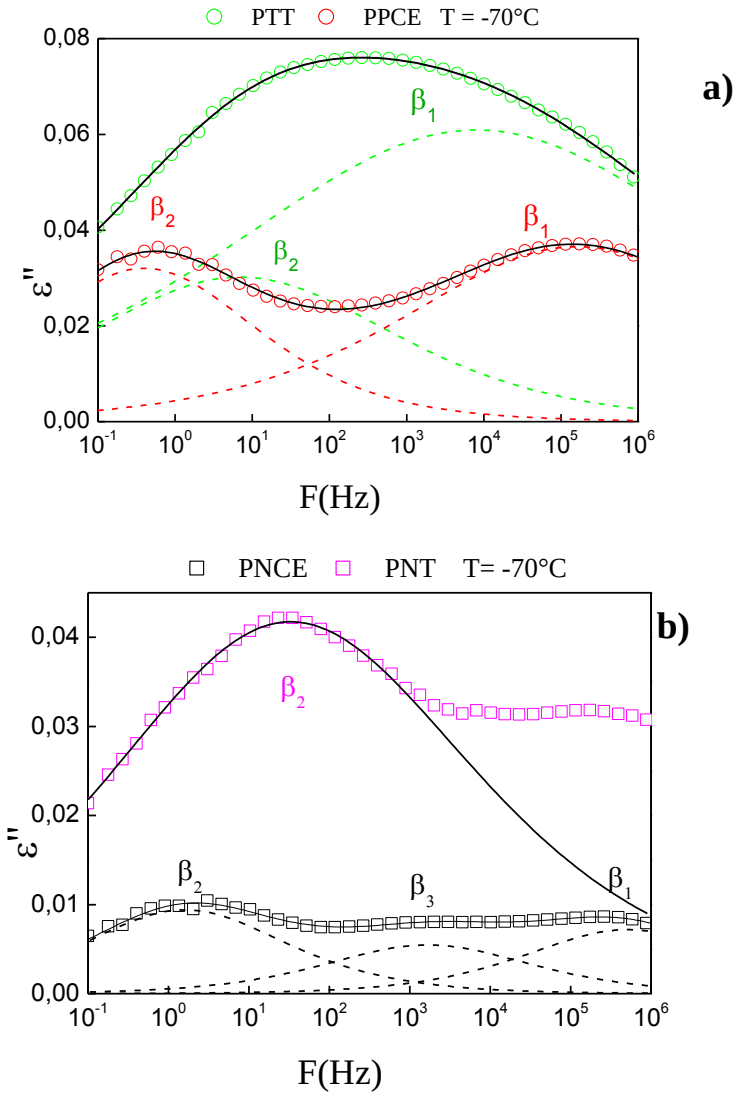

Figure 4.50: (a) Subglass relaxations of PPCE(○) compared to those of PTT (○) at T= -70°C [Soccio, Nogales et al., 2012]. (b) Subglass relaxations of PNCE(□) and PNT (□) at T= -70°C. In both cases, continuous lines represent best fits according to CC equation, dashed lines show the separated contribution of the different relaxation processes (green: PTT; red: PPCE; black: PNCE; pink: PNT) .

The β relaxation processes observed below Tg for both PPT and PNT appear as broad maxima. It has been proposed that the β relaxation for PTT and PNT is composed of two processes, designated as β_2 and β_1 in order of increasing frequency [Soccio, Nogales et al., 2012]. Multimodal shapes of the glassy dynamics has been in different homopolymers and copolymers both experimentally [Bravard &Boyd 2003; Nogales et al., 2006; Soccio, Nogales et al., 2014; Martin-Fabiani et al., 2013] and by molecular dynamics simulation [Boyd & Boyd, 2001]. It has been proposed that the multimodal shape of the β relaxation in aromatic polyesters consist of the contribution of the three conformationally flexible bonds of the monomer, namely, the aromatic ring carbon to ester carbon bond (CA-C), the ester ether oxygen to aliphatic carbon bond (O-C) and the aliphatic carbon-carbon bond (C-C). Computer simulation suggests that the O-C bond should relax faster than the C-C one and both faster than the CA-C bond [Boyd & Boyd, 2001]. This latter bond is responsible for the β* relaxation appearing in polyesters based on 2,6-naphthalenedicarboxylic acid like Poly(ethylene naphthalene-2,6-dicarboxylate) (PEN) [Bravard & Boyd, 2003; Nogales et al., 2000] or Poly(butylene naphthalene-2,6-dicarboxylate) (PBN) [Soccio, Nogales et al., 2008]. The corresponding relaxation times for the β relaxations of PPT and PNT have been included in Fig.4.48 for sake of comparison. From the graph it is clear that τ_{max} values of the low frequency process (β_2) of PPCE, PNCE and P(PCExNCEy) random copolymers are comparable with those of the β_2 process for PPT and PNT. In a similar way, although the relaxation time data of the β_1 process for PPCE and P(PCExNCEy) random copolymers appear somehow at lower temperatures, they are similar to those of the β_1 relaxation for PTT as far as the activation energy is concerned.

The molecular origin of the β_1 relaxation can be associated to the relaxation of the ester oxygen linked to the aliphatic carbon of the diol subunit. The β_1 relaxation of NCE monomeric units is expected to overcome a higher energy barrier as compared to PCE ones even if it is not so evident in the studied composition range (the Ea varies from 33 kJ/mol for PPCE to 37 kJ/mol for PPCE80). The glycolic part of NCE unit is characterized by the presence of two methyl groups in *β*-position with respect to the oxygen atom, instead of two hydrogen atoms as in PPCE. The presence of these two methyl groups could be the responsible of the hindering of this mode in PNCE in respect to PPCE. This fact supports the idea that the molecular origin of the

β_1 relaxation is related to the distinct arrangement of the glycolic group attached to the ester one.

As to the low frequency process, figure 4.48 shows that the slope of $\log_{10}\tau max$ vs reciprocal temperature and consequently the corresponding activation energy E_a, keeps almost a constant value of ≈62 kJ mol $^{-1}$ both in PPCE, PNCE and in P(PCE80NCE20) copolymer (the other copolymers present similar activation energies). This result indicates that the molecular origin of the β_2 process can be associated with a bond that is present in both repeating units forming the copolymers: the chemical link between the aromatic ring carbon to the ester carbon.

Finally, the weak β_3 relaxation, observed in PNCE can be associated with the chair-chair conformational changes of the aliphatic ring (see figure 4.51) [Mc Crum et al., 1967].

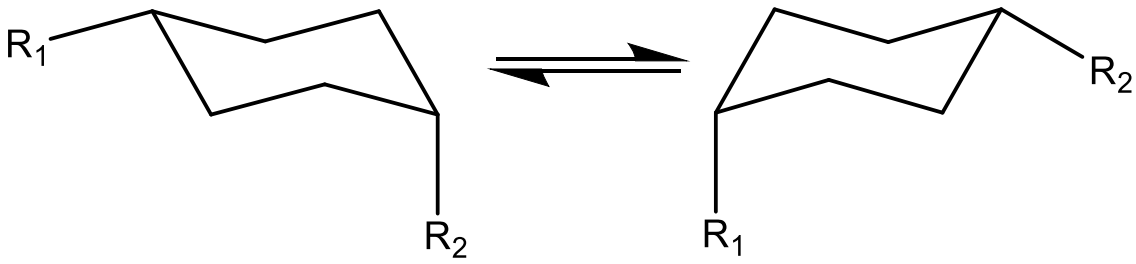

Figure 4.51: Conformational flip chair-chair of the aliphatic ring

As a matter of fact, a deeper analysis of the relaxation profile of P(PCE80NCE20) copolymer revealed the presence of this mode in this polymer too, even if its contribution is too weak to be fitted properly.

In PPCE, as in the other copolymers, the weak β_3 relaxation is impossible to detect being hidden by the more intense β_1 relaxation. As already stated, the presence of the two $-CH_3$ groups in NCE co-units is responsible of the reduction of chain mobility and consequently of the inhibition of β_1 relaxation, that make now detectable β_3 contribution (Fig. 4.47).

4.4.5.2 α Relaxation

The intense alpha process appears above the calorimetric glass transition temperature as previously reported and has been associated to the segmental dynamics of the amorphous phase. Figure 4.52 shows the α relaxation curves of PPCE, PNCE and P(PCE80NCE20) at different temperatures, that have been chosen to exhibit similar frequencies of the maximum loss.

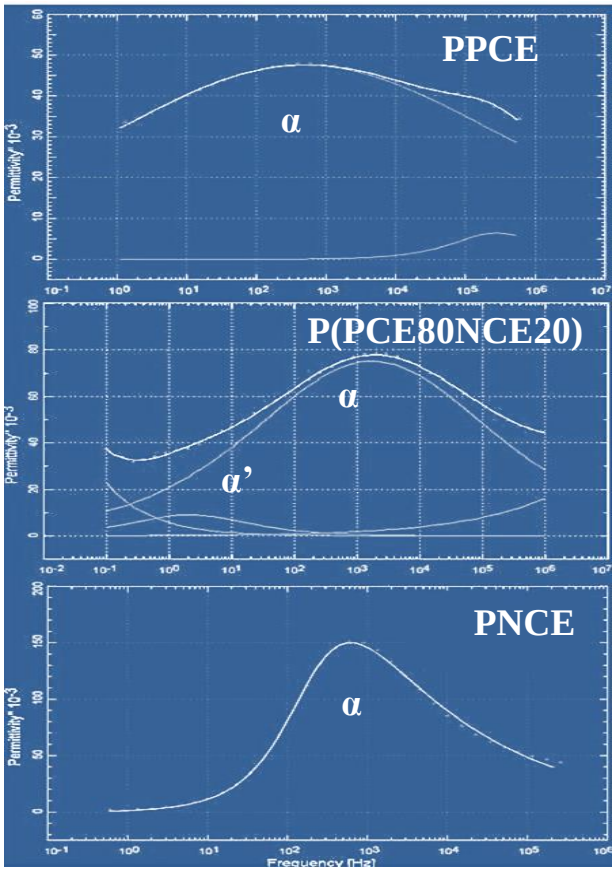

Figure 4.52: α relaxation for PPCE at T=45ºC, P(PCE80NCE20) at T=40ºC and PNCE at T= 50ºC.

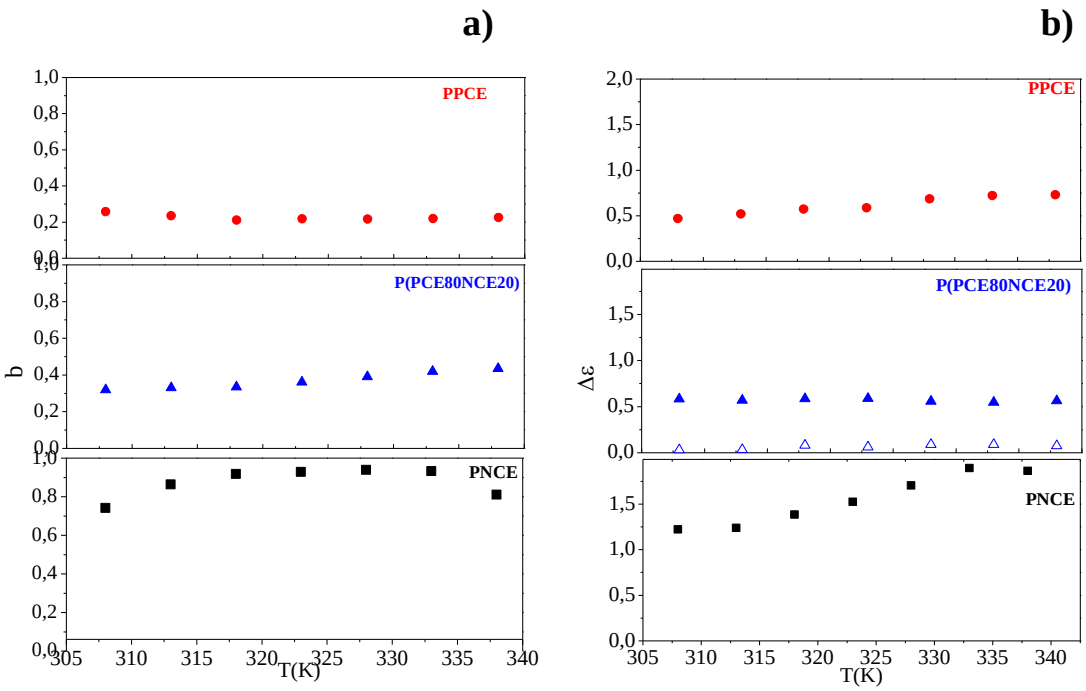

Figure 4.53: Symmetric broadening b of the α relaxation (a) and dielectric strength (b) as a function of temperature for PPCE at T=45ºC(●), P(PCE80NCE20) at T=40ºC (▲) and PNCE at T= 50ºC (■). Open symbols (Δ) indicates the dielectric strength for the α' relaxation detected in P(PCE80NCE20).

The α relaxation of amorphous PNCE is characterized by a relatively narrow peak in ε'' as a function of frequency, while the peak is broaden for the semicrystalline PPCE and P(PCE80NCE20) (a similar behaviour has been observed for the other copolymers). For all the polymers under study, at higher frequencies the less intense contribution of the β relaxation region is also revealed.

For P(PCE80NCE20) a broadening in the low frequency side of the α relaxation is detected. This effect, previously reported [Soccio, Nogales et al., 2012] for PTT-PNT system, can be ascribed to an additional α-process, called α' appearing at lower frequencies as crystallinity develops and corresponding to the segmental relaxation of a confined rigid amorphous phase coexisting with the initial one. Consequently an additional Havrliak –Negami contribution must be taken into account to consider a second alpha process. The presence of the α' phase was already detected by dynamic mechanical thermal analysis (see paragraph 4.4.2).

The broadening parameter *b* of the amorphous PNCE homopolymer and semicrystalline PPCE and P(PCE80NCE20) is showed in figure 4.53a. Its value is of about 0.8 for the

amorphous sample, remaining almost constant with the increasing of temperature due to the absence of crystallization, while is lower for the semicrystalline samples (about 0.2-0.3).

As concerns the dielectric strength (Figure 4.53b), Δε of PNCE homopolymer is higher than that of the semicrystalline PPCE and P(PCE80NCE20) in the whole temperature range considered.

The evolution of both *b* and Δε parameters reflect the amorphous nature of PNCE with respect to the semicrystalline PPCE and P(PCE80NCE20). In fact, while amorphous materials are characterized by a narrow (high *b* value) and intense (high Δε value) α relaxation peak, semicrystalline samples present broad (low *b* value) and weak (low Δε value) α relaxation peak [Soccio, Nogales et al., 2007].

Figure 4.54 shows the α relaxation for PNCE and PNT amorphous homopolymers. The curves have been normalized with respect to ε''_{max} and F_{max} to compare the peak shape of each sample. As observed, the shape of the α relaxation, for similar temperature conditions, is nearly the same for the two homopolymers, with the broadening *b* parameter being around 0.8 for both PNCE (figure 4.53 a) and PNT [Soccio, Nogales et al., 2012]. This result highlights that the nature of the six carbon ring, aliphatic or aromatic, does not affect the segmental dynamics in terms of homogeneity of the process.

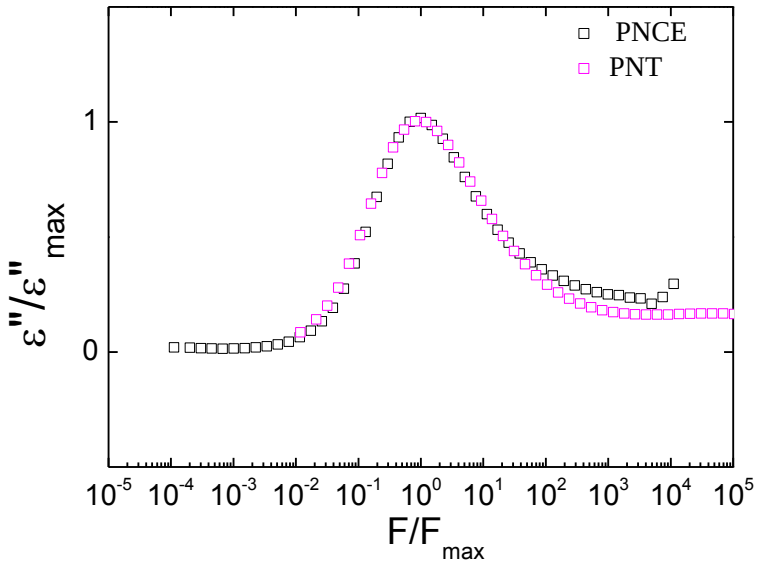

Figure 4.54: Normalized ε'' values for PNCE at T=45ºC(□),and PNT at T= 80ºC (□)

In Figure 4.48, together with the β-relaxation τ_{max} values at low temperatures, the α-relaxation τ_{max} evolution is also reported at higher temperature.

In the amorphous state, the frequency of α-relaxation maximum loss exhibits a typical Vogel Fulcher Tamann (VFT) dependence:

:

$$\tau_{\max} = \tau_0 \exp\left(\frac{DT_0}{T - T_0}\right) \qquad [32]$$

where τ_0 is a characteristic time, T_0 is the Vogel temperature, and D is the fragility strength parameter [Richert & Angell 1998]. This behaviour is characteristic of cooperative segmental motions appearing above the glass transition temperature. To obtain accurate fits, and in accordance with a Angell's proposal, [Angell, 1997]] a value of τ_0 of 10^{-14}s was assumed. Continuous lines in Figure 4.48 represent the best fits of the experimental α-relaxation τ_{max} values to equation 31.

The fragility strength parameter D and the Vogel temperature T_0, calculated for the only amorphous sample PNCE, are 6.0 and 246 K, respectively. The same parameters for the corresponding aromatic polymer PNT, previously determined, are: D = 6.2 and T_0= 290 [Soccio, Nogales et al., 2012]. As expected on the basis of the increased backbone flexibility due to the presence of the aliphatic ring, PNCE shows lower T_0 value. Interestingly, the D parameter is not similarly affected. This result indicates that the fragility is not so sensible to the nature of the ring and is on the same lines as the segmental dynamics results (Figure 4.54).

As shown in Figure 4.48, the α-relaxation τ_{max} values for PPCE and P(PCE80NCE20) shift toward lower temperature, in accordance with the calorimetric results (see Chapter X). Further considerations are limited by the semicrystalline nature of these two samples.

4.4.6 Conclusions

The introduction of neopenthyl glycol along the PPCE macromolecular chain has been carried out by the polycondensation reaction of 1,4-dimethylcyclohexanedicarboxylate with 1,3-propanediol and neopenthyl glycol. This easy synthesis strategy allowed the preparation of a new class of aliphatic polyesters with improved properties with respect

to the parent homopolymer. Moreover, the final material properties can be effectively tailored simply varying the copolymer composition.

As expected, the introduction of neopenthyl glycol sub-unit in the PPCE resulted in a decrease of the crystallinity degree and melting point, due to a decrement of chain symmetry and regularity. The higher the mol% of NCE co-units, the greater the effect on these properties. As a consequence, the mechanical properties and the biodegradation rate turned out to be influenced. As a matter of fact it has been observed a decrease in the elastic modulus and an increase in the elongation to break till to an elastomeric behaviour.

The biodegradation rate in compost resulted in all cases higher than that of PPCE, and once again dependent on the copolymer composition: the higher the NCE mol%, the higher the weight losses of the copolymers under study.

The subglass dynamics of PPCE homopolymer and of the copolymers is characterized by the existence of two processes, β_1 and β_2, which have been assigned to the relaxation of the bond between the ester oxygen and the aliphatic carbon of the diol subunit, and to the bond between the aliphatic ring carbon to the ester carbon, respectively. The comparison between PPCE and PNCE reveals that this latter presents and additional process, labelled as β_3, at intermediate frequencies between β_1 and β_2, that has been assigned to the conformation changes of the aliphatic ring. The presence of the two methyl groups in PNCE determine a decrease of the β_1 intensity, enabling β_3 relaxation to be detected in the dielectric spectrum.

It is notable all the new materials are potentially bio-based and biodegradable, and can be candidates for substituting some traditional petroleum-based polymers in specific applications.

4.5 Aliphatic multiblock poly(ester urethane)s based on 1,4-trans-cyclohexane dicarboxylic acid and Poly(buthylene succinate)

A family of poly(ester urethane)s obtained by chain extending hydroxyl-terminated polyester prepolymers has been studied. Poly(butylene cyclohexanedicarboxylate) has been coupled in different mass ratios with two poly(butylene succinate)-based random copolymers containing ether linkages. So, five high molecular weight bio-based poly(ester urethane)s have been designed. The effect of the chemical composition and of the mass ratio of the two blocks in the final polymer have been evaluated by characterizing the materials from the molecular, thermal and mechanical point of view. In addition, envisioning a food packaging application, biodegradation in compost and measurement of the gas barrier properties have been carried out and correlated to the polymer chemical structure. The activation energy of the gas permeation process has been calculated, too.

4.5.1. Prepolymer synthesis and characterization

The purified and dried hydroxyl-terminated prepolymer powders, whose molecular structure is represented in Figure 4.55, have been synthesized following the procedure explained in paragraph 3.2.2 (PBCE-OH) and 3.2.3.2 (P(BSxBDGy)-OH). They have been characterized from the molecular and thermal point of view. The data have been collected in Table 4.27.

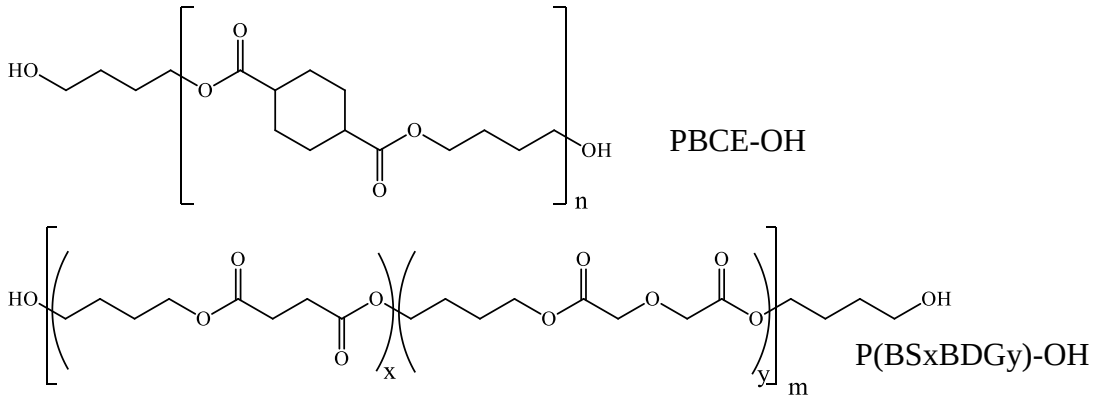

Figure 4.55: Chemical structure of PBCE-OH (above) and P(BSxBDGy)-OH (below).

The molecular weight has been determined by GPC and 1H-NMR, showing comparable results (Table 4.26). 1H-NMR has been employed also to verify the chemical structure and composition of the P(BSxBDGy)-OH (Figure 4.56) and PBCE-OH (Figure S1). In all cases the spectra are consistent with the expected structure and the composition of the P(BSxBDGy)-OH is very close to the feed. The areas of the peaks of h aliphatic proton of the succinic subunit located at 2.61 ppm and of the k protons of the diglycolic subunit at 4.24 ppm have been used to deduce the copolymer composition (Figure 4.56).

Table 4.27. Molecular and thermal characterization data of OH-terminated prepolymers.

Polymer	M_n[a]	PDI[a]	M_n[b]	BS mol%[b]	T_g (°C)	T_m (°C)	ΔH_m (J/g)
PBCE-OH	7700	2.7	4100	-	n.d.	171	46
P(BS70BDG30)-OH	9300	2.9	6200	68.5	-30	89	58
P(BS50BDG50)-OH	8600	2.6	4900	49.2	-32	61	40

a) determined by GPC
b) determined by 1H-NMR

Due to the catalyst employed and the high temperatures involved in the reaction, the P(BSxBDGy)-OH display a random distribution of the comonomeric sequences [Gigli, Lotti et al., 2012].

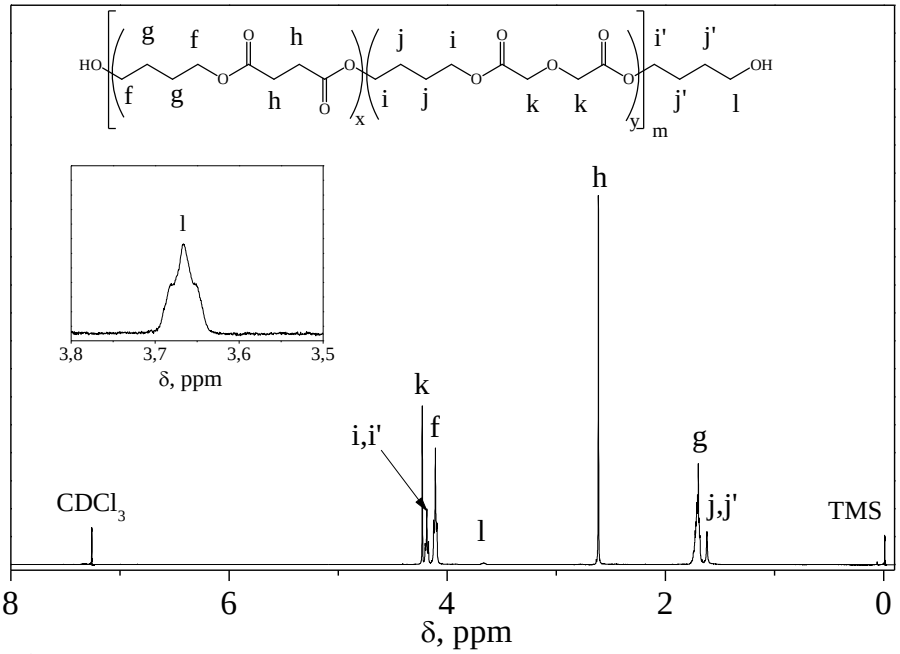

Figure 4.56. ^{1}H-NMR spectrum of P(BS70BDG30)-OH with resonance assignments. In the inset, an enlargement of the section showing the terminal groups.

The molecular weights have been determined by GPC and ^{1}H-NMR. M_n from ^{1}H-NMR has been calculated according to the following formula, as previously described [Fabbri et al., 2016]:

$$M_n = DP * M_{w,unit} + X \qquad [33]$$

where DP is the degree of polymerization determined by NMR, $M_{w,unit}$ is the molecular weight of each polymer repeating unit (226 g/mol for PBCE, 177 g/mol for P(BS70BDG30) and 182 g/mol for P(BS50BDG50)) and X is the molecular weight of the terminal butanediol (100% hydroxyl-terminated polymers have been considered).

It can be noticed from Table 4.26 that the molecular weights calculated by NMR and GPC are comparable. Polydispersity is a bit higher than the theoretical value of polycondensation reactions, probably because of the selected reaction conditions (high excess of butanediol, shorter reaction time and lower temperature), which have been optimized to achieve a high concentration of hydroxyl terminal groups.

The thermal transitions, obtained from I scan DSC, have been reported in **Table 4.27**. All three samples are semicrystalline polymers, but the melting and glass transition temperatures present some differences. In particular, PBCE-OH show a T_m of about 170 °C, while the PBS-based prepolymers display much lower melting endotherms, below 90°C, and T_g well below room temperature. These effects are due to two main factors: the presence of a comonomeric unit and linear aliphatic nature of the macromolecular chain.

4.5.2. Polymer synthesis, molecular and thermal characterization

High molecular weight multiblock copolymers were prepared by chain extending PBCE-OH (A) with P(BS50BDG50)-OH (B) and P(BS70BDG30)-OH (C) in different mass percentages (see paragraph 3.2.4.2). The polymers obtained are thus A50B50, A30B70, A50C50, A30C70, where the values in the abbreviations represent the feed mass percentages of each prepolymer. Chain extended PBCE was also considered.

In **Figure 4.57**, the general chemical formula of the resulting poly(ester urethane)s is represented. After the purification process, no unreacted HDI was detected by ^{1}H-NMR. In **Figure 4.58** the spectrum of A50B50 is reported as an example. With z, w and y are

labelled the protons of the reacted chain extender located at d 3.15 ppm, 1.34 ppm and 1.25 ppm, respectively. All the spectra are consistent with the awaited structure.
In **Table 4.28** the molecular, thermogravimetric and wettability characterization data are contained.

Table 4.28: Molecular, thermogravimetric and wettability characterization data.

Polymer	M_n	PDI	T_{onset}	T_{max}	WCA (°)
PBCE	36000	2.7	328	420	98 ± 3
A50B50	37000	3.0	315	414	90 ± 3
A30B70	52400	3.3	313	403	90 ± 3
A50C50	35500	3.2	313	414	87 ± 2
A30C70	51000	2.8	303	395	84 ± 1

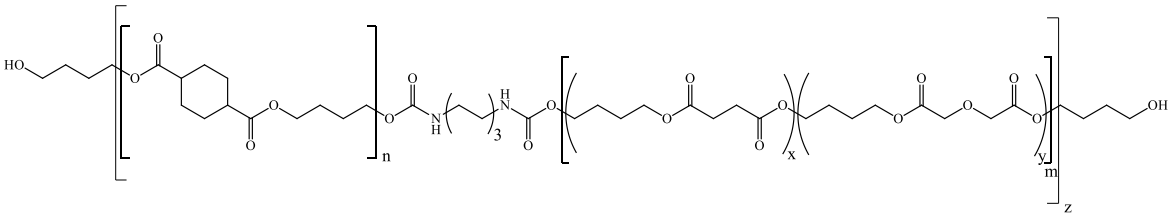

Figure 4.57: Chemical structure of PBCE-based multiblock poly(ester urethane)s.

As it can be seen from Table 4.28, the chain extension process resulted in a significant increase of the polymer molecular weight. From the polymer purified powders, thin film have been obtained by compression moulding. Before characterizing, they have stored at room temperature for at least two weeks in order to achieve equilibrium crystallinity.

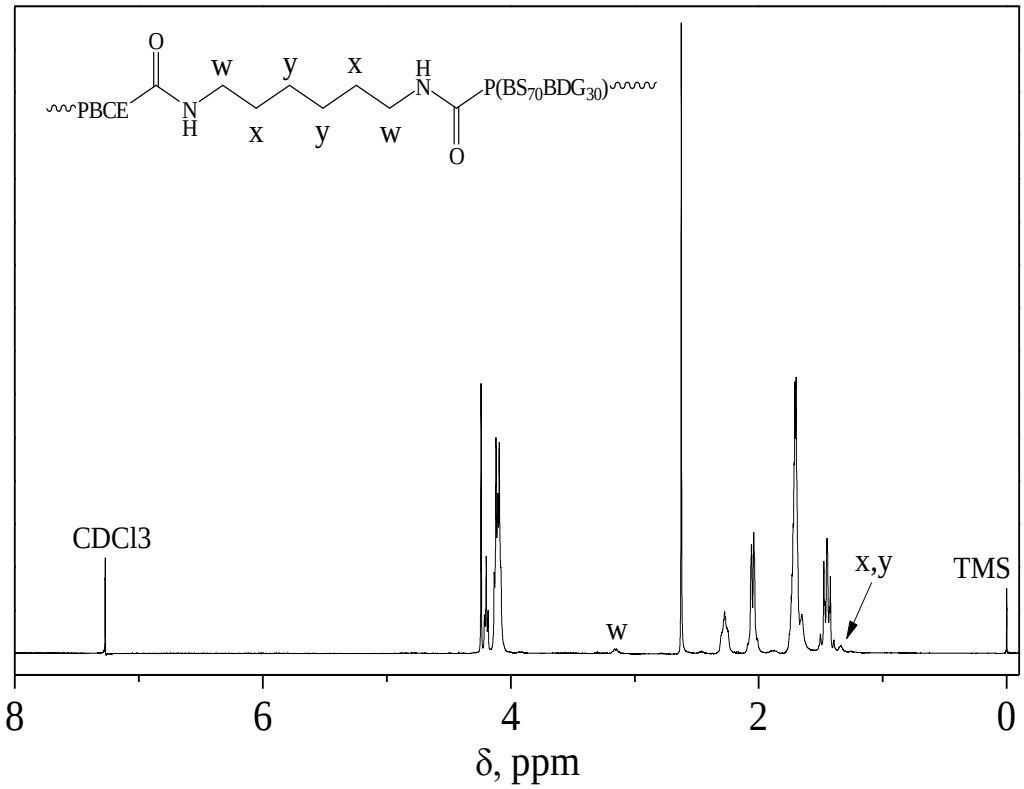

Figure 4.58: ^{1}H-NMR spectrum of A50B50 with resonance assignments.

Afterwards, the thermal stability has been analysed by TGA under nitrogen flux. The temperatures relative to the degradation onset (T_{onset}) and to the maximum weight loss rate (T_{max}) have been reported in **Table 4.28**. The thermal degradation of the polymers under study is characterized by a one-step weight loss, that start above 300°C. The PBCE is the more stable material, thanks to the presence of the aliphatic ring, which confers good thermal resistance [Gigli et al., 2014 (b)]. For the copolymers, it can be observed that the higher the amount of PBCE blocks, the higher the stability. For equal PBCE content, the lower the amount of butylene diglycolate co-units (BDG) the higher the stability, as previously observed. [Gigli. Lotti et al., 2012]

The main thermal transition data of the multiblock copolymers under study are reported in **Table 4**.29.

Table 4.29: Thermal characterization data and degree of crystallinity.

I scan								
Polymer	**T_g (°C)**	**ΔC_p (J/°C g)**	**$T_{m,1}$ (°C)**	**$T_{m,2}$ (°C)**	**$\Delta H_{m,1}$ (J/g)**	**$\Delta H_{m,2}$ (J/g)**	**$T_{cc,1}$ (°C)**	**$T_{cc,2}$ (°C)**
PBCE	10	0.056	-	166	-	34	-	143
A50B50	-34	0.303	44	141	9	13	8	116
A30B70	-31	0.366	63	132	18	7	31	104
A50C50	-29	0.444	49	114	3	20	-	96
A30C70	-32	0.470	47	109	9	6	-1	90

Figure 4.59 contains the melting endotherms of PBCE and the multiblock copolymers. The glass transition of PBCE is not clearly visible due to the high crystallinity of this sample, while all the copolymers display a T_g of about -30°C, due to the flexibilizing effect imparted by the linear aliphatic PBS-based chains. In all cases a single T_g is visible, indicating good miscibility in the amorphous phase (**Figure 4.59**).

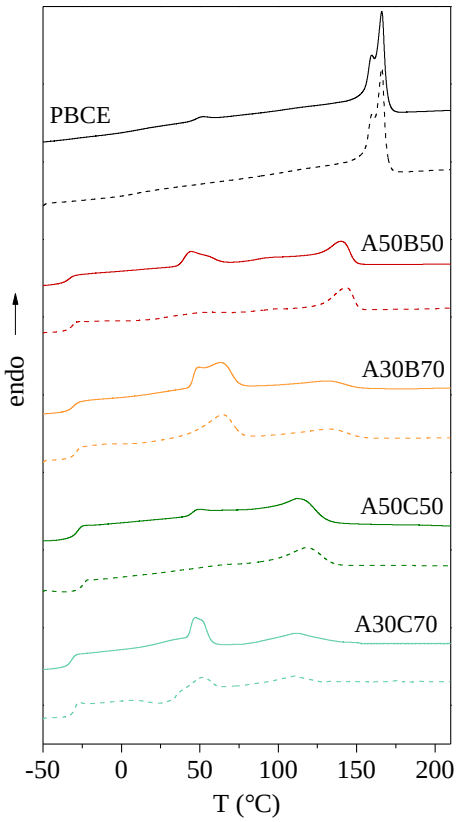

Figure 4.59. Calorimetric curves of PBCE and multiblock copolymers. Solid lines: 1st scan; dash lines: 2nd scan after melt quenching.

As to the melting phenomenon, PBCE homopolymer displays a very high melting temperature. The melting phenomenon is characterized by multiple peaks, ascribed to fusion and recrystallization processes, as already observed for this and other aliphatic polyesters. [Soccio et al., 2007; Soccio et al., 2008 (c); Soccio et al.,2009; Gigli, Lotti et al., 2012]. On the contrary, the copolymers are marked out of two well distinct melting endotherms, whose intensity well correlates with their composition (**Figure 4.59**). In each copolymer, to a higher amount of PBS-based blocks corresponds a higher intensity of the lower temperature melting endotherm ($\Delta H_{m,1}$ in **Table 4.29**). Similarly, an increased content of PBCE blocks resulted in a more intense melting endotherm at higher temperatures ($\Delta H_{m,2}$ in **Table 4.29**). Moreover, as already observed for the prepolymers, the P(BS70BDG30) block (B) displayed an higher capacity to crystallize with respect to P(BS50BDG50) (C) in the poly(ester urethane)s (**Figure 4.59**). The T_m follows a similar trend. It is worth highlighting that the presence of P(BS50BDG50) caused the formation of less perfect PBCE crystals with respect to multiblock copolymers containing P(BS70BDG30), as well indicated by the lower of the T_m (**Table 4.29**).

Deeper investigation on the nature of the crystalline phase have been carried out by WAXS and the results have been displayed in **Figure 4.60**.

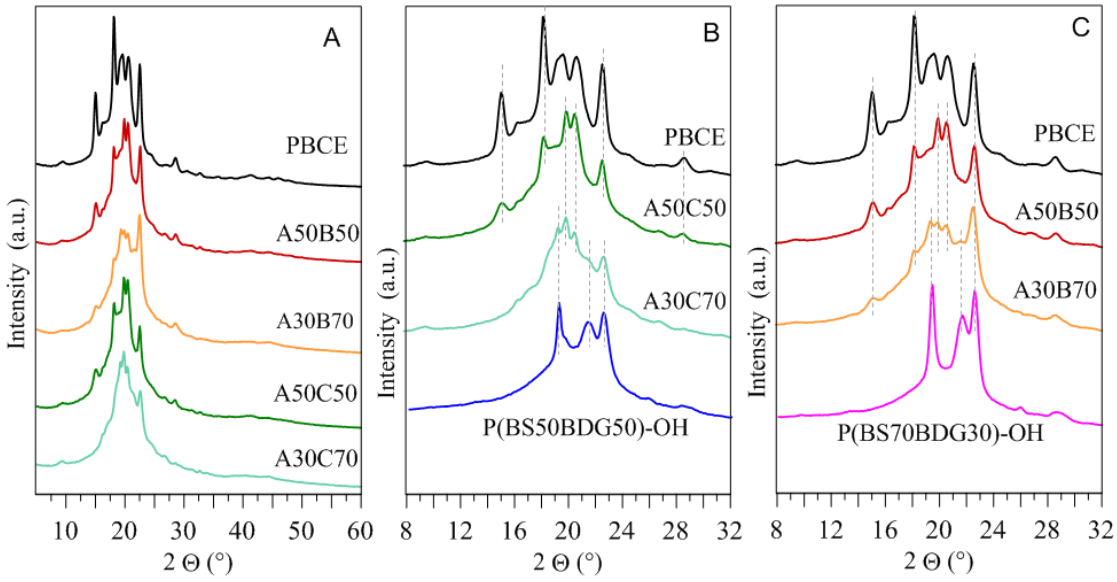

Figure 4.60: X-ray diffraction patterns of PBCE and multiblock copolymers. In A the spectra of the five polymers under study are reported, B contains the PBCE pattern together with those of the copolymers containing P(BS50BDG50), in C are collected the patterns of PBCE and of P(BS70BDG30) containing copolymers.

All the copolymers show broader and more convoluted peaks with respect to the PBCE homopolymer, suggesting a significant drop of the crystallinity degree. The analysis of the diffraction profiles reveals that all the samples contain more than one crystal phase. PBCE sample shows strong peaks at 15.0°, 18.1°, 20.6°, 22.5°, 28.6° that can be assigned to the main PBCE crystal phase, and broader peaks at 9.3°, 16.25°, 19.2°, 19.6°, 24.5°, probably due to a secondary PBCE phase. The copolymers richer in PBCE blocks display a XRD pattern very similar to that of PBCE, but contain an extra peak at 19.9° that confirms the presence of an extra crystalline phase (**Figure 4.60**). In the copolymers containing a higher amount of PBS-based blocks, the PBS crystalline phase becomes indeed more evident (**Figure 4.60**). Therefore, the XRD results are in perfect agreement with the DSC ones.

Further information about the ability to crystallize of each block in the poly(ester urethane)s has been deduced by second DSC scan (after melt quenching, data are reported in table S4) and by subjecting the samples to a controlled cooling rate from the melt.

The second DSC scan evidenced that all the samples cannot be obtained in a completely amorphous state (**Figure 4.59**, dotted curves). As a matter of fact, both crystalline phases are able to develop in all the copolymers, with the exception of A50C50. In this sample, the PBS phase crystallization was completely depressed by the quenching.

Non-isothermal experiments ratified the above mentioned findings. In the A50C50 sample PBS crystals were not able to grow even at low cooling rates. **Table 4.29** reports the temperature of the maximum of the crystallization peaks in non-isothermal experiments (T_{cc}). In all the copolymers a significant reduction of the PBCE ability to crystallize has been observed.

Two factors contribute to this behaviour: the amount of each block in the final polymer and the chemical structure of the PBS-based blocks. In particular, the higher the amount of a block, the higher its ability to crystallize. The higher the amount of BDG sequences in the PBS-based blocks, the lower the ability to crystallize of the PBS phase, due to a hampering effect caused by the presence of the BDG comonomeric unit.

4.5.3 Mechanical characterization

Tensile tests have been carried out on PBCE and multiblock copolymers to analyse their mechanical behaviour. Stress-strain curves have been reported in **Figure 4.61** and the corresponding data (elastic modulus E, stress at yield σ_y, elongation at yield ε_y, stress at break σ_b, and elongation at break ε_b) are contained in **Table 4**.30 As it can be observed, the presence of PBS-based blocks, deeply affected the mechanical properties of PBCE homopolymer. Generally speaking, a lowering of the elastic modulus and of the stress at yield and an increase of the elongation at break has been observed.

Table 4.30: Mechanical characterization data of PBCE and multiblock copolymers.

Polymer	E (MPa)	σ_y (MPa)	ε_y (%)	σ_b (MPa)	ε_b (%)
PBCE	811 ± 39	32 ± 3	14 ± 2	27 ± 2	78 ± 11
A50B50	190 ± 11	13 ± 1	16 ± 2	13 ± 1	318 ± 33
A30B70	250 ± 33	12 ± 2	11 ± 2	14 ± 3	276 ± 24
A50C50	131 ± 5	-	-	13 ± 1	480 ± 36
A30C70	140 ± 22	8 ± 1	17 ± 3	10 ± 2	506 ± 55

This effect strongly depends on the nature of the PBS-based block. Indeed, copolymers containing P(BS50BDG50) display a higher ε_b and a lower E as compared to those containing P(BS70BDG30) blocks, because of the higher crystallinity degree of the latter.

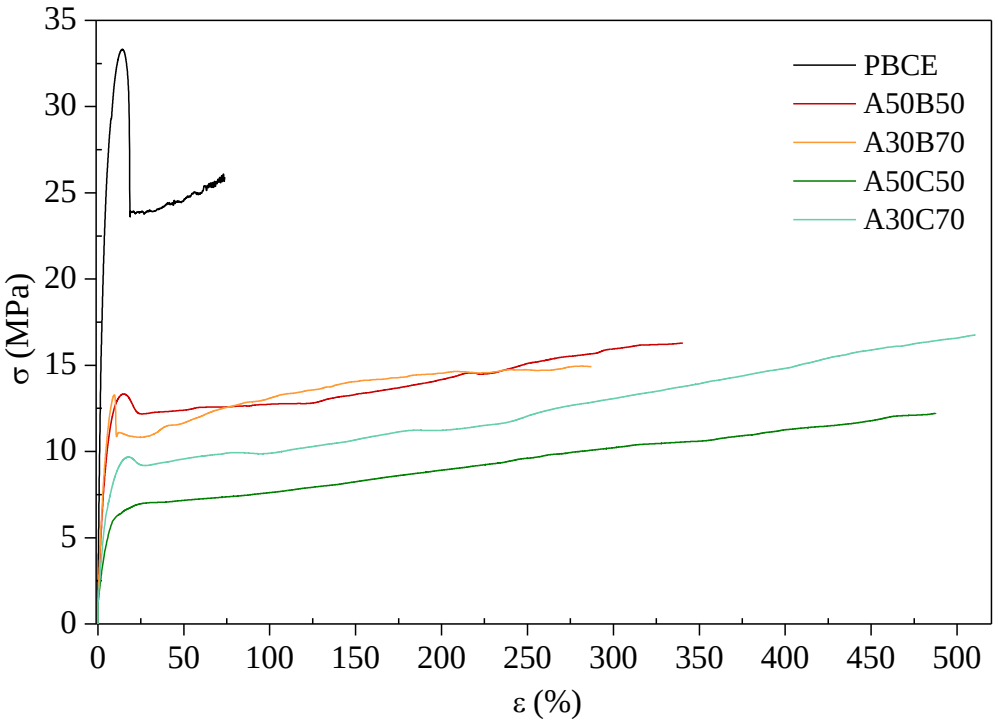

Figure 4.61: Representative stress-strain curves of PBCE and multiblock copolymers.

Interestingly, A50C50 does not show the yield point and behaves as an elastomeric material (**Figure 4.61**). To investigate its resistance to loading-unloading stresses, cyclic tensile measurements have been conducted on this sample (**Figure 4.62**). The loading-unloading path is characterized by a high elasticity, with a recovery of about 85% even after 20 cycles (**Figure 4.62**). The difference between the first and the second cycle can be explained on the basis of the reorientation of the macromolecules and the crystallization during straining. [Andronova & Albertsson, 2006] From the second cycle the loading-unloading curve sticks to a fixed path, with a very small hysteresis and both the unloading curve and the residual strain are quite independent from the cycle number.

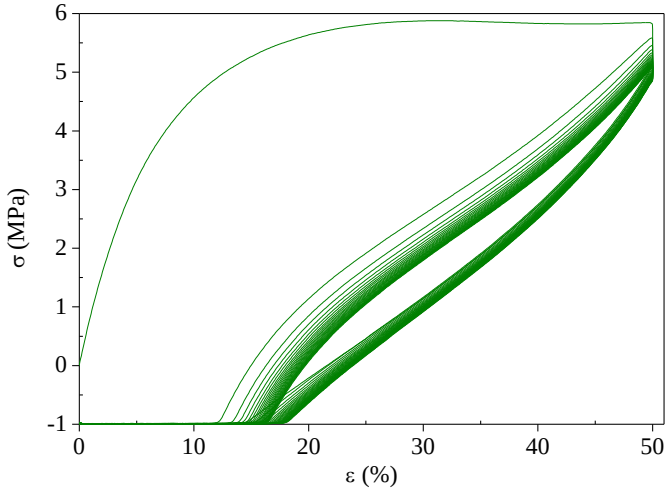

Figure 4.62: Hysteresis behaviour of A50C50 upon cyclic loading (20 cycles).

4.5.4 Barrier properties

The existence of mass transport through polymeric material, represented by the process of gas permeation, migration, and sorption (permeability behavior) is well known and it is identified as the quantification of permeates transmission, gas or vapor, through a resisting material [Pauly, 1999; Galić et al., 2000]. As a consequence, the gas transfer is normally associated with the quantitative evaluation of the barrier properties of a plastic material.

Taking into account that a polymeric film is characterized by a rate of food respiration or gas permeability which vary with the operating temperature, the barrier properties evaluation has been performed at 8°C (fruit and vegetables average storage temperature), 15°C (abusing temperature) and 23°C (standard temperature) [Pao et al.,1998; Marklinder & Eriksson, 2015]. The samples performances have been studied with respect to different gases such as O_2, N_2, CO_2, and C_2H_4. The permeability of polymers to gases or water vapor is often presented as GTR (Gas Transmission Rate). [Robertson, 2006; Mangaraj & Goswami, 2009]. GTR values ($cm^3/cm^2\ d\ bar$), together with Solubility (S, $cm^3/cm^2\ bar$), Diffusivity (D, cm^2/sec) and Time Lag (t_L, *sec*), have been recorded for pure gases.

Figure 4.63 reports the GTR values recorded for all samples under the different temperatures considered.

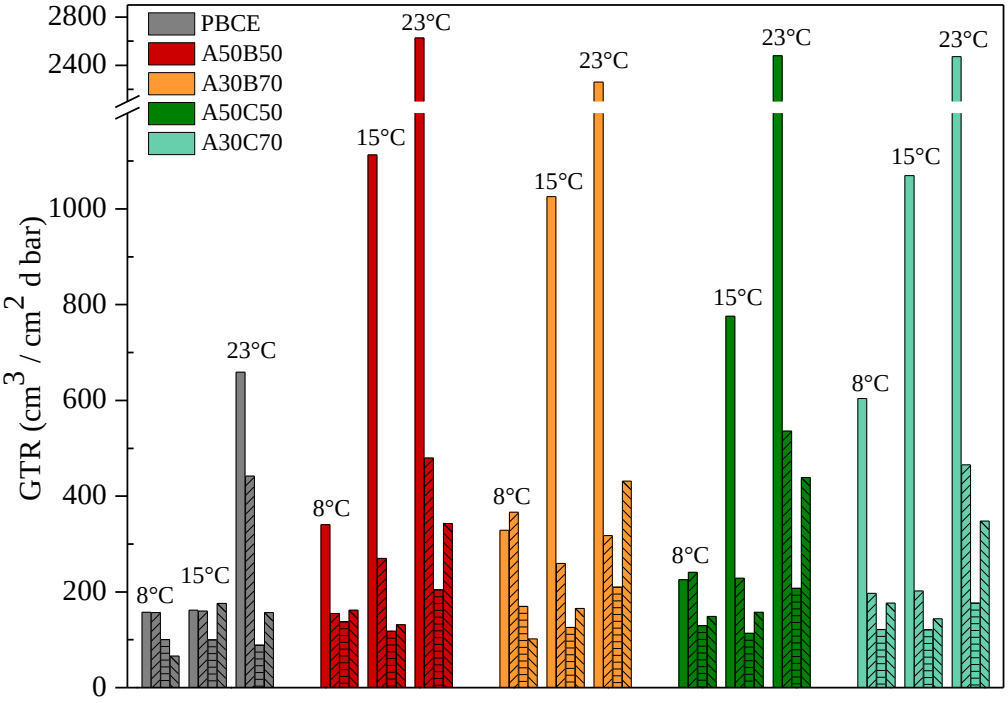

Figure 4.63 GTR to CO_2 (empty bars), O_2 (// pattern), N_2 (= pattern) and C_2H_4 (\\ pattern) for PBCE and multiblock copolymers at 8, 15 and 23°C.

In **Table S5** have been collected all the permeability data to CO_2 and the sample thickness, while in **Table S6** the perm-selectivity ratio to all the different gases at the studied temperatures are contained. It has been demonstrated that the perm-selectivity ratio is a definite value for each polymer under determinate conditions, as it depends on several factors, such as chemical structure and temperature [Siracusa et al., 2015; Genovese et al. 2014; Gigli et al., 2014 (a)].

As it can be observed from **Figure 4.63**, the GTR behavior is strictly linked to the chemical structure of the polymers under evaluation. For all samples at all the temperature studied, the CO_2 is more permeable than O_2 and N_2, despite the larger molecular diameter. Moreover, the multiblock copolymers display a much higher permeability as compared to PBCE homopolymer, due to their higher flexibility and lower crystallinity (**Table 4.29**).

The C_2H_4 gas transmission rate is quite low, but higher than that of N_2. Since ethylene is responsible of accelerated senescence of fruit and vegetables, the C_2H_4 permeation across the package is welcomed as it would improve the food shelf-life and quality.

As expected, the temperature has a significant influence on the gas transmission through the material and it strictly depends on the gas. It is well known that the mechanisms

driving the adsorption/desorption permeability, solubility and diffusion phenomena are all closely dependent on the temperature [Lee et al., 2008; Robertson, **2006**].

As it can be seen in **Figure 4.63**, CO_2 GTR shows a consistent increment with the temperature increase, due to the fast and chaotic motion of this gas. On the contrary, for O_2, N_2 and C_2H_4 only a moderate increase/dependence has been recorded. This result is highly interesting because a slow packaging crossing by the O_2, N_2 and C_2H_4 molecules can help avoiding a high-level of food respiration rate, the film collapse and an accelerate food ripening, respectively.

D, S and t_L data (**Table S5**) have been recorded for CO_2 at 23°C and in some cases also at 8°C and 15°C. The D value, linked to the kinetic parameters, increases with GTR increase, due to the gas diffusion rise throughout the polymer wall [Siracusa,; Blanco et al., **2012**; Mrkić et al., **2006**]. The S value, which correlates to the gas solubility into the matrix, decreases as the GTR increases, because the interaction between polymer and gas is not favorable. Finally, the t_L value, correlated to the time required to achieve equilibrium of the permeability processes, is in good accordance with the GTR value. As GTR increases t_L decreases, meaning that less time is necessary to reach the steady-state. All data well fit a standard behavior.

4.5.5 Activation energy of gas transport process

In order to describe the dependence of the permeation on the temperature, an Arrhenius type-equation has been employed to calculate the activation energy for gas transmission (E_{GTR}), heat of solution (H_S) and diffusion (E_D) processes. The mathematical relations used are well described in the related scientific literature [Siracusa et al., 2015]. The activation energy is deduced by calculating the value of the slope ($-E_a/R$) of the Arrhenius straight line, where R is the gas constant (8.314 J/mol K). Natural logarithmic (ln) of GTR, S and D compared with the reciprocal of the absolute temperature (1/T) have been reported as an example in **Figure 4.64** for the A50C50 sample, together with the indication of the calculated linear regression of the corrected experimental points fittings. Moreover, In **Table S7** are contained the corresponding activation energies for the gas transmission rate (E_{GTR}), the Heat of Solution (H_S) and the Diffusion (E_D) process in the range of 8-23°C for all gases, with the corresponding R^2 factor (between brackets).

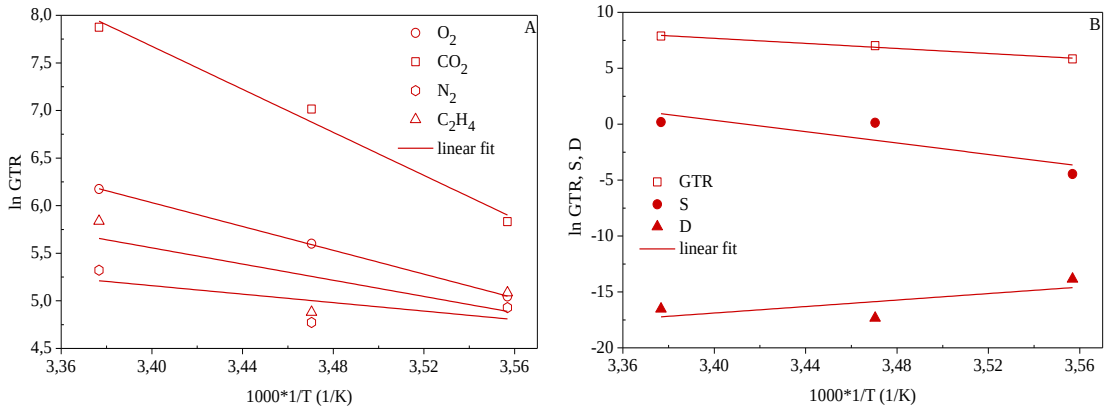

Figure 4.64: A) GTR of O_2, CO_2, N_2, C_2H_4 as a function of 1/T (K) for A50C50; B) GTR, S, D of CO_2 as a function of 1/T (K) for A50C50.

It can be evicted that in most cases the data well fit the theoretical relation (high R^2 coefficients), indicating a good correlation between permeability and temperature for all gases. The corresponding E_{GTR} (**Table S6**) is very high, especially for CO_2, while is lower for O_2, N_2 and C_2H_4 gases. This behavior confirms the assumption that CO_2 molecules move faster than the other gas molecules. Therefore, the permeability to CO_2 is higher than to the other studied gases.

For CO_2 the solubility increases by increasing the temperature. Consequently, the permeability displays the same trend. However, a linear trend was recorded not for all samples. This confirms the difficulty to observe a standard behavior. As the Solubility is linked to the polymer chemical structure, its trend confirms that the gases interact differently with the matrix. The corresponding H_S shows a fluctuant value. The same conclusion could be formulated for the E_D value. As it is well known from the literature, [Atkins & Jones, **2012**] high activation energy implies more sensitivity to temperature variations. It has been found that the permeation process is very well correlated to the temperature variation, while the sorption/diffusion process shows consistent deviation, being more dependent on polymer structure. The trend varies in fact by changing the gas and the temperature, and therefore underlines the importance of performing the barrier properties measurements at different storage conditions.

4.5.6 Composting

Biodegradation evaluation has been carried out through composting experiments. Weight losses as a function of the incubation time are reported in **Figure 4.65**. No mass decrease has been observed in the time scale explored for PBCE, as also previously reported [Gigli, Lotti et al., 2014 (a); Gigli, Govoni et al., 2014)] while the multiblock copolymers underwent a significant decrease of molecular weight.

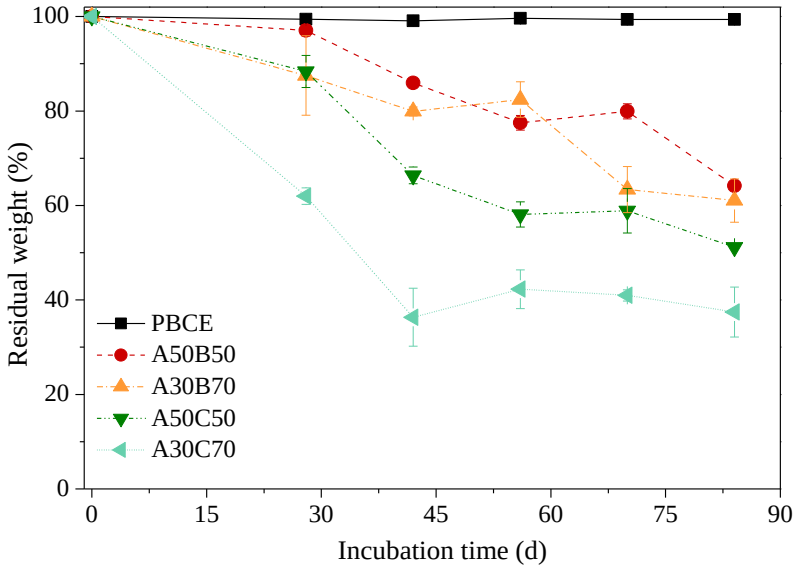

Figure 4.65. Weight losses of PBCE and multiblock copolymers as a function of the incubation time.

In particular, among the different factors affecting polymer biodegradation, such as molecular weight, melting temperature, crystallinity and surface hydrophilicity, [Gigli, Negroni et al., 2012; Gigli, Negroni et al., 2013 (a and b)], the last two played the major role for the polymer here studied.

Indeed, A30C70 is the more hydrophilic (**Table 4.27**) and the less crystalline material (**Table 4.28**), therefore its weight loss reached about 63%. On the other hand, A50B50 and A30B50, whose crystallinity degree and surface wettability are comparable, degraded to a similar extent (about 40% weight loss). Lastly, A50C50 lost about 50% of its initial weight in 84 days of incubation. Notwithstanding a similar crystallinity degree as compared to A50B50 and A30B50, its higher wettability caused a more pronounced degradation.

The surface morphology of the partially degraded samples has been observed by SEM (**Figure 4.66**).

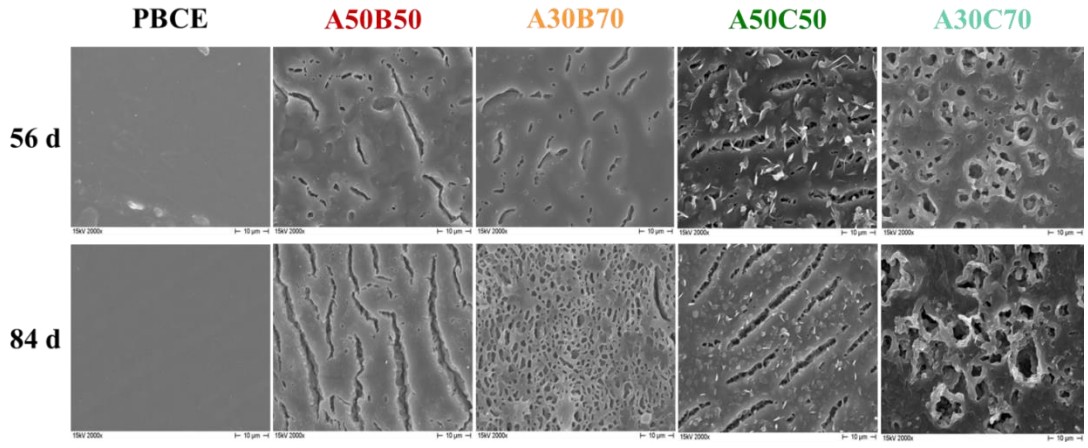

Figure 4.66. SEM micrographs of PBCE and multiblock copolymers at different incubation times.

Before composting, all the polymers displayed a smooth surface. While PBCE surface remained unchanged, the copolymer films show a significant modification. In fact, cracks and holes, whose intensity increased with the incubation time, appear on the surface, clearly evidencing the proceeding of the degradation process.

As it is well known, the polymer degradation by microorganisms is a surface eroding process. The more accessible and less packed amorphous regions are preferentially degraded (at least in the first stages), giving rise to an increase of the degree of crystallinity. To better highlight this effect, WAXS analyses and crystallinity degree measurements have been carried out. X-ray diffraction patterns of the polymers under study are reported in **Figure 4.66** as a function of the composting time.

It is clearly visible an increase of the degree of crystallinity, more evident for the multiblock copolymers than for PBCE. As a matter of fact A50B50, A30B70, A50C50 and A30C70 indeed display an increase of X_c of 46%, 54%, 73% and 83% respectively (**Table S8**). Such increment occurs prevalently during the first 56 days of incubation, while in the last part of the experiment only a slight changes are observed. The trend observed perfectly matches with the gravimetric measurements: the higher the weight losses, the higher the X_c increase.

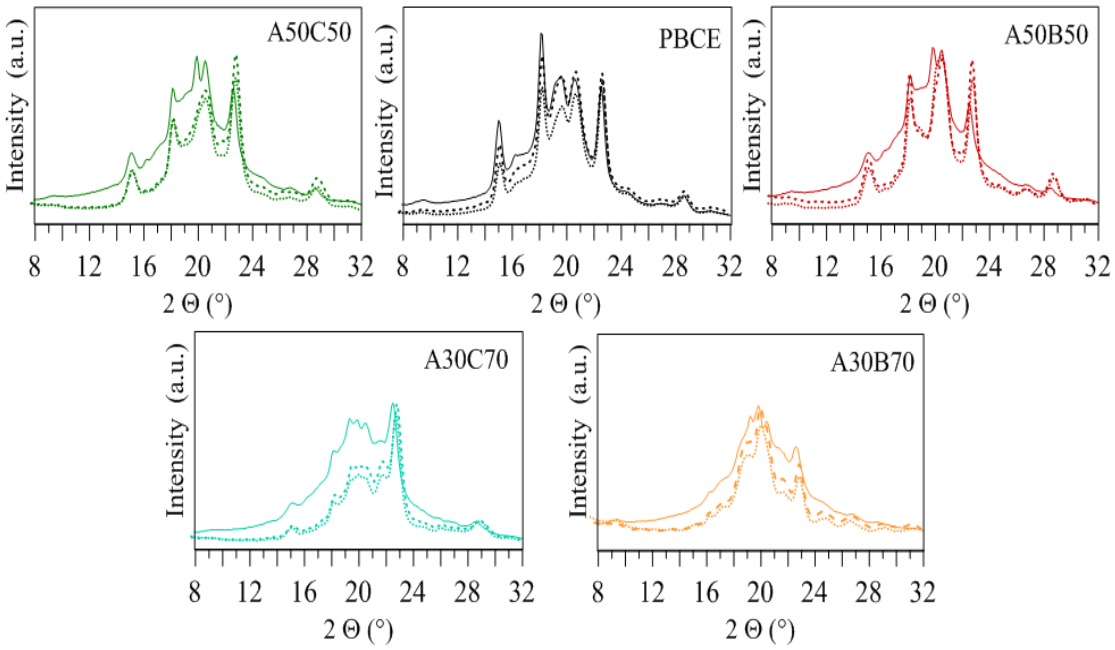

Figure 4.66. X-ray diffraction patterns of PBCE and multiblock copolymers as a function of the composting time. Solid lines: 0 d, dash lines: 56 d, dot lines: 84 d.

4.5.7 Conclusions

The chain extension technique allowed for the preparation of five new high molecular weight poly(ester urethane)s. The building blocks, hydroxyl-terminated polyester prepolymers, are obtainable from renewable resources. The final materials are therefore fully bio-based, with the exception of HDI chain extender. However, its molar percentage in the final polymer is in all cases below 6%.

The results evidence that by playing with two different factors, i.e. the chemical composition and the mass ratio of each prepolymer block in the final mixture, it is possible to design a class of materials with peculiar and promising properties for food packaging.

The unique combination of soft and hard segments and the introduction of different amounts of ether linkages in the polymer backbone, permits to improve the mechanical behaviour and the biodegradation rate of the PBCE homopolymer, although preserving its good thermal resistance and the promising gas barrier properties.

In this respect it is very important to underline that the polymers here presented display superior barrier performances to CO_2 and O_2 not only with respect to other biodegradable materials employed for food packaging, such as poly(caprolactone) and poly(lactic acid), but also as compared to PP, HDPE and LDPE [Mensitieri et al., 2011].

e

5.

CONCLUSIONS

CONCLUSIONS

In the present PhD Thesis new compostable polymers, very attractive candidates for the production of flexible food packaging films, have been successfully synthesized and characterized. Such new materials have been designed as chemical modification of some interesting aliphatic polyesters, some of them already used in food packaging applications, such as PLA.

The results presented in this PhD Thesis highlighted that copolymerization, realized through different synthetic strategy, represents a winning approach to modulate the polymer performances according to the desired application.

As pointed out by the results discussed in the present PhD Thesis, solid-state properties and biodegradation rate can be tailored acting on chemical structure, copolymer composition and polymer architecture: in particular, type and amount of comonomeric units and sequence distribution along macromolecular chain deeply affect the material final properties, changing the ability of the parent homopolymer to crystallize and the hydrophobic/hydrophilic ratio. More specifically, the introduction of different amounts of ether- or thio-ether linkages or short ramifications along macromolecular backbone of parent homopolymer, or simply acting on *soft*/*hard* ratio in block structures permitted to modulate mechanical behaviour and biodegradation rate of the parent homopolymer, without compromising the good properties.

Among these, the good barrier properties: as an example, the synthesized polymers revealed to be suitable, for modified atmosphere packaging (MAP) of fresh product, since they possess very low permeability to oxygen, that gives rise to oxidation processes, with consequent deterioration of the chemical-physical and organoleptic properties of the packaged food. Their barrier properties to this gas have proved to be even better than that of commercial Poly(lactic acid) (PLA), already approved by Food and Drug Administration and widely used in packaging applications.

It is worth noting that all the employed synthetic strategies are simple, eco-friendly, versatile and cost-effective processes. All of them are solvent-free in order to be in conditions close to those used to scale up the process, for a reasonable low-cost industrial production.

Nowadays the largest challenge of polymer scientists is in fact to manufacture, at a reasonably low cost, biodegradable polymers with well-balanced biodegradability and

performances, starting from renewable sources and employing low-environmental-impact processes.

In this view, aliphatic polyesters, and above all those here presented, are industrially very appealing; they are currently obtained from fossil carbon sources at an acceptable cost, but many of their monomers can be also prepared from renewable resources (Bechthold et al., 2008; Madhavan, Nampoothiri et al., 2010Colonna et al., 2011a; 2011b; Luckachan & Pillai, 2011;).

Relying on competitive price and performances, bioplastics will target growth markets where new production capacity will be added and serve existing markets by retrofitting existing production assets from oil-based products to green ones.

Of course, the results herein discussed only represent a starting point towards a real application of the polyesters studied; upscalability of the synthesis process has to be proved and deeper investigations of polymer processability, interactions with food and ecotoxicity are necessary.

The path is still long and arduous because each achievement has to face scientific, technological and economic hurdles before reaching the status of practical viability. To that end, biomass researchers, microbiologists, synthetic chemistry, and process engineers are making use of their individual expertise and collaborate to develop materials for human prosperity and a more sustainable society.

REFERENCES

Albertsson, A.C.; Srivastava, R.K.; *Advanced Drug Delivery Reviews*, **2008**, 60(9),1077-1093.

Albertsson, A.C.; Varma, I.K.; *Advances in Polymer Science*, Springer-Verlag Berlin Heidelberg, **2002**, 157.

Ali Shah, A.; Hasan, F.; Hameed, A.; Ahmed, S.*; Biotechnology Advances*; **2008**, 26, 246-265.

Allegra, G.; Marchessault, R.H.; Bloembergen, S.J.; *Polymer Science, Part B: Polymer Physics*; **1992**, 30, 809.

Amanatidou, A.; Slump, R. A.; Gorris, L. G. M. and Smid, E. J. ; *J. Food. Sci.;* **2000,** 65, 61–66.

Andronova, N., Albertsson,. A.C.; *Biomacromolecules*, **2006**, 7(5), 1489-95.

Angell, C.A.; *Polymer* **1997,** *38,* (26), 6261-6266

Arutchelvi, J.; Sudhakar, M.; Arkatkar, A.; Doble, M.; Bhaduri, S.; Uppara, P. V.; *Indian J. Biotechnol.*, **2008**, 7, 9.

ASTM D 6400-04 "Standard specification for compostable plastics";

ASTM D 6002-96 (Reapproved 2002)^{e1} "Standard guide for assessing the compostability of environmentally degradable plastics".

Atkins, P.; Jones, L.; *Chemical principles: The Quest for Insight*, 5th edition: Freeman WH & Co., New York, USA, **2012**.

Auras, R.; Harte, B.; Selke, S.; *Macromol. Biosci.*, **2004**, 4, 835–864.

Averous, L. and Boquillon, N.; *Carbohydrate Polymers*, **2004**, 56(2), 111–122.

Barry-Ryan, C. and Beirne, D. O.; *Int J. Food Sci. Technol*., **2000**, 35, 243–254.

Barry-Ryan, C.; Pacussi, J. M. and Beirne, D. O.; *J. Food Sci,*, **2000,** 65, 726–730.

Bastioli, C.; *Handbook of Biodegradable Polymers,* Rapra Technology, **2005**.

Baur, V.H.; *Makromol. Chem*., **1966**, 98, 297.

Bechthold, I.; Bretz, K.; Kabasci, S.; Kopitzky, R.; Springer, A.; *Chem. Eng. Technol.*, **2008**, 31 647–654.

Berti, C ; Binassi, E. ; Celli, A.; Colonna, M.; Fiorini M.; Marchese P.; Marianucci E.; Gazzano M.; Di Credico F.; Brunelle D.J.; *Journal of Polymer Science Part B: Polymer Physics*, **2008**, 46(6), 619.

Berti, C.; Celli, A.; Marchese, P.; Marianucci, E.; Barbiroli, G.; Di Credico, F.; *Macromolecular Chemistry and Physics*, **2008**, 209, 1333-1344.

Berti, C.; Binassi, E.; Colonna, M.; Fiorini, M.; Kannan, G.; Kanaram, S.; Mazzacurati, M.; *Bio-Based Terephthalate Polyesters*. US 20100168461 A1, **2010**.

Berti, C.; Celli, A.; Marchese, P.; Marianucci, E.; Sullalti, S.; Barbiroli, G.; *Macromolecular Chemistry and Physics*, **2010**, 211(14), 1559.

Bikiaris; *Biodegradable Polyesters*, 1st Edition, Wiley-VCH Verlag GmbH & Co. KGaA, **2015**.

Bioplastics Facts and Figures; <www.european-bioplastics.org.>, **2016**.

Blanco, I.; Siracusa, V.; *J. Therm. Anal. Calorim.*, **2013**, 112(3), 1171.

Boyd, S.U.; Boyd, R.H.; *Macromolecules*, **2001**, 34(20), 7219-7229.

Boyer, R. F.; *Rubber Chemistry and Technology*, **1963**, 36, 1303-1421.

Bravard, S.P.; Boyd, R.H.; *Macromolecules*, **2003**, 6(3), 741-748.

Cai, J.; Liu, C.; Cai, M.; Zhu, J.; Zuo, F.; Hsiao, B.; Gross, R. A.; *Polymer*, **2010**, 51, 1088.

Cannarsi, M.; Baiano, A.; Marino, R.; Sinigaglia, M. and Del Nobile, M. A.; *Meat Science*, **2005**, 70(2), 259-265.

Carothers, W.H.; *Polymerization, Chem. Rev.*, **1931**, 8, 353-426.

Carothers, W.H.; *Trans. Faraday Soc*., **1936**, 32-39.

Chaiwong, C., Rachtanapun, P., Wongchaiya, P., Auras, R., & Boonyawan, D.; *Surface and Coatings Technology*, **2010**, 204(18–19), 2933-2939.

Chang, P.R.; Jian, R.; Yu, J.; Ma, X.; *Food Chemistry*, **2010**, 120, 736-740.

Chatani, Y.; Okita, Y.; Tadokoro, H.; Yamashita, Y.; *Polim. J.* **1970**, *1*, 555.

Chen, C.C. and White, J.L.; *Polym. Eng. Sci*., **1993**, 33, 923-930.

Chen, H.B.; Wang, X.L.; Zeng, J.B.; Li, L.L.; Dong, F.X.; Wang, Y.Z.; *Ind. Eng. Chem. Res*., **2011**, 50, 2065.

Chen, G.-Q.; Patel, M.K.; *Chem. Rev*., **2012**, 112, 2082-2099.

Chrissafis, K.; Paraskevopoulos, K. M.; Bikiaris, D. N.; *Thermochim. Acta*, **2005**, 435(2), 142-150.

Cohn, D.; Lando, G.; Sosnik, A.; Garty, S.; Levi, A.; *Biomaterials*, **2006**, 27, 1718.

Conn, R.E.; Kolstad, J.J.; Borzelleca, J.F.; Dixler, D.S.; Filer, Jr. L.J.; LaDu, Jr. B.N. et al.; *Food and Chemical Toxicology*, **1995**, 33(4), 273.

Davis, G., & Song, J. H.; *Industrial Crops and Products*, **2006**, 23(2), 147-161.

De Azeredo, H. M. C.; *Food Research International*, **2009**, 42(9), 1240-1253.

De Leiris, P.; "Water activity and permeability," in *Food Packaging and Preservation*, M. Mathlouthi, Ed., pp. 213–233, Elsevier Applied Science, New York, NY, USA, **1986**.

Diaz, A.; Katsarava, R.; Puiggali, J.; *Int. J Mol. Sci.*, **2014**, 15, 7064-7123.

Di Franco, C. R.; Cyras, V. P.; Busalmen, J. P.; Ruseckaite, R. A. and Va´zquez, A.; *Polymer Degradation and Stability*, **2004**, 86(1), 95-103.

Dorsch R.R., Miller R.W.: Tuomela M.: Academic dissertation in microbiology, "Degradation of lignin and other 14C-labelled compounds in compost and soil with an emphasis on white-rot fungi, Helsinki, **2002**, <http://ethesis.helsinki.fi>

Drumright, R.E.; Gruber, P.R.; Henton, D.E.; *Polylactic acid technology. Adv. Mater*., **2000**, 12, 1841-1846.

Duda, A.; Penczek, S.; *Biopolymers*, Wiley-VCH, Weinheim, Germany, Vol. 3b, Ch. 12, **2002**.

Dusunceli, N.; Colak, O.U.; *Int. J. Plasticity*, **2008**, 24, 1224–1242.

EN 13.432, *Packaging –Requirements for Packaging Recoverable Through Composting And Biodegradation-Test Scheme and Evaluation Criteria for the Final Acceptance of Packaging, European Standard. European Committee for Standardization*, Brussels, Belgium, **2005**.

Endo, T.; Handbook of RingOpening Polymerization, Wiley-VCH Verlag GmbH & Co. KGaA, **2009**.

Fabbri, M. ; Gigli, M.; Gamberini, R.; Lotti, N.; Gazzano, M.; Rimini, B.; Munari, A.; *Polym. Degrad. Stab.*, **2014**, 108, 223–231.

Fabbri, M.,. Soccio, M, Gigli, M., Guidotti, G., Gamberini, R., Gazzano, M., Siracusa, V., Rimini, B., Lotti, N., Munari, A.; *Polymer*, **2016**, 83, 154-161.

Farber, J. N., Harris, L. J., Parish, M. E., Beuchat, L. R., Suslow, T. V., Gorney, J. R., Garrett, E. H. and Busta, F. F.; *Rev. Food Sci. Food Safety*, **2003**, 2,142–160.

Feuilloley, P.; Cesar, L.; Benguigui, L.; Grohens, Y.; Pillin, I.; Bewa, H.; Lefaux, S.; Jamal, M.; *J Polym Environ*, **2005**, 13, 349.

Flory, P.J.; *J. Am. Chem. Soc*., **1936**, 58, 1877.

Flory, P.J.; *J. Am. Chem. Soc*., **1939**, 61, 3334.

Flory, P.J.; *J. Am. Chem. Soc*., **1942**, 64, 2205.

Flory, P.J.; *J. Chem. Phys*., **1947**, 15, 684.

Flory, P.J.; *Principles of Polymer Chemistry*, Ithaca, NY, **1953**.

Fujimaki, T.; *Polym. Degrad. Stab.*, **1998**, 59, 209–214.

Galić, J.; Galić, K.; Kurtanjek, M.; Ciković, N.; *Polym. Test.,* **2000**, 20, 49-57.

Galić, K. and Ciković, N.; *Polymer Testing*, **2001**, 20, 599-606.

Gan, Z.; Abe, H.; Doi, Y.; *Biomacromolecules*, **2001**, 2, 313-321.

Gazzano, M.; Viscardo, M.; Focarete, M.L.; Scandola, M.; Gross, R.A.; *J Polym Sci Pol Phys* **2003**, 41, 1009.

Genovese, L.; Gigli, M.; Lotti, N.; Gazzano, M.; Siracusa, V.; Munari, A.: Dalla Rosa, M.; *Industrial & Engineering Chemichal Research*, **2014**, 53, 10965-10973.

George, S.C.; Thomas, S.; *Prog. Polym. Sci*, **2001**, 26(6), 985-1017.

George, S.M., Puglia, D., Kenny, J.M., Causin, V., Parameswaranpillai, J., and Thomas, S.*; Ind. Eng. Chem. Res.*, **2013**, 52 (26), 9121–9129.

Ghanbarzadeh, B.; Almasi, H.; and Entezami, A. A.; *Industrial Crops and Products*, **2011**, 33(1), 229–235.

Gigli, M.; Lotti, N.; Gazzano, M.; Finelli, L.; Munari, A.; *React. Funct. Polym*., **2012**, 72, 303–310.

Gigli, M.; Negroni, A.; Soccio, M.; Zanaroli, G.; Lotti, N.; Fava, F.; Munari, A.; *Green Chem*., **2012**, 14, 2885-2893.

Gigli, M.; Negroni, A.; Soccio, M.; Zanaroli, G.; Lotti, N.; Fava, F.; Munari, A.; *Polym. Degrad. Stab.*, **2013**, 98, 934-942. (a)

Gigli, M.; Negroni, A.; Zanaroli, G.; Lotti, N.; Fava, F.; Munari, A.; *React. Funct. Polym*., **2013**, 73, 764-771. (b)

Gigli, M.; Lotti, N.; Gazzano, M.; Finelli, L.; Munari, A.; *Polym. Eng. Sci*., **2013**, 53, 491-501. (a)

Gigli, M.; Lotti N., Gazzano M.; Siracusa V.; Finelli L., Munari A.; Dalla Rosa M.; *Industrial & Engineering Chemical Research*, **2013**, 52, 12876−12886. (b)

Gigli, M.; Govoni, M.; Lotti, N.; Giordano, E. D.; Gazzano, M.; Munari, A.; *RSC Adv.*, **2014**, 4, 32965-32976.

Gigli, M.; Lotti, N.; Gazzano, M.; Siracusa, V.; Finelli, L.; Munari, A.; Dalla Rosa, M.; *Polymer Degradation and Stability*, **2014**, 105, 96-106. (a)

Gigli, M., Lotti, N., Vercellino, M., Visai, L., Munari, A.; *Material Science and Engineering: C*, **2014**, 34, 86-97. (b)

Gigli, M., Fabbri, M., Lotti, N., Gamberini, R., Rimini, B.; Munari, A.; *European Polymer Journal*, **2016**, 75 431–460.

Göpferich, A.; *Biomaterials*, **1996**, 17, 103.

Grima, S.; Bellon-Maurel, V.; Feuilloley, P.; Silvestre, F.; *Journal of Polymers and the Environment*, **2000**, 8(4), 183.

Gross R.A., Kalra B.; *Science*, **2002**, 297, 803.

Gross R.A., Ganesh M., Lu W.; *Trends in Biotechnology*, **2010**, 28, 435.

Gupta, B.; Revagade, N.; and Hilborn, J.; *Prog. Polym. Sci*., **2007**, 32 (4), 455–482.

Hakkarainen, M.; *Adv. Polym. Sci*., **2002**, 157, 113–138.

Halek, G.W.; *American Chemical Society*, **1988**, 16, 195.

Halpi, J.C.; Kardos, K.L.; *J. Appl. Phys.* **1972**, 43, 2235–2241.

Havriliak, S.; Negami, S. *Polymer* **1967,** *8* (4), 161.

Helfland, E.; Lauritzen J.I.; *Macromolecules*, **1973**, 6, 631.

Highlights in bioplastics, IBAW publications, **2006**.
http://www.biodeg.net/fichiers/Highlights%20in% 20Bioplastics%20(Eng).pdf.

Hotchkiss, J. H.; *Safety considerations in active packaging. In: Active Food Packaging*, Springer US, **1995**.

Ichikawa, Y.; Kondo, H.; Igarashi, Y.; Noguchi, K.; Okuyama, K.; Washiyama, J.; *Polymer*, **2000**, 41, 4719-4727; **corrigendum** *Polymer*, **2001**, 42, 847.

Ikada, Y.; Tsuji, H.; *Macromol. Rapid Commun*., **2000**, 21, 117.

Ingrao, C.; Tricase, C.; Cholewa-Wójcik, A.; Kawecka, A.; Rana R.; Siracusa, V.; *Science of the Total Environment*, **2015**, 537, 385 –398.

Jakubowicz, I.; *Polymer Degradation and Stability*, **2003**, 80, 39-43.

Jamshidian, M.; Tehrany, E.A.; Cleymand, F.; Leconte, S.; Falher, T.; Desobry, S.; *Carbohydr. Polym.*, **2012**, 87, 1763-1773.

Jérôme, C.; Lecomte, P.; *Advanced Drug Delivery Reviews*, **2008**, 60, 1056.

Jiang, R.; Quirk, R.P.; White, J.L.; and Min, K.; *Polym. Eng. Sci*., **1991**, 31, 1545.

Klug, H.P.; Alexander, L.E. *X-ray diffraction procedures for polycrystalline and amorphous materials.* New York: Wiley Interscience, **1974.**

Kofinas, P.; Cohen, R.E.; Halasa, A.F.; *Polymer* **1994**, *35*, 1229.

Koutny, M.; Lemaire, J.; Delort, A.M.; Chemosphere, **2006**, 64, 1243-1252.

Kowalski, A.; Duda, A.; and Penczek, S.; *Macromolecules*, **2000**, 33, 7359–7370.

Kremer, F.; Schonhals, A., *Broadband Dielectric Spectroscopy*. Springer Verlag: Heidelberg, **2002.**

Lee, D. S.; Yam, K. L.; Piergiovanni, L.; *Food Packaging: Science and Tecnology*, CRC, Taylor & Francis Group: London, **2008**.

Lee, S. H.; Kim, M.N.; *Int Biodeterior Biodegradation*. **2010**, 64, 184-190.

Legras, R.; Dekoninck, J.M.; Vanzieleghem, A.; Mercier, J.P.; Nield E.; *Polymer*, **1986**, 27, 109.

Li D.; Xia Y.N.; *Advanced Materials*, **2004**, 16, 1151.

Liu, C.; Liu, F.; Cai, J.; Xie, W.; Long, T. E.; Turner, S. R.; Lyons, A.; Gross, R. A.; *Biomacromolecules*, **2011**, 12, 3291

López, O.V.; Castillo, L.A.; García, M.A.; Villar, M.A.; Barbosa, S.E.; *Food Hydrocolloids*, **2015**, 43, 18-24

Lu, L.X. and Xu, F.; *Packaging Technology and Science*, **2009**, 22, 107-113.

Lucas, N.; Bienaime, C.; Belloy, C.; Queneudec, M.; Silvestre, F.; Nava-Saucedo, J.E.; *Chemosphere*, **2008**, 73, 429.

Luckachan, G.E.; Pillai, C.K.S.; *J Polym Environ*, **2011**, 19, 637.

Lunt, J.; *Polym. Degrad. Stab.*, **1998**, 59, 145.

Madhavan Nampoothiri, K.; Rajendran Nair, N.; John, R.P.; *Bioresour. Technol*., **2010**, 101, 8493 –8501.

Mandelkern, L.; *Crystallization of Polymers*, McGraw-Hill, New York, **1954**.

Mandelkern L.; *Crystallization and melting in 'Comprehensive polymer science'* (eds.: G. Allen and J. C. Bevington) Pergamon Press, Oxford, vol. 2, **1989**.

Mangaraj, S.; Goswami, T.K.; Mahajan, P.V.; *Food Eng. Rev.* **2009**, 1, 133-158.

Mark, H.; Whitby, G. S.; *Interscience*, New York, **1940**.

Marklinder, I.; Eriksson, M. K.; *British Food Journal*, **2015**, 117(6), 1764-1776.

Martin-Fabiani, I.; Linares, A.; Nogales, A.; Ezquerra, T.A.; *Polymer*, **2013**, 54(21), 5892-5898.

Mc Crum, N.G.; Read, B.E.; Williams, G.; *Anelastic and Dielectric Effects in Polymeric Solids*, Wiley, London , **1967**.

Mecking, S.; *Int. Ed. Engl*. **2004**, 43, 1078.

Menges, M.G.; Penelle, J.; Le Fevere de Ten Hove, C.; Jonas, A.M.; Schmidt-Rohr, K.; Macromolecules, **2007**, 40, 8714.

Mensitieri et al.; *Trends in Food Science & Technology*, **2011**, 22, 72-80.

Miyata, T. ; Masuko, T.; *Polymer*, **1998**, 39, 1399–1404.

Mochizuki, M.; Hirami M.; *Polym. Adv. Technol*., **1997**, 8, 203.

Mochizuki, M.; Mukai, K.; Yamada, K.; Ichise, N.; Murase, S.; Iwaya, Y.; *Macromolecules*, **1997**, 30, 7403-7407.

Mrkic, S.; Galic, K.; Ivankovic, M.; Hamin S.; Cikovic, N.; *J. Appl. Polym. Sci.*, **2006**, 99, 1590–1599.

Müller, A.J.; Balsamo, V.; Arnal, M.L.; *Lect. Notes Phys*., **2007**, 714, 229.

Müller, R.J.; *Biopolymers, General Aspects and Special Applications*, , Wiley-VCH Verlag GmbH, Weinheim, **2003**, 10, 365–374.

Mukai, K.; Yamada, K.; Doi Y.; *Int. J. Biol. Macromol.*, **1993**, 15, 361.

Nair, L.S.; Laurencin, C.T.; *Prog. Polym. Sci.*, **2007**, 32, 762.

Nogales, A.; Denchev, Z.; Sics, I.; Ezquerra, T.A.; *Macromolecules*, **2000**, 33(25), 9367-9375.

Nogales, A.; Sanz, A.; Ezquerra, T.A.; *Journal of Non-Crystalline Solids*, **2006**, 352(42-49), 4649-4655.

Ohlsson, T. and Bengtsson, N.; *Minimal Processing Technologies in the Food Industry*, 1st ed. CRC Press, Washington, DC, **2002**.

Okada, M.; *Prog. Polym. Sci.*, **2002**, 27, 87.

Olivato, J.B., Grossmann M.V.E.; Yamashita F.; Eiras D.; Pessan L.A.; *Carbohydrate Polymers*, **2012**, 87 2614–2618.

Ortega-Toro, R.; Contreras, J.; Talens, P.; Chiralt, A.; *Food packaging and shelf life*, **2015**, 5, 10–20.

Pankaj, S.K.; Bueno-Ferrer, C.; Misra, N.N.; O'Neill, L.; Jiménez, A.; Bourke, P.; Cullen, P.J.; *Innovative Food Science and Emerging Technologies*, **2014**, 21, 107–113.

Pao, S.; Brown, G.E.; Schneider, K.R.; *Journal of Food Science*, **1998**, 63(2), 359-362.

Pasha, I.; Saeed, F.; Tauseef Sultan, M.; Rafiq Khan M.; Rohi, M.; *Critical Reviews in Food Science and Nutrition*, **2014**, 54, 340–351.

Paul, D.R.; *Control of phase structure in polymer blends, in Functional Polymers*, Plenum Press, New York, **1989**.

Pauly, A.S.; Permeability and diffusion data in *Polymer Handbook*; Brandrup, J.; Immergut, E.H.; Grulke, E.A., Eds.; John Wiley & Sons, New York, NY, USA, 4th Edition, **1999**.

Papageorgiou, G.Z.; Bikiaris, D.N.; *Polymer*, **2005**, 46, 12081–12092.

Papageorgiou, G.Z.; Bikiaris, D.N. ; Biomacromolecules, **2007**, 8, 2437-2449.

Pepels, M.P.F.; Hansen, M.R.; Goossens, H.; Duchateau, R.; *Macromolecules*, **2013**, 46, 7668.

Plastics – the Facts **2015**. An analysis of European plastics production, demand and waste data.

Rabinovitch E.; *Trans. Faraday Soc.*, **1937**, 33, 1225.

Rasal, R.M.; Janorkar, A.V. and Hirt, D.E.; *Progr. Polym. Sci.*, **2010**, 35, 338–356.

Regulation (EC) No 1935/2004 of the European Parliament and of the Council of 27

October **2004** on materials and articles intended to come into contact with food and repealing Directives 80/590/EEC and 89/109/EEC.

Regulation (EU) No 10/2011 of 14 January **2011** on plastic materials and articles intended to come into contact with food.

Richert, R.; Angell, C. A.; *Journal of Chemical Physics*; **1998**, 108, (21), 9016-9026

Rizzarelli, P.; Puglisi, C.; Montaudo, G.; *Polym. Degrad. Stab.*, **2004**, 85, 855.

Robertson, G. L.; *Food Packaging Principles and Practice*, second Edition, CRC Taylor & Francis Group, **2006**, 4, 63.

Roy, P.K.; Hakkarainen, M.; Varma, I.K.; Albertsson, A.C.; *Environ. Sci. Technol.*, **2011**, 45, 4217.

Rudnik E.; *Compostable Polymer Materials*, Elsevier, Amsterdam, **2008**.

Russo, G. M.; Simon, G. P.; and Incarnato, L.; *Macromolecules*, **2006**, 39(11), 3855-3864.

Sanchez, I.C.; Eby, R.K.; *Journal of research of the Notional Bureau of Standards - A. Physics and Chemistry*, **1973**, 77A(3), 353.

Sandhya; *LWT-Food. Sci. Technol*., **2010**, 43, 381–392.

Scott, G.; *Polymer Degradation and Stability*, **2000,** 68, 1.

Shirahama, H.; Kawaguchi, Y.; Aludin, M.S.; Yasuda, H.; *J. Appl. Polym. Sci*., **2001**, 80, 340.

Siracusa, V.; Rocculi, P.; Romani, S.; & Rosa, M.D.; *Trends in Food Science & Technology*, **2008**, 19(12), 634–643.

Siracusa, V.; *International Journal of Polymer Science*, **2012**, 2012, 1-11.

Siracusa, V.; Blanco, I.; Romani, S.; Tylewicz, U.; Rocculi, P.; Dalla Rosa, M.; *J. Appl. Polym. Sci.*, **2012**, 125, E390-E401.

Siracusa, V.; Lotti, N.; Munari, A.; Dalla Rosa, M.; *Polym. Degr. Stab*., **2015**, 119, 35-45.

Soccio, M.; Lotti, N.; Finelli, L.; Gazzano, M.; Munari, A.; *Eur. Polym. J.*, **2007**, 43, 3301-3313.

Soccio, M.; Nogales, A.; Lotti, N.; Munari, A.; Ezquerra, T.A.; *Physical Review Letters*. **2007**, 98(3), 037801-1 - 037801-4.

Soccio, M.; Lotti, N.; Finelli, L.; Gazzano, M.; Munari, A.; *Eur. Polym. J.*, **2008**, 44, 1722–1732. (a)

Soccio, M.; Lotti, N.; Finelli, L.; Gazzano, M.; Munari, A.; *Journal of Polymer Science, Part B: Polymer Physics*, **2008**, 46, 170-181. (b)

Soccio, M.; Lotti, N.; Finelli, L.; Munari, A.; *Journal of Polymer Science, Part B: Polymer Physics*, **2008**, 46, 818-830. (c)

Soccio, M.; Nogales, A.; Garcia-Gutierrez, M.C.; Lotti, N.; Munari, A.; Ezquerra, T.A.; *Macromolecules*, **2008,** 41(7), 2651-2655.

Soccio, M.; Lotti, N.; Finelli, L.; Munari, A.; *Eur. Polym. J.*, **2009**, 45, 171-181.

Soccio, M.; Lotti, N.; Gigli, M.; Finelli, L.; Gazzano, M.; Munari, A.; *Polym. Int.* **2012**, 61, 1163-1169.

Soccio, M.; Nogales, A.; Ezquerra, T.A.; Lotti, N.; Munari, A .; *Macromolecules*, **2012**, 45(1), 180-188.

Soccio, M.; Lotti, N.; Munari, A.; *J. Therm. Anal. Calorim.*, **2013**, 114(2), 677-688.

Soccio, M.; Nogales, A.; Martin-Fabiani, I.; Lotti, N.; Munari, A.; Ezquerra, T.A.; *Polymer*, **2014**, 55(6), 1552-1559.

Sokolsky-Papkov, M.; Agashi, K.; Olaye, A.; Shakesheff, K.; Domb, A.J.; *Adv. Drug Deliv. Rev.*, **2007**, 59, 187–206.

Sorrentino, A.; Gorrasi, G.; & Vittoria, V.; *Trends in Food Science & Technology*, **2007**, 18(2), 84-95.

Stempfle, F.; Ortmann, P.; Mecking, S.; *Macromol. Rapid Commun.*, **2013**, 34, 47.

Suyama, T.; Tokiwa, Y.; Ouichanpagdee, P.; Kanagawa, T.; Kamagata, Y.; *Applied and Environmental Microbiolology*, **1998**, 64, 5008.

Themelis, N.J.; Castaldi, M.J.; Bhatti, J.; Arsova, L.; *Energy and Economic Value of Non-recycled Plastics (NRP) and Municipal Solid Wastes (MSW) That are Currently Landfilled in the Fifty States*, Columbia University, Report of Earth Engineering Center, **2011**.

Thompson, A.; Taylor, B. N. editors. *Guide for the Use of the International System of Units (SI), special publication 811*. U.S. Dept. Of Commerce, NIST-Natl. Inst. of Standards and Technology, **2008.**

Trzaskowski, J.; Quinzler, D.; Baehrle, C.; Mecking, S.; *Macromol. Rapid Commun.*, **2011**, 32, 1352.

Tserki, V.; Matzinos, P.; Pavlidou, E.; Vachliotis, D.; Panayiotou, C.; *Polymer Degradation and Stability*, **2006**, 91, 367.

Van der Zee, M.; *Structure-biodegradability relationship of polymeric material*, Dissertation University of Twente, Enschede, The Netherlands, 213, **1997**.

Van Krevelen, D. W. *Properties of Polymers*; Elsevier: Amsterdam, **1997**

Van Natta, F.J.; Hill, J.W.; Carothers, W.H.; *J. Am. Chem. Soc.*, **1934**, 57, 455.

Vanhaecht, B.; Rimez, B.; Willem, R.; Biesemans, M.; Koning, C.E.; *Journal of Polymer Science Part A: Polymer Chemistry*, **2002**, 40, 1962-1971.

Varadarjan, S.; Miller, D.J.; *Biotechnol. Progr*., **1999**, 15, 845–854.

Varma, I.K.; Albertsson, A.C.; Rajkhowa, R.; Srivastava, R.K.; *Prog. Polym. Sci*., **2005**, 30, 949.

Vert, M.; *Biomacromolecules*, **2005**, 6, 538.

Vieira, M.; Altenhofen, M.; Oliveira, L.; and Masumi, M.; *Eur. Polym. J*, **2011**, 47, 254–263.

Vilela, C.; Silvestre, A.J.D.; Meier, M.A.R.; *Macromol. Chem. Phys*., **2012**, 213, 2220.

Von Burkersroda, F.; Schedl, L.; Göpferich, A.; *Biomaterials*, **2002**, 23, 4221.

Wendling, J.; Suter, U.W.; *Macromolecules*, **1998**, 31, 2509.

Windle, A.H.; Golombok, C.; Donald, A.M.; Mitchell, G.R.; *Faraday Discuss*., Chem. Soc., 79-55, **1985**.

www.compost.org.

Xing, Y.; Li, X.; Xu, Q.; Jiang, Y.; Yun, J. and Li, W.; *Innovat. Food Sci. Emerg. Technol*., **2010**, 11, 684–689.

Xu, J.; Guo, B.H.; *Biotechnol. J*., **2010**, 5, 1149–1163.

Yokesahachart, C.; Yoksan, R.; *Carbohydrate Polymers*, **2011**, 83, 22–31.

Yoo, E.S.; Im, S.S.; *J. Polym. Sci. Polym. Phys*., **1999**, 37, 1357–1366.

Yoshie, N.; Inoue, Y.; You, H.Y.; Okui, N.; *Polymer*, **1994**, 35, 1931.

Zhang, J.; Sun, X.; *Biomacromolecules*, **2004**, 5, 1446–1451.

Zhang, Y.; Liu, Z.; *Starch-based edible films in environmentally compatible food packaging*, Woodhead Publishing, England, **2008,** 108–136,.

Zheng, Y.; Yanful, E.K.; Bassi, A.S.; *Crit. Rev. Biotechnol*., **2005**, 25, 243.

Zhu, J.; Li, X.; Chen, L.; Li, L.; *Carbohydrate Polymers*, **2014**, 104, 1-7.

Zimmermann, H.; *Developments in polymer degradation*, Applied Science Publishers, London, **1984,** 5, 89.

SUPPLEMENTARY MATERIAL

Table S1. Percentage of increment /decrement (+/-) of CO_2 GTR data after ageing treatments.

Sample	R^2	4 days	8 days	12 days	16 days	20 days	30 days	40 days
Thermal ageing								
PHD	0.1	+37	+47	+30	+54	+119	+30	+36
P(HD85TED15)	0.1	-21	-22	-32	-31	+17	-4	-9
P(HD70TED30)	0.3	-11	-17	-23	-25	+8	-26	-32
P(HD55TED45)	0.1	-5	-29	-21	-12	+36	-4	+2
PTED	0.1	+10	+26	-4	+19	+59	+7	+21
LDPE	0.4	+15	+1	+1	+0	+72	+78	+32
Photo ageing								
PHD	0.2	+38	+90	+27	+57	+88	+30	+84
P(HD85TED15)	0.3	-18	+21	-18	+5	-24	+14	+37
P(HD70TED30)	0.9	+7	-12	-19	-34	-37	-36	-52
P(HD55TED45)	0.3	+12	-10	-6	-10	-5	-1	-13
PTED	0.8	-10	-18	-22	-42	-23	-39	-47
LDPE	0.6	+21	+17	-9	+24	+45	+42	+53

Table S2 Mechanical data after contact with food simulants.

Polymer	Untreated		DW		AA		EtOH		i-O	
	E (MPa)	**ε_b (%)**	**E (MPa)**	**ε_b (%)**	**E (MPa)**	**ε_b (%)**	**E (MPa)**	**ε_b (%)**	**E (MPa)**	**ε_b (%)**
PHD	400±21	80±6	373±19	43±1	436±10	50 ±3	433±37	70±4	242±17	142±22
P(HD85TED15)	361±6	742±67	353±5	271 ±31	345±17	185±34	420±13	87 ±15	334 ±3	847 ±51
P(HD70TED30)	246±13	907±56	218±13	680 ± 2	245±16	156±34	261±15	180±1	244±33	1153 ±61
P(HD55TED45)	222±9	842±23	236±14	66 ±6	261±24	7 ±1	165±17	60±9	235±9	52 ±13
PTED	201±7	856±81	-	-	-	-	-	-	-	-
LDPE	135±6	824±36	172±28	356 ±63	165±16	492±58	131±21	348±34	160 ±3	617 ±49

Table S3. Percentage of increment /decrement (+/-, %) of CO_2 GTR data after contact with food simulants.

Sample	DW	AA	E	i-O	CO_2/O_2
PHD	+35	-82	+84	-14	3.9
P(HD85TED15)	-9	+25	+11	-36	8.0
P(HD70TED30)	+52	-33	-29	+16	9.4
P(HD55TED45)	-15	-21	-19	-64	10.1
PTED	--	--	-3	-33	10.4
LDPE	+88	+72	+35	+8	3.7

DW: Distilled Water, AA: Acetic Acid, E: Ethanol, i-O: iso-Octane

Table S4: Thermal characterization data (II scan DSC after quenching from the melt).

	II scan					
Polymer	T_g (°C)	ΔC_p (J/°C g)	$T_{m,1}$ (°C)	$\Delta H_{m,1}$ (J/g)	$T_{m,2}$ (°C)	$\Delta H_{m,2}$ (J/g)
PBCE	9	0.141	-	-	166	33
A50B50	-34	0.330	52	3	143	13
A30B70	-31	0.389	64	16	134	8
A50C50	-29	0.440	-	-	119	17
A30C70	-32	0.451	51	2	110	4

Table S5. Permeability data of CO_2 gas at 8, 15 and 23°C and film thickness

Polymer	***PBCE***	***A50B50***	***A30B70***	***A50C50***	***A30C70***
Thickness (µm)	146±14	241±13	163±3	262±8	263±29
		8°C			
GTR (cm^3/cm^2 d bar)	157 ± 1	341 ± 2	329 ± 2	226 ± 1	604 ± 1
S 10^2(cm^3/cm^2 bar)		1.2± 0.3			27 ± 1
D 10^8(cm^2/s)		100 ± 30			4.2± 0.1
t_L (s)		130 ± 40			1070 ± 40
		15°C			
GTR (cm^3/cm^2 d bar)	160 ± 1	1113 ± 2	1026 ± 4	776 ± 2	1070 ± 1
S (cm^3/cm^2 bar)		1.10 ± 0.01	1.40 ± 0.01	0.38 ± 0.01	1.40 ± 0.01
D 10^8 (cm^2/s)		3.00± 0.01	3.90± 0.07	5.80 ± 0.03	1.40± 0.01
t_L (s)		130 ± 40	3000 ± 60	1678 ± 7	3080 ± 6
		23°C			
GTR (cm^3/cm^2 d bar)	659 ± 2	2627 ± 5	2263 ± 5	2480 ± 8	2473 ± 5
S (cm^3/cm^2 bar)	1.20 ± 0.01	1.20 ± 0.01	1.30 ± 0.01	1.30 ± 0.01	1.40 ± 0.03
D 10^8 (cm^2/s)	0.93 ± 0.01	6.7 0± 0.01	5.40± 0.02	5.50±0.03	3.20±0.07
t_L (s)	3810 ± 30	1716 ± 3	2126 ± 6	1775 ± 10	1370 ± 30

Table S6: Perm-selectivity values at 8,15 and 23°C.

Polymer	CO_2/O_2	CO_2/N_2	CO_2/C_2H_4	CO_2/O_2	CO_2/N_2	CO_2/C_2H_4	CO_2/O_2	CO_2/N_2	CO_2/C_2H_4
	8°C			**15°C**			**23°C**		
PBCE	1.01	1.57	2.41	1.01	1.62	0.92	1.49	7.42	4.20
A50B50	2.19	2.46	2.11	4.12	9.41	8.45	5.47	12.83	7.67
A30B70	3.06	4.93	3.40	5.31	8.82	7.45	7.12	10.76	5.24
A50C50	0.94	1.74	1.51	3.39	6.83	4.91	4.63	11.92	5.65
A30C70	3.06	4.93	3.40	5.31	8.82	7.45	5.30	13.97	7.09

Table S7.: Activation energy for the gas transmission rate (E_{GTR}), the Heat of Solution (H_S) and the Diffusion (E_D) process at 8, 15 and 23°C. In the brackets the linear regression coefficients (R^2).

Polymer	E_{GTR} (J/mol)	H_S (J/mol)	E_D (J/mol)	E_{GTR} (J/mol)	H_S (J/mol)	E_D (J/mol)
	O_2			**CO_2**		
PBCE	48 ± 0.16 (0.8)	-	--	66 ± 0.11 (0.8)	--	--
A50B50	52 ± 0.16 (1)	--	--	94 ± 0.13 (1)	211 ± 0.18 (0.7)	-121 ± 0.13 (0.5)
A30B70	-6 ± 0.22 (0.2)	116 ± 0.24 (1)	100 ± 0.13 (1)	89 ± 0.10 (1)	-9 ± 0.07 (1)	30 ± 0.03 (1)
A50C50	37 ± 0.10 (0.7)	--	--	111 ± 0.19 (1)	108 ± 0.15 (1)	-5 ± 0.20 (1)
A30C70	40 ± 0.21 (0.8)	--	--	65 ± 0.22 (1)	76 ±0.19 (1)	-10 ± 0.22 (0.0)
	N_2			**C_2H_4**		
PBCE	-6 ± 0.11 (0.8)	--	--	39 ± 0.20 (0.6)	--	--
A50B50	19 ± 0.10 (0.5)	--	--	35 ± 0.05 (0.6)	--	--
A30B70	10 ± 0.13 (0.2)	--	--	67 ± 0.21 (1)	--	--
A50C50	22 ± 0.28 (0.6)	--	--	50 ± 0.12 (0.8)	--	--
A30C70	17 ± 0.12 (0.8)	--	--	32 ± 0.03 (0.6)	--	--

Table S8: **Table S2.** Degree of crystallinity as a function of the composting time

	X_c (%)		
Polymer	**0 d**	**56 d**	**84 d**
PBCE	38	39	41
A50B50	28	38	41
A30B70	26	37	40
A50C50	26	43	45
A30C70	24	40	44

PUBBLICATIONS

The following list of publications collects all papers produced during the doctoral period:

1. Laura Genovese, Matteo Gigli, Nadia Lotti, Massimo Gazzano, Valentina Siracusa, Andrea Munari, Marco Dalla Rosa; Biodegradable PE-like aliphatic polyesters containing ether linkages: synthesis, solid-state and barrier properties; Industal and Engineering Chemistry Research 2014, 53, 10965 −10973.
2. Laura Genovese, Nadia Lotti, Massimo Gazzano, Lara Finelli, Andrea Munari; New eco-friendly random copolyesters based on poly(propylene cyclohexanedicarboxylate): structure-properties relationships, eXPRESS Polymer Letters, 2015, 9(11), 972–983.
3. Laura Genovese, Nadia Lotti, Massimo Gazzano, Valentina Siracusa, Marco Dalla Rosa, Andrea Munari; Novel biodegradable aliphatic copolyesters based on poly(butylene succinate) containing thioether-linkages for sustainable food packaging applications. *In press* in Polymer degradation and stability (2016), *http://dx.doi.org/10.1016/j.polymdeg.*
4. Matteo Gigli, Laura Genovese, Nadia Lotti, Andrea Munari, Marco Dalla Rosa, Valentina Siracusa; Gas barrier and thermal behavior of biodegradable PE-like long chain polyesters after stressed treatments. *Under review* in Polymer-Plastics Technology and Engineering

Scientific contributions to national and international congresses:

1. L.Genovese, M. Gigli, N. Lotti, M. Gazzano, V. Siracusa, A.Munari, M. Dalla Rosa; Novel pe-like eco-friendly polymers containing ether-linkages for food packaging applications; European Polymer Federation congress (EPF 2013); Pisa (Italy), 16th-21th June, 2013.
2. L. Genovese, M. Gigli, N. Lotti, M. Gazzano, V. Siracusa, A. Munari, M. Dalla Rosa; Novel pe-like eco-friendly polymers containing ether-linkages for food packaging applications; VI conferenza internazionale Energythink; Bologna (Italy), 27th November 2013.
3. L. Genovese, N. Lotti, M. Gazzano, L. Finelli, A. Munari; New eco-friendly random copolyesters based on Poly(propylene cyclohexanedicarboxylate): structureproperties relationships; 2nd international conference on Bio-based Polymers and Composites; Visegrád (Hungary), 24th-28th August 2014.
4. N. Lotti, L.Genovese, M. Gazzano, L. Finelli, V. Siracusa, M.Dalla Rosa, A. Munari; Biodegradable aliphatic copolyesters containing thio-ether linkages for sustainable food packaging applications; Convegno dell'Associazione Italiana di Chimica per l'Ingegneria (AICIng 2014); Lecce, 14th-17th september 2014.
5. L. Genovese, A.Linares, T. Ezquerra, A. Nogales, M.Soccio, N. Lotti, A. Munari, Molecular dynamics of Poly(propylene 1,4- cyclohexanedicarboxylate) and its copolymers with Poly(neopenthyl glycol 1,4-cyclohexanedicarboxylate) as revealed by broadband dielectric spectroscopy; European polymer federation congress (EPF 2015); Dresden, 21th -26th june 2015.
6. L. Genovese; Novel eco-friendly random copolyesters for packaging applications: synthesis and characterization; Macrogiovani 2015. Bologna, 6th july 2015.
7. L. Genovese, M. Soccio, N. Lotti, M. Gazzano, L. Finelli, V. Siracusa, M. Dalla Rosa, A. Munari; Biodegradable aliphatic copolyesters containing thio-ether linkages for sustainable food packaging applications; 5th International Conference on Biobased and Biodegradable Polymers (BIOPOL-2015), Donostia-San Sebastián (Spain), 6th-9th October 2015.
8. M. Soccio, L. Genovese, N. Lotti, M. Gazzano, V.Siracusa, E. Salatelli, F. Balestra, A.Munari; New biodegradable PLA-based triblock copolymers for

sustainable food packaging; 5th International Conference on Biobased and Biodegradable Polymers (BIOPOL-2015), Donostia-San Sebastián (Spain), 6th-9th October 2015.

9. M. Negrin, M. Mariani , E. Macerata, G. Consolati, F. Quasso, L. Genovese, M. Soccio, N. Lotti, A. Munari; Effect of gamma irradiation on novel fully aliphatic Poly(Propylene/Neopenthyl Glycol Cyclohexanedicarboxylate) random copolymers; Advances in Materials & Processing Technologies Conference, Madrid (Spain), 14 - 17 December 2015

Participation to congresses

1. European Polymer Federation congress (EPF 2013); Pisa(Italy), 16th-21th June, 2013.
2. VI International conference Energythink; Bologna (Italy), 27th November 2013.
3. Polymers from renewable resources and biodegradable polymers, Bologna (Italy), 29th November 2013.
4. XXXV Convegno-Scuola AIM "Mario Farina"- Characterization of Polymeric Materials; Gargnano (Italy), 19th-23th may 2014.
5. 2nd international conference on Bio-based Polymers and Composites; Visegrád (Hungary), 24th-28th August 2014.
6. European polymer federation congress (EPF 2015); Dresden (Germany), 21th - 26th june 2015.
7. Macrogiovani 2015, Associazione Italiana di Chimica e tecnologia delle macromolecole (AIM). Bologna (Italy), 6 july 2015.

Experience abroad

Institute for the structure of matter, Spanish National Research Council (CSIC), Madrid (Spain), October 2014 – March 2015.

Research project: Study of structure-dynamic relationships in new ecofriendly copolymers by broad band dielectric spectroscopy.

Acknowledgments

Eccomi giunta infine ai ringraziamenti.

Chi mi conosce un pochino sa che non sono affatto brava in questo genere di cose e che preferirei disegnarli i miei ringraziamenti, piuttosto che esprimerli a parole.

Proverò comunque a riassumere in poche righe la mia gratitudine verso tutti coloro che mi sono stati accanto in questi tre anni e che, in modi diversi, mi hanno aiutata a raggiungere questo importante obiettivo.

Grazie alla Prof.ssa Lotti e al Prof. Munari che mi hanno dato la possibilità di iniziare questo percorso nel mondo dei materiali polimerici e della ricerca universitaria, facendomi da costante guida e supporto.

Grazie a Matteo, che nonostante le spedizioni in discarica, le lunghe giornate di lavoro, e tante altre piccole avventure, è stato un costante punto di riferimento con i suoi preziosi consigli e insegnamenti, un'ispirazione ed esempio con le sue idee e la voglia di fare.

Grazie a Michela S. che durante questo ultimo anno ha condiviso con me non solo l'ufficio, ma anche risate e momenti tristi, esperienze di vita, modi di dire spagnoli e soprattutto la sua esperienza di donna di scienza e la sua forza.

Grazie a Martina e Michela C., colleghe e amiche, siamo cresciute insieme qui al DICAM, abbiamo imparato tanto e abbiamo condiviso ogni tipo di stato d'animo durante questi anni. Grazie soprattutto per le piccole cose, che sono quelle che portano il sole nei giorni bui, grazie per i caffè, i pranzi, gli oroscopi di Rob e le chiacchiere, e per tutto il resto.

Grazie a Giulia, per questi ultimi mesi, per i suoi sorrisi e il suo non scoraggiarsi davanti alle difficoltà.

Grazie a Vilma, indispensabile per la sopravvivenza del DICAM e a tutta l'amministrazione per la loro pazienza e abilità nel districare le matasse della burocrazia.

Grazie a Paola per i suoi insegnamenti durante i primi mesi e a tutti i ragazzi che in questi anni ho conosciuto qui al DICAM e con i quali ho condiviso esperienze, belle e brutte, cibo e laboratori.

Grazie al Dott. Massimo Gazzano e alla Prof.ssa Valentina Siracusa per il loro fondamentale apporto scientifico, al Prof . Tiberio Ezquerra e a tutto il gruppo

SoftMatPol del CSIC di Madrid per avermi accolta tra loro e avermi regalato un'importante esperienza di vita, tanti incoraggiamenti e qualche parola di spagnolo.
Grazie alle Montelline, Magda e Daniela, per aver ascoltato i miei sfoghi, per la birra nei calici, i progetti artistici e le serate di lavoro attorno al tavolo della cucina.
Non può mancare un ringraziamento alla mia famiglia e agli amici di sempre, anche se più o meno lontani, costante presenza nella mia vita e porto sicuro dove rifugiarmi al riparo dalle tempeste.
Dulcis in fundo, grazie a te Emanuele, per essermi stato vicino anche quando ci separavano più di mille chilometri e per continuare a prenderti cura di me giorno per giorno adesso che dividiamo la stessa casa. Grazie perché mi sopporti anche quando sono insopportabile e perché mi tieni la mano quando ho la testa tra le nuvole e sto per cadere. Grazie per i caffè, i manicaretti dietetici da master chef, i telefilm e le fughe in altri mondi. Grazie di farmi sentire felice almeno una volta ogni giorno.

Grazie a tutti, di cuore.
Laura